universität wien

DISSERTATION

Titel der Dissertation

Functional and molecular characterization of proteins involved in Mg^{2+} and K$^+$ homeostasis

Verfasser

Mag.rer.nat Gerhard Sponder

angestrebter akademischer Grad

Doktor der Naturwissenschaften (Dr.rer.nat.)

Wien, 2011

Table of contents

1.1. Summary

Transport processes across cellular membranes have been a challenging and fascinating field of research for the past 50 years.

Mrs2p and its bacterial homolog CorA belong to a large family of Mg^{2+} transporters. Common characteristics of members of this family are two transmembrane domains (TMs) in the C-terminal part of the protein and the highly conserved G-M-N motif at the end of TM 1. In order to obtain new insights into the molecular mechanisms of regulation of these transporters, mutational analyses on members of the CorA/*MRS2* family were performed. For CorA from *Thermotoga maritima* we confirmed the key gating role of residue Leu294 by forming a mechanical barrier for ion permeation. Mutations at this position strongly affect the ability of the channel to close the ion conduction pathway, which is eventually lethal for the cell.

In contrast, our studies on *MRS2* suggest that the regulation of Mg^{2+} transport is more complex in eukaryotic members of this family. We performed a comparative analysis of the crystal structure of *T. maritima* CorA and the structure of the N-terminal domain of *Saccharomyces cerevisiae* Mrs2p, including the pore forming TM 1. We thereby identified amino acid residues most likely involved in gating of the channel. Our results show that in Mrs2p, Met309 is the equivalent to Leu294 in CorA and fulfils a similar function in gating the channel. However, mutations at this position do not lead to a complete deregulation of the closing mechanism as observed for Leu294 in CorA. A second gate formed by Val315 was identified but appears to be less important in controlling ion translocation.

By structure-based sequence analysis, we identified a potential cation binding site putatively involved in sensing the intramitochondrial Mg^{2+} concentration. However, our attempts to experimentally demonstrate the involvement of the highly conserved amino acid Asp97 in formation of a cation binding site did not yield a clear result.

We also performed a random mutational analysis of the highly conserved G-M-N motif of Mrs2p. It has been shown that even conservative single amino acid substitutions in this motif abolish the transport activity of CorA and Mrs2p. Surprisingly, we identified a series of mutants with sequences completely different from G-M-N, but still able to transport Mg^{2+}. However, these mutants exhibited reduced selectivity for Mg^{2+}. Our results suggest that the G-M-N motif plays a central role for the substrate specificity in the CorA/Mrs2p family.

Besides Mrs2p the genome of *S. cerevisiae* encodes a homologous protein, namely Lpe10p. In this study Lpe10p was investigated in more detail. Deletion of *LPE10* or *MRS2* similarly leads to impaired growth on non-fermentable carbon sources. However, in contrast to deletion of *MRS2*, deletion of *LPE10* results in a strong reduction of the mitochondrial membrane potential. Lpe10p alone cannot form a Mg^{2+}-selective channel but it is able to hetero-oligomerize with Mrs2p and thereby reduces the conductance of the Mrs2p channel. Our results indicate that the interplay between the two proteins is important to maintain the mitochondrial Mg^{2+} homeostasis in *S. cerevisiae*.

Compared to Lpe10p or CorA, *S. cerevisiae* Mrs2p has an exceptionally long C-terminus. We performed site-directed mutagenesis on the non-conserved positively charged KRRRK motif and created a C-terminally truncated version of Mrs2p. While the KRRRK motif does not appear to be crucial for the function, large deletions in the C-terminal part of the protein strongly affect the transport activity of the channel.

The second part of this thesis focuses on the biochemical characterization of the two yeast members of the MDM38/LETM1 family. Mdm38p has previously been characterized as an essential factor for mitochondrial K^+/H^+ exchange in *S. cerevisiae*. In a genome-wide suppressor screen, the proteins Mrs7p and Ydl183cp were identified as strong suppressors of the *MDM38* deletion. While Mrs7p exhibits a high sequence similarity to Mdm38p and Letm1, Ydl183c appears to be an unrelated protein. Since these proteins only have one predicted transmembrane domain, it is unlikely that they form the K^+/H^+ exchanger. Mdm38p/Letm1 and Mrs7p were found to form high molecular weight complexes in the inner mitochondrial membrane suggesting that they form homo-multimers or rather associate as a cofactor with the so far unidentified K^+/H^+ exchanger. To tackle this question, we aimed here at identifying the interaction partners of Mrs7p, and expected to find the antiporter among them.

1.2. Zusammenfassung

Transportprozesse durch Zellmembranen sind ein herausforderndes und faszinierendes Forschungsgebiet.

Mrs2p und sein bakterielles Homolog CorA gehören zu einer großen Familie von Mg^{2+} Transportern. Charakteristische Eigenschaften der Mitglieder dieser Familie sind zwei Transmembrandomänen (TMs) im C-terminalen Bereich der Proteine und das hochkonservierte Motiv G-M-N am Ende der TM 1. Um weitere Einblicke in die molekularen Mechanismen der Regulation dieser Transporter zu bekommen, wurden Mutationsanalysen an Mitgliedern der CorA/*MRS2* Familie durchgeführt. Bei CorA von *Thermotoga maritima* konnte die Schlüsselrolle der Aminosäure Leu294 als Schleuse des Kanals bestätigt werden. Mutationen an dieser Position haben eine starke Auswirkung auf die Fähigkeit des Ionenkanals die Pore zu schließen und sind letal für die Zelle.

Im Gegensatz dazu deuten unsere Ergebnisse mit *MRS2* darauf hin, dass die Regulation des Ionentransports in den eukaryotischen Vertretern der Familie wesentlich komplexer ist. Wir haben eine vergleichende Strukturanalyse der Kristallstrukturen von *T. maritima* CorA und der N-terminalen Domäne von *Saccharomyces cerevisiae* Mrs2p durchgeführt. Es konnten Aminosäuren identifiziert werden, die höchstwahrscheinlich am Schließen des Kanals beteiligt sind. Unsere Ergebnisse zeigen, dass Met309 in Mrs2p und Leu294 in CorA eine gleichwertige Rolle in der Regulation des Ionenflusses spielen. Mutationen an dieser Position führen aber nicht zu einer vollständigen Deregulierung des Schließmechanismus, wie es bei Leu294 von CorA beobachtet wurde. Eine zweite Schleuse (von Val315 gebildet) wurde ebenfalls identifiziert - scheint aber für die Kontrolle des Ionentransports eine untergeordnete Rolle zu spielen.

Durch strukturbasierende Sequenzanalyse konnte auch eine potentielle Kationenbindungsstelle identifiziert werden, die als Messfühler der intramitochondrialen Mg^{2+} Konzentration fungiert. Die Beteiligung der hochkonservierten Aminosäure Asp97 an der Bildung einer Kationenbindungsstelle konnte experimentell aber nicht eindeutig gezeigt werden.

Zusätzlich wurde das hochkonservierte G-M-N Motiv von Mrs2p mittels Zufallsmutagenese analysiert. In früheren Arbeiten wurde gezeigt, dass sogar konservative Substitutionen einzelner Aminosäuren in diesem Motiv nicht toleriert werden und die Transportaktivität von CorA und Mrs2p stark minimieren. Eine Serie von Mutanten zeigt aber noch immer Transportaktivität, obwohl die Sequenzen überraschend stark von der Sequenz G-M-N

abweichen. Die Selektivität dieser Mutanten für Mg^{2+} war aber reduziert. Diese Ergebnisse lassen darauf schließen, dass das G-M-N Motiv eine zentrale Rolle für die Substratselektivität der CorA/Mrs2p Familie spielt.

In der vorliegenden Arbeit wurde auch die Funktion von Lpe10p, dem Homolog von Mrs2p in Hefe, genauer untersucht. Die Deletion von *LPE10* oder *MRS2* führt in beiden Fällen zu einem Wachstumsdefekt auf nicht-fermentierbaren Kohlenstoffquellen. Im Gegensatz zur Deletion von *MRS2* führt die Deletion von *LPE10* aber zusätzlich zu einer starken Reduktion des mitochondrialen Membranpotentials. Lpe10p alleine kann keinen Mg^{2+} selektiven Ionenkanal bilden, es bildet aber Heterooligomere mit Mrs2p, die zu einer Reduktion der Leitfähigkeit des Mrs2p Kanals führen. Unsere Ergebnisse zeigen, dass die Interaktion zwischen den beiden Proteinen eine entscheidende Rolle für die mitochondriale Mg^{2+} Homöostase in *S. cerevisiae* spielt.

Im Vergleich zu Lpe10p oder CorA, besitzt Mrs2p einen ungewöhnlich langen C-Terminus. Wir haben eine ortspezifische Mutagenese am nicht-konservierten, positiv geladenem KRRRK Motiv durchgeführt und eine C-terminale Verkürzung des Mrs2 Proteins hergestellt. Während das KRRRK Motiv selbst keine entscheidende Rolle für die Transportaktivität des Kanals spielt, führt die größere Deletion am C-Terminus zu eine starken Reduktion der Funktionalität des Kanals.

Im zweiten Teil dieser Arbeit wurden zwei Mitglieder der MDM38/LETM1 Familie aus Hefe charakterisiert. In vorangegangenen Studien wurde Mdm38p bereits als essentieller Faktor im mitochondrialen K^+/H^+ Austausch in *S. cerevisiae* beschrieben. In einer genomweiten Suche nach Suppressoren, wurden die Proteine Mrs7p und Ydl183cp als starke Suppressoren der *MDM38* Deletion identifiziert. Während Mrs7p eine große Ähnlichkeit zu Mdm38p aufweist, scheint Ydl183c ein nicht verwandtes Protein zu sein. Da beide Proteine vermutlich nur eine Transmembrandomäne besitzen, ist es relativ unwahrscheinlich, dass sie den aktiven K^+/H^+ Austauscher alleine bilden. Mdm38p/Letm1 und Mrs7p wurden als Teil von Proteinkomplexen mit hohem Molekulargewicht in der inneren Mitochondrienmembran nachgewiesen. Diese Beobachtung lässt darauf schließen, dass diese Proteine Homomultimere formen oder- noch wahrscheinlicher- als Cofaktoren mit dem bisher unbekannten K^+/H^+ Austauscher assoziieren. Um diese Fragestellung zu klären, wurde versucht Interaktionspartner von Mrs7p zu identifizieren, mit der Erwartung den verantwortlichen Antiporter zu finden.

2. Introduction

2.1. The importance of magnesium in living cells

Magnesium has a crucial function in countless biological processes; it acts as cofactor with ATP in multiple enzymatic reactions, interacts with exonuclease III, ribonuclease H and hairpin ribozymes (Garcia Vescovi, et al., 1996; McCarthy, et al., 2005; Romani, 2007). The ion exerts a stabilizing function on membranes and protein complexes, e.g. in the absence of Mg^{2+} ribosomal subunits are disassembled (Smith and Maguire, 1998). Furthermore Mg^{2+} plays an important role in signaling processes, extracellular magnesium concentrations exert a regulatory effect on K^+ and Ca^{2+} channels in the plasma membrane (Brunet, et al., 2005) and stress caused by Mg^{2+} depletion in yeast results in a rise of cellular Ca^{2+} concentrations which in turn triggers the calcineurin signaling pathway, a major regulator of environmental stress conditions (Wiesenberger, et al., 2007).

Cellular total magnesium concentrations are in the order of about 14-30 mM, only a small fraction of which is found in the free ionized form (~ 0.5 mM), whereas the vast majority is bound to negatively charged ligands, like phosphate, ATP, RNA and DNA (Romani and Scarpa, 1992; Jung, et al., 1997; Maguire and Cowan, 2002). Altered Mg^{2+} levels are observed in a variety of human diseases. Changes in the intracellular concentration of the ion in myocytes were reported in several cardiovascular diseases (Murphy, 2000). Furthermore, due to its important role in glucose metabolism, hypomagnesia is implicated in insulin resistance and diabetes (Garfinkel and Garfinkel, 1988; de Valk, 1999; Humphries, et al., 1999; Kao, et al., 1999).

2.2. Magnesium transport systems in prokaryotes

2.2.1. The CorA family of magnesium transporters

Members of the CorA family are ubiquitous throughout eubacteria and archaea, with sequence homologies ranging from 98% between *E. coli* CorA and that of *S. typhimurium* to 15-20% in more distantly related species (Smith, et al., 1993; Kehres, et al., 1998).

CorA was the first molecularly characterized magnesium transport protein. The name CorA originates from its ability to transport cobalt besides of magnesium, which is toxic for the cell at higher concentrations. The deletion of CorA therefore confers resistance to high cobalt concentrations in the growth medium (Hmiel, et al., 1986; Hmiel, et al., 1989; Snavely, et al., 1989).

In 2006 three crystal structures of *Thermotoga maritima* CorA have been published independently with a resolution of 3.9 Å, 2.9 Å and 3.7 Å, respectively (Lunin, et al., 2006; Eshaghi, et al., 2006; Payandeh and Pai, 2006).

The crystal structures unisonously demonstrated that CorA is a homopentamer with two transmembrane helices (TMs). The ion conduction pathway is entirely formed by TM 1, while five TM 2 domains form an outer anchoring ring in the membrane. The channel has a narrow entrance (~ 5 Å) and a wide mouth (~ 20 Å). The N-terminal domain of the protein is localized in the cytoplasm and folded into a seven stranded parallel/antiparallel ß-sheet (ß 1-7), sandwiched between two sets of α-helices (α1, α2, α3 and α4, α5, α6). The helices α5, α6 are called "willow helices" and extend towards the membrane (α5) and back (α6). This cytosolic domain is followed by an unusually long (~100 Å) stalk helix (α7) forming the funnel and TM 1 (Figure 1) (Lunin, et al., 2006).

The short loop connecting TM 1 and TM 2 is missing in all published structures, indicating a high flexibility (Lunin, et al., 2006; Eshaghi, et al., 2006; Payandeh and Pai, 2006). The helix forming TM 2 domain ends with the highly conserved KKKKWL motif (Lunin, et al., 2006). In the pentameric structure these lysine residues form the "basic sphincter", a highly positively charged ring around the pore at the membrane-cytosol interface. This high accumulation of positive charge is counterbalanced by a high number of negatively charged residues, mainly aspartic acid and glutamic acid residues situated in the tips of α5 and α6 as well as in the loop connecting the two willow helices (Lunin, et al., 2006).
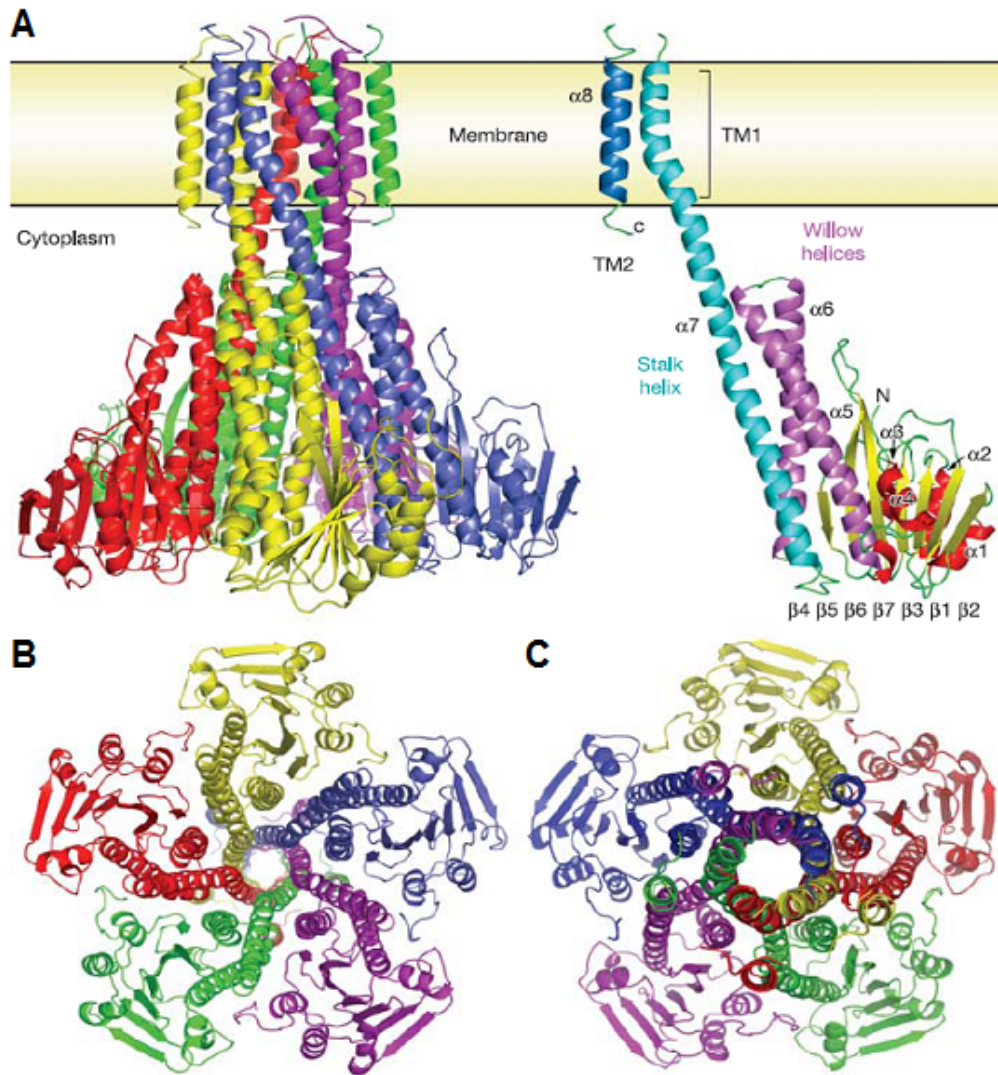
Figure 1: Structure of the CorA Mg^{2+} channel: (**A**), Ribbon diagram of the CorA pentameric complex, viewed in the plane of the membrane. On the right a single unit of the CorA channel highlighting the following structural features is shown: Stalk helix and inner TM1 helix (turquoise), outer helix TM 2 (dark blue) and willow helices (purple). The α-helices 1-4 are colored in red and β - sheets in yellow. The membrane surface is indicated. (**B**) View from the intracellular region. (**C**), View from the periplasm. Adapted from (Lunin, et al., 2006)

Magnesium exhibits several exceptional characteristics: a fully hydrated ion has a diameter of 5 Å which is approximately the same size as a glucose molecule, whereas the unhydrated cation is only about 0.65 Å in diameter (Maguire, 2006b). The finding that cation hexaammines, mimicking the hydrated ion, are able to block the channel suggests that initially the fully hydrated ion interacts with CorA (Kucharski, et al., 2000). In most CorA homologs as well as in Mrs2p and Alr1p the short loop connecting TM 1 and TM 2 contains negatively

charged residues, suggesting that this is the initial interaction site for Mg^{2+} (Weghuber, et al., 2006; Wachek, et al., 2006). In view of the high transport rates of members of the CorA/Mrs2 family, the concept that hydrated magnesium ions literally bind to the loop through strong ionic interactions has been questioned recently (Moomaw and Maguire, 2010).

The ring of asparagines (Asn314) from the highly conserved F/Y-G-M-N motif located at the end of TM 1 completely blocks the entrance of the channel at the membrane-periplasm interface in the closed channel conformation (Lunin, et al., 2006). Further constrictions of the pore are formed by Met302 in the center of the membrane and at the membrane-cytosol interface the bulky, hydrophobic amino acids Leu294 and Met291, narrow the pore to 2.5 Å in the closed state. Leu294 in combination with the positive potential of the basic sphincter is supposed to be the major barrier for ion movement (Lunin, et al., 2006; Payandeh, et al., 2008; Eshaghi, et al., 2006).

How is sensing the intracellular Mg^{2+} concentration linked to opening and closing of the channel? Recent data obtained from structural and mutational analyses led to the identification of two Mg^{2+} binding sites (Asp89 in helix α3 and Asp253 in the stalk helix) in the intracellular domain of the protein (Figure 1). A secondary site was proposed to coordinate the ion indirectly through water molecules (Lunin, et al., 2006; Eshaghi, et al., 2006; Payandeh and Pai, 2006; Maguire, 2006b).

According to the model proposed by Payandeh et al., ion binding to these sites would have a stabilizing effect in the closed conformation. Under this condition the αßα domain (helices α1-4 and the ß-sheet) of one monomer would associate with the stalk helix of the neighboring monomer. Mg^{2+} dissociation in contrast would allow rotation of the αßα domain away from the stalk helix. Also the helices α5 and α6 would undergo a rearrangement relative to one another and relative to helix α7. These large conformational changes result in opening of the hydrophobic gate formed by Leu294 and might also propagate on the periplasmatic gate (for a detailed description see Figure 2) (Payandeh and Pai, 2006; Payandeh, et al., 2008).
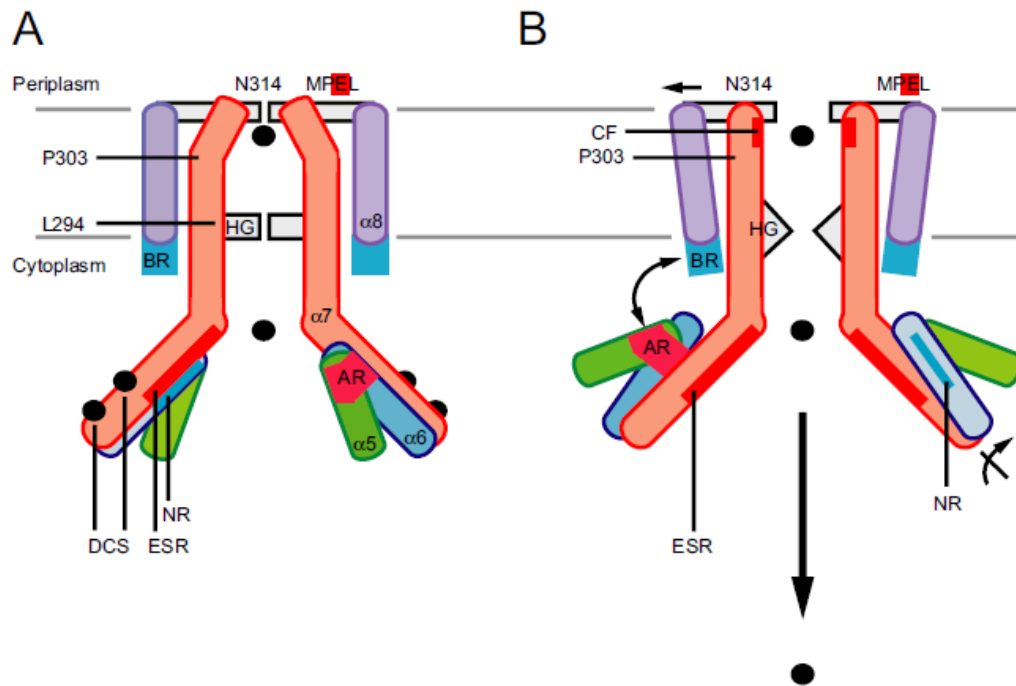
Figure 2: A proposed gating model for CorA. (**A**) Cations (black spheres) bound to the DCS (divalent cation sensor) sites have a stabilizing effect on the closed conformation of the channel. (**B**) Dissociation of Mg^{2+} from the DCS sites destabilizes the interactions between the intracellular electrostatic sink residues (ESR) and the neutralizing residues (NR) through charge repulsion and initiates the transition to the open state. The structural reorganization brings the acidic ring (AR, negatively charged residues situated in the tips of α5 and α6 and in the loop connecting the two willow helices) in proximity to the basic sphincter (BR). The interaction between AR and BR may affect the position of TM 2 and the short loop connecting TM 1 and TM 2 and possibly leads to opening of the periplasmic mouth of the channel. Rotation of α6 around α7 generates a torque along α7, which produces a gating force on the hydrophobic gate (HG) and possibly the periplasmic Pro303 gate. The Asn314 side chains (of the G-M-N motif) are displaced from the pore entrance and uncover the carbonyl funnel (CF). The α1-4/ß1-7 domain has been omitted for clarity. Adapted from (Payandeh, et al., 2008).

Recently, also an iris-like mechanism has been proposed for opening and closing of the channel. This model of Chakrabarti et al. proposes that only small conformational changes are necessary for gating of the channel. The α7 helix exhibits kinks at two sites, at Pro303, near the periplasmatic gate and at Gly274 leading to a widening of the ion conduction pathway in the cytosol (Chakrabarti, et al., 2010). Together with its extraordinary length of ~100 Å the α7 helix was proposed to operate like a lever transmitting conformational changes in the cytosolic domain to the constrictions in the transmembrane region and the mouth of the pore and eventually opening the channel (Chakrabarti, et al., 2010; Maguire, 2006b).

As the channel opens, after the initial interaction of the hydrated ion with residues in the loop between TM 1 and TM 2, the ion hydration shell is removed and the ion passes through the pore. Interestingly, no charged amino acid is present in the pore-forming TM 1 helix as well as in the membrane-anchoring TM 2, indicating that no interaction between the positively charged ion and negatively charged amino acid residues is necessary for the transport process. Mg^{2+} rather interacts with the backbone carbonyls while passing the membrane (Payandeh and Pai, 2006; Maguire, 2006b; Payandeh, et al., 2008). In contrast, the cytosolic portion of the stalk helix contains negatively charged or polar residues contributing to a negative electrostatic potential that attracts Mg^{2+} to exit the membrane-spanning domain (Lunin, et al., 2006; Payandeh and Pai, 2006; Eshaghi, et al., 2006).

2.2.2. The MgtA and MgtB transport systems

Besides CorA, two other systems mediating magnesium influx, termed MgtA and MgtB, have evolved in prokaryotes (Hmiel, et al., 1989). MgtA as well as MgtB do not exhibit any similarity to CorA. Members of the MgtA/B class are found primary in eubacteria (for review see Maguire et al. 2006: Magnesium transporters: properties, regulation and structure) (Maguire, 2006a) and belong to the family of P-type ATPases, using one molecule ATP per transport cycle (Tao, et al., 1995).

The most striking physiological difference between CorA and the MgtA/MgtB system is their regulation. In contrast to the constitutively expressed members of the CorA family, expression of MgtA and MgtB is regulated by the two-component signal transduction system PhoPQ and Mg^{2+} itself serves as the sensing signal (Smith, et al., 1998; Groisman, 2001). Although both proteins are very similar, they exhibit some differences regarding their transport activity. Unlike MgtA, MgtB is highly temperature sensitive and looses its activity at 20°C (Snavely, et al., 1989).

2.2.3. The MgtE family of Mg^{2+} transporters

MgtE from *Bacillus firmus* was identified in the lab of Michael Maguire in a genomic library screen to complement the magnesium dependent growth defect of the *S. typhimurium* triple deletion strain MM281, which lacks all three known magnesium transport systems CorA, MgtA and MgtB (Smith, et al., 1995).

MgtE encodes a 34 kDa protein with no similarity to other magnesium transporters like CorA or the MgtA/MgtB system and therefore seems to represent a new class of Mg^{2+} transporters.

Members of the MgtE family are found in both Eubacteria and Archaea (Townsend, et al., 1995). Human and mouse homologs have been characterized as well e.g. the solute carriers SLC41A1 and SLC41A2 (Wabakken, et al., 2003; Goytain and Quamme, 2005a; Goytain and Quamme, 2005b; Kolisek, et al., 2008).

Recently, Hattori et al. have published the crystal structure of full-length MgtE from *Thermus thermophilus* at 3.5 Å and the cytosolic domain in presence and absence of Mg^{2+} at 2.3 Å and 3.9 Å, respectively (Hattori, et al., 2007). The transporter in its homodimeric form has ten transmembrane helices and exhibits a continuous ion-conducting pathway, formed mainly by TM 5 and TM 2 and partly by TM 1 helices. A mechanism for regulation of the transporter has been proposed in which the cytosolic part of the MgtE dimer functions as Mg^{2+} sensor triggering conformational changes. The presence of Mg^{2+} leads to dimerization of the cation binding site (CBS) domains and the connecting helices are fixed via Mg^{2+} mediated interactions with the cytosolic and membrane-spanning domains. Low intracellular Mg^{2+} concentrations in contrast lead to a higher flexibility of the cytosolic domain and an opening of the pore (Figure 3) (Hattori, et al., 2007).
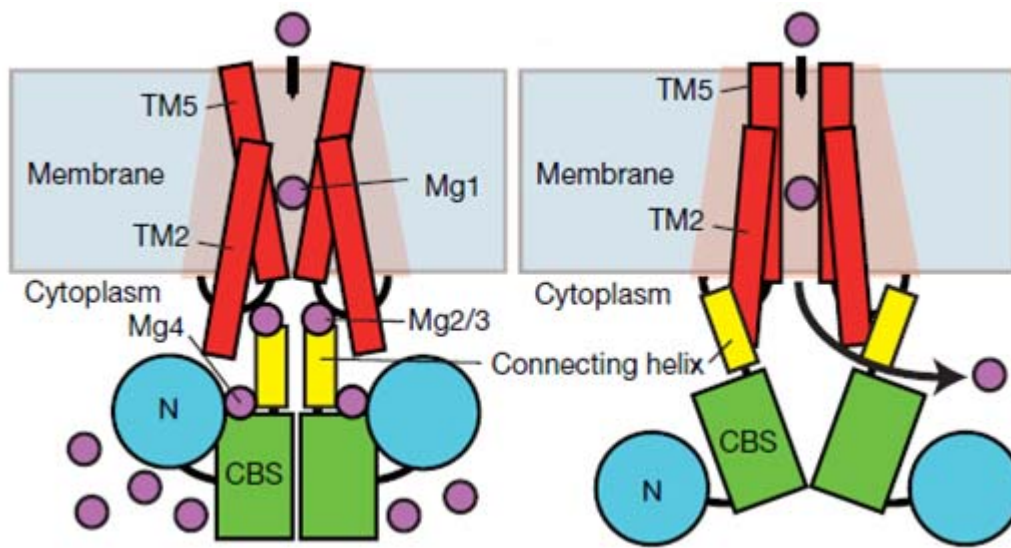
Figure 3: Proposed gating mechanism of MgtE. The closed state at a high intracellular Mg^{2+} concentration (left). The open state at a low intracellular Mg^{2+} concentration (right), CBS= cation binding site. Modified from (Hattori, et al., 2007)

Although the available structure resembles a channel, it was proposed that MgtE acts as secondary active transporter, based on the conformation of the pore in closed state (Hattori, et al., 2007). However, recent data obtained from patch clamping experiments characterize MgtE as a highly selective Mg^{2+} channel (Hattori, et al., 2009).

2.3. Magnesium transport in eukaryotes

2.3.1. The protein Alr1p controls Mg^{2+} uptake through the plasma membrane in yeast cells

Alr1p was the first characterized magnesium transporter in eukaryotic cells and is distantly related to the mitochondrial Mrs2p and the bacterial CorA (MacDiarmid and Gardner, 1998; Bui, et al., 1999; Wachek, et al., 2006). Homologs of Alr1p are found in other fungi and some protozoa but not in higher eukaryotic organisms. The protein is localized in the plasma membrane and is essential for viability of yeast cells in standard rich and synthetic media (MacDiarmid and Gardner, 1998; Graschopf, et al., 2001). A Mg^{2+} concentration of 30 μM is sufficient to support normal growth of wild-type cells in synthetic medium. Upon deletion of

ALR1, cells require 50 mM Mg^{2+} to reach wild-type growth rates. It has been shown that expression of the bacterial Mg^{2+} transporter CorA is able to partially compensate the deletion of *ALR1* (Graschopf, et al., 2001). However unlike the constitutively expressed CorA and Mrs2p, expression and turn-over of Alr1p is regulated by the intracellular Mg^{2+} concentration. Cells incubated in the presence of 1 to 10 mM Mg^{2+} exhibit a reduced stability of the protein and it was proposed that Alr1p is internalized via the endocytic pathway and subsequently delivered to the vacuole for degradation (Graschopf, et al., 2001).

The yeast genome encodes a close homolog of *ALR1*, named *ALR2*. The two proteins have a sequence identity of 69%. The most striking difference between the two proteins is the strongly reduced Mg^{2+} transport activity of *ALR2*, which is due to an amino acid substitution in the loop region connecting the two TM domains (Wachek, et al., 2006). Other members of the CorA-Mrs2p-Alr1p superfamily predominantly have a negatively charged residue in the loop region at the position + 6 relative to the F/Y-G-M-N motif often followed by a second negatively charged residue (Bui, et al., 1999; Weghuber, et al., 2006). Alr1p exhibits a glutamic acid residue at this position, while in Alr2p a positively charged arginine residue is found. As a consequence, even high copy expression of Alr2p is not able to elevate the cellular Mg^{2+} concentration to wild-type levels in an *alr1Δ* strain (Wachek, et al., 2006).

Alr1p and Alr2p were shown to form homo- and heterooligomers, however due to the relatively low stability of the proteins no higher oligomeric states than tetramers could be shown experimentally (Wachek, et al., 2006).

2.3.2. Mrs2p forms a Mg^{2+} selective channel of high conductance in the inner mitochondrial membrane

The nuclear gene *MRS2* encodes a 54 kDa protein localized in the inner mitochondrial membrane (Bui, et al., 1999). *MRS2* was originally found together with several other genes (e.g. *MRS3* and *MRS4*) to be essential for splicing of mitochondrial group II introns and to suppress a splice defect when overexpressed (Koll, et al., 1987). However, unlike the other *MRS* genes, *MRS2* was the only gene essential for splicing of all four group II introns in the mitochondrial pre-mRNA and deletion of the gene additionally caused a growth defect on non-fermentable carbon sources (*petite*-phenotype) also in intron-less yeast strains. Further effects of the *MRS2* deletion are a reduction in cytochrome b levels and absence of cytochrome a.a3. Since these effects were also found in intron-less yeast strains, an additional function for Mrs2p was proposed (Wiesenberger, et al., 1992).

Mrs2p exhibits low sequence similarity to the bacterial CorA protein, in fact conservation of the primary sequence is virtually absent except for the motif F/Y-G-M-N and the end of the first transmembrane domain (Knoop, et al., 2005). In spite of the low sequence identity, CorA and Mrs2p were shown to be functional homologs. Expression of a fusion protein between CorA of *S. typhimurium* and the first 48 amino acids of Mrs2p localized correctly to the inner mitochondrial membrane and partially suppressed the *pet* phenotype of *mrs2Δ* cells (Bui, et al., 1999). Recently it was also demonstrated that Mrs2p is functional in a *S. typhimuruium* strain lacking all major magnesium transport systems (Svidova, S., manuscript in preparation) Furthermore, chemical cross-linking experiments (Kolisek, et al., 2003) and Blue-native PAGE (Schindl, et al., 2007) provided evidence that Mrs2p forms high molecular weight complexes (most likely pentamers), which is consistent with data obtained from analysis of the CorA crystal structure (Lunin, et al., 2006; Eshaghi et al., 2006; Payandeh and Pai, 2006).

Mg^{2+} concentrations in eukaryotic cells are in the low millimolar range and remain relatively unaffected even when extracellular concentrations are altered drastically (Jung and Brierley, 1999; Beeler, et al., 1997). Addition of magnesium to the growth medium therefore does not rescue the *pet* phenotype of *mrs2Δ* cells. As a consequence the double deletion of *ALR1* and *MRS2* exhibits a synthetic phenotype with strongly reduced growth on fermentable as well as non-fermentable carbon sources (Bui, et al., 1999). In contrast, overexpression of *ALR1* increases cellular Mg^{2+} concentrations by a factor of 1.5 and therefore has as a mild suppressive effect on the *pet* phenotype caused by deletion of *MRS2* (Gregan, et al., 2001b).

Kinetic characteristics and ion selectivity of the Mrs2p channel were extensively studied in our laboratory. Changes in mitochondrial Mg^{2+} concentrations can be measured by the fluorescent dye mag-fura-2 (Kolisek, et al., 2003). Isolated mitochondria are loaded with the membrane-permeant acetoxymethyl ester of the dye. The dye is subsequently entrapped and activated by mitochondrial esterases. Basal mitochondrial Mg^{2+} concentrations measured in nominally Mg^{2+} free buffer are in the range of 0.6-0.7 mM. Upon stepwise addition of Mg^{2+} a fast and highly regulated uptake of ions takes place and steady state plateau levels are reached within 50 seconds. The facts that magnesium uptake *via* Mrs2p is temperature insensitive and that influx rates are in the range of 150 µM s-1 for wild-type cells characterize Mrs2p as a channel (Kolisek, et al., 2003).

The driving force for Mg^{2+} influx *via* the Mrs2p channel is the high, inside negative membrane potential ($\Delta\Psi$) of -130 to -160 mV generated by the electron transport chain. Given a potential of -160 mV, Mg^{2+} influx into mitochondria would theoretically continue until Mg^{2+}

concentrations of approx. 1450 mM are reached if 10 mM Mg^{2+} is applied outside. This is far above the mitochondrial matrix Mg^{2+} concentration of 5 mM reached with 10 mM Mg^{2+} outside in isolated mitochondria (Kolisek, et al., 2003). A tight regulation of the channel is therefore imperative.

Patch clamping experiments with giant lipid vesicles fused with inner mitochondrial membrane were used to study conductivity and selectivity of the channel. Permeability of the Mrs2p channel was tested for Ca^{2+}, Mn^{2+}, Co^{2+}, and Ni^{2+}. However, the channel was only permeable for Mg^{2+} with a very high conductance of 155 pS and for Ni^{2+} a significantly lower conductance of 43 pS was observed. Addition of the known CorA/Mrs2p channel inhibitor Co(III)-hexaammine (Robinson and Wang, 1996; Kucharski, et al., 2000) lowered the conductance to 33 pS, which equals vesicles prepared from *mrs2Δ* mitochondria (Schindl, et al., 2007).

For CorA of *S. typhimurium* it has been shown that the F/Y-G-M-N motif at the end of TM 1 helix is essential for Mg^{2+} transport and represents a "Mg^{2+} signature sequence" involved in maintenance of selectivity of the channel (Szegedy and Maguire, 1999; Knoop, et al., 2005). Even conservative mutations at one of these positions are not tolerated and entirely abolish transport activity (Szegedy and Maguire, 1999). Substitution of glycine in this motif by alanine strongly reduces Mg^{2+} influx (Kolisek, et al., 2003). Interestingly, for CorA as well as for Mrs2p only single amino acid substitutions have been tested for their effect on magnesium transport activity, but no random mutagenesis of the whole motif was performed so far.

Another common feature of the CorA/Alr1p/Mrs2p family is the presence of one or two negatively charged amino acids in the short loop connecting the two membrane spanning domains following the F/Y-G-M-N motif. By acting as a topogenic signal, this loop is considered to be important for the correct insertion of the protein into the inner mitochondrial membrane (Baumann, et al., 2002). Furthermore, these negatively charged residues are believed to be important for electrostatic attraction of Mg^{2+} ions to the channel pore and to represent the initial contact site of the hydrated ion with the protein (Lunin, et al., 2006; Eshaghi, et al., 2006 ; Payandeh and Pai, 2006 ; Wachek, et al., 2006 ; Weghuber, et al., 2006 ; Hu, et al., 2009). At least for the prokaryotic CorA family, this model of electrostatic attraction and interaction of the Mg^{2+} ion with negatively charged loop amino acid residues has been questioned recently. Based on mutational analysis of the loop region, Moomaw et al. suggested that the loop region plays an important role rather as selectivity filter and in

accelerating the dehydration process of the hydrated ion than in the so far believed function of attracting Mg^{2+} to the channel entrance by a direct electrostatic interaction (Moomaw and Maguire, 2010). However, yeast and mammalian Mrs2 proteins exhibit two negatively charged glutamic acid residues at these positions, a conservative substitution of Glu341 and Glu342 by aspartic acid does not affect the function of yeast Mrs2p, whereas positively charged lysine residues at these positions result in a complete loss of mitochondrial Mg^{2+} uptake (Weghuber, et al., 2006).

A specific feature of yeast Mrs2p is an exceptionally long C-terminal sequence following the TM 2 helix, which is neither present in plant or human homologs nor in CorA. This C-terminal extension contains an arginine-rich motif (ARM) which has initially been considered as potential RNA binding domain (Schmidt, et al., 1998). Mutational analysis of this sequence revealed that deletion of this basic region, reduced activity of the Mrs2p channel significantly, however, overexpression of this mutant variant basically compensated for its lower activity (Weghuber, et al., 2006). Nevertheless this positively charged sequence stretch appears to be a potential candidate for a "basic sphincter" in *S. cerevisiae* Mrs2p.

2.3.3. The role of Lpe10p in mitochondrial Mg^{2+} homeostasis

During sequencing of the yeast genome a homolog of *MRS2* has been identified, named *LPE10*. The respective gene encodes for a protein of 47 kDa localizing to the inner mitochondrial membrane. Phylogenetic analysis of the CorA/MRS2 family suggests that *MRS2* and *LPE10* evolved from a common ancestor by gene duplication (Knoop, et al., 2005). Overall sequence identity between Mrs2p and Lpe10p is 32%, the apparent size difference is mostly due to the C-terminal extension of Mrs2p, not present in Lpe10p (Gregan, et al., 2001a).

The phenotype caused by deletion of *LPE10* is very similar to that observed for deletion of *MRS2*. In mitochondria of yeast cells lacking *LPE10* splicing of group II introns is impaired and cells are respiratory deficient but viable if provided with fermentable substrates (*petite* phenotype) (Gregan, et al., 2001a). The *pet* phenotype can also be observed in intron-less strains pointing to a more general function of *LPE10* in yeast mitochondria. The simultaneous deletion of both genes leads only to a slightly stronger phenotype on non-fermentable carbon

sources (Gregan, et al., 2001a). Despite of their sequence similarity and comparable phenotypes both proteins cannot substitute for each other when expressed at low copy number. Overexpression of Mrs2p in a *lpe10Δ* background suppresses the petite phenotype weakly, whereas Lpe10p exhibits no significant effect in *mrs2Δ* cells (Sponder, et al., 2010). Interestingly, the above mentioned fusion between the first 48 amino acids of Mrs2p and CorA of *S. typhimurium* as mentioned before restored growth of cells lacking *LPE10* to a certain degree (Gregan, et al., 2001a).

In this study *LPE10* was investigated in more detail to better understand the function and the interplay of this protein with Mrs2p in regard to magnesium transport (Sponder, et al., 2010).

2.4. Mitochondrial K$^+$/H$^+$ exchange and volume homeostasis

Mitochondria are vital organelles of eukaryotic cells. They serve as power plants converting pyruvate, the end product of glycolysis via the citric acid cycle and oxidative phosphorylation into energy in the form of ATP.

Mitochondria possess two membrane systems reflecting their endosymbiotic origin. The outer mitochondrial membrane (OM) has a composition similar to the eukaryotic plasma membrane and exhibits a high permeability for solutes and ions. Porins, integral ß-barrel proteins, form pores in the outer mitochondrial membrane with a diameter of 2-3 nm, large enough to allow passive diffusion of e.g. sugars, amino acids or ions up to a size of 600 Da (Zeth and Thein, 2010; Menze, et al., 2005).

In contrast, the inner mitochondrial membrane (IM) has similarity to bacterial membrane systems and is highly folded into cristae increasing the surface for enzymes of the electron transport chain and ATP synthesis (Garlid and Paucek, 2003). Unlike the OM, the inner membrane is highly impermeable, even to small molecules or ions. This impermeability is an essential prerequisite for the establishment of an electrochemical gradient across the membrane and thereby for ATP production (Bernardi, 1999; Garlid and Paucek, 2003).

Electrons of NADH or FADH2 are funneled to oxygen through the respiratory chain and this process drives the ejection of H$^+$ by redox pumps (Bernardi, 1999). Due to the low passive permeability of the membrane, the ejection of protons leads to the buildup of a pH gradient (ΔpH) of about 0.3 units (Garlid and Paucek, 2003) and an electrical potential gradient ($\Delta\Psi$). The proton-electrochemical gradient ($\Delta\mu$H) is about -150 to -200 mV and most of the gradient is present in the form of a membrane potential under physiological conditions (Bernardi, 1999). This proton motive force is used to drive different mitochondrial transport processes e.g. the import of nuclear encoded proteins, ion transport and most importantly it is essential for ATP synthesis via the F_0/F_1 ATPase (Bernardi, 1999).

The requirement of a strong proton-electrochemical gradient for ATP synthesis, however, poses a problem: it is a strong driving force for the uptake of K$^+$ and other cations *via* diffusive processes. Physiological potassium concentrations in the cytosol are very high - in the range of 150 mM. The high, inside negative membrane potential would favour K$^+$ uptake to an electrochemical equilibrium of approximately 150 M. The same applies for other positively charged ions e.g. Na$^+$ with 5 mM (Bernardi, 1999). Energized mitochondria

therefore represent infinite sinks for potassium accompanied by influx of water, resulting in swelling and eventual lysis of the organelle (Garlid and Paucek, 2003). As stated previously, the inner mitochondrial membrane in general has a low permeability to ions and protons, nevertheless ions can pass the membrane by diffusive processes (leaks) and at the same time the inner mitochondrial membrane has a high permeability to water (Garlid and Paucek, 2003; Mitchell, 1961). Net uptake or loss of K^+ consequently leads to osmotic swelling or shrinkage of the organelle (Bernardi, 1999). To overcome this danger, Peter Mitchell postulated in 1961 the existence of proton/cation antiporters regulating mitochondrial osmolarity and volume (Mitchell, 1961; Mitchell, 1966).

For more than five decades, great effort has been made to prove Mitchell's postulate and to identify the responsible proteins of the cation/H^+ exchange systems. However, the experimental demonstration of electroneutral K^+/H^+ antiport in mitochondria was complicated by the presence of different electrophoretic transport systems for K^+ and H^+ in the inner mitochondrial membrane (Garlid, et al., 1986).

The finding that cation/H^+ antiport activity can be demonstrated by monitoring changes in the mitochondrial volume (swelling) has proven to be an extremely useful tool in examining these transport processes. Swelling of the organelle results in changes in light scattering and can therefore easily be followed (Azzone and Massari, 1971; Azzone, et al., 1976; Blondin, et al., 1969). Classical swelling experiments as described in (Blondin, et al., 1969; Douglas and Cockrell, 1974; Mitchell and Moyle, 1969) were carried out with isolated non-respiring mitochondria in acetate-based media. The inner mitochondrial membrane is highly permeable to the protonated form of acetic acid. Incubation of mitochondria in Na-acetate resulted in fast swelling, in contrast swelling in K-acetate was extremely slow. This finding suggested that mitochondria obviously posses a very active Na^+/H^+ exchange mechanism and an inactive or latent K^+/H^+ antiporter (Douglas and Cockrell, 1974; Nakashima and Garlid, 1982; Welihinda, et al., 1993; Rosen and Futai, 1980). However, fast swelling in K-acetate medium could be achieved by addition of the drug nigericin, an artificial K^+/H^+ exchanger (Figure 4).
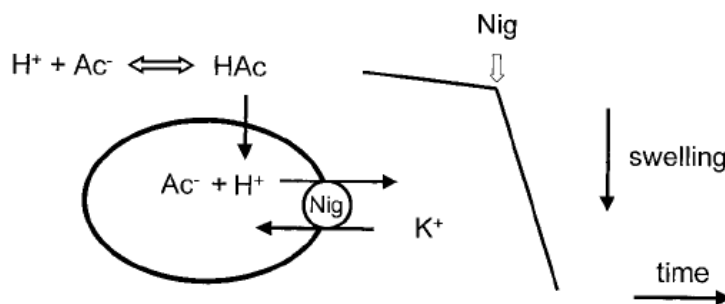
Figure 4: Nigericin induced swelling of mitochondria in acetate medium. Isolated, non-respiring mitochondria rapidly swell upon addition of the electroneutral K^+/H^+ exchanger nigericin. Nigericin leads to K uptake, followed by rapid diffusion of acetic acid. This leads to a net-uptake of K-acetate and eventually to swelling due to an increased uptake of water. Swelling can be followed by a decrease in light-scattering of the organelle. Adapted from (Bernardi, 1999))

Conversely, sole addition of a protonophore (e.g. FCCP) or a K^+ ionophore (e.g. valinomycin) does not lead to fast swelling. Only if these two transport processes are coupled fast swelling can be observed (Figure 5) (Mitchell and Moyle, 1969; Douglas and Cockrell, 1974; Azzone, et al., 1976; Bernardi, 1999).
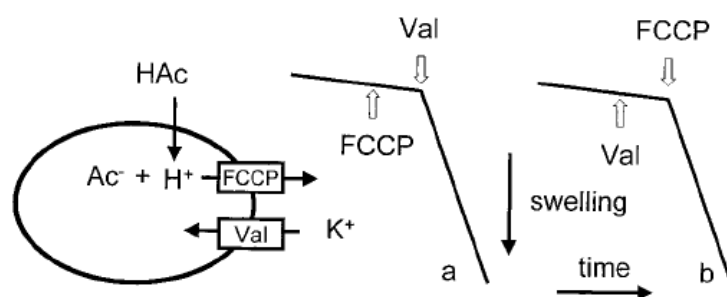
Figure 5: Swelling of isolated mitochondria, the effects of FCCP and valinomycin. Due to the low permeability of the membrane to protons and K^+, deenergized mitochondria in acetate medium swell only in the presence of both, a protonophore (FCCP) and a K^+ ionophore (valinomycin). Equivalent to nigericin, FCCP and valinomycin together mediate electroneutral K^+/H^+ exchange resulting in net uptake of K-acetate and swelling of the organelle. Adapted from (Bernardi, 1999))

These experiments in principle allow an experimental demonstration of the postulated K^+/H^+ antiport. Nevertheless, the latent K^+/H^+ exchanger needs to be activated, which is in contrast to the Na^+/H^+ antiporter. Treatment of isolated mitochondria with EDTA and A-23187, a

$2H^+/Me^{2+}$ exchanger alters the permeability of the mitochondrial membrane for K^+ (Figure 5) (Dordick, et al., 1980). This effect was initially explained with the transport of K^+ by A-23187. Later it became clear that A-23187 does not transport K^+ itself, but leads to depletion of the mitochondrial matrix for divalent cations (Bernardi, 1999; Cockrell, 1973; Mitchell and Moyle, 1969; Chappell, 1968).
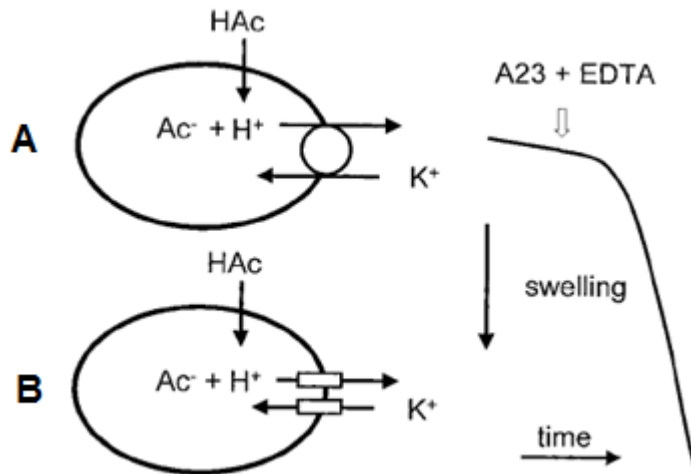
Figure 6: Stimulation of K-acetate uptake by A-23187 and EDTA. Non-respiring mitochondria in acetate medium exhibit rapid swelling after incubation with A-23187 and EDTA. Net-uptake of K-acetate can either be mediated by an electroneutral K^+/H^+ exchanger (scheme **A**) or by coupling of two independent, electrical H^+ and K^+ fluxes (scheme **B**). Adapted from (Bernardi, 1999)

Depletion of the mitochondrial matrix for divalent cations (mostly Mg^{2+} and Ca^{2+}) seems to unmask conductances for H^+ and K^+. However, as shown in Figure 6, this experiment cannot dissect between K^+/H^+ exchange mediated by the postulated, electroneutral K^+/H^+ exchanger and coupling of two independent uniport processes for K^+ and H^+, respectively (Bernardi, 1999).

This question was solved by passive swelling experiments in K-nitrate medium. The nitrate anion is membrane permeable. Depletion of the mitochondrial matrix for divalent cations by A-23187 and EDTA should lead to swelling, reflecting K^+ uptake. However, swelling only occurred after addition of the protonophore FCCP. This demonstrates that the two conductances are coupled (Bernardi, 1999).

It was not clarified, if K^+ influx in these experiments only occurred via the K^+/H^+ exchanger alone or if other transport pathways for K^+ were present as well (Duszynski and Wojtczak, 1977; Bernardi, et al., 1989). Furthermore, the effect of A-23187 on the permeability of the mitochondrial membrane for K^+ was controversially discussed (Garlid, 1980; Pfeiffer and Lardy, 1976).

The demonstration that K^+ and H^+ fluxes are intrinsically electroneutral was finally accomplished with an experiment in isolated, energized mitochondria (Figure 6).

Mitochondria were treated with a very low concentration of valinomycin in low K-sucrose buffer. The inside negative membrane potential induces an inward directed K^+ flux mediated by the K^+ ionophore valinomycin. The K^+ concentration outside decreases until a new steady state is reached. This steady-state is perturbed by addition of A-23187 and induces a phase of net K^+ efflux, increasing the K^+ concentration outside to a new steady-state, which is insensitive to further addition of A-23187. This steady state is based on K^+ influx, mediated by valiomycin and K^+ efflux via the endogenous K^+/H^+ exchanger. The balance is destroyed by further addition of valinomycin inducing a new phase of K^+ uptake and nigericin resulting in further K^+ efflux (Figure 7). This experiment demonstrated that A-23187 unmasks an endogenous, electroneutral K^+/H^+ exchanger, mediating K^+ efflux against the K^+-electrochemical gradient. A-23187 obviously does not transport K^+ itself, since further addition of the ionophore does not alter the steady-state (Dordick, et al., 1980; Shi, et al., 1980; Bernardi, 1999).
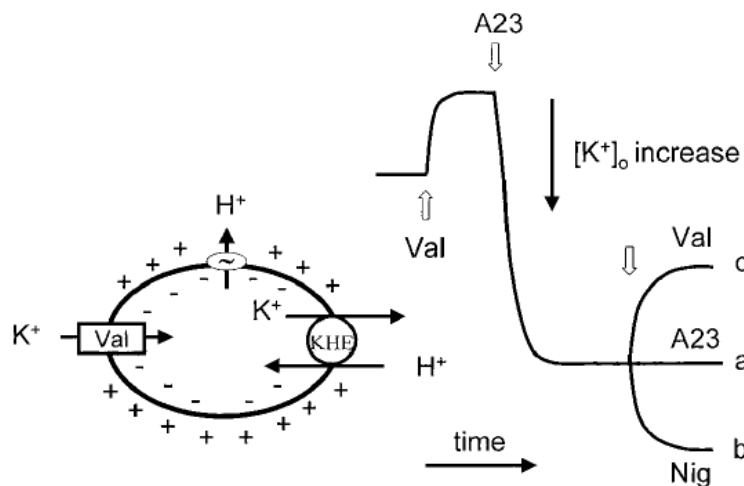
Figure 7: Endogenous mitochondrial K^+/H^+ exchange is intrinsically electroneutral and activated by depletion for Me^{2+}. Addition of valinomycin to energized mitochondria in low K^+ buffer leads to K^+ influx driven by the inside, negative membrane potential and the K^+ concentration outside decreases. A-23187 induces K^+ efflux by activating the endogenous K^+/H^+ exchanger, until a new steady state with higher outside K^+ concentration is established. Further addition of valinomycin leads to enhanced K^+ uptake, whereas addition of nigericin leads to increased K^+ efflux. In contrast, a second dose of A-23187 does not alter the steady-state. Adapted from (Bernardi, 1999))

The existence of a K^+/H^+ exchanger counterbalancing the diffusive influx of K^+ solves the problem of mitochondrial volume homeostasis but at the same time creates a threat for energy conservation in the form of an electrochemical potential gradient. A constantly active exchanger using the proton motive force to pump K^+ out of the mitochondrial matrix would

result in a break-down of the proton-chemical gradient and consequently of energy production (Garlid and Paucek, 2003).

These considerations led Garlid and colleagues to propose the "Mg^{2+} carrier brake hypothesis". According to this hypothesis a matrix solute would act as reversible inhibitor of the K^+/H^+ exchanger. Electrophoretic influx of K^+ is osmotically accompanied by influx of water leading to swelling of the organelle and dilution of matrix solutes. Volume increase would consequently reduce the inhibitor concentration and activate the exchanger (Garlid, 1980; Garlid, 1978; Garlid, 1979).

Based on the observation that K^+ efflux is induced by anions able to form complexes with divalent cations (e.g. citrate, phosphate) but not by anions weakly interacting with divalent cations (e.g. malate, succinate), the role of the inhibitor was attributed to Mg^{2+} with a K_i of 200-400 µM in heart and liver mitochondria (Nakashima and Garlid, 1982; Kakar, et al., 1989)

Another argument, that Mg^{2+} is the regulatory cation, is the fact that unlike Ca^{2+}, Mg^{2+} concentrations are relatively stable (Nakashima, et al., 1982).

The Mg^{2+} carrier brake hypothesis represents a mechanism which balances K^+ influx and K^+ extrusion *via* the K^+/H^+ exchanger thereby preventing futile cycling of K^+ and minimizing the energetic cost for volume homeostasis. In this model Mg^{2+} serves as a volume sensor. Swelling is caused by the net uptake of salts, and the anions of these salts (e.g. citrate and phosphate) would decrease the matrix free Mg^{2+} concentration, inhibitory Mg^{2+} bound to the K^+/H^+ antiporter would dissociate and thereby activating it (Garlid and Paucek, 2003).

This theory is not without controversy. It was clearly demonstrated that the antiporter is reversibly inhibited by Mg^{2+} in swelling experiments (Azzi, et al., 1984; Dordick, et al., 1980; Garlid, et al., 1986). However, the availability of the Mg^{2+} sensitive fluorescent dye mag-fura-2 allowed for the first time to directly examine changes in the matrix free Mg^{2+} concentration. Changes of matrix Mg^{2+} concentrations upon different swelling conditions were examined and the authors concluded that Mg^{2+} concentrations do not change in a manner compatible with the proposed role of Mg^{2+} being a volume sensor (Jung and Brierley, 1999).

Possible alternative regulatory mechanisms for the K^+/H^+ exchanger are changes in matrix protein concentration or mechanical signals caused by a stronger contact between the outer and the inner membrane upon swelling. Also a complete equilibration between mitochondrial matrix and the cytoplasm through transient opening of the mitochondrial permeability transition pore was discussed (Jung and Brierley, 1999).

Further studies demonstrated that an increased matrix volume itself stimulates the K^+/H^+ exchanger by an unknown mechanism (Brierley, et al., 1984; Bernardi and Azzone, 1983) and that amphiphilic amines (e.g. antidepressants, antihistamines, antiarrhythmics and local anesthetics) inhibit the antiporter. Also quinine exhibits an inhibitory effect (Nakashima and Garlid, 1982; Jung, et al., 1984; Dordick, et al., 1980). These inhibitors proved to be useful for the demonstration that mammalian mitochondria have two distinct monovalent cation/proton antiporters, a Na^+ selective and a latent non selective antiporter. This non-selective system transports various monovalent cations e.g. Na^+, K^+, Li^+, Rb^+ and Cs^+. Due to the high abundance of K^+ in the cell, this non-selective system primarily mediates an exchange of K^+ for H^+ and is therefore often referred to as K^+/H^+ antiporter (Brierley, et al., 1994; Beavis and Garlid, 1990).

An important finding however was that DCCD irreversibly inhibits the K^+/H^+ antiporter. DCCD is a general inhibitor for ion transport proteins interacting with carboxylic groups in the hydrophobic core of these membrane proteins (Azzi, et al., 1984; Dordick, et al., 1980). Interestingly, DCCD only reacts with the activated K^+/H^+ exchanger. Quinine and appropriate matrix Mg^{2+} concentrations therefore protect the antiporter from inhibition (Garlid, et al., 1986; Martin, et al., 1984; Martin, et al., 1986).

Special protocols have been developed to purify the responsible proteins using radiolabeled DCCD. The K^+/H^+ exchange activity was attributed to a 82 kDa protein from rat heart and beef heart mitochondria (Martin, et al., 1984; DiResta, et al., 1986). Efforts to purify the protein to homogeneity were in part successful. The 82 kDa protein was reconstituted into liposomes where it mediated electroneutral $^{86}Rb^+$ transport, which was sensitive to Mg^{2+} and quinine. These results were confirmed later with the K^+ sensitive, fluorescent dye PBFI. However, determination of the amino acid sequence and identification of the corresponding gene failed (Li, et al., 1990; Brierley and Jung, 1988).

2.4.1. Mitochondrial K⁺/H⁺ exchange in S. cerevisiae

Experiments to prove the existence of the mitochondrial K^+/H^+ and Na^+/H^+ exchangers and attempts to purify the candidate proteins have been carried out with mammalian mitochondria (Mitchell and Moyle, 1969; Nakashima and Garlid, 1982; Martin, et al., 1984; DiResta, et al., 1986; Garlid, et al., 1991).

Initial results obtained with the classical light scattering assay showed that mitochondria of yeast cells do not possess a specific Na^+/H^+ exchanger (Welihinda, et al., 1993). However, Na^+/H^+ exchange was later attributed to NHX1/NHA2. Antiport activity was measured by ^{22}Na uptake form acetate medium, a significantly more sensitive method which could determine the very low transport activity of this antiporter (Numata, et al., 1998; Kapus, et al., 1988). Although deletion of the NHX1/NHA2 gene abolishes ^{22}Na uptake, these results have been questioned recently (Nass and Rao, 1999). According to Brett et al. and Qiu et al. Nhx1p/Nha2p is not localized in the inner mitochondrial membrane but mediates Na^+/H^+ exchange in vacuoles and late endosomes (Brett, et al., 2005; Qiu and Fratti, 2010).

Accordingly, to date it is not clear if yeast mitochondria, analogously to mammalian mitochondria, possess two distinct proton/cation exchangers, a specific antiporter for Na^+ and a non-specific one transporting virtually all monovalent cations, referred to as the K^+/H^+ antiporter.

2.4.2. The role of the MDM38 (MKH1)/MRS7 (YPR125)/LETM1 family in mitochondrial K⁺/H⁺ exchange

Mdm38p is a nuclear encoded, 65 kDa protein localized in the inner mitochondrial membrane (Nowikovsky, et al., 2004). The gene was originally found in a screen for genes involved in mitochondrial distribution and morphology (Dimmer, et al., 2002). Deletion of the open reading frame *YOL027* (*MDM38*) results in fragmentation of the mitochondrial network and reduced growth on non-fermentable carbon sources (Dimmer, et al., 2002; Nowikovsky, et al., 2004). Fermentative growth is reduced as well, indicating that deletion of *MDM38* affects also other functions than mitochondrial energy production.

The simultaneous deletion of *MDM38* and *MRS2* exhibits a synthetic growth defect; cells fail to grow on non fermentable carbon sources and are rho 0 (devoid of mitDNA) (Nowikovsky, et al., 2004). A strong indication for an involvement of *MDM38* in mitochondrial K^+-

homeostasis came from the observation that mitochondria of *mdm38Δ* cells are heavily swollen lacking the typical cristae structures, have a severely reduced mitochondrial membrane potential and strongly increased K^+ content of 84%. Mg^{2+} and Na^+ contents are increased by about 40% and 10%, respectively (Nowikovsky, et al., 2004).

As previously described, passive swelling experiments with non-respiring yeast mitochondria of DBY747 cells in KOAc buffer showed a high swelling capacity after addition of A-23187 and EDTA, and swelling is strongly inhibited by quinine and DCCD, comparable to mammalian mitochondria. In contrast, mitochondria of *mdm38Δ* cells did not exhibit rapid swelling as they are already swollen. Importantly, addition of the K^+/H^+ ionophore nigericin to the growth medium restored growth of *mdm38Δ* cells on non-fermentable carbon sources, strongly indicating a primary role of Mdm38p in K^+/H^+ antiport (Nowikovsky, et al., 2007).

Submitochondrial particles (SMPs) loaded with the H^+- and K^+-sensitive fluorescent dyes BCECF and PBFI proved to be in particular useful for a direct characterization of proton and cation fluxes across the inner mitochondrial membrane (Froschauer, et al., 2005; Brierley and Jung, 1988). The advantage of the SMP system is that the milieu on both sides can be controlled at will and that SMPs are not swollen prior to the measurements. An obligatory coupled transport of K^+ and H^+ can be observed in SMPs when either a K^+ or pH concentration gradient between the inside and outside of SMPs is applied. This electroneutral K^+/H^+ exchange is absent in *mdm38Δ* mitochondria but could be induced by addition of nigericin (Froschauer, et al., 2005).

Despite the strong evidence for a direct involvement of *MDM38* in K^+ homeostasis, recently, Frazier et al. suggested a role of *MDM38* in the translation of mitochondrially encoded proteins. This conclusion was based on the finding that Mdm38p was found to be associated with newly synthesized mitochondrial proteins *via* ribosomes. An interaction of the protein with ribosomes was also found in the absence of translation products (Frazier, et al., 2006).

The authors reported reduced levels of the respiratory chain complexes III and IV in *mdm38Δ* mitochondria. Interestingly, steady state levels of Cox1p, Cox2p, cytochrome b (Cob), the nuclear encoded Rip1p of complex III and also to some extent Cox3p were diminished, in contrast, Atp6p levels were not reduced but a stable pool of unassembled Atp6p accumulated in mitochondria. Other membrane complexes e.g. Tim22p were not affected in *mdm38Δ* cells. This led the authors to propose that *MDM38* is a factor of a so far uncharacterized Oxa1p-

independent protein export and insertion pathway in mitochondria (Frazier, et al., 2006; Bauerschmitt, et al., 2010).

However, reduced levels of respiratory chain complexes, impaired protein export and insertion into the mitochondrial membrane observed in $mdm38\Delta$ mitochondria, may alternatively arise as secondary effects of a deletion of this gene. The question if these effects were caused by impaired K^+ homeostasis, the reduced membrane potential or the fact that $mdm38\Delta$ mitochondria are heavily swollen was subsequently addressed by Nowikosky et al. (Nowikovsky, et al., 2007). The finding of Frazier et al. that Cox2p, cytochrome b and Cox3p levels are reduced upon deletion were indeed confirmed. Interestingly, this effect could be efficiently reversed by addition of nigericin, pointing to a direct involvement of *MDM38* in K^+/H^+ exchange. Furthermore, doxycycline induced down-regulation of *MDM38* was used, to follow the consequences of loss of the protein in the course of time. Levels of mitochondrially expressed proteins remained unaffected over 50 hours. In contrast loss of K^+/H^+ exchange activity, swelling and a drop in the mitochondrial membrane potential occurred early. These results strongly indicated that the primary effect of down-regulation of *MDM38* was the impairment of K^+/H^+ exchange (Nowikovsky, et al., 2007). A defect in K^+ homeostasis furthermore leads to morphological changes of both types of organelles, mitochondria and vacuoles. Mitochondria are heavily swollen, the mitochondrial network is disrupted and a close association between mitochondria and vacuoles can be observed eventually resulting in mitophagy, a degradative uptake of mitochondrial material by vacuoles (Priault, et al., 2005; Nowikovsky, et al., 2007).

The yeast genome encodes a close homolog of *MDM38*, named *MRS7* (*YPR125*). In fact, this gene was identified as multi-copy suppressor of *MRS2* (Waldherr, et al., 1993). *MDM38* and *MRS7* exhibit about 40% sequence identity and both have one predicted transmembrane domain (Nowikovsky, et al., 2004). Compared *to MDM38*, the growth defect caused by deletion of *MRS7* on non-fermentable carbon sources is significantly less pronounced and on fermentative media loss of *MRS7* has no effect at all. Overexpression of *MRS7* rescues the growth defect of $mdm38\Delta$ cells pointing to a functional homology of these two proteins (Nowikovsky, et al., 2004; Zotova, et al., 2010) Furthermore, Frazier et al. found both proteins *MDM38* and *MRS7* associated with ribosomes and *MRS7* coeluted with Protein A-tagged Mdm38p and *vice versa* (Frazier, et al., 2006). Taken these findings together, *MRS7*

appears to be less important for normal mitochondrial function and is therefore, in contrast to *MDM38*, poorly characterized.

Homologs of *MDM38* and *MRS7* are found in all sequenced eukaryotes and the human homolog, *LETM1,* is implicated in the hereditary disease Wolf-Hirschhorn syndrome (WHS). The Wolf-Hirschhorn syndrome is caused by a heterozygous deletion of a region of variable length on the short arm of chromosome 4 (Endele, et al., 1999; Zollino, et al., 2003). Clinical hallmarks of this disease are severe growth and mental retardation, hypotonia, midline fusion defects and facial dysmorphism (Johnson, et al., 1976; Wilson, et al., 1981). Several genes are affected by this deletion and the extent of the deletion correlates with the severity of the syndrome. Interestingly, the complete WHS phenotype including seizures frequently leading to death involves the hemizygous deletion of *LETM1* (Zollino, et al., 2000).

LETM1 has also one predicted transmembrane domain in the N-terminal part of the protein exhibiting the highest sequence similarity to Mdm38p (Nowikovsky, et al., 2004). The C-terminal part of the protein contains two EF-hand calcium binding domains and a leucine zipper domain. Very recently *LETM1* was identified in a genome-wide RNAi screen in *Drosophila* S2 cells as being an essential factor for coupled Ca^{2+}/H^+ exchange. Patch clamping experiments with permeabilized S2 cells exhibited reduced Ca^{2+} uptake in the absence of Letm1. From this and reconstitution experiments of Letm1 in liposomes the authors concluded that the protein forms a Ca^{2+}/H^+ antiporter mediating Ca^{2+} transport into mitochondria and extrusion of H^+ (Jiang, et al., 2009). This conclusion is surprising, considering the inside directed driving force for cation uptake, Ca^{2+} uptake is expected to be mediated by a uniporter or a channel. In contrast, cation/H^+ antiporters are expected to rather extrude cations from energized mitochondria. Consequently, down-regulation of the Ca^{2+}/H^+ antiporter would result in increased Ca^{2+} levels in mitochondria (Mitchell, 1966).

In summary, the role of *MRS7, MDM38* and *LETM1* is highly controversially discussed and a function of these proteins in different biological processes has been implicated. This thesis focuses on the characterization of *MRS7,* specifically aiming at the identification of its interaction partners.

3. Results

3.1. Publication I

Functional analysis of the conserved hydrophobic gate region of the magnesium transporter CorA

Svidová S., Sponder G., Schweyen R.J., Djinović-Carugo K.

Functional analysis of the conserved hydrophobic gate region of the magnesium transporter CorA

Soňa Svidová [a], Gerhard Sponder [a], Rudolf J. Schweyen [a,†], Kristina Djinović-Carugo [b,c,*]

[a] Department of Microbiology, Immunobiology and Genetics, Max F. Perutz Laboratories, University of Vienna, Dr. Bohrgasse 9/4, A-1030 Vienna, Austria
[b] Department for Structural and Computational Biology, Max F. Perutz Laboratories, University of Vienna, Campus Vienna Biocenter 5, A-1030 Vienna, Austria
[c] Department of Biochemistry, Faculty of Chemistry and Chemical Technology, University of Ljubljana, Ljubljana, Slovenia

ABSTRACT

The Leu294 residue in the cytoplasmic neck of *Thermotoga maritima* CorA is considered to be the main gate for Mg^{2+} transport. We created three site-directed mutants at this position: in the Leu294Asp and Leu294Gly mutants we observed a defect in closing of the pore, while in the Leu294Arg mutant not only gating, but also the regulation of Mg^{2+} uptake was affected. Our results confirmed the importance of the Leu294 for gating of Mg^{2+} transport and in addition revealed the influence of the charge and structural features of the amino acid residues on the gating mechanism.

© 2010 Elsevier B.V. All rights reserved.

1. Introduction

Magnesium transporters of the CorA family are widely distributed amongst Eubacteria and Archaea. The CorA gene encodes a constitutively expressed integral membrane protein [1]. Previous investigations showed that it is essential for bacterial growth [2] but standard rich media provide sufficient magnesium concentrations for growth [3].

In the last years three crystal structures of *Thermotoga maritima* CorA have been published [4–6]. All showed that the transporter exists in a pentameric form, consisting of a cytosolic funnel shaped part, linked to the transmembrane region by long α7 helices (Fig. 1a, b). The pore is formed by the first trans-membrane helices and surrounded by the second trans-membrane helices, which anchor the complex in the membrane and end in a highly conserved positively charged motif (KKKKWL) called "basic sphincter". In the cytoplasmic neck of the pore a hydrophobic ring is created by residues Leu294 and Met291, surrounded by the aforementioned basic sphincter (Fig. 1c). This concentration of positive charges and the significant conservation of the bulky hydrophobic residues at positions 291 and 294 in the CorA protein family is considered to be of high importance for gating of Mg^{2+} ions. Opening and closing of the gate is most probably regulated by interaction of the Mg^{2+} ion with a divalent cation sensing site (DCS), placed between Asp89 in the α3 helix in the N-terminal part of one monomer and Asp253 of the α7 helix of the adjacent monomer [4–6]

(Fig. 1b). A second DCS site, involving residues Glu88 and Asp175, was identified by Eshaghi et al. [5] and Payandeh et al. [6] (Fig. 1b).

The exact gating mechanism of the TmCorA transporter could not been revealed yet. It has been proposed that binding of the Mg^{2+} ions to the DCS sites evokes a structural rearrangement of the cytosolic domain causing positively charged residues of the basic sphincter to close the pore by drawing the negative charges away from the middle of the pore, and thereby preventing the positively charged Mg^{2+} ion to pass. Removal of Mg^{2+} from the DCS sites would cause a movement of the N-terminal domain, resulting in drawing the basic sphincter away from the neck of the pore and allowing the Mg^{2+} ion to pass [4]. According to the recently performed 110-ns molecular-dynamics simulations, based on the CorA structures published by Eshaghi et al. [5] and Payandeh et al. [8], the binding or unbinding of Mg^{2+} ions to the DCS sites evokes structural rearrangements of the cytosolic domains and the α7 helices transmit these changes to the gate region causing closing or widening of the pore [7].

Leu294 in the hydrophobic ring is the critical residue for Mg^{2+} gating. It creates a strong energetic barrier for ion permeation and probably controls the movement of Mg^{2+} ions indirectly through the movement of water. According to Payandeh et al. [8], not only an energetic, but also a mechanic barrier can influence the uptake of Mg^{2+} and "opening sensitivity" of the transporter. To investigate this hypothesis in more detail, this mutational study was focused on Leu294 which was mutated to 15 different amino acids using random PCR mutagenesis. After a preliminary screen, three of these mutants representing different types of amino acids: positively charged hydrophilic arginine, negatively charged hydrophilic aspartic acid and small neutral glycine, were chosen for closer investigations.

* Corresponding author. Campus Vienna Biocenter 5, A-1030 Vienna, Austria. Tel.: +43 1 4277 52203/52201; fax: +43 1 4277 9522.
*E-mail address:* kristina.djinovic@univie.ac.at (K. Djinović-Carugo).
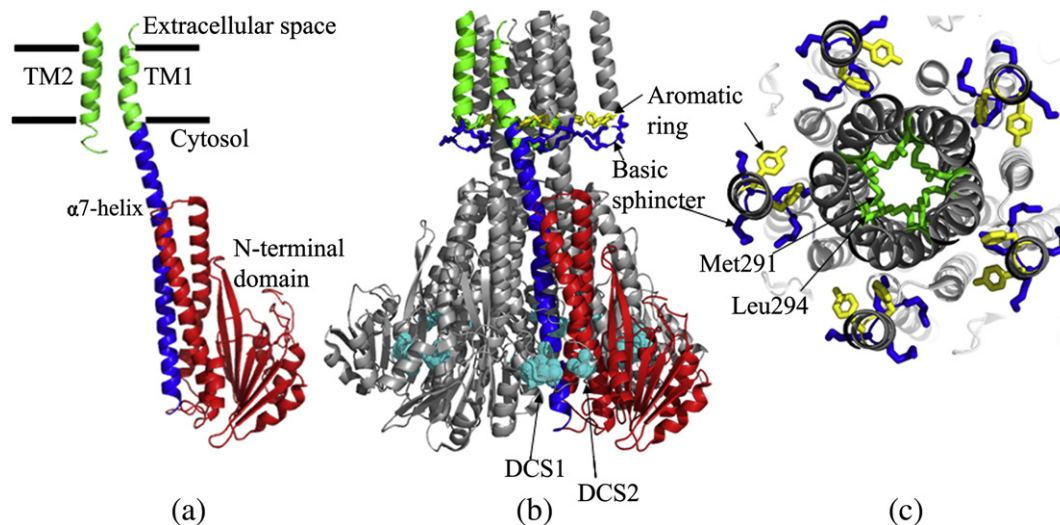
Fig. 1. Structure of the TmCorA Mg^{2+} transporter. (a) Single monomer: green — transmembrane domains TM1 and TM2, blue — α7 helix, red — N-terminal domain. (b) Side view of the homopentamer: cyan — DCS sites 1 and 2. (c) View from the top: blue — basic sphincter, yellow — aromatic ring, green — the gate forming residues Leu294 and Met291.

2. Materials and methods

2.1. Bacterial strains, growth media and genetic procedures

Salmonella enterica serovar *Typhimurium* strain LB5010 was used as wild-type reference.

Salmonella enterica serovar *Typhimurium* strain MM281 (DEL485 (leuBCD)mgtB::MudJ;mgtA21::MudJ;corA45::mudJ;zjh1628::Tn10 (cam) Cam^R, Kan^R, Mg^{2+} dependent) was kindly provided by M.E. Maguire. It lacks all major magnesium transport systems *CorA*, *MgtA* and *MgtB* and requires Mg^{2+} concentrations in millimolar range for growth.

Strains were grown in LB medium (10 g tryptone, 5 g yeast extract, 10 g NaCl per liter) with ampicillin (100 µg/ml). MM281 required addition of 10 mM $MgCl_2$.

LB plates contained 2% Difco™ Agar Noble, minimizing possible Mg^{2+} contamination.

2.2. Plasmid constructs

The *Thermotoga maritima* CorA coding sequence was kindly provided by S. Eshaghi and used as template for PCR. The sequence was amplified using the following primers: TmCorwoSfw 5′-CGCGGATCCGAGGAAAA-GAGGCTGTCTGC-3′ and TmCorrev 5′-TCCCCCGGGTCACAGC-CACTTCTTT-TTCTTG-3′. The 1035 bp PCR product was cut with BamHI and SmaI restriction enzymes and cloned into the pQE80L vector with an IPTG-inducible promoter.

2.3. Random PCR mutagenesis

In order to introduce various amino acid substitutions in CorA, an overlap extension PCR according to Pogulis et al. [9] was used.

Random mutagenesis of the Leu294 amino acid with the mutagenic forward primer 5′-GCGGTCTTCTTGATGTGTACCTTTCGAGTGTAAGTAA-CAAAACAAACGAAGTGATGAAGGTNNNACCATCATAGCG-3′ and the reverse primer 5′-CGCTATGATGGTNNNCACCTTCATCACTTCGTTTG-TTTTGTTACTTACACTCGAAAGGTACACATCAAGAA-GACCGC-3′ was performed with mutagenic PCR according to standard protocols. PCR product was cut with BamHI and PstI restriction enzymes and cloned into a BamHI and PstI digested pQE CorA construct. Correctly ligated constructs were identified by deletion of the BsaBI restriction site in the CorA gene, resulting in a silent mutation from a thymine to a cytosine. No additional mutations were found by sequencing.

2.4. Complementation assays on solid media

The CorA, MgtA, MgtB deletion strain MM281 was transformed with pQE80L constructs harbouring TmCorA or mutated versions thereof. Single colonies were inoculated in LB medium containing 10 mM $MgCl_2$ and grown over night. The cultures were washed twice with 0.7% saline, adjusted to an OD_{600} of 0.1, and diluted 1:10, 1:100 and 1:1000 and spotted on LB plates containing 100 mM $MgCl_2$ or on standard LB plates, both supplemented with different IPTG concentrations (0; 0.01; 0.1 mM). The cultures were incubated for 24 h at 37 °C.

2.5. Growth curves

Overnight cultures of MM281 cells transformed with the aforementioned plasmid constructs were grown in LB medium with 10 mM $MgCl_2$, washed twice with LB and inoculated to an OD_{600} of 0.1 into liquid LB medium containing different concentrations of $MgCl_2$ and IPTG.

2.6. Measurement of Mg^{2+} uptake by spectrofluorometry

For these measurements cells were grown in low-phosphate LB medium in order to minimize complexation of Mg^{2+} by an excess of phosphate, which might cause variation in Mg^{2+} concentration. The measurements have been performed as described previously [10].

2.7. PAGE and western blotting

Overnight cultures of MM281 cells transformed with the aforementioned plasmid constructs were washed twice with LB medium and diluted in fresh LB + Amp medium to an OD_{600} of 0.1. Expression was induced by adding 0.05 mM IPTG for 3 h. Equivalents of 3 ml culture with an OD_{600} of 0.5 were taken. The cell pellet was resuspended in 20 µl SDS-Laemmli buffer and 20 µl 8 M Urea and sonicated for 5 s. After 15 min centrifugation at 13,000 rpm, equal volumes of supernatant were loaded on 10% SDS/polyacrylamide gels, blotted and labelled with an antiserum against the 6xHis tag (Qiagen).

3. Results

There are several hydrophobic constrictions along the TmCorA ion conduction pathway. The narrowest one is formed by the highly conserved residues Leu294 and Met291 [4–6]. They are considered to

be part of the potential "hydrophobic gate" [4,8]. To verify this hypothesis our mutations targeted the Leu294, we analysed mutants containing three different residues: positively charged arginine, negatively charged aspartic acid and small glycine.

3.1. Effect of positive charge at position 294 on gating of CorA: Leu294Arg mutant

In the growth complementation assay the Leu294Arg mutant showed similar growth as the wild-type TmCorA on plates without $MgCl_2$ and with different IPTG concentrations, which means, that the change from hydrophobic leucine to the hydrophilic, positively charged arginine does not cause a dramatic change in the protein function (Fig. 2). While on plates containing 100 mM $MgCl_2$ and 0.1 mM IPTG the wild-type TmCorA exhibited a growth defect, probably caused by Mg^{2+} overdose, the Leu294Arg mutant was still able to grow indicating decreased transport efficiency of this mutant (Fig. 2).

Mg^{2+} uptake measurements of the Leu294Arg mutant showed slower Mg^{2+} influx and lower steady-state values (~80% of wild-type values) (Fig. 3) suggesting that (i) the pore of the transporter is smaller than in wild-type TmCorA; (ii) the sensitivity of CorA to Mg^{2+} or the regulation of opening and closing of the pore was affected.

The growth curves of cells transformed with TmCorA Leu294Arg mutant (Fig. 4a, b, c) support these hypotheses. In liquid medium supplemented with 0.05 mM IPTG the cells grew much slower than those with wild-type TmCorA (Fig. 4b), while the shapes of the curves remained similar, pointing to a lower Mg^{2+} transport capacity of this mutant. The same was true for cells growing in medium with 0.05 mM IPTG and 3 mM $MgCl_2$ (Fig. 4c). We did not observe any indications of Mg^{2+} overdose, not even after 11 hour incubation (results not shown), suggesting that closing of the transporter remained tightly regulated. In medium without $MgCl_2$ the cells with Leu294Arg mutant
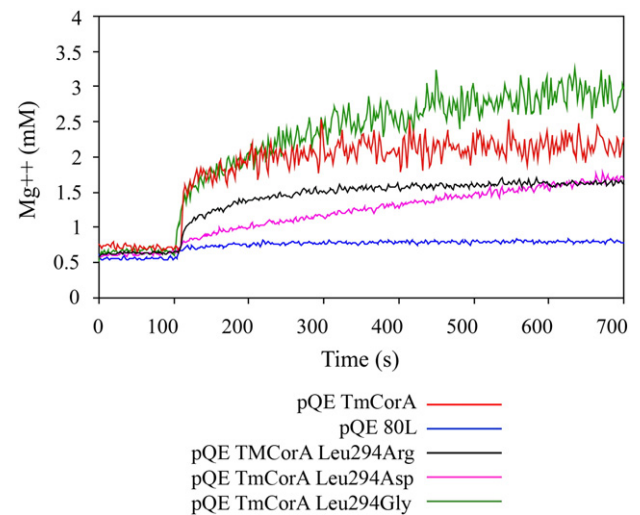
Fig. 3. Representative recordings of Mg^{2+} uptake. *S. typhimurium* strain MM281 which lacks all three known magnesium transport systems was transformed with plasmids indicated. The representative recordings show changes in fluorescence intensity of Mag-Fura-2 monitored over 10 min time after adding 10 mM $MgCl_2$. The pQE TmCorA and pQE80L empty constructs served as positive and negative control.

were unable to grow, exactly like those with wild-type TmCorA (Fig. 4a).

3.2. Effect of negative charge at position 294 on gating of CorA: Leu294Asp mutant

Cells transformed with TmCorA Leu294Asp mutant showed a growth defect on medium containing 0.1 mM IPTG as well as on media containing 0.1 mM IPTG and 100 mM $MgCl_2$ in the growth complementation assay (Fig. 2). This suggests either a higher Mg^{2+}
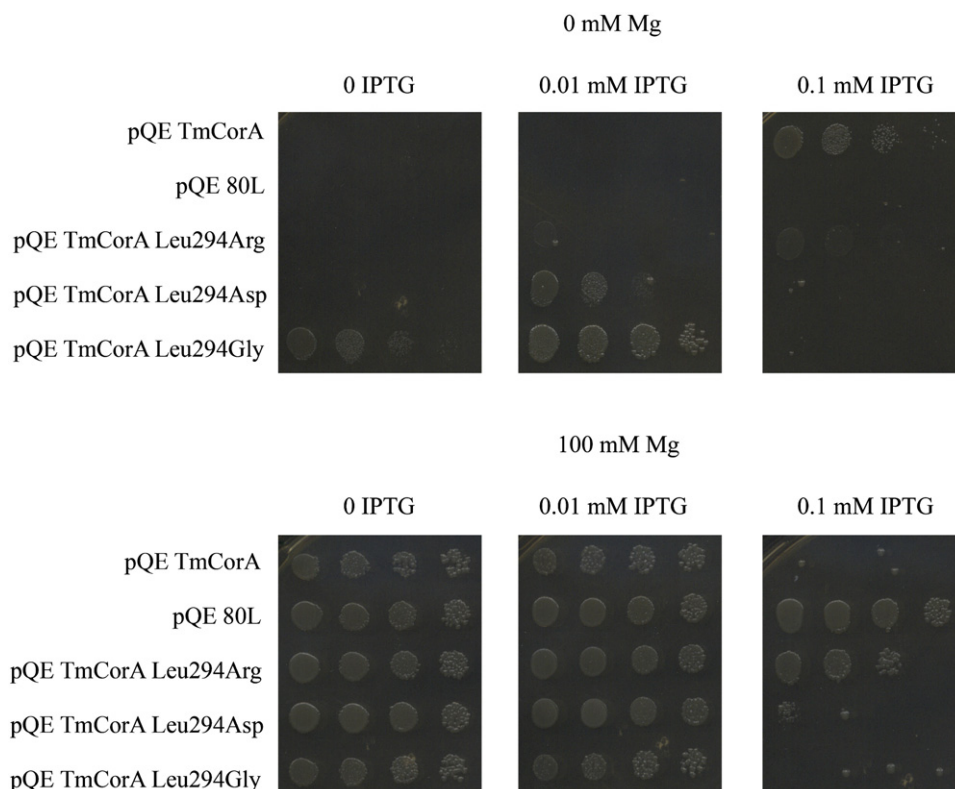
Fig. 2. Growth complementation assay of the gating mutants. *S. typhimurium* strain MM281 which lacks all three known magnesium transport systems was transformed with plasmids indicated. The pQE TmCorA and pQE80L empty constructs served as positive and negative control.
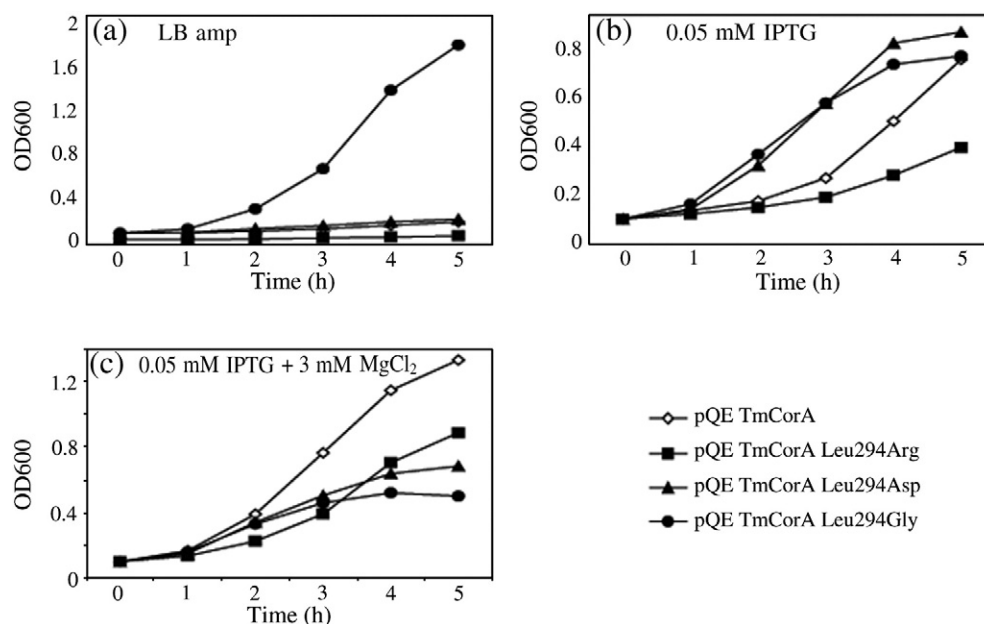
**Fig. 4.** Effect of gating mutations in different liquid medium. Growth curves of the *S. typhimurium* strain MM281 which lacks all three known magnesium transport systems, transformed with plasmids indicated. Cells were grown over night in LB amp medium containing 10 mM MgCl$_2$. Cultures were diluted to an OD$_{600}$ of 0.1 and grown over 5 h. The data were averaged from three independent experiments.

transport capacity, which might be caused by a defect in the regulation process of the opening and closing of the channel or in the closing itself, leading to Mg^{2+} overdose during the 24 hour incubation and consequently to a toxic effect of this protein at high expression levels.

Mg^{2+} uptake of Leu294Asp mutant increased slowly and did not reach a steady-state level within a time period of 600 s (Fig. 3), suggesting that the pore is neither completely open nor can it close properly, causing slow, constant Mg^{2+} uptake, leading finally to a Mg^{2+} overdose. This mutation apparently causes a defect in the regulation of opening and closing or/and in the closing process itself, which was corroborated by the growth curves (Fig. 4a, b, c): neither cells transformed with the TmCorA nor cells transformed with the Leu294Asp mutant were able to grow in medium without MgCl$_2$ (Fig. 4a). In medium containing 0.05 mM IPTG we observed rapid growth but after 4 h a steady-state phase was reached, probably due to a Mg^{2+} overdose (Fig. 4b). In medium containing 0.05 mM IPTG and 3 mM MgCl$_2$ the shape of the Leu294Asp mutant growth curve differed from that of the wild-type TmCorA: the mutant cells grew significantly slower, reaching only an OD$_{600}$ of 0.6 (~50% of the wild-type CorA) (Fig. 4c), which indicates a Mg^{2+} overdose caused by the constant Mg^{2+} uptake depicted in Fig. 3.

3.3. Effect of removal of side chain at position 294 on gating of CorA: Leu294Gly mutant

As expected, the Leu294Gly mutant was even more Mg^{2+} sensitive than the Leu294Asp variant. The cells did not grow on plates containing 0.1 mM IPTG suggesting a defect in the closing and/or in the regulation of the transporter and the growth on plates containing 0.01 mM IPTG points to a higher Mg^{2+} uptake capacity compared to the wild-type TmCorA (Fig. 2). In case of the Leu294Gly mutant the cells also grew on plates without additional MgCl$_2$ or IPTG (Fig. 2) which might be due to not tight enough regulation of the used plasmid, leading to leaky expression of the CorA gene in the absence of IPTG. This was tested by determination of expressed CorA levels using western blots (Fig. 6). The low expression level of the wild-type TmCorA protein was not sufficient to provide cells with enough Mg^{2+} in a low Mg^{2+} medium, but in the case of the Leu294Gly mutant cells

are able to take up enough Mg^{2+} to survive. This observation supports the suggested increased Mg^{2+} transport ability of the Leu294Gly mutant, which was also observed in Mg^{2+} uptake measurements (Fig. 3). The Mg^{2+} influx was as fast as in cells transformed with wild-type TmCorA, but it did not reach a steady-state, which indicates a defect in the closing of the transporter.

In liquid medium containing 0.05 mM IPTG we observed fast growth of the Leu294Gly cells, followed by a steady-state after 4 h (Fig. 4b). In medium supplemented with 0.05 mM IPTG and 3 mM MgCl$_2$ the cells stopped to grow already after 3 h, reaching only ~40% of the wild-type level, and contrary to the wild-type cells, they began to die (Fig. 4c). This effect can be related not only to an increased Mg^{2+} transport ability but also to a closing defect of the transporter. Increased Mg^{2+} transport ability of the Leu294Gly mutant (Fig. 3) allowed growth of the cells also in medium without any supplements (Fig. 4a), suggesting eminent structural changes caused by this mutation.

In order to confirm that the higher Mg^{2+} uptake capacity of this mutant is due to the Leu294Gly mutation, we used Co(III)hexamine, a known blocker of the CorA transporter [8,11,12]. We compared the wild-type *Salmonella typhimurium* strain LB5010, which has all major Mg^{2+} uptake systems (CorA, MgtA, MgtB) with strain MM281 deficient for these genes, transformed with wild-type TmCorA and with TmCorA Leu294Gly mutant. In liquid LB medium (Fig. 5) strain LB5010 grew fast, whereas strain MM281 containing the Leu294Gly mutation showed reduced growth, and strain MM281 with wild-type TmCorA did not grow at all. After addition of 3 mM Co(III)hexamine, growth of LB5010 cells and MM281 cells containing wild-type TmCorA remained unchanged, whereas growth of MM281 cells with the Leu294Gly mutation was completely inhibited proving that growth of cells under low Mg^{2+} conditions is the result of this mutation.

4. Discussion

Gating of the TmCorA magnesium transporter is a complex process, involving several events resulting in structural rearrangements of the pentamer: binding of Mg^{2+} ions to the regulatory DCS site(s) with consequent rearrangements of α-helices in the N-terminal domain, the pore-forming α7 helices and the basic sphincter are considered to lead collectively to conformational changes in the gating region. Leu294 lies
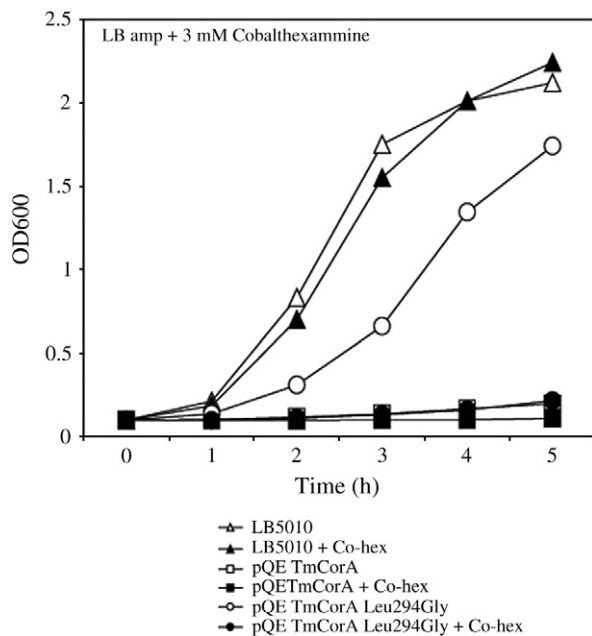
Fig. 5. Effect of Co(III)hexamine, inhibitor of the CorA-mediated magnesium transport. Growth curves of the *S. typhimurium* strains LB5010 (wild-type strain) transformed with pQE80L parental vector and MM281 (*corAΔ*, *mgtAΔ*, *mgtBΔ*) transformed with pQE80 TmCorA and pQE80 TmCorA L294G in the presence or absence of cobalt hexamine. The data were averaged from three independent experiments.

in the 15 Å long region termed MM stretch (spanning residues Met291 to Met301) proposed to play a central role in controlling the ionic conduction profile by representing both a steric as well as an electrostatic bottleneck for Mg^{2+} translocation [7]. This region involves a series of hydrophobic residues among which Leu at position 294 plays a critical role in the gating process. The effects of the Leu294 mutation to Asp and Gly may be mechanistically and structurally explained by local structural and electrostatic changes due to introduction of a negatively charged or a small amino acid residue with no side chain.

In case of glycine, the absence of the side chain could on one hand cause a wider opening of the pore and on the other impair its complete closing. This is in agreement with results of Payandeh et al. [8], who showed that exchange of Leu294 to a hydrophobic amino acid with a smaller side chain (Ile, Val or Ala) results in an increased ability of cells to grow on media supplemented with low $MgCl_2$ concentrations.

In case of introduction of an aspartic acid at position 294, the negatively charged side chains coming from five protomers repulse each other and thereby maximise the distance between them, leading to the incapacity of the transporter to properly close and to maintain a stable magnesium concentration in the cell. Furthermore, slow magnesium uptake of this mutant indicates that Mg^{2+} ions are probably trapped in the ring of negative charges.
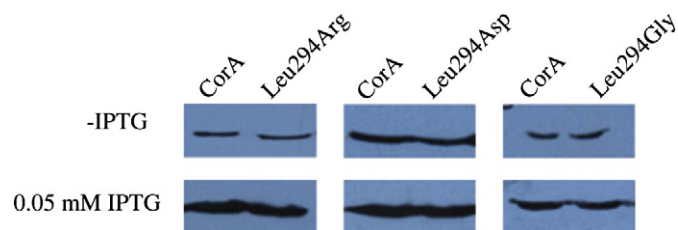

Fig. 6. Western blot analysis of whole cell samples. *S. typhimurium* strain MM281 which lacks all three known magnesium transport systems was transformed with plasmids indicated. The synthesis of CorA protein and variants thereof was induced by addition 0.05 mM IPTG for 3 h.

The effects observed with the Leu294Arg mutant cannot only be explained by local changes. Concentration of positively charged arginine residues in this region might have two opposite effects: repulsion of the positively charged residues causing a local structural distortion, and/or repulsion of the Mg^{2+} ion and hindering its passing through the pore. Both effects can explain the slow-down of Mg^{2+} transport, but not the low steady-state values observed in Mg^{2+} uptake measurements, which indicate a change in the regulation of Mg^{2+} influx. According to Payandeh et al. a valine mutation at position 294 can alter Mg^{2+}-binding properties of the transporter [8]. Due to the distance of ~65 Å between the Leu294 and the DCS sites a direct interaction seems impossible. Since the loss of Mg^{2+} ions from DCS sites can induce conformational rearrangements of the magnesium-binding domains, transmitted to the gate region by the α7 helices and leading to changes allowing ions to pass through [7,8], also a reverse process might be possible. Certain mutations in the gate region may evoke structural rearrangements of the α7 helices leading to conformational changes in the DCS sites, resulting in their changed affinity to Mg^{2+} ions.

5. Concluding remarks

In summary, we confirmed the importance of the Leu294 as a mechanical barrier to Mg^{2+} permeation. We furthermore propose an additional function of this residue in the regulation of Mg^{2+} uptake. Since Mg^{2+} transport involves multiple coordinated structural movements, further structural and functional analyses will be required to fully understand the molecular basis of this process.

Acknowledgements

References

[1] R.L. Smith, J.L. Banks, M.D. Snavely, M.E. Maguire, Sequence and topology of the CorA magnesium transport systems of *Salmonella typhimurium* and *Escherichia coli*. Identification of a new class of transport protein, J. Biol. Chem. 268 (1993) 14071–14080.

[2] M. Webb, The utilization of magnesium by certain Gram-positive and Gram-negative bacteria, J. Gen. Microbiol. 43 (1966) 401–409.

[3] R.L. Smith, M.E. Maguire, Microbial magnesium transport: unusual transporters searching for identity, Mol. Microbiol. 28 (1998) 217–226.

[4] V.V. Lunin, E. Dobrovetsky, G. Khutoreskaya, R. Zhang, A. Joachimiak, D.A. Doyle, A. Bochkarev, M.E. Maguire, A.M. Edwards, C.M. Koth, Crystal structure of the CorA Mg2+ transporter, Nature 440 (2006) 833–837.

[5] S. Eshaghi, D. Niegowski, A. Kohl, D. Martinez Molina, S.A. Lesley, P. Nordlund, Crystal structure of a divalent metal ion transporter CorA at 2.9 angstrom resolution, Science 313 (2006) 354–357.

[6] J. Payandeh, E.F. Pai, A structural basis for Mg2+ homeostasis and the CorA translocation cycle, EMBO J. 25 (2006) 3762–3773.

[7] N. Chakrabarti, C. Neale, J. Payandeh, E.F. Pai, R. Pomes, An iris-like mechanism of pore dilation in the CorA magnesium transport system, Biophys. J. 98 (2010) 784–792.

[8] J. Payandeh, C. Li, M. Ramjeesingh, E. Poduch, C.E. Bear, E.F. Pai, Probing structure–function relationships and gating mechanisms in the CorA Mg2+ transport system, J. Biol. Chem. 283 (2008) 11721–11733.

[9] R.J. Pogulis, A.N. Vallejo, L.R. Pease, In vitro recombination and mutagenesis by overlap extension PCR, Meth. Mol. Biol. 57 (1996) 167–176.

[10] E.M. Froschauer, M. Kolisek, F. Dieterich, M. Schweigel, R.J. Schweyen, Fluorescence measurements of free [Mg2+] by use of mag-fura 2 in *Salmonella enterica*, FEMS Microbiol. Lett. 237 (2004) 49–55.

[11] L.M. Kucharski, W.J. Lubbe, M.E. Maguire, Cation hexaammines are selective and potent inhibitors of the CorA magnesium transport system, J. Biol. Chem. 275 (2000) 16767–16773.

[12] M. Kolisek, G. Zsurka, J. Samaj, J. Weghuber, R.J. Schweyen, M. Schweigel, Mrs2p is an essential component of the major electrophoretic Mg2+ influx system in mitochondria, EMBO J. 22 (2003) 1235–1244.

3.2. Publication II

Functional analysis of the conserved GMN motif of the yeast mitochondrial magnesium transporter Mrs2p *

Svidová S., Sponder G., Khan M.B., Carugo O., Schweyen R.J., Djinović-Carugo K.

* Manuscript in preparation

Functional analysis of the conserved GMN motif of the yeast mitochondrial magnesium transporter Mrs2p

Soňa Svidová[1], Gerhard Sponder[1], Muhammad Bashir Khan[3], Oliviero Carugo[2,3], Rudolf J. Schweyen[1†], Kristina Djinović-Carugo[3,4*]

[1]Department of Microbiology, Immunobiology and Genetics, Max F. Perutz Laboratories, University of Vienna, Vienna, Austria

[2]Department of General Chemistry, University of Pavia, Pavia, Italy

[3]Department of Structural and Computational Biology, Max F. Perutz Laboratories, University of Vienna, Vienna, Austria

[4]Department of Biochemistry, Faculty of Chemistry and Chemical Technology, University of Ljubljana, Ljubljana, Slovenia

*Correspondence address: Campus Vienna Biocenter 5, A-1030 Vienna, Austria

Phone: +43-1-4277-52203/52201

Fax: +43-1-4277-9522

E-mail: kristina.djinovic@univie.ac.at

[†] Deceased on 15th of February 2009

Abstract

The highly conserved G-M-N motif of the CorA-Mrs2-Alr1 family of Mg^{2+} transporters has been proven to be essential for Mg^{2+} transport. Here we performed random mutagenesis of the G-M-N sequence of *Saccharomyces cerevisiae* Mrs2p and employed an unbiased genetic screen. We obtained a large amount of mutants still capable of Mg^{2+} transport, albeit below the wild-type level. Some selected mutants displayed reduced growth in the presence of Mn^{2+} and Zn^{2+} ions. We conclude that the G-M-N motif can be partially replaced by certain combinations of amino acids. Furthermore, we show that this motif also plays a role in ion selectivity, being part of the selectivity filter together with the flanking negatively charged loop at the entrance of the channel, to which selectivity function has primarily been assigned.

1. Introduction

As the most abundant divalent cation within cells, magnesium is required for numerous cellular functions, including coordination to nucleotide triphosphates, membrane stability, regulation of gene transcription, DNA replication, enzyme catalysis, and protein synthesis [1,2,3,4,5]. Maintenance of Mg^{2+} concentrations within a certain range is therefore critical for cell viability. Cellular membranes are impermeable to divalent cations, which necessitates transmembrane channels or carriers that allow Mg^{2+} to pass through in a controlled manner.

Members of the large, heterogeneous CorA/Mrs2/Alr1 protein superfamily, found in prokaryotes, eukaryotic organisms, as well as in plants are high-affinity Mg^{2+} uptake systems enabling growth of bacterial and yeast cells even in very low external Mg^{2+} concentrations. Mutants lacking these transporters cannot survive without being provided with high external Mg^{2+} concentrations [6,7,8,9,10,11].

The *MRS2* gene encodes a 54 kDa integral protein of the inner mitochondrial membrane (Mrs2p). Yeast cells lacking *MRS2* are respiratory deficient and therefore exhibit a growth defect on non-fermentable substrates ("*petite* phenotype") [23]. Besides *MRS2*, *S. cerevisiae* expresses a homologous protein known as Lpe10p. Its deletion also results in a "*petite* phenotype" [15] and additionally in a considerable reduction of the mitochondrial membrane potential ($\Delta\Psi$) [27].

Mrs2p is a distant relative of the bacterial Mg^{2+} transporter CorA, which three-dimensional crystal structure has already been revealed [12,13,14]. Conservation of the primary sequences in the CorA/Mrs2/Alr1 protein superfamily is in the range of 15-20% [6,8]. Despite of the low primary sequence homology there are several structurally conserved features, in particular the two α-helices in the large N-terminal part and two trans-membrane helices (TM1, TM2) near the C-terminus connected by a short conformationally flexible loop [15]. The sequence G-M-N, a motif within TM1 and the presence of bulky hydrophobic amino acids in the predicted gate region at the intracellular/intramitochondrial end of the pore are the only universally conserved features, indicating an essential role for the function of these proteins [8,12,13,14].

Mrs2p-mediated Mg^{2+} transport has been extensively studied using the Mg^{2+} sensitive, fluorescent dye mag-fura-2, where it was shown that Mrs2p mediates rapid, highly regulated Mg^{2+} uptake into mitochondria [9]. Isolated mitochondria respond within seconds to a rise in the external magnesium concentration with a rapid increase of the mitochondrial free Mg^{2+} concentration (150 μM s^{-1}) [9]. The high conductance of ~150 pS obtained in patch-clamp recordings, characterizes Mrs2p as a channel [19] and preliminary data on the Mrs2p homologue, *Salmonella typhimurium* CorA, suggest a similar high conductance [16]. The assumption of a common mechanism of Mg^{2+} transport for Mrs2p and CorA is supported by the fact that Mrs2p can be functionally replaced by CorA [15] and *vice versa* (this study). Furthermore, Mg^{2+} transport is in both cases inhibited by cobalt(III)-hexaammine, an analogue for the hydrated Mg^{2+} ion [17,18,19].

Mrs2p is able to mediate Ni^{2+} transport, albeit with a 3.5-fold lower conductance (~45 pS) compared to Mg^{2+}, whereas it is not permeable for Ca^{2+}, Mn^{2+} or Co^{2+} [19]. Additionally, suppression of Mg^{2+} currents in the presence of Co^{2+} was observed suggesting Co^{2+} to interact with the pore [19]. This is different to *S. typhimurium* CorA and yeast Alr1p for which transport of Ni^{2+} as well as of Co^{2+} has been reported [6,17].

As noted above, the G-M-N motif at the C-terminal end of the first transmembrane helix is the signature sequence of the CorA/Mrs2/Alr1 protein superfamily. The crystal structure of *Thermotoga maritima* CorA revealed that main-chain carbonyl groups of the G-M-N motif are exposed into the center of the pore entrance on the periplasmic side and form a polar strip suited for interaction with cations [13]. Lunin et al. proposed that the ring of five Asn314 side chains of the G-M-N motif in the CorA pentamer at the periplasmic entrance occlude the pore in the closed state [12]. The G-M-N motif has been shown to be critical for the function of CorA and even conservative single point mutations completely abolish Mg^{2+} transport [20]. This was also confirmed for Mrs2p where single mutations in the G-M-N motif were introduced [9]. This suggests that this sequence is indispensable for the function,

possibly through suitably positioning the periplasmic loop implicated in initial binding of the hydrated Mg^{2+} [12] and in assisting in the dehydration process [16].

In order to further investigate the importance and role of the G-M-N motif we performed random PCR mutagenesis on the G-M-N triplet to obtain mutants harbouring all possible amino acid combinations and identified those still capable of transporting Mg^{2+}. The active mutants were further characterized using *in vivo* and *in vitro* studies showing that the G-M-N motif can be in part functionally replaced by certain combinations of amino acids. Furthermore, our results corroborate the notion that this motif plays an important role in ion selectivity.

2. Materials and Methods

2.1 Yeast and bacterial strains, growth media and genetic procedures

2.1.1 Bacterial cells

Escherichia coli DH10B F⁻ endA1 recA1 galE15 galK16 nupG rpsL ΔlacX74 Φ80lacZΔM15 araD139 Δ(ara,leu)7697 mcrA Δ(mrr-hsdRMS-mcrBC) λ⁻

Salmonella enterica serovar Typhimurium transmitter strain LB5010: metA22 metE551 ilv-452 leu-3121 trpC2 xyl-404 galE856 hsdL6 hsdSA29 hsdSB121 rpsL120 H1-b H2-e, n, x flaA66 nml (-) Fel-2(-)

Salmonella enterica serovar Typhimurium strain MM281 DEL485 (leuBCD)mgtB::MudJ;mgtA21::MudJ;corA45::mudJ;zjh1628::Tn10(cam) Cam^R, Kan^R, Mg $^{2+}$ dependent) was kindly provided by M.E. Maguire. It lacks all three major magnesium transport systems *CorA, MgtA* and *MgtB* and therefore requires medium containing Mg^{2+} concentrations in the millimolar range.

Salmonella enterica serovar Typhimurium strain MM 1927
DEL485 (leuBCD);mgtB::MudJ;mgtA21::MudJ;corA45::mudJ;zjh1628::Tn10(cam)
CamR, KanR, pALTER-CorA (AmpR)

Strains were grown in LB medium (1% tryptone, 0.5% yeast extract, 1% NaCl) with ampicillin (100 µg/ml). MM281 required addition of 10 mM MgCl₂. LB plates contained 2% Difco Agar Noble minimizing possible Mg contamination.

2.1.2 Yeast cells

The yeast *S. cerevisiae* DBY747 *mrs2Δ* deletion strain (DBY mrs2-1, short) has been described previously [22,23,24].

Yeast cells were grown in rich medium (1% yeast extract, 2% peptone dextrose) with 2% glucose as a carbon source (YPD).

2.1.3 Plasmid constructs

The construct YEp351 MRS2-HA was described previously [15].
For cloning of *MRS2* into the vector pGEX-3X with IPTG-inducible promoter the primers
M2GEXfw: 5'-CGCGGATCCCCAATCGGCGTCTCCTGG-3' and
MRS2HiXrev: 5'-TGCTCTAGATCAATGGTGATGGTGATGG-3' were used. The resulting PCR fragment was cloned into the vector via BamHI and XbaI restriction sites.

2.1.4 Random PCR mutagenesis

In order to introduce various amino acid substitutions in Mrs2p, overlap extension PCR according to Pogulis et al. [25] was used. No additional mutations were found by sequencing.

Random mutagenesis of the GMN motif of the *MRS2* was performed with the mutagenic forward primer 5'-GCATCTGTTCTGCCGGCGTTCTATNNNNNNNNNTTAAAGAATTTCATCGAGGAGAGTG -3' and the reverse primer 5'-

CACTCTCCTCGATGAAATTCTTTAANNNNNNNNNNATAGAACGCCGGCAGA
ACAGATGC -3' according to standard protocols.

PCR products were digested with XhoI and EcoRI and cloned into an XhoI and EcoRI
digested pGEX-MRS2 construct. For transformation into the DH10B *Escherichia coli*
strain standard calcium chloride method was used. Correctly ligated constructs were
identified by deletion of the BsmI restriction site of the *MRS2* gene, resulting in a
silent mutation from an adenine to a guanine.

2.2 Identification of tolerated substitutions

A total of 45,600 constructs were pooled and transformed into the *S. typhimurium*
LB5010 transmitter strain. A total of 46,848 construct were pooled and transformed
into the *S. typhimurium* MM281 strain, plated on LB plates supplemented with 10
mM $MgCl_2$ and replicaplated on LB plates containing 0.05 mM IPTG to induce
protein expression. 49 mutants able to grow on this medium were sequenced. No
additional mutations were found by sequencing.

2.3 Serial dilutions

For serial dilutions on plates, cells were grown in liquid LB medium containing 10
mM $MgCl_2$ at 37°C over night, washed twice with LB medium, adjusted to an A_{600} of
1 and diluted to an A_{600} 0.1, 0.01 and 0.001. Serial dilutions were spotted onto LB
medium plates containing different concentrations of $MgCl_2$, IPTG, $MnCl_2$ or $ZnCl_2$
and incubated for 24 h.

2.4 Isolation of mitochondria and measurement of changes in the intramitochondrial Mg^{2+} concentrations by spectrofluorometry

Isolation of mitochondria by differential centrifugation and ratiometric determination
of intramitochondrial Mg^{2+} concentrations ($[Mg^{2+}]_m$) dependent on various external
concentrations ($[Mg^{2+}]_e$) was performed as previously reported [9].

3. Results and discussion

3.1 Screening of triple G-M-N mutants

According to the studies of Szegedy and Maguire [20] and Kolisek et al. [9] a single amino acid substitution in the G-M-N motif of CorA or Mrs2p is sufficient to abolish Mg^{2+} transport. Since even single conservative mutations in the G-M-N motif are not tolerated we performed a triple site random mutagenesis screen in order to address the question whether any other amino acid combination can substitute for this unique and universally conserved motif.

Since large-scale isolation of mitochondria from yeast is very time consuming and therefore not suitable for high throughput analyses, we decided to develop a bacterial system for screening for functional G-M-N mutants. Based on the fact, that Mrs2p can be functionally replaced by its bacterial homologue CorA [15], we assumed that Mrs2p expressed in the *S. typhimurium* strain MM281 depleted of all major Mg^{2+} transport systems (CorA, MgtA and MgtB), could complement the Mg^{2+} transport deficiency. *S. typhimurium* strain MM1927, lacking the magnesium uptake systems MgtA and MgtB and over-expressing only CorA was used as the positive control. As depicted in Fig. 1, growth of MM281 cells is only supported at a high magnesium concentration of 10 mM. MM281 cells expressing Mrs2p virtually grow like MM1927 also without addition of external $MgCl_2$. This experiment clearly proved the ability of Mrs2p to complement the *corAΔmgtAΔmgtBΔ* induced Mg^{2+} deficiency of strain MM281 and enabled us to investigate our G-M-N mutants of Mrs2p in bacteria.

After transforming the mutant library into strain MM281, we replicaplated the transformants on LB plates without additional Mg^{2+} but supplemented with 0.05 mM IPTG to induce protein expression. These conditions restrict growth exclusively to mutants still able to transport Mg^{2+}.

Surprisingly, we obtained a considerable amount of mutants able to grow without additional Mg^{2+} supplementation. We sequenced 66 mutants, 7 of which contained the G-M-N motif itself (showing the functional dominance of this sequence), while 59 contained mutations of the G-M-N motif, 5 of which appeared twice. These 59

mutants were analyzed further using a growth complementation assay on plates supplemented with different IPTG concentrations to investigate, how their Mg^{2+} transport activity differs from the wild-type Mrs2p. In the complementation assay four "+" were attributed to cells able to grow at all four dilution steps, while "-" represents no growth at all on the plate (Tab. 1).

Bacterial cells transformed with wild-type *MRS2* were able to grow on plates with only 0.03 mM IPTG. In contrast, the analyzed mutants exhibited only poor growth at this IPTG concentration or did not grow at all. Upon stronger expression (IPTG concentrations of 0.035 – 0.05 mM) viability and growth of most of the mutants improved (Tab. 1). These results indicate that several G-M-N triple mutants still exhibited Mg^{2+} transport albeit at lower efficiency than wild-type Mrs2p.

3.2 Sequences of the functional mutants

The prominent feature of the identified amino acid sequences of functional mutants is their divergence from the G-M-N canonical motif. A glycine at the first position was observed only twice (4%), a methionine appeared twice (4%) in the second position, and in only one case there was an asparagine in the third position. The only mutant resembling the wild type protein was characterized by the presence of a G-T-N tripeptide instead of G-M-N.

Interestingly, about 80% of the functional mutants had a positively charged residue in the G-M-N motif. In 59% of the cases this occurred in the first position, in 18% of the cases in the second position, and only in 4% of the cases in the third position. However, the co-presence of two positively charged amino acids was uncommon (only in about 10% of the cases). There was only one evident correlation between two positions: in the 59% of the cases in which the first position was occupied by a positively charged residue, a small and hydrophobic amino acid (Val, Ile or Leu) tended to occupy the third position.

By contrast, few negatively charged residues were observed in the functional mutants, i.e. only six times in the first position and twice in the other two positions. No other clear trends were observed.

In a previous mutation analysis of the G-M-N motif of S. typhimurium CorA, none, even the most conservative single mutations (A-M-N, G-A-N, G-C-N, G-I-N, G-M-A, G-M-L, G-M-Q) were tolerated [20]. A mutational study of Mrs2p performed by Kolisek et al. [9] also confirmed the importance of the G-M-N motif: mutation to A-M-N reduced Mg^{2+} uptake to the level of the *mrs2Δ* mutant. These findings are in agreement with our results, as these mutants were not identified amongst the functional mutants which are much more divergent from the native motif G-M-N.

3.3 The effects of mutations of the G-M-N sequence on cation selectivity of Mrs2p

We subsequently performed a growth complementation assay on plates containing 0.05 mM IPTG and different concentrations of divalent cations (Ca^{2+}, Co^{2+}, Mn^{2+} and Zn^{2+}), known substrates of the yeast plasma membrane Mg^{2+} uptake system Alr1p, a homologue of Mrs2p [26]. We selected 10 mutants for this assay (Tab. 2, 3), in which we examined if the presence of the aforementioned divalent cations in the growth medium influenced the growth of mutants compared to wild-type Mrs2p.

Seven of the chosen mutants had a positively charged amino acid (K, R, H) in the first position and a small, hydrophobic residue in the third position (like 35% of the analyzed mutants). The last three mutants did not fit in the pattern "positively charged – X – hydrophobic", and were chosen as representatives of very well (R-A-W), medium (R-R-T) and poorly (R-V-H) complementing mutant variants.

In case of Ca^{2+} and Co^{2+} we did not observe any difference (results not shown) in the growth complementation assay compared to plates not supplemented with cations, suggesting that no transport or blockage of the channel by these ions occured. In a study employing patch clamp electrophysiology on giant lipid vesicles fused with inner-mitochondrial membranes, Mrs2p was permeable for Mg^{2+} and Ni^{2+} but not for Ca^{2+}, Mn^{2+} or Co^{2+}. However, suppression of Mg^{2+} currents in the presence of Co^{2+} was observed [19]. In our case, an effect of Co^{2+} was observed, neither on wild-type Mrs2p, nor on the investigated mutants. This might be caused by the different techniques used: patch-clamp recordings on single ion channels enable very precise measurements of the ion currents and tight control of ionic conditions on both sides of

the channel which is not possible in a growth complementation assay on plates. Furthermore, ion concentrations used in the patch-clamp experiments were much higher ($\sim 1000x$ higher in this case) than concentrations used *in vivo*. For this reason, we cannot properly compare the results of the growth complementation assay and the patch-clamping experiments. The Co^{2+} concentration used in the growth complementation assay might have been too small to cause suppression of Mg^{2+} influx *in vivo*.

The three tested concentrations of $MnCl_2$ reduced growth of all mutants, whereas growth of cells harboring wild-type *MRS2* remained unaffected. The negative effect of $MnCl_2$ increased with increasing concentrations of the cation (Tab. 2). Furthermore, the growth defect was differently pronounced in the mutants: the top three least affected are characterized by positively charged residues in the first and the second position (K-R-L; R-R-T), while the two most affected mutants, that exhibited good growth in the absence of cations, carry Arg at the first, and Leu at the third position (R-Q-L; R-V-L) (Tab. 2).

The effect of $ZnCl_2$ was similar to $MnCl_2$, however the growth defect of the mutants was less severe and the differences between the mutants less pronounced (Tab. 3). Moreover, rising $ZnCl_2$ concentrations had only a moderately increasing negative effect on growth of the cells. The three least affected and the two most affected mutants were the same as those identified in the Mn^{2+} case.

The R-V-H, R-A-W and R-R-T mutants do not significantly differ from the "positively charged - X - hydrophobic" set, suggesting that the absence of a hydrophobic amino acid in the third position does not critically affect ion selectivity, when combined with a small hydrophobic or positively charged residue in the second place.

3.4 Mg^{2+} influx into isolated mitochondria

In order to directly investigate Mg^{2+} influx into isolated mitochondria of selected mutants we used the Mg^{2+}-sensitive dye mag-fura-2 (Fig. 2). The mutants were selected on the basis of good (R-M-V, R-F-V, R-C-V), medium (R-Q-L) or poor (R-V-H) growth complementation capacity in *S. typhimurium* strain MM281 (Tab. 1). After addition of $MgCl_2$ to a concentration of 1 mM Mg^{2+} a lack of the characteristic

rapid Mg^{2+} influx [9] was observed in most mutants, together with significantly lower steady-state Mg^{2+} levels (Fig. 2). The only exception was the R-Q-L mutant, which lacked rapid Mg^{2+}influx, but finally reached a mitochondrial Mg^{2+} concentration comparable to the wild-type level during the subsequent 100 seconds. After addition of $MgCl_2$ to the final concentration of 3 mM Mg^{2+}, we observed Mg^{2+} influx in all mutants, however, it did not reach the final steady-state level of wild-type Mrs2p. The differences between mutants were minimal, with the exception of the R-Q-L mutant, which again reached almost wild-type Mg^{2+} levels.

These results show that all investigated mutants maintained a certain ability to transport Mg^{2+} in *S. typhimurium* cells (Tab. 1) and mutants R-V-H, R-M-V, R-F-V, R-C-V and R-Q-L also in yeast mitochondria (Fig. 2), albeit in both systems the transport activity was significantly decreased compared to the wild type protein.

4. Conclusions

The asparagine residues of the G-M-N motif have been proposed to block the entrance of the channel in the closed conformation [12]. Furthermore, this motif has been implicated in suitably orienting the flexible, negatively charged loop at the mouth of the pore for interaction with the hydrated magnesium ion. The loop connecting TM1 and TM2 appears to form the initial interaction site for hydrated Mg^{2+} and likely participates in the dehydration process of the ion required prior to its entrance into the pore of the channel [12,16,18]. The high conductance of Mrs2p [19] and CorA [16] channels may be based on a mechanism which involves electrostatic interactions of the loop residues with the hydration shell of Mg^{2+} and not with the ion itself [16].

Our study on the G-M-N motif identified viable triple mutants hosting a positively charged residue. At a first glance, the presence of positively charged residues in functional mutants might seem counterintuitive as these mutations could in fact hinder the transport of Mg^{2+} ions by electrostatic repulsion. However, since it is structurally unfeasible for all three amino acid residues of the motif to be in direct contact with the ion, it is more probable that these residues form a structural motif critical for ion uptake, which can be partially accomplished by different amino acid combinations, eventually leading to a functionally equivalent structure.

Changes in the positioning of the loop could lead to an improved interaction with cations with a different diameter of the hydration shell, like Zn^{2+} or Mn^{2+}, and cause blockage of the channel by these ions and changes in the selectivity.

In order to assess the impact of mutations in the G-M-N motif on the selectivity of Mrs2p, we performed growth complementation assays on plates supplemented with different cations (Ca^{2+}, Co^{2+}, Mn^{2+} and Zn^{2+}).

Our results show that mutations in the G-M-N motif lead to reduced growth of the cells in presence of Mn^{2+} and Zn^{2+}. This can take place *via* two possible mechanisms: (i) Mn^{2+} and Zn^{2+} are transported through the pore and the growth defect is caused by Mn^{2+}/Zn^{2+} overdose, or (ii) Mn^{2+} and Zn^{2+} ions enter the channel where they get trapped and block the channel for Mg^{2+} transport causing the growth defect by Mg^{2+} deficiency.

In summary we conclude, that although the highly conserved G-M-N motif is important for Mg^{2+} transport, it can be functionally replaced by certain combinations of amino acid residues. Most frequently a positively charged residue in the first and a hydrophobic residue in the third position were found. Our studies suggest that the G-M-N motif plays a role in ion dehydration as well as in ion selectivity, being therefore part of the selectivity filter together with the flanking negatively charged loop, at the entrance of the Mrs2p channel. The concurrent involvement of the G-M-N motif in the gating process and in ion selectivity as well, might be the molecular basis for its universal conservation throughout the phyla.

Table 1

S. typhimurium strain MM281 was transformed with plasmids indicated, serially diluted and replicaplated on plates with increasing IPTG concentrations. The number of pluses corresponds to the number of dilution steps exhibiting growth.

Sequence	0.03 mM IPTG	0.035 mM IPTG	0.04 mM IPTG	0.045 mM IPTG	0.05 mM IPTG
G-M-N	++++	++++	++++	++++	++++
R-F-V*	+	++++	++++	++++	++++
R-I-L	+	++++	++++	++++	++++
R-M-V	+	++++	++++	++++	++++
R-Q-I	+	++++	++++	++++	++++
R-Q-L*	+	++++	++++	++++	++++
R-V-L*	+	++++	++++	++++	++++
L-R-C	++	+++	+++	++++	++++
R-A-W	+	++++	+++	++++	++++
R-V-M	+	++++	+++	++++	++++
I-R-I	++	+++	++	++++	++++
K-A-I	-	++++	+++	++++	++++
K-R-L	-	++++	+++	++++	++++
R-F-I	+	++++	+++	++++	+++
R-V-I	+	++++	+++	++++	+++
R-N-L	-	+++	+++	++++	++++
R-P-L	+	+++	+++	++++	+++
C-F-L	++	++	++	+++	++++
R-G-F	+	+++	+++	+++	+++
R-S-V	+	+++	+++	++++	++
R-C-V	-	++	++	++++	++++
F-R-L*	+	++	++	+++	+++
D-F-G	+	++	+	+++	+++
K-A-M	-	++	++	+++	+++
R-F-Y	+	++	++	+++	++
R-R-T	-	++	++	+++	+++
V-R-A	+	++	++	++	+++
V-R-C	+	++	++	++	+++
D-F-P*	+	++	+	++	+++
E-F-P	+	++	++	++	++
K-H-V	-	++	++	+++	++
E-Q-V	+	++	+	++	++
G-D-M	+	++	+	++	++
K-Y-I	-	++	++	++	++
R-T-Y	-	++	++	++	++
E-F-A	+	+	+	++	++
G-T-N	+	+	+	++	++
K-M-L	-	++	+	++	++
P-D-L*	-	+	++	++	++
R-F-Q	-	++	+	++	++
R-V-H	-	+	+	+++	++
R-Y-S	-	++	++	++	+
R-F-S	-	+	+	++	++
T-S-E	+	+	+	+	++
E-S-K	-	+	+	++	+
F-R-E	-	+	+	++	+
K-I-T	-	+	+	++	+
P-N-V	-	+	+	+	+
P-R-L	-	+	+	+	+
P-T-L	-	-	-	+	+

∗ Mutants which appeared two times.

Table 2

S. typhimurium strain MM281 was transformed with plasmids indicated, serially diluted and replicaplated on plates with 0.05 mM IPTG and different $MnCl_2$ concentrations. The number of pluses corresponds to the number of dilution steps exhibiting growth.

Sequence	0 mM $MnCl_2$	0.01 mM $MnCl_2$	0.03 mM $MnCl_2$	0.1 mM $MnCl_2$
G-M-N	++++	++++	++++	++++
K-R-L	++++	+++	+++	++
R-A-W	++++	+++	++	++
R-R-T	+++	+++	+++	++
K-A-I	++++	++	++	+
R-M-V	++++	++	++	+
R-C-V	++++	+	+	+
R-F-V	++++	+	+	+
R-Q-L	++++	+	+	+
R-V-L	++++	+	+	+
R-V-H	++	++	+	+

Table 3

S. typhimurium strain MM281 was transformed with plasmids indicated, serially diluted and replicaplated on plates with 0.05 mM IPTG and different $ZnCl_2$ concentrations. The number of pluses corresponds to the number of dilution steps exhibiting growth.

Sequence	0 $ZnCl_2$	0.001 mM $ZnCl_2$	0.005 mM $ZnCl_2$	0.01 mM $ZnCl_2$	0.1 mM $ZnCl_2$
-	-	-	-	-	-
G-M-N	++++	++++	++++	++++	+++
K-R-L	++++	+++	+++	+++	++
R-R-T	+++	+++	+++	+++	++
R-A-W	++++	+++	+++	++	+
K-A-I	++++	++	++	++	+
R-C-V	++++	++	++	++	+
R-F-V	++++	++	++	++	+
R-M-V	++++	++	++	++	+
R-Q-L	++++	++	++	++	+
R-V-L	++++	++	++	++	+
R-V-H	++	++	++	++	++

Figure 1

Growth complementation assay of the MM281 mutant strain by ScMrs2**.**

Over night cultures of MM1927 and MM281 were transformed with plasmids indicated, serially diluted and spotted on LB medium plates with 10 mM magnesium or 0.05 mM and 0.025 mM IPTG concentrations and incubated on 37°C for 24 hours.
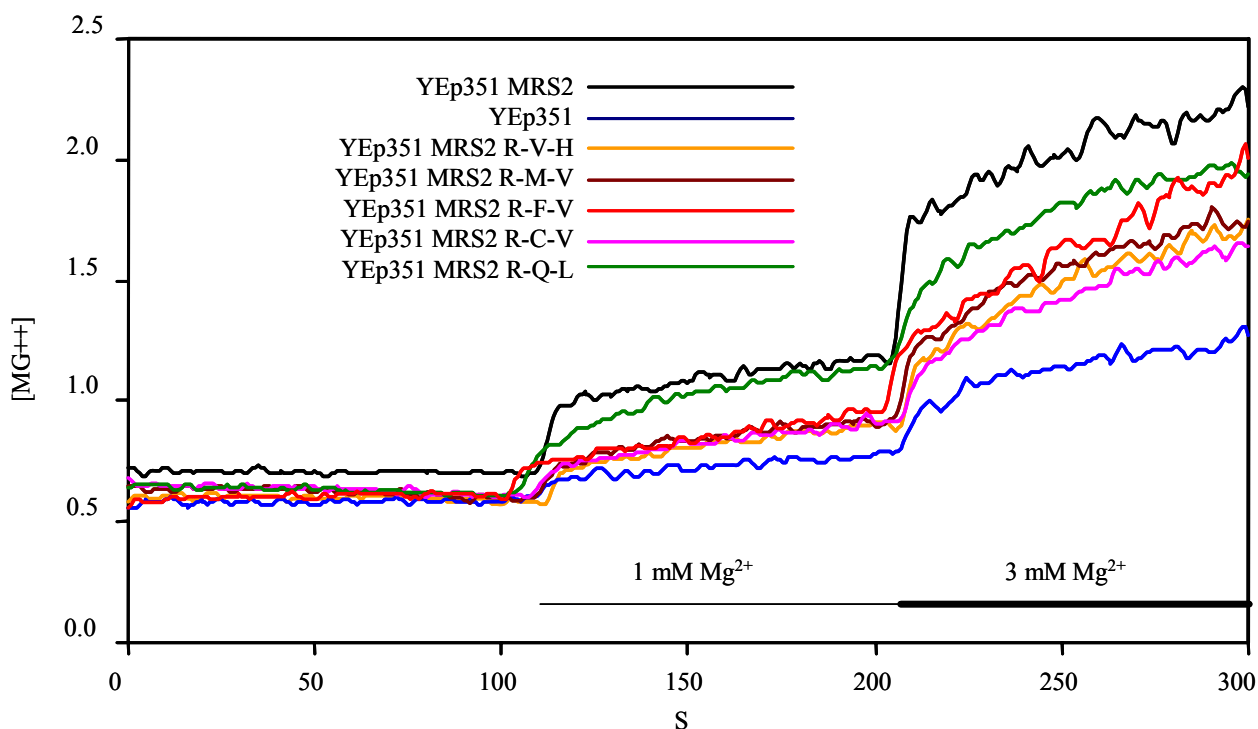
Figure 2

Representative recordings of [Mg^{2+}] uptake.

S. cerevisiae strain DBY747 *mrs2Δ* was transformed with the indicated plasmids and mitochondria were isolated. The representative recordings show changes in fluorescence intensity of mag-fura-2 monitored over 300 seconds after step-wise addition of $MgCl_2$.

References

[1] J.A. Cowan, Metallobiochemistry of magnesium. Coordination complexes with biological substrates: site specificity, kinetics and thermodynamics of binding, and implications for activity, Inorg. Chem. 30 (1991) 2740- 2747.

[2] J.A. Cowan, Metal Activation of Enzymes in Nucleic Acid Biochemistry, Chem Rev 98 (1998) 1067-1088.

[3] J.A. Cowan, T. Ohyama, K. Howard, J.W. Rausch, S.M. Cowan, S.F. Le Grice, Metal-ion stoichiometry of the HIV-1 RT ribonuclease H domain: evidence for two mutually exclusive sites leads to new mechanistic insights on metal-mediated hydrolysis in nucleic acid biochemistry, J Biol Inorg Chem 5 (2000) 67-74.

[4] C.E. Dann, 3rd, C.A. Wakeman, C.L. Sieling, S.C. Baker, I. Irnov, W.C. Winkler, Structure and mechanism of a metal-sensing regulatory RNA, Cell 130 (2007) 878-892.

[5] G.J. Quigley, M.M. Teeter, A. Rich, Structural analysis of spermine and magnesium ion binding to yeast phenylalanine transfer RNA, Proc Natl Acad Sci U S A 75 (1978) 64-68.

[6] R.C. Gardner, Genes for magnesium transport, Curr Opin Plant Biol 6 (2003) 263-267.

[7] A. Graschopf, J.A. Stadler, M.K. Hoellerer, S. Eder, M. Sieghardt, S.D. Kohlwein, R.J. Schweyen, The yeast plasma membrane protein Alr1 controls Mg2+ homeostasis and is subject to Mg2+-dependent control of its synthesis and degradation, J Biol Chem 276 (2001) 16216-16222.

[8] V. Knoop, M. Groth-Malonek, M. Gebert, K. Eifler, K. Weyand, Transport of magnesium and other divalent cations: evolution of the 2-TM-GxN proteins in the MIT superfamily, Mol Genet Genomics 274 (2005) 205-216.

[9] M. Kolisek, G. Zsurka, J. Samaj, J. Weghuber, R.J. Schweyen, M. Schweigel, Mrs2p is an essential component of the major electrophoretic Mg2+ influx system in mitochondria, EMBO J 22 (2003) 1235-1244.

[10] M. Wachek, M.C. Aichinger, J.A. Stadler, R.J. Schweyen, A. Graschopf, Oligomerization of the Mg2+-transport proteins Alr1p and Alr2p in yeast plasma membrane, FEBS J 273 (2006) 4236-4249.

[11] J. Weghuber, F. Dieterich, E.M. Froschauer, S. Svidova, R.J. Schweyen, Mutational analysis of functional domains in Mrs2p, the mitochondrial Mg2+ channel protein of Saccharomyces cerevisiae, FEBS J 273 (2006) 1198-1209.

[12] V.V. Lunin, E. Dobrovetsky, G. Khutoreskaya, R. Zhang, A. Joachimiak, D.A. Doyle, A. Bochkarev, M.E. Maguire, A.M. Edwards, C.M. Koth, Crystal structure of the CorA Mg2+ transporter, Nature 440 (2006) 833-837.

[13] S. Eshaghi, D. Niegowski, A. Kohl, D. Martinez Molina, S.A. Lesley, P. Nordlund, Crystal structure of a divalent metal ion transporter CorA at 2.9 angstrom resolution, Science 313 (2006) 354-357.

[14] J. Payandeh, E.F. Pai, A structural basis for Mg2+ homeostasis and the CorA translocation cycle, EMBO J 25 (2006) 3762-3773.

[15] D.M. Bui, J. Gregan, E. Jarosch, A. Ragnini, R.J. Schweyen, The bacterial magnesium transporter CorA can functionally substitute for its putative homologue Mrs2p in the yeast inner mitochondrial membrane, J Biol Chem 274 (1999) 20438-20443.

[16] A.S. Moomaw, M.E. Maguire, Cation selectivity by the CorA Mg2+ channel requires a fully hydrated cation, Biochemistry 49 5998-6008.

[17] R.L. Smith, M.E. Maguire, Microbial magnesium transport: unusual transporters searching for identity, Mol Microbiol 28 (1998) 217-226.

[18] L.M. Kucharski, W.J. Lubbe, M.E. Maguire, Cation hexaammines are selective and potent inhibitors of the CorA magnesium transport system, J Biol Chem 275 (2000) 16767-16773.

[19] R. Schindl, J. Weghuber, C. Romanin, R.J. Schweyen, Mrs2p forms a high conductance Mg2+ selective channel in mitochondria, Biophys J 93 (2007) 3872-3883.

[20] M.A. Szegedy, M.E. Maguire, The CorA Mg(2+) transport protein of Salmonella typhimurium. Mutagenesis of conserved residues in the second membrane domain, J Biol Chem 274 (1999) 36973-36979.

[21] J. Payandeh, C. Li, M. Ramjeesingh, E. Poduch, C.E. Bear, E.F. Pai, Probing structure-function relationships and gating mechanisms in the CorA Mg2+ transport system, J Biol Chem 283 (2008) 11721-11733.

[22] H. Koll, C. Schmidt, G. Wiesenberger, C. Schmelzer, Three nuclear genes suppress a yeast mitochondrial splice defect when present in high copy number, Curr Genet 12 (1987) 503-509.

[23] G. Wiesenberger, M. Waldherr, R.J. Schweyen, The nuclear gene MRS2 is essential for the excision of group II introns from yeast mitochondrial transcripts in vivo, J Biol Chem 267 (1992) 6963-6969.

[24] J. Gregan, M. Kolisek, R.J. Schweyen, Mitochondrial Mg(2+) homeostasis is critical for group II intron splicing in vivo, Genes Dev 15 (2001) 2229-2237.

[25] R.J. Pogulis, A.N. Vallejo, L.R. Pease, In vitro recombination and mutagenesis by overlap extension PCR, Methods Mol Biol 57 (1996) 167-176.

[26] C.W. MacDiarmid, R.C. Gardner, Overexpression of the Saccharomyces cerevisiae magnesium transport system confers resistance to aluminum ion, J Biol Chem 273 (1998) 1727-1732.

[27] Sponder, G., Svidova, S., Schindl, R., Wieser, S., Schweyen, R. J., Romanin, C., Froschauer, E. M. and Weghuber, J. (2010). Lpe10p modulates the activity of the Mrs2p-based yeast mitochondrial Mg2+ channel. *Febs J* **277,** 3514-25.

3.3. Publication III

Lpe10p modulates the activity of the Mrs2p-based yeast mitochondrial Mg^{2+} channel

Sponder G., Svidova S., Schindl R., Wieser S., Schweyen R.J., Romanin C., Froschauer E.M., Weghuber J.

Lpe10p modulates the activity of the Mrs2p-based yeast mitochondrial Mg^{2+} channel

Gerhard Sponder[1], Sona Svidova[1], Rainer Schindl[2], Stefan Wieser[2], Rudolf J. Schweyen[1], Christoph Romanin[2], Elisabeth M. Froschauer[1,]*and Julian Weghuber[2,]*

1 Max F. Perutz Laboratories, Department of Microbiology, Immunology and Genetics, Vienna, Austria
2 Institute of Biophysics, University of Linz, Austria

Correspondence

J. Weghuber, Institute of Biophysics, University of Linz, Altenbergerstraße 69, 4040 Linz, Austria
Fax: +43 732 2468 29284
Tel: +43 732 2468 9266
E-mail: julian.weghuber@jku.at

*These authors contributed equally to this work

Saccharomyces cerevisiae Lpe10p is a homologue of the Mg^{2+}-channel-forming protein Mrs2p in the inner mitochondrial membrane. Deletion of *MRS2*, *LPE10* or both results in a petite phenotype, which exhibits a respiratory growth defect on nonfermentable carbon sources. Only coexpression of *MRS2* and *LPE10* leads to full complementation of the *mrs2Δ/lpe10Δ* double disruption, indicating that these two proteins cannot substitute for each other. Here, we show that deletion of *LPE10* results in a loss of rapid Mg^{2+} influx into mitochondria, as has been reported for *MRS2* deletion. Additionally, we found a considerable loss of the mitochondrial membrane potential ($\Delta\Psi$) in the absence of Lpe10p, which was not detected in *mrs2Δ* cells. Addition of the K$^+$/H$^+$-exchanger nigericin, which artificially increases $\Delta\Psi$, led to restoration of Mg^{2+} influx into mitochondria in *lpe10Δ* cells, but not in *mrs2Δ/lpe10Δ* cells. Mutational analysis of Lpe10p and domain swaps between Mrs2p and Lpe10p suggested that the maintenance of $\Delta\Psi$ and that of Mg^{2+} influx are functionally separated. Cross-linking and Blue native PAGE experiments indicated interaction of Lpe10p with the Mrs2p-containing channel complex. Using the patch clamp technique, we showed that Lpe10p was not able to mediate high-capacity Mg^{2+} influx into mitochondrial inner membrane vesicles without the presence of Mrs2p. Instead, coexpression of Lpe10p and Mrs2p yielded a unique, reduced conductance in comparison to that of Mrs2p channels. In summary, the data presented show that the interplay of Lpe10p and Mrs2p is of central significance for the transport of Mg^{2+} into mitochondria of *S. cerevisiae*.

Structured digital abstract

- MINT-7905005: *LPE10* (uniprotkb:Q02783) *physically interacts* (MI:0915) with *MRS2* (uniprotkb:Q01926) by *anti tag coimmunoprecipitation* (MI:0007)
- MINT-7905028: *LPE10* (uniprotkb:Q02783) and *LPE10* (uniprotkb:Q02783) *covalently bind* (MI:0195) by *cross-linking study* (MI:0030)
- MINT-7905072: *LPE10* (uniprotkb:Q02783) and *MRS2* (uniprotkb:Q01926) *covalently bind* (MI:0195) by *cross-linking study* (MI:0030)

Abbreviations

BN-PAGE, Blue native PAGE; HA, haemagglutinin; JC-1, 5,5′,6,6′-tetrachloro-1,1′,3,3′-tetraethylbenzimidazolocarbocyanine iodide; [Mg^{2+}]$_e$, external Mg^{2+} concentration; [Mg^{2+}]$_m$, inner mitochondrial Mg^{2+} concentration; WT, wild-type; $\Delta\Psi$, mitochondrial membrane potential.

Introduction

The inner mitochondrial membrane forms a tight barrier to the passage of cations. Their movement across this barrier requires the action of transporters and ion channels. Physiological studies suggest that uptake of cations is driven by the inside-negative membrane potential of the organelle, whereas extrusion from mitochondria occurs against the electrochemical gradient by the influx of protons [1,2]. Mrs2p was the first molecularly identified cation channel of mitochondria [3]. It forms an oligomeric, Mg^{2+}-selective channel of high conductance in the inner mitochondrial membrane, whose probability of being open is controlled by the Mg^{2+} concentration inside the organelle [4,5].

Mrs2p is distantly related to the bacterial Mg^{2+} transport protein CorA [6] and to the Mg^{2+} transport protein Alr1p in the plasma membrane of fungi [7]. Proteins of this superfamily are characterized by two adjacent transmembrane domains (TM1 and TM2) in their C-terminal part, an F/YGMN motif at the end of TM1, a short loop with a surplus of negative charges connecting TM1 and TM2 [8], and a series of helical structures in the long N-terminal protein part. Crystallization and X-ray diffraction analysis of the *Thermotoga maritima* transporter CorA, determined in a closed state, have revealed a homopentamer with a membrane pore formed by five TM1 helices and a funnel-shaped structure composed of the N-terminal extension of TM1 in the cytoplasm [9,10].

Vertebrates express only a single *MRS2* gene in their mitochondria, whereas plant genomes contain at least 10 *MRS2*-related genes, whose products are not restricted to mitochondria [11,12]. The genome of *Saccharomyces cerevisiae* encodes not only Mrs2p but also a homologue with 32% sequence identity, which has been named Lpe10p. Like Mrs2p, it is located in the inner mitochondrial membrane with an N_{in}–C_{in} orientation, and it has been reported to be involved in Mg^{2+} uptake as well, but the mode of action remains undefined [13]. Notably, disruption of only one of *mrs2Δ* or *lpe10Δ* has been shown to cause a growth defect on nonfermentable carbon sources (petite phenotype) and a reduction in mitochondrial Mg^{2+} content [13,14].

Here, we found that deletion of *LPE10* led to a loss of Mg^{2+} influx, comparable to what is seen with *MRS2* deletion, but also resulted in a prominent decrease in the mitochondrial membrane potential (ΔΨ). To obtain further insights into the diverse functions of Lpe10p and Mrs2p, we constructed Mrs2-Lpe10p fusion proteins and investigated their ability to transport Mg^{2+} and to oligomerize. The results presented indicate an influence of Lpe10p on the size of Mrs2p-containing complexes, and show a direct interaction between Lpe10p and Mrs2p. Furthermore, single-channel recordings of giant lipid vesicles with fused inner mitochondrial membranes revealed a significantly decreased conductance for the Mrs2p channel if Lpe10p was coexpressed. On the basis of these results, we assume that Lpe10p has the potential to interact with the Mrs2p-based Mg^{2+} channel and, in addition, modulates its activity.

Results

Secondary structure prediction of Lpe10p

Full-length secondary structure prediction of *S. cerevisiae* Lpe10p and Mrs2p [5,13,15] reveals similarities to *Arabidopsis thaliana* Mrs2–7 [11], and *T. maritima* CorA [16]. As shown in Fig. S1, secondary structure similarity is particularly high in the α-helical regions N-terminal to TM1, which appear to be homologous to helices α5, α6 and α7 (highlighted in blue, yellow and green) of *T. maritima* CorA, whose tertiary structure has been solved [10]. A unique feature of Mrs2p is the extended C-terminus containing a box of positively charged amino acids [15], which is absent in Lpe10p and other members of the Mrs2p family.

Complementation of *mrs2Δ* and *lpe10Δ* mutants as well as the *mrs2Δ/lpe10Δ* double mutant with Mrs2p and Lpe10p

Chromosomal deletion of *LPE10* (*lpe10Δ* mutant) results in growth reduction on nonfermentable substrates (petite phenotype), which is less pronounced than that resulting from *MRS2* disruption [13]. We analysed the complementation of strains with deleted *MRS2* and/or *LPE10* by Mrs2p or Lpe10p expressed from episomal high copy number (H) or low copy number (L) vectors (Fig. 1). In the cross-wise combinations, $(MRS2)_L$ and $(MRS2)_H$ partly complemented *lpe10Δ*, whereas Lpe10p did not detectably restore growth of *mrs2Δ* cells. The double disruption *mrs2Δ/lpe10Δ* was only partly complemented by $(MRS2)_H$. Interestingly, coexpression of $(MRS2)_H$ and $(LPE10)_L$ fully restored growth of double-disruption cells, whereas the presence of $(MRS2)_H$ and $(LPE10)_H$ led to only weak complementation. These data suggest
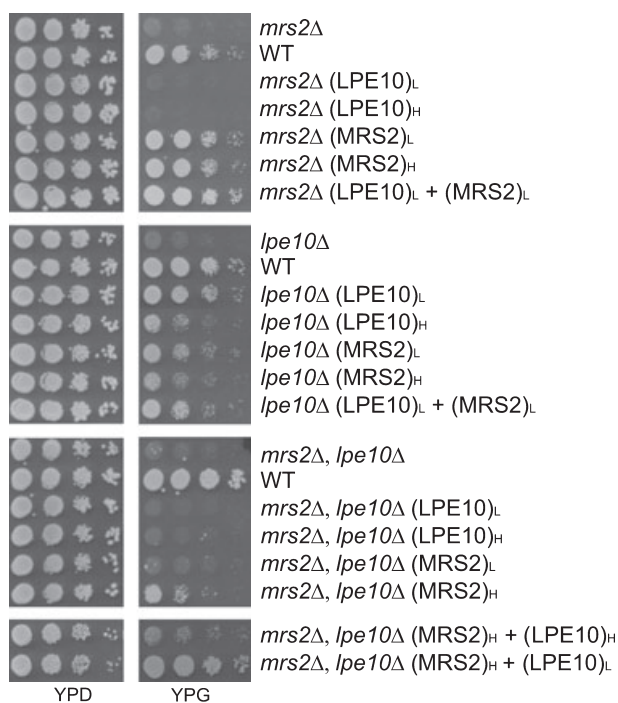
Fig. 1. Growth phenotypes of yeast strains with deleted *MRS2* and/or *LPE10*. Serial dilutions of DBY 747 *mrs2*Δ, DBY747 *lpe10*Δ and the double-deletion strain DBY747 *mrs2*Δ/*lpe10*Δ expressing MRS2 or LPE10 from high (H) or low (L) copy number vectors were spotted on fermentable (YPD) or nonfermentable (YPG) plates and incubated at 28 °C for 3 or 6 days, respectively.

that mitochondrial Mg^{2+} homeostasis in yeast may be dependent on the relative expression levels of Mrs2p and Lpe10p, with the latter playing an inhibitory role if overexpressed. Consistently, high copy number expression of Lpe10p reduced growth.

To determine whether parts of Mrs2p and Lpe10p are exchangeable, we created Mrs2-Lpe10p and Lpe10p-Mrs2p fusion proteins in an attempt to examine respective domain functions (Fig. 2A). Secondary structure prediction data revealed two coiled-coil domains for Mrs2p [15], which turned out to be helical structures homologous to helices α5/α6 and α7 of *T. maritima* CorA [10]. We chose the fusion site between α6 and α7. The chimeric proteins were expressed at similar levels (Fig. 2B), but only weakly restored growth of *mrs2*Δ and also *lpe10*Δ mutant cells. We detected slightly better complementation on expression of Lpe10-Mrs2p fusion proteins, which contained the pore of Mrs2p (Fig. 2C). It is noteworthy that complementation with Lpe10-Mrs2p was more pronounced in both single disruption backgrounds. However, neither of the chimeras could restore growth of *mrs2*Δ/*lpe10*Δ mutant cells.

Loss of high-capacity Mg^{2+} influx in *lpe10*Δ mitochondria is partly restored by Mrs2-Lpe10p fusion proteins

Our previous studies with Eriochrome blue as an indicator to measure Mg^{2+} concentration in mitochondrial extracts have revealed that mitochondria from *LPE10* disruptants contain lower steady-state concentrations of Mg^{2+} than mitochondria from wild-type (WT) cells [13]. Alternatively, we used the Mg^{2+}-sensitive dye mag-fura 2 to determine changes in free ionized inner mitochondrial Mg^{2+} ($[Mg^{2+}]_m$) [4], with the aim of examining whether disruption of *LPE10* affects Mg^{2+} influx into mitochondria isolated from these mutant cells (Fig. 3A). The resting $[Mg^{2+}]_m$ of *lpe10*Δ mitochondria was slightly reduced (to 0.4–0.5 mM) as compared with that of mitochondria overexpressing Lpe10p (0.8 mM) in nominally Mg^{2+}-free buffer. When the external Mg^{2+} concentration $[Mg^{2+}]_e$ was increased stepwise to final concentrations of 1 and 3 mM, *lpe10*Δ mitochondria lacked the rapid, Mg^{2+}-dependent influx. High copy number expression of Lpe10p led to an increased rate of uptake of Mg^{2+} upon addition of 1 and 3 mM $[Mg^{2+}]_e$. Expression of Mrs2–Lpe10p or Lpe10–Mrs2p chimeric proteins partially restored Mg^{2+} influx in *lpe10*Δ mitochondria. In particular, the presence of the Lpe10-Mrs2p chimeric protein resulted in almost complete restoration of Mg^{2+} influx.

In *mrs2*Δ mitochondria expressing the Mrs2-Lpe10p fusion protein, Mg^{2+} influx was similar to that in *lpe10*Δ, with both mutants restoring the influx to a considerable degree (Fig. 3B). We did not find influx of Mg^{2+} into mitochondria isolated from *mrs2*Δ/*lpe10*Δ cells expressing the Mrs2-Lpe10p chimeric proteins (data not shown).

We conclude that the presence of endogenous Lpe10p or Mrs2p in combination with expression of Mrs2-Lpe10p chimeric proteins is sufficient to restore moderate influx of Mg^{2+} into mitochondria.

Deletion of *LPE10* causes reduction of mitochondrial membrane potential (ΔΨ)

We have shown that Mg^{2+} influx of Mrs2p channels is dependent on ΔΨ as a driving force [4]. Using the ΔΨ-sensitive dye 5,5′,6,6′-tetrachloro-1,1′,3,3′-tetraethyl-benzimidazolocarbocyanine iodide (JC-1), we analysed ΔΨ of *lpe10*Δ and *lpe10*Δ/*mrs2*Δ mitochondria, and observed a pronounced loss of relative ΔΨ as compared with WT or *mrs2*Δ mitochondria. Expression of (LPE10)$_H$ in *lpe10*Δ or *mrs2*Δ/*lpe10*Δ cells restored ΔΨ close to WT levels, meaning that the loss of
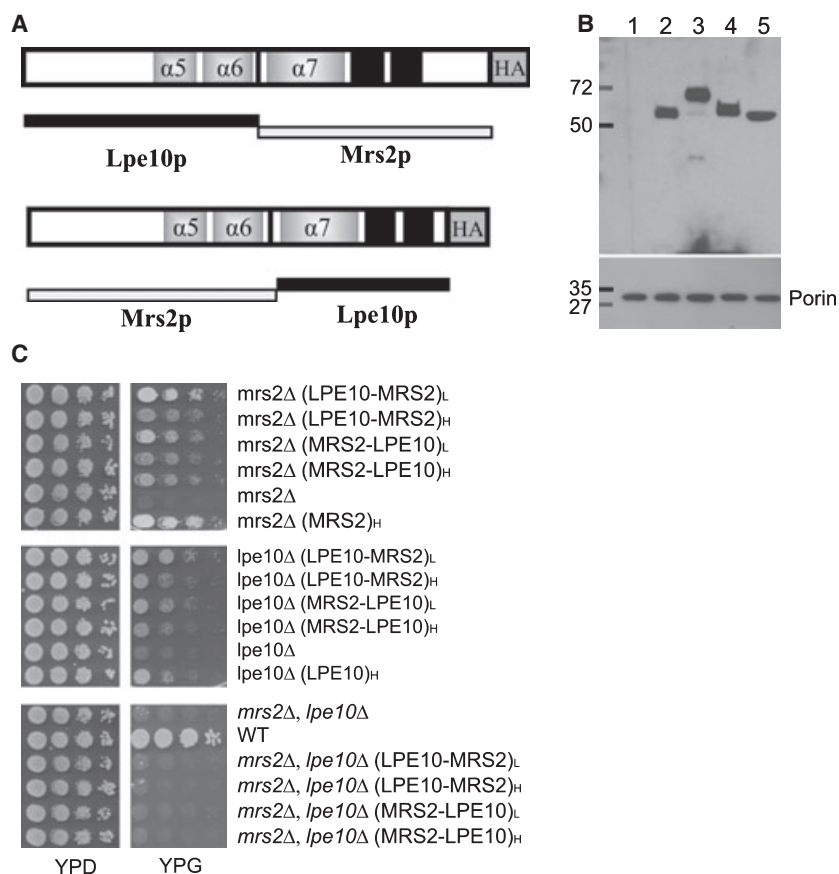
Fig. 2. Characterization of Lpe10-Mrs2p chimeric proteins. (A) Schematic representation of two chimeric proteins with indicated transmembrane (black boxes) and helical regions (α5–α7). (B) Western blot analysis of isolated mitochondria from *mrs2Δ/lpe10Δ* cells transformed with an empty plasmid (lane 1) or a high copy number vector expressing MRS2–HA (lane 2), LPE10–HA (lane 3), LPE10–MRS2–HA (lane 4) or MRS2–LPE10–HA (lane 5). The samples were separated by SDS/PAGE, and proteins were visualized by immunoblotting with an antiserum against HA. The porin protein was used as a loading control. (C) Serial dilutions of DBY 747 *mrs2Δ*, DBY747 *lpe10Δ* and the double-deletion strain DBY747 *mrs2Δ/lpe10Δ* expressing Lpe10-Mrs2p or Mrs2-Lpe10p fusion proteins from high (H) or low (L) copy number vectors were spotted onto fermentable (YPD) or nonfermentable (YPG) plates and incubated at 28 °C for 3 or 6 days, respectively.

$\Delta\Psi$ was dependent on the *lpe10Δ* deletion. Consistently, $(MRS2)_H$ failed to restore $\Delta\Psi$ (Fig. 4A).

Expression of $(LPE10–MRS2)_L$ in the *mrs2Δ/lpe10Δ* background led to restoration of $\Delta\Psi$ up to levels comparable to those detected with full-length Lpe10p present, whereas $(MRS2–LPE10)_L$ was less efficient (Fig. 4A). This is in good agreement with the better complementation and Mg^{2+} influx restoration in *lpe10Δ* cells by the Lpe10-Mrs2p chimeric protein.

We assume that deletion of *LPE10* caused a disturbance in the maintenance of $\Delta\Psi$, which could be a major cause of the substantial reduction in Mg^{2+} influx. To further test this hypothesis, we repolarized *lpe10Δ* mitochondria to determine whether Mg^{2+} influx could be restored. Addition of nigericin, an Na^+, K^+/H^+ ionophore, to the growth medium or to isolated mitochondria is known to restore $\Delta\Psi$ in yeast mutants [17]. Thus, we used mag-fura 2 to measure Mg^{2+} influx into mitochondria isolated from *lpe10Δ* cells pretreated with nigericin. We found Mg^{2+} influx to be restored nearly to WT levels, whereas no significant Mg^{2+} influx could be detected in repolarized mitochondria from *mrs2Δ/lpe10Δ* cells (Fig. 4B). Addi-

tion of nigericin did not have an effect on Mg^{2+} influx into mitochondria isolated from WT cells (data not shown). These experiments clearly showed that Lpe10p has a key regulatory role by maintaining $\Delta\Psi$. However, mitochondria with deleted Lpe10p still retained 30% of WT $\Delta\Psi$. The remaining level might explain why high copy number expression of Mrs2p in *mrs2Δ/lpe10Δ* cells led to weak growth restoration in the absence of Lpe10p.

The F/YGMN motif is essential for the Mg^{2+} transport activity of Lpe10p

The conserved F/YGMN motif in TM1 of CorA-like proteins cannot be varied without loss of Mg^{2+} uptake [4,18]. We performed site-directed mutagenesis, replacing the F/YGMN motif of Lpe10p with ASSV, resulting in the mutant Lpe10-J1. These amino acid substitutions were chosen to create a nonfunctional pore, without substantially affecting the charge or polarity of the protein in this region, which could lead to incorrect folding. Growth of mutant *lpe10Δ* or *mrs2Δ* cells expressing $(LPE10–J1)_H$ was only
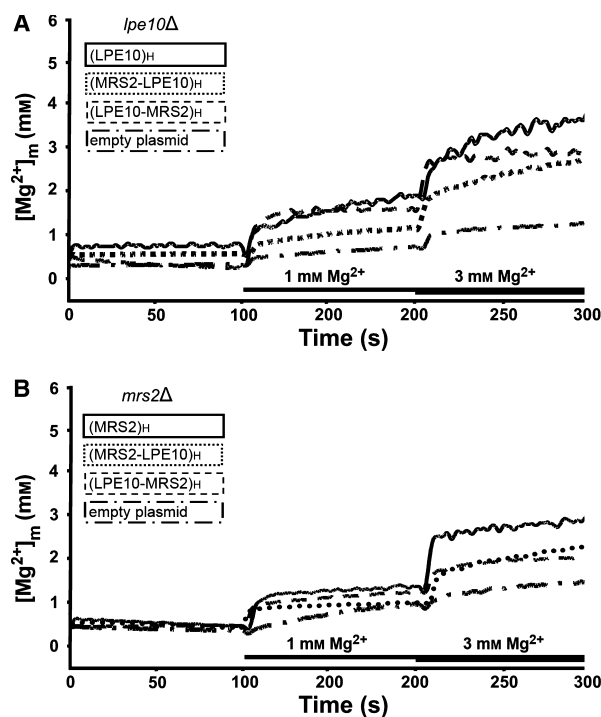
Fig. 3. Expression of Lpe10-Mrs2p chimeric proteins restores Mg^{2+} influx into isolated mitochondria from *lpe10Δ* or *mrs2Δ* cells. $[Mg^{2+}]_e$-dependent changes in $[Mg^{2+}]_m$ in *lpe10Δ* (A) or *mrs2Δ* (B) mitochondria isolated from cells expressing either Lpe10p, Mrs2p or Lpe10-Mrs2p chimeric proteins from a high copy number vector. Mitochondria were loaded with the Mg^{2+}-sensitive fluorescent dye mag-fura 2, and $[Mg^{2+}]_m$ values were determined in nominally Mg^{2+}-free buffer or upon addition of Mg^{2+} to the level of $[Mg^{2+}]_e$, as indicated in the figure. Note that the framing of the different samples (solid, dotted, dashed or dash–dotted lines, respectively) matches the style of the individual traces (identical description in Figs 4B and 5B). Representative curve traces of four individual measurements are shown.

Fig. 4. Chromosomal deletion of *LPE10* leads to loss of $\Delta\Psi$. Mitochondria isolated from *mrs2Δ*, WT, *lpe10Δ* or *mrs2Δ/lpe10Δ* yeast cells transformed with various *MRS2*-containing or *LPE10*-containing high (H) or low (L) copy number plasmids were incubated with JC-1, and the intensity changes of the monomeric and multimeric forms were recorded (A). Relative $\Delta\Psi$ was determined as described in Experimental procedures. (B) $[Mg^{2+}]_e$-dependent changes in $[Mg^{2+}]_m$ in WT, *lpe10Δ* or *mrs2Δ/lpe10Δ* mitochondria. As indicated in some experiments, 1 μM nigericin was added prior to measurements. Representative curve traces of four individual measurements are shown.

minimally restored, and the double-deletion mutant failed to grow (Fig. 5A). (LPE10–J1)$_H$ led to only a minor decrease in $\Delta\Psi$ ($\sim 10\%$) as compared with the level of WT mitochondria, but Mg^{2+} influx could not be detected (Fig. 5B) if this mutant was present in *lpe10Δ* cells. These data suggest that the F/YGMN motif of Lpe10p is critical for restoration of Mg^{2+} influx, possibly in conjunction with Mrs2p. By contrast, mutations in this motif did not affect the ability of the protein to maintain $\Delta\Psi$.

Homo-oligomerization and hetero-oligomerization of Mrs2p and Lpe10p

For a better understanding of how expression of Lpe10p influences the assembly of the Mrs2p channel, we performed cross-linking, Blue native (BN)-PAGE

and coimmunoprecipitation experiments. Initially, we tested for the potential of Lpe10p to homo-oligomerize. Mitochondria were isolated from *mrs2Δ/lpe10Δ* double-disruption cells expressing [LPE10–haemagglutinin (HA)]$_H$, and treated with the chemical cross-linker oPDM. We found that the anti-HA serum reacted with a major product representing the Lpe10p-HA monomer (50.4 kDa), and upon addition of the cross-linker, additional bands of higher molecular mass of ~ 110 kDa and ~ 160 kDa, as expected for an Lpe10p-HA dimer and possibly trimer, respectively, were obtained (Fig. 6A). Accordingly, Lpe10p was apparently able to form homo-oligomers, as previously shown for Mrs2p [4]. However, we cannot exclude the presence of an undefined protein interacting with
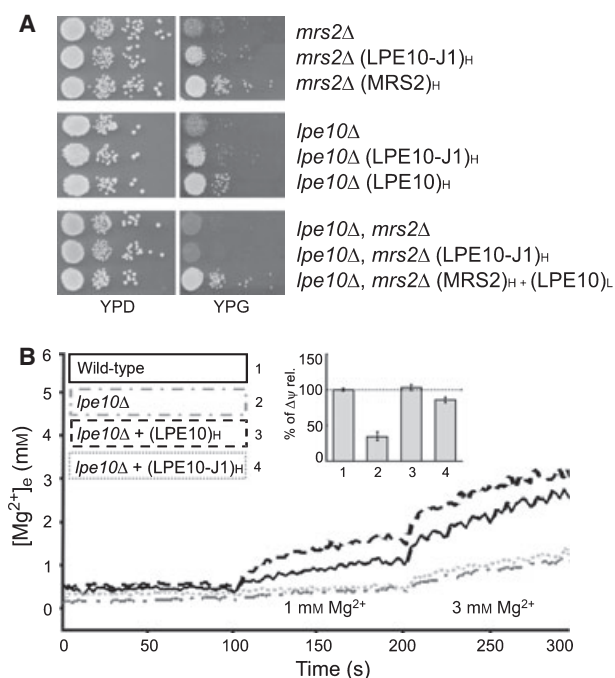
Fig. 5. The highly conserved F/YGMN motif is essential for the Mg^{2+} influx mediated by Lpe10p. (A) Serial dilutions of *mrs2Δ* or *lpe10Δ* or the double-deletion strain *mrs2Δ/lpe10Δ* transformed with high (H) or low (L) copy number plasmids expressing MRS2, LPE10 or the mutant variant LPE10–J1, were spotted on fermentable (YPD) or nonfermentable (YPG) plates and incubated at 28 °C for 3 or 6 days, respectively. (B) $[Mg^{2+}]_e$-dependent changes in $[Mg^{2+}]_m$ in WT or *lpe10Δ* mitochondria expressing WT LPE10 or the mutant variant LPE10–J1 from a high copy number plasmid. Representative curve traces of three individual measurements are shown. Mitochondrial membrane potential was determined as described in Experimental procedures for wild-type (1) and *lpe10Δ* (2) cells, as well as for *lpe10Δ* cells expressing LPE10 (3) or the mutant version LPE10–J1 (4) from high copy number plasmids.

Lpe10p on addition of the cross-linking reagent. We did not detect Lpe10p complexes as large as Mrs2p oligomers, which were shown to be homopentameric [4]. When we coexpressed $(LPE10–HA)_H$ and $(MRS2-Myc)_H$ and added oPDM, anti-HA serum recognized Lpe10p-HA-containing complexes, which were increased in size as compared with those detected without coexpression of Mrs2p-Myc (Fig. 6B, upper picture). Incubation of the same blot with anti-myc serum resulted in identification of Mrs2p-Myc-containing complexes of high molecular mass, which were of similar size as the largest complexes found with the anti-HA serum (Fig. 6B, lower picture). Interestingly, no intermediate dimeric or trimeric assemblies were detected in Mrs2p-cross-linking experiments in the absence of Lpe10p [4].

We continued with BN-PAGE experiments, and transformed *mrs2Δ/lpe10Δ* cells with different combi-

nations of Mrs2p-Myc, Mrs2p-HA or Lpe10p-HA (64, 57.5 and 50.4 kDa, respectively). Proteins from isolated mitochondria were separated by BN-PAGE according to Schagger *et al.* [19]. As shown in Fig. 6C, expression of $(LPE10–HA)_L$ or $(LPE10–HA)_H$ resulted in a band with an apparent molecular mass of ~ 230 kDa (lanes 2 and 3). Upon coexpression of $(MRS2-Myc)_H$ and $(LPE10–HA)_L$ or $(LPE10–HA)_H$, the anti-HA serum recognized additional bands of ~ 300 and 400 kDa, and the intensity of the band at ~ 230 kDa decreased markedly (Fig. 6C, lanes 4 and 5). No bands were visible when proteins of mitochondria lacking an HA tag were immunoblotted (Fig. 6C, lane 1). These results strengthened our assumption that Lpe10p is involved in the assembly of the Mrs2p-based Mg^{2+} channel *in vivo*.

To confirm a direct interaction between Lpe10p and Mrs2p, we performed coimmunoprecipitation experiments. Mitochondria from *mrs2Δ/lpe10Δ* double-disruptant cells coexpressing LPE10–HA and MRS2-Myc, as well as mitochondria from cells expressing either LPE10–HA or MRS2-Myc or the empty vectors, were used. Upon coexpression of LPE10–HA and MRS2-Myc, both proteins were detected in the anti-HA immunoprecipitate (Fig. 6D, elution fractions, lanes 1 and 5). In the control experiments with mitochondria from cells expressing only LPE10–HA, the protein was found unbound (Fig. 6D, supernatant fraction, lane 3) as well as bound to HA-coated beads (Fig. 6D, elution fraction, lane 3). If mitochondria from cells expressing only MRS2-Myc were used, the respective protein was exclusively found in the unbound fraction (Fig. 6D, supernatant fraction, lane 4). These results confirm a tight interaction between the two proteins.

Lpe10p modulates the conductance of the Mrs2p channel

To initially investigate whether Lpe10p is able to generate a homomeric Mg^{2+}-permeable channel in the absence of Mrs2p, we used single-channel patch clamp recordings on giant lipid vesicles fused with inner mitochondrial membranes from $(LPE10)_H$-expressing *mrs2Δ/lpe10Δ* cells. We have previously used this technique to characterize the Mrs2p-based high-conductance channel with a calculated conductance of ~ 155 pS [5]. Inside-out patches were studied in a 105 mM $MgCl_2$-based pipette solution and an *N*-methyl-D-glucamine gluconate-based bath solution. Current traces at test potentials ranging from $+5$ to -35 mV resulted in an increase in single-channel amplitudes with decreasing potentials in four of 14 experiments, consistent with Mg^{2+}-permeable channels
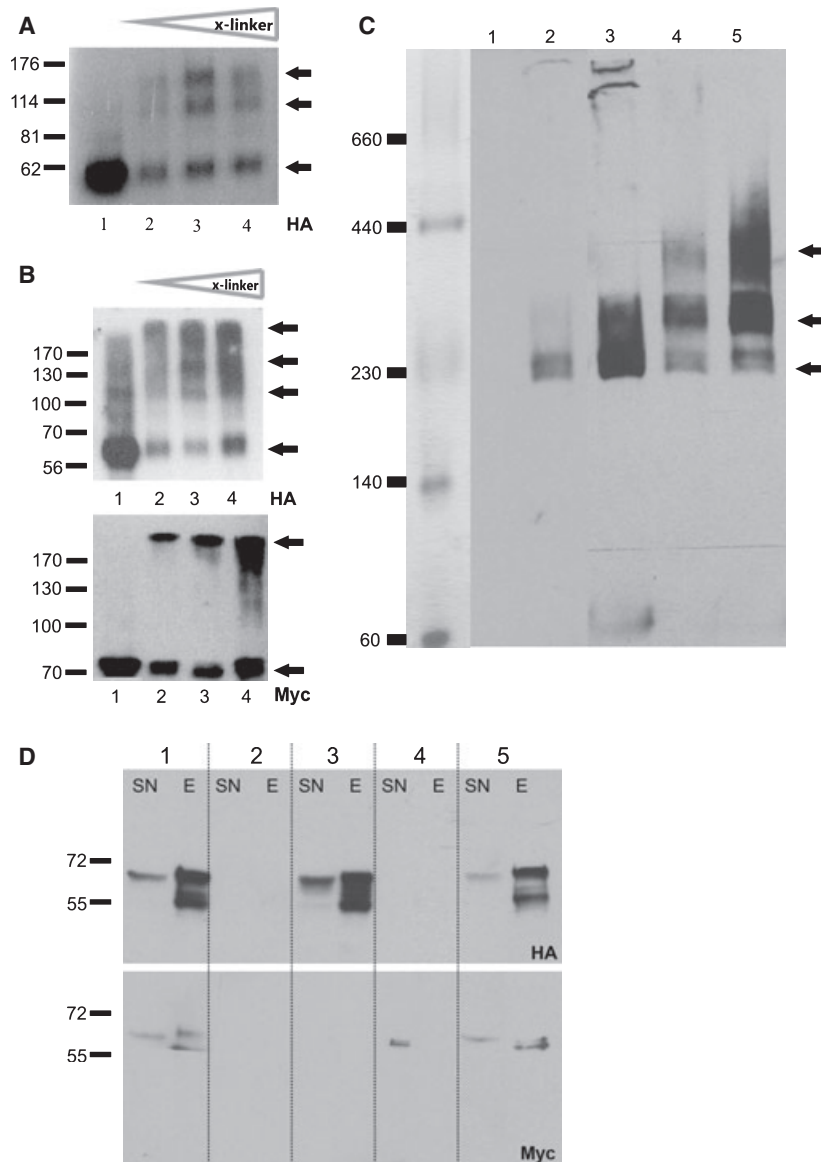
Fig. 6. Lpe10p influences the Mrs2p channel complex. (A) Isolated mitochondria of *lpe10Δ* cells transformed with LPE10–HA-expressing high copy number plasmid were incubated in sulfhydryl buffer without (lane 1) or with the chemical cross-linker oPDM at final concentrations of 30 μM (lane 2), 100 μM (lane 3) and 300 μM (lane 4), separated by SDS/PAGE, and analysed by immunoblotting with anti-HA serum. (B) Isolated mitochondria of *mrs2Δ/lpe10Δ* cells transformed with LPE10–HA and MRS2–Myc from multicopy plasmids were incubated in sulfhydryl buffer without (lane 1) or with the chemical cross-linker oPDM (lanes 2–4; 30, 100 or 300 μM, respectively), separated by SDS/PAGE, and analysed by immunoblotting with anti-HA serum (upper blot) or anti-Myc serum (lower blot). (C) High molecular mass complexes containing Lpe10p-HA and/or Mrs2p-Myc detected by BN-PAGE. Mitochondria of *mrs2Δ/lpe10Δ* cells were transformed with an empty plasmid (lane 1) or the following proteins expressed from high (H) or low (L) copy number plasmids: (LPE10–HA)$_L$ (lane 2), (LPE10–HA)$_H$ (lane 3), (MRS2-Myc)$_H$ and (LPE10–HA)$_L$ (lane 4) or (MRS2-Myc)$_H$ and (LPE10–HA)$_H$ (lane 5). Samples were solubilized in 1.2% laurylmaltoside, and products were visualized anti-HA serum. (D) Coimmunoprecipitation experiments with Lpe10p-HA and Mrs2p-Myc. Isolated mitochondria of *mrs2Δ/lpe10Δ* cells expressing LPE10–HA and MRS2-Myc from high copy number plasmids (lanes in blot area 1), the empty vectors (lanes in blot area 2), LPE10–HA or Mrs2-Myc alone (lanes in blot area 3 and 4, respectively) and coexpressing LPE10–HA from a low and Mrs2-Myc from a high copy number vector (lanes in blot area 5) were solubilized and incubated with anti-HA serum-coated beads. Unbound (supernatant, SN) and bound (elution, E) fractions were separated by SDS/PAGE, and analysed by immunoblotting with anti-HA serum (upper blot) or anti-Myc serum (lower blot).

(Fig. 7A). A current–voltage relationship determined at negative potentials yielded a single-channel conductance of 61 ± 5 pS (Fig. 7C). No single-channel events were recorded in the other 10 experiments. As a similar conductance of 67 ± 4 pS (in three of 15 experiments) was also observed in vesicles from *mrs2Δ/lpe10Δ* cells [5], resulting from channel activity of unknown origin, we suggest that Lpe10p is not capable of forming a detectable Mg^{2+}-permeable channel in the absence of Mrs2p.

As we found a significant effect of Lpe10p expression on the size of Mrs2p-containing complexes (Fig. 6), we examined whether the presence of Lpe10p might affect the characteristics of the Mrs2p channel (e.g. its conductance of ∼ 155 pS) in giant lipid vesicles. Current traces

of mitochondrial vesicles from cells expressing (LPE10)$_H$ and (MRS2)$_H$ revealed unique single-channel amplitudes at negative potentials of −15 and −35 mV as compared with *mrs2Δ/lpe10Δ* vesicles with or without expressed Lpe10p (Fig. 7B). Current–voltage relationships recorded from vesicles expressing Lpe10p and Mrs2p determined within +5 and −45 mV revealed a novel conductance of 103 ± 5 pS in four of seven experiments, with a reversal potential of +22 mV (Fig. 7B). Mrs2p channels yielded a reversal potential of > 40 mV in identical solutions [5]. The typical conductance of vesicles expressing Mrs2p only (∼ 155 pS) was not observed, whereas the conductance from a channel of unknown origin (61 pS) was also observed in one of seven experiments (data not shown). We conclude that
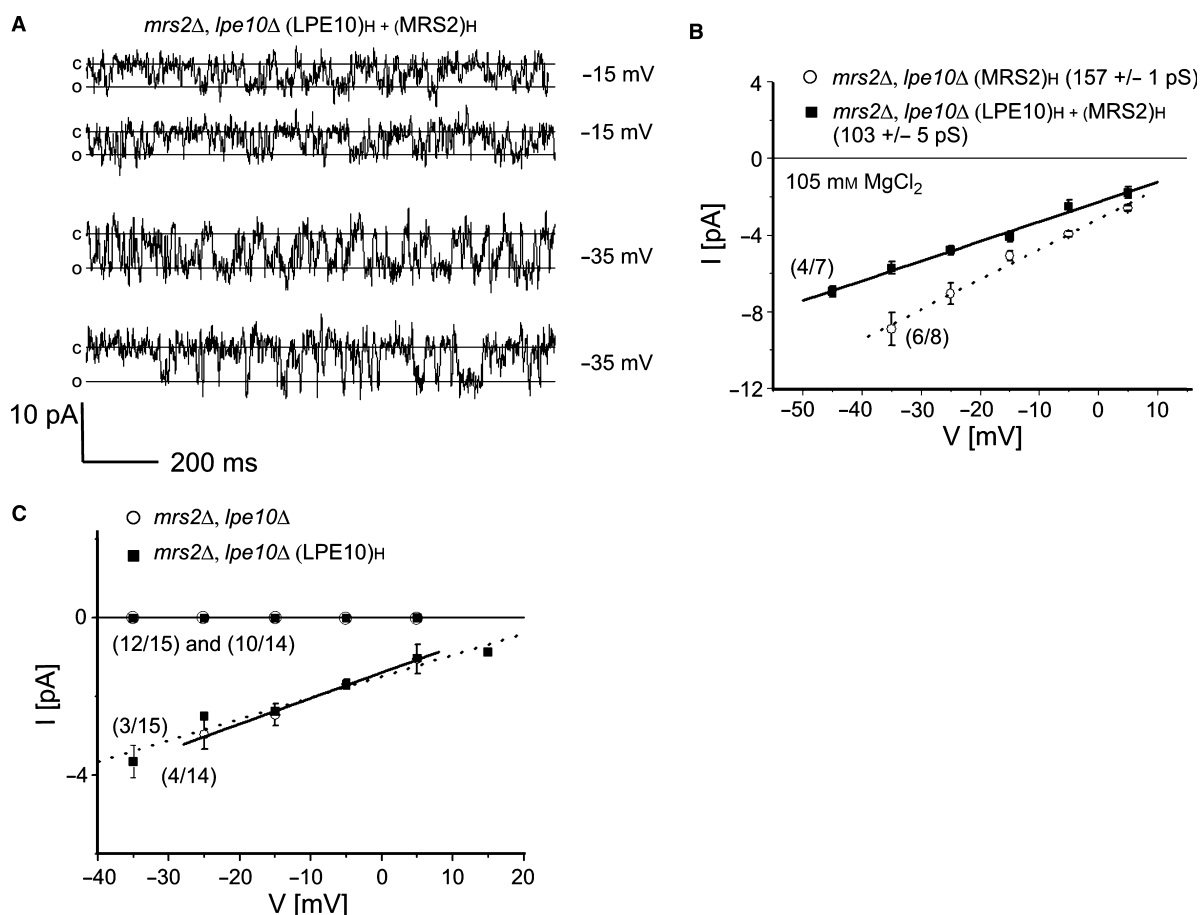
Fig. 7. Coexpression of Lpe10p and Mrs2p results in a unique single-channel conductance. Single-channel currents were obtained in an inside-out configuration from reconstituted giant vesicles fused with the inner mitochondrial membrane. (A) Recordings of vesicles overexpressing Lpe10p and Mrs2p from a multicopy plasmid were performed in the *mrs2Δ/lpe10Δ* background. Mg^{2+} (105 mM) was used as a charge carrier, and currents were recorded at −15 and −35 mV. (B) Current–voltage relationships were determined from amplitude histograms of single-channel currents at the indicated potentials, and yielded a conductance of 103 ± 5 pS (*n* = 4/7) for Lpe10p and Mrs2p coexpression; overexpression of Mrs2p resulted in a conductance of 157 ± 1 pS (*n* = 6–8). (C) Current–voltage relationships of endogenous single-channel currents of vesicles in the *mrs2Δ/lpe10Δ* background yielded a similar conductance (67 ± 4 pS, *n* = 3–15) as for overexpression of Lpe10p in a similar background (61 ± 5 pS, *n* = 4/14). In the remaining experiments, no single-channel currents were detected.

Lpe10p assembles with Mrs2p, thereby leading to a novel conductance of the Mrs2p channel.

Discussion

If the mitochondrial inner membrane protein Lpe10p and its homolog in *S. cerevisiae*, Mrs2p, fulfilled exactly the same functions, it would have been sufficient to retain one of the two proteins during evolution. In fact, the proteins cannot substitute for each other, and expression of one of the proteins in the *mrs2Δ/lpe10Δ* background is not sufficient to fully restore cell growth. We showed that only high copy number expression of Mrs2p weakly restored growth in the double-disruption strain, whereas Lpe10p failed to do so. In addition, Lpe10p and Mrs2p chimeric proteins were designed, and these restored Mg^{2+} influx in *mrs2Δ* as well as in *lpe10Δ* cells. Expression of a chimeric protein consisting of the N-terminal part of Lpe10p and the C-terminal region of Mrs2p, including its pore, restored growth and Mg^{2+} influx better than expression of a chimeric protein composed of the N-terminal part of Mrs2p and the C-terminal end of Lpe10p. Using mag-fura 2 for the detection of free, ionized Mg^{2+} inside mitochondria, we demonstrated that mitochondria of *lpe10Δ* cells lack the rapid Mg^{2+} influx, similar to mitochondria from *mrs2Δ* cells [4].

Interestingly, measurements of $\Delta\Psi$ revealed that deletion of *LPE10* goes along with a pronounced drop in $\Delta\Psi$, which was not observed if *MRS2* was deleted. As it is necessary to use $\Delta\Psi$-dissipating (valinomycin) and $\Delta\Psi$-increasing (nigericin) chemicals for the calibration of JC-1, i.e. setting artificial minimum and maximum $\Delta\Psi$ levels, it is not possible to determine absolute values of $\Delta\Psi$ reduction. However, expression of Lpe10p in *lpe10Δ* or *mrs2Δ/lpe10Δ* cells restored $\Delta\Psi$ to WT levels. Addition of nigericin, a K^+/H^+ ionophore, restored $\Delta\Psi$ and, as a consequence, Mg^{2+} influx in *lpe10Δ* mitochondria. We also found that expression of the Lpe10-Mrs2p chimeric protein re-established $\Delta\Psi$ to a significant degree, whereas the Mrs2-Lpe10p chimera failed to do so. Furthermore, mutation of the conserved F/YGMN motif of Lpe10p led to a strong decrease in Mg^{2+} influx, but no significant impact on $\Delta\Psi$. As Mrs2p forms an Mg^{2+} channel, the primary driving force for this system is the membrane potential, rather than pH changes in the mitochondrial matrix (ΔpH). However, we cannot fully exclude the possibility that deletion of Lpe10p also influences ΔpH, and that some of the effects of nigericin are attributable to changes in ΔpH.

Our findings led us to assume that both Mrs2p and Lpe10p physiologically contribute to the assembly of a functional Mg^{2+} channel. Moreover, Lpe10p is additionally involved in the maintenance of $\Delta\Psi$ *in vivo*, a function that remains even with a mutated F/YGMN motif. It remains to be determined in what way Lpe10p has an impact on the membrane potential of yeast mitochondria, thereby setting the driving force for the influx of Mg^{2+}.

In vitro chemical cross-linking assays and BN-PAGE experiments revealed homo-oligomeric Lpe10p complexes similar to those formed by Mrs2p [4]. Thus, potential domains for oligomerization are present in the protein encoded by *LPE10*, which is not surprising, given the similarities in secondary structure between Mrs2p and Lpe10p. BN-PAGE experiments showed a size shift of the Lpe10p complex if Mrs2p was coexpressed. Finally, using coimmunoprecipitation, we were able to pull down the entire Mrs2 protein complex, and clearly identified Lpe10p as a member of this. These findings demonstrate a tight interaction of both proteins within this complex. We speculate that Lpe10p is a structural as well as modulating factor of the Mrs2p channel complex, leading to a stronger phenotype of *LPE10* deletion than the *MRS2* mutant itself. Additionally, reduction of $\Delta\Psi$ may also have adverse effects on the function of other mitochondrial proteins.

Single-channel recordings on giant lipid vesicles with overexpressed Lpe10p isolated from *mrs2Δ/lpe10Δ* cells, as previously reported [5], did not reveal an Lpe10p-specific Mg^{2+}-permeable channel activity. However, coexpression of Lpe10p and Mrs2p decreased the Mrs2p channel conductance from ~ 155 to ~ 103 pS. Therefore, our data suggest that Lpe10p plays an important role in the physiological formation of the mitochondrial Mg^{2+} channel with a unique conductance resulting from heteromeric assembly of Mrs2p and Lpe10p. Whereas direct binding of matrix Mg^{2+} to the N-terminal domain of Mrs2p results in fast closing of the channel [8,9], the reduction of the Mrs2p channel conductance by $\sim 30\%$ (from ~ 155 to ~ 103 pS) suggests a possible regulatory role of Lpe10p in addition to its impact on $\Delta\Psi$. As compared with the Mg^{2+} conductance of 40 pS mediated by the mammalian TRPM7 channel [20,21], the conductance of 155 pS of the Mrs2p channel is surprisingly high. It is tempting to speculate that Mg^{2+} influx at strong, negative mitochondrial potentials is somewhat limited by this heteromeric Lpe10-Mrs2p channel assembly with a reduced conductance, whereas a decrease in Lpe10p expression levels leading to a reduction in mitochondrial potential might be compensated by the higher conductance of the homomeric Mrs2p channel.

In mammalian cells, only a single Mrs2p homolog has been identified [22,23]. Owing to the activity of numerous other 'modern' Mg^{2+} transporters [24], Lpe10p might be redundant in mammalian cells, whereas its presence in yeast, which lacks modern Mg^{2+} transporters, is obligatory.

Finally, we would like to propose a new name for *LPE10* (yeast ORF YPL060w), as *LPE* has only been the systematic name for many uncharacterized genes of *S. cerevisiae* [13]. We suggest calling it *MFM1* (Mrs2 function modulating factor 1), a synonym that best reflects the function of the protein.

Experimental procedures

Yeast strains, growth media and genetic procedures

The yeast *S. cerevisiae* DBY747 WT strain, the isogenic *mrs2Δ* deletion strain (DBY *mrs2-1*), the *lpe10Δ* deletion strain (DBY *lpe10-1*) and the *mrs2Δ/lpe10Δ* double-disruption (DBY747 *mrs2-2 lpe10-2*) have been described previously [3,13,14]. Yeast cells were grown to stationary phase in rich medium (YPD) with 2% glucose (Sigma Aldrich, Schnelldorf, Germany) as a carbon source.

Plasmid constructs

The plasmid construct YEp351 MRS2–HA [3] was digested with *Sac*I and *Sph*I and cloned into an empty YEp112 vector cut with the same restriction enzymes. The generated YEp112 MRS2–HA construct was digested with *Not*I and dephosphorylated (Antarctic Phosphatase, NEB), and a cassette coding for the myc epitope tag was cloned in frame with *MRS2* at the *Not*I site, resulting in the construct YEp112–MRS2–Myc.

To create Lpe10-Mrs2p-HA and Mrs2-Lpe10p-HA fusion proteins, a *Bcl*I restriction site was introduced at position 780 by use of overlap extension PCR according to [25]. The mutagenic forward primer 5′-AGTCTCCTAAGG**A**TG**A**TCATTCGGACTTGGAAATGC-3′ (mismatched bases in bold) and the mutagenic reverse primer 5′-GCATTTCCAAGTCCGAA**T**GA**T**CATCCTTAGGAG ACT-3′ were used in combination with the forward primer 5′-GTTGTCCTCCACCAAGAATAACTCTC-3′ and the reverse primer 5′-CCGCCACTGAAGTAAACCCC-3′. A double amino acid change (Asn261 to Asp and Phe262 to His) was thereby introduced, but this did not interfere with growth on nonfermentable carbon sources (data not shown). The resulting construct YEp351 MRS2–HA* *Bcl*I was digested with *Sph*I and *Bcl*I, and the isolated fragment was cloned into an *Sph*I-digested and *Bcl*I-digested YEp351 LPE10 vector [13] to generate the construct YEp351 MRS2–LPE10. The YEp351 LPE10 construct was digested

with *Sph*I and *Bcl*I, and the isolated fragment was cloned into an *Sph*I-cut and *Bcl*I-cut YEp351 MRS2–HA* *Bcl*I vector to create the YEp351 LPE10–MRS2–HA construct (N-terminal 281 amino acids of Lpe10p and C-terminal 250 amino acids of Mrs2p). The YEp351 MRS2–LPE10 construct was linearized with *Not*I, and a cassette coding for the HA epitope tag was cloned in frame with the *MRS2–LPE10* fusion gene, resulting in the construct YEp351 MRS2–LPE10–HA (N-terminal 260 amino acids of Mrs2p and C-terminal 135 amino acids of Lpe10p). Both this and the YEp351 LPE10–MRS2–HA construct were cut with *Sac*I and *Sph*I, and cloned into an *Sac*I-digested and *Sph*I-digested YCp111 vector, resulting in the constructs YCp111 MRS2–LPE10–HA and YCp111 LPE10–MRS2–HA.

The plasmid construct YEp351 MRS2–HA was digested with *Sac*I and *Sph*I, and cloned into an empty YCp111 vector digested with the same restriction enzymes, resulting in the construct YCp111 MRS2–HA. The constructs YCp LPE10–HA and YEp351 LPE10–HA have been previously described [13].

In order to mutate the F/YGMN motif of Lpe10p to ASSV, overlap extension PCR was used with the mutagenic forward primer 5′-GCTCTATTCCTGTCTATCGCTAGCT CTGTTCTGGAAAGTTTCATAGAAG-3′ and the mutagenic reverse primer 5′-CTTCTATGAAACTTTCCAGA ACAGAGCTAGCGATAGAACCCAGGAATAGAGC-3′, in combination with the forward primer 5′-AAGCTTGCA TGACTGCAGGTCGACTC-3′ and the reverse primer 5′-GAATTCGAGCTCGGTACCCGGGGATAA-3′. Verification of positive clones was performed by restriction analysis with *Nhe*I, and the mutation was indicated Lpe10–J1. No additional mutations were found by sequencing.

Isolation of mitochondria and measurement of $[Mg^{2+}]_m$ by spectrofluorometry

Isolation of mitochondria and the measurement of Mg^{2+} influx into mitochondria were performed as previously described [4]. In some experiments, mitochondrial preparations equivalent to 1 mg of total mitochondrial protein were treated with 1 μM nigericin (Sigma-Aldrich, Germany) 5 min prior to the measurement.

BN-PAGE

Eighty micrograms of isolated mitochondrial protein was extracted by addition of 40 μL of extraction buffer (750 mM aminocaproic acid, 50 mM Bis–Tris/HCl, pH 7.0) and laurylmaltoside to a final concentration of 1.2%. After incubation on ice for 30 min, the samples were centrifuged at 45 000 *g* for 30 min, and the supernatant was supplemented with a 0.25 volume of sample buffer (500 mM aminocaproic acid, 5% Serva blue G). The solubilized protein solution was analyzed by BN-PAGE on a 5–18% linear polyacrylamide gradient [19]. The gel was blotted

onto a poly(vinylidene difluoride) membrane, which was stained with Coomassie Blue reagent or analysed by immunoblotting with an HA antiserum.

Chemical cross-linking and PAGE

Thirty micrograms of total mitochondrial protein was mixed with loading buffer containing β-mercaptoethanol, and samples were heated to 80 °C for 4 min before being loaded onto SDS/PAGE gels. HA protein-containing bands were visualized by the use of an anti-HA serum (Covance), and myc protein-containing bands by an anti-Myc serum (Sigma-Aldrich). Chemical cross-linking experiments were performed as previously reported [4], using the cross-linking reagent oPDM (Sigma Aldrich).

Coimmunoprecipitation

Five milligrams of mitochondrial protein was resuspended in solubilization buffer (500 mM NaCl, 100 mM Tris/HCl, pH 7.8), and membrane proteins were solubilized by addition of Triton X-100 to a final concentration of 1.2% and incubation for 30 min at 4 °C under gentle rotation. After centrifugation at 43 000 *g* for 30 min (4 °C) to remove nonsolubilized mitochondrial debris, the Triton X-100 concentration of the supernatant was reduced to 0.8%. One hundred microliters of Protein A Dynabeads (Invitrogen, Lofer, Austria) was washed with solubilization buffer + 0.8% Triton X-100. Coating of the beads was performed with an HA antibody (Covance) in the same buffer for 30 min at 4 °C under rotation. HA-coated beads were washed twice and incubated with the clarified supernatant for 1 h at 4 °C under gentle rotation. After the binding reaction, the supernatant was removed, and the beads were washed three times with solubilization buffer including 0.8% Triton X-100. Proteins were eluted from the beads by heating for 5 min at 80 °C in SDS sample buffer. The supernatant and the elution fraction were analyzed on a 10% SDS/polyacrylamide gel, and western blotting was performed as described above.

Determination of ΔΨ

Isolated yeast mitochondria equivalent to 50 μg of total mitochondrial protein were incubated with 0.5 μM JC-1 (Molecular Probes, NL) for 7 min at room temperature. The sample was spun down and resuspended in 2 mL of 0.6 M sorbitol buffer supplemented with 0.5 mM ATP, 0.2% succinate and 0.01% pyruvate. The intensity changes of the monomeric form (low energy, 540 nm) and of the multimeric form (high energy, 590 nm) were recorded with the Scan mode of a Perkin Elmer LS55 luminescence photometer. Data collection was performed with FL WINLAB4. For calibration, similar samples were treated in parallel,

either with nigericin (1 μM), to determine the maximum of energization, or carbonyl cyanide p-(trifluoromethoxy)-phenylhydrazone (1 μM), to determine the minimum of energization, respectively. These datasets were used to calculate a calibration curve for every single measurement for the determination of the percentage of relative ΔΨ.

Patch clamp recordings of ion channels

Single-channel currents at various test potentials were recorded, as previously described [5], from giant lipid vesicles fused with inner mitochondrial membrane vesicles, using the patch clamp technique [26].

Computer analysis

Secondary structure analysis (prediction of transmembrane domains, helices and loops) of *S. cerevisiae* Mrs2, *S. cerevisiae* Lpe10, *A. thaliana* Mrs2-7 and *T. maritima* CorA was performed with Jpred3, a consensus method for protein secondary structure prediction at the University of Dundee.

Acknowledgements

References

1 Iwatsuki H, Lu YM, Yamaguchi K, Ichikawa N & Hashimoto T (2000) Binding of an intrinsic ATPase inhibitor to the F(1)FoATPase in phosphorylating conditions of yeast mitochondria. *J Biochem* **128**, 553–559.

2 Rodriguez-Zavala JS & Moreno-Sanchez R (1998) Modulation of oxidative phosphorylation by Mg^{2+} in rat heart mitochondria. *J Biol Chem* **273**, 7850–7855.

3 Bui DM, Gregan J, Jarosch E, Ragnini A & Schweyen RJ (1999) The bacterial magnesium transporter CorA can functionally substitute for its putative homologue Mrs2p in the yeast inner mitochondrial membrane. *J Biol Chem* **274**, 20438–20443.

4 Kolisek M, Zsurka G, Samaj J, Weghuber J, Schweyen RJ & Schweigel M (2003) Mrs2p is an essential component of the major electrophoretic Mg^{2+} influx system in mitochondria. *EMBO J* **22**, 1235–1244.

5 Schindl R, Weghuber J, Romanin C & Schweyen RJ (2007) Mrs2p forms a high conductance Mg^{2+} selective channel in mitochondria. *Biophys J* **93**, 3872–3883.

6 Niegowski D & Eshaghi S (2007) The CorA family: structure and function revisited. *Cell Mol Life Sci* **64**, 2564–2574.

7 Graschopf A, Stadler JA, Hoellerer MK, Eder S, Sieghardt M, Kohlwein SD & Schweyen RJ (2001) The yeast plasma membrane protein Alr1 controls Mg^{2+} homeostasis and is subject to Mg2+-dependent control of its synthesis and degradation. *J Biol Chem* **276**, 16216–16222.

8 Payandeh J & Pai EF (2006) A structural basis for Mg^{2+} homeostasis and the CorA translocation cycle. *EMBO J* **25**, 3762–3773.

9 Eshaghi S, Niegowski D, Kohl A, Martinez MD, Lesley SA & Nordlund P (2006) Crystal structure of a divalent metal ion transporter CorA at 2.9 angstrom resolution. *Science* **313**, 354–357.

10 Lunin VV, Dobrovetsky E, Khutoreskaya G, Zhang R, Joachimiak A, Doyle DA, Bochkarev A, Maguire ME, Edwards AM & Koth CM (2006) Crystal structure of the CorA Mg^{2+} transporter. *Nature* **440**, 833–837.

11 Gebert M, Meschenmoser K, Svidova S, Weghuber J, Schweyen R, Eifler K, Lenz H, Weyand K & Knoop V (2009) A root-expressed magnesium transporter of the MRS2/MGT gene family in Arabidopsis thaliana allows for growth in low-Mg^{2+} environments. *Plant Cell* **21**, 4018–4030.

12 Knoop V, Groth-Malonek M, Gebert M, Eifler K & Weyand K (2005) Transport of magnesium and other divalent cations: evolution of the 2-TM-GxN proteins in the MIT superfamily. *Mol Genet Genomics* **274**, 205–216.

13 Gregan J, Bui DM, Pillich R, Fink M, Zsurka G & Schweyen RJ (2001) The mitochondrial inner membrane protein Lpe10p, a homologue of Mrs2p, is essential for magnesium homeostasis and group II intron splicing in yeast. *Mol Gen Genet* **264**, 773–781.

14 Wiesenberger G, Waldherr M & Schweyen RJ (1992) The nuclear gene MRS2 is essential for the excision of group II introns from yeast mitochondrial transcripts in vivo. *J Biol Chem* **267**, 6963–6969.

15 Weghuber J, Dieterich F, Froschauer EM, Svidova S & Schweyen RJ (2006) Mutational analysis of functional domains in Mrs2p, the mitochondrial Mg^{2+} channel protein of Saccharomyces cerevisiae. *FEBS J* **273**, 1198–1209.

16 Maguire ME (2006) The structure of CorA: a Mg(2+)-selective channel. *Curr Opin Struct Biol* **16**, 432–438.

17 Nowikovsky K, Reipert S, Devenish RJ & Schweyen RJ (2007) Mdm38 protein depletion causes loss of mitochondrial K^+/H^+ exchange activity, osmotic swelling and mitophagy. *Cell Death Differ* **14**, 1647–1656.

18 Szegedy MA & Maguire ME (1999) The CorA Mg(2+) transport protein of Salmonella typhimurium. Mutagen-esis of conserved residues in the second membrane domain. *J Biol Chem* **274**, 36973–36979.

19 Schagger H, Cramer WA & von Jagow G (1994) Analysis of molecular masses and oligomeric states of protein complexes by blue native electrophoresis and isolation of membrane protein complexes by two-dimensional native electrophoresis. *Anal Biochem* **217**, 220–230.

20 Monteilh-Zoller MK, Hermosura MC, Nadler MJ, Scharenberg AM, Penner R & Fleig A (2003) TRPM7 provides an ion channel mechanism for cellular entry of trace metal ions. *J Gen Physiol* **121**, 49–60.

21 Nadler MJ, Hermosura MC, Inabe K, Perraud AL, Zhu Q, Stokes AJ, Kurosaki T, Kinet JP, Penner R, Scharenberg AM *et al.* (2001) LTRPC7 is a Mg.ATP-regulated divalent cation channel required for cell viability. *Nature* **411**, 590–595.

22 Piskacek M, Zotova L, Zsurka G & Schweyen RJ (2009) Conditional knockdown of hMRS2 results in loss of mitochondrial Mg(2+) uptake and cell death. *J Cell Mol Med* **13**, 693–700.

23 Zsurka G, Gregan J & Schweyen RJ (2001) The human mitochondrial Mrs2 protein functionally substitutes for its yeast homologue, a candidate magnesium transporter. *Genomics* **72**, 158–168.

24 Quamme GA (2010) Molecular identification of ancient and modern mammalian magnesium transporters. *Am J Physiol Cell Physiol* **298**, C407–C429.

25 Pogulis RJ, Vallejo AN & Pease LR (1996) In vitro recombination and mutagenesis by overlap extension PCR. *Methods Mol Biol* **57**, 167–176.

26 Hamill OP, Marty A, Neher E, Sakmann B & Sigworth FJ (1981) Improved patch-clamp techniques for high-resolution current recording from cells and cell-free membrane patches. *Pflugers Arch* **391**, 85–100.

Supporting information

The following supplementary material is available:
Fig. S1. Secondary structure prediction of CorA and its homologues in yeast and plants.

This supplementary material can be found in the online version of this article.

Please note: As a service to our authors and readers, this journal provides supporting information supplied by the authors. Such materials are peer-reviewed and may be re-organized for online delivery, but are not copy-edited or typeset. Technical support issues arising from supporting information (other than missing files) should be addressed to the authors.

3.4. Publication IV

Structural and functional characterization of the N-terminal domain of Mrs2 – the Mg^{2+} transporter of the yeast inner mitochondrial membrane *

Khan M.B., Sponder G., Sjöblo B., Svidová S. Carugo O., Schweyen R.J.,
Djinović-Carugo K.

*   Manuscript in preparation

Structural and functional characterization of the N-terminal domain of Mrs2 – the Mg^{2+} transporter of the yeast inner mitochondrial membrane

Muhammad Bashir Khan[1], Gerhard Sponder[2], Björn Sjöblom[1], Soňa Svidová[2], Rudolf J. Schweyen[2†], Oliviero Carugo[1,3], Kristina Djinović-Carugo[1, 4,*]

[1]Department for Structural and Computational Biology, Max F. Perutz Laboratories, University of Vienna, Vienna, Austria

[2]Department of Microbiology, Immunobiology and Genetics, Max F. Perutz Laboratories, University of Vienna, Vienna, Austria

[3]Department of Chemistry, University of Pavia, Pavia, Italy

[4]Department of Biochemistry, Faculty of Chemistry and Chemical Technology, University of Ljubljana, Ljubljana, Slovenia

*Correspondence e-mail: kristina.djinovic@univie.ac.at
[†] Deceased in February 2009

Abstract

Mrs2 transporters are distantly related to the major bacterial Mg^{2+} transporter CorA, and to Alr1, located in the plasma membranes of lower eukaryotes. Common characteristics of all Mrs2 proteins are the presence of a large N-terminal soluble domain followed by two adjacent trans-membrane helices (TM1, TM2) near their C-termini and the highly conserved F/Y-G-M-N sequence motif at the end of TM1. Here we determined the crystal structure of the N-terminal domain of Mrs2, a Mg^{2+} transporter of the yeast inner mitochondrial membrane. The N-terminal domain of Mrs2, was crystallized and its crystal structure solved at 1.3 Å resolution. The fold displays differences compared to the prokaryotic CorA N-terminal domain structure. Analytical gel filtration and dynamic light scattering demonstrated that the N-terminal domain of Mrs2 forms a homo-pentamer at low salt solutions. Analysis of the structure allowed us to identify residues forming a hydrophobic gate as well as residues involved in formation of a putative magnesium sensing site. Validation of the putative gating residues by introducing amino acids residues with different characteristics, confirmed the involvement of these amino acids in the gating process. In contrast, mutational analysis of the putative Mg^{2+} sensing site did not yield a clear result. We furthermore explored the role of the exceptional long C-terminus of *S. cerevisiae* Mrs2 and in particular a positively charge stretch in the C-terminal part of the protein and its potential role as "the basic sphincter".

Keywords: magnesium transport, Mrs2, matrix located domain, *Saccharomyces cerevisiae*, hydrophobic gate, magnesium binding site.

1. Introduction

The magnesium ion, Mg^{2+}, is essential for many biochemical processes and remains the only major biological ion whose transport mechanism is still not fully understood. It is present at a total cellular concentration of 15–25 mM in both prokaryotic and mammalian cells (Ikari et al, 2008; Lunin et al, 2006; Mobasheri et al, 1998). It plays important roles in stabilizing macromolecules, in binding to nucleotides and it acts as cofactor of many enzymes. By regulating activities of ion channels and transporters, Mg^{2+} also influences cell volume and signalling processes (Ikari et al, 2008; Mobasheri et al, 1998). In the cytosol, the majority of Mg^{2+} is bound to adenosine-5'-triphosphate (ATP) and other phosphonucleotides and to a number of different enzymes. In all cells, Mg^{2+} serves as an essential structural element for ribosomes and membranes and as a required cofactor for ATP in the catalytic pocket of multiple enzymes. In prokaryotes, Mg^{2+} has also been identified as an important regulatory signal essential for virulence (Eshaghi et al, 2006; Lunin et al, 2006).

The metal ion transporters (MIT) found in all kingdoms of life are essential membrane proteins which transport metal ions across membranes. Among these transporters the CorA family is responsible for Mg^{2+} uptake in most prokaryotes. Until now it is the most extensively studied magnesium transporter. Three lower resolution crystal structures (2.9, 3.7, and 3.9 Å) (Eshaghi et al, 2006; Lunin et al, 2006; Payandeh & Pai, 2006) of *Thermatoga maritima* CorA (Tm-CorA) and of the cytoplasmic soluble domain of *Vibrio parahemolyticus* zinc transporter ZntB (Vp-ZntB) structure (1.9 Å) show a homopentameric assembly (Tan et al, 2009). The structures of full-length Tm-CorA exhibit two trans-membrane α-helices (TM1, TM2) per monomer and a large intracellular funnel shaped assembly. On the other hand the two structures of the cytoplasmic domain of Tm-CorA (1.85 Å) (Lunin et al, 2006) and *Archaeoglobus fulgidus* CorA (Af-CorA) (2.9 Å) show dimeric arrangements of the CorA subunits, which might be due to crystal packing effects (Payandeh & Pai, 2006).

Mrs2 transporters form the major mitochondrial Mg^{2+} uptake system in yeast, plants and mammals (Kolisek et al, 2003; Li et al, 2001; Schock et al, 2000; Zsurka et al, 2001) and

are essential for mitochondrial biogenesis (Walker et al, 1982). Human mitochondrial Mrs2 promotes multidrug resistance in gastric cancer cells by regulating p27, cyclin D1 expression and cytochrome C release (Chen et al, 2009). Mrs2 transporters are distantly related to the major bacterial Mg^{2+} transporter CorA. The amino acid sequence identity and similarity between N-terminal domains of Tm-CorA and Mrs2 form *Saccharomyces cerevisiae* are 11% and 40%, respectively, while the corresponding numbers for the full sequences of the two transporters are 15% and 31%, respectively.

Mrs2 transporters are also related to the Alr1 subfamily, which is restricted to lower eukaryotes. Members of this family form the major Mg^{2+} uptake system of the plasma membrane. Expression of Alr1 is essential for growth of yeast cells, except when cultured in media with unphysiologically high Mg^{2+} (Graschopf et al., 2001). Some of these transporters can in part functionally replace each other which strongly supports the idea that they are homologues (Bui et al, 1999; Li *et al*, 2001; Zsurka *et al*, 2001; Kehres and Maguire, 2002) [Svidova et al submitted].

Despite low sequence identity among all members of the CorA-Mrs2-Alr1 superfamily overall structural features seem to be in part conserved for the N-terminal domain and trans-membrane portion. On the other hand, considerable differences in the C-terminal region following the TM2 can be anticipated from the sequence analysis.

Common features between the CorA, Mrs2 and Alr1 families are the presence of two adjacent trans-membranes helices (TM1, TM2) at the C-terminus and the highly conserved F/Y-G-M-N sequence motif at the end of TM1. The N-terminus of Tm-CorA is characterized by a large cytoplasmic domain that forms a funnel-shaped assembly in the active pentamer. Two divalent cation sensing sites (DCS) which regulate opening and closing of the transporter were mapped to the N-terminal domain of CorA (Eshaghi et al, 2006).

Mrs2 is inserted in the inner mitochondrial membrane while Alr1 is located in the cytoplasmic membrane. The orientation of these transporters in their membranes is such

that both the large N-terminal and the shorter C-terminal part are oriented towards the mitochondrial matrix in case of Mrs2 and to cytoplasm in case of Alr1, resulting in a N_{in} - C_{in} topology. A short loop connecting the two TMs is exposed to the inter-membrane space in case of Mrs2, while it is oriented towards the periplasm in case of Alr1

Although the sequences of CorA-Mrs2-Alr1 superfamily are extremely divergent, these proteins appear to exploit the membrane potential to drive Mg^{2+} uptake (Froschauer et al, 2004; Kolisek et al, 2003)

The cation selectivity of CorA and Mrs2 was attributed to their signature motifs (CorA: YGMNFxxMPEL, Mrs2: xGMNxxxFIEE) (Kehres et al, 1998; Worlock & Smith, 2002). This has also been shown for the zinc transporter family ZntB (GxxG[I,V]NxGGxP). The motif is located at the end of TM1 on the outer surface of the membrane followed by the short loop connecting TM1 and TM2 which tends to be disordered in the crystal structures (Lunin et al, 2006; Payandeh & Pai, 2006). The molecular details of Mg^{2+} transport across the membrane are not yet completely understood. Possible Mg^{2+} gating mechanisms through the trans-membrane domain were proposed for Tm-CorA (Lunin et al, 2006; Payandeh & Pai, 2006). Residue Asn314 of the GMN motif at the external entrance to the pore together with a pair of hydrophobic rings formed by Met291 and Leu294, respectively, were suggested to play important roles in gating of the channel and possible ion dehydration/rehydration steps.

Balancing Mg^{2+} levels is vital for normal cellular function. Homeostasis is maintained by a delicate balance of transport activities across the plasma and organelle membranes. A mechanism for regulation of the transport activity has been proposed for bacterial transporter Tm-CorA (Eshaghi et al, 2006; Lunin et al, 2006; Payandeh et al, 2008; Payandeh & Pai, 2006). In absence of sufficient intracellular Mg^{2+} levels, Mg^{2+} ions bound between monomers are released, the N-terminal domain of the protomers move as a rigid body, where as the willow helices (two antiprallel helices at the N-terminus) undergo a rearrangement with respect to one another and relative to stalk helix (pore forming helices). This causes a torque along the stalk helix. The torque propagates onto the intracellular hydrophobic gates (Met291 and Leu294) and possibly activates the

periplasmic gate by interaction of the cytoplasmic N-terminal, acidic residues and the C-terminal, basic residues. This causes impingement on Asn314 residues through movement of TM2, the MPEL motif (loop connecting TM1 and TM2) and thus allow Mg^{2+} ion to flow through (Lunin et al, 2006; Payandeh et al, 2008).

By now many genes have been reported from plants, bacteria and animals encoding for proteins involved or mediating Mg^{2+} transport (Gardner, 2003). We still have limited information not only about their biological and physiological functions but also about their structures and the capability and mechanism of Mg^{2+} transport. The low sequence homology of the eukaryotic Mrs2 transporters with prokaryotic magnesium transporter Tm-CorA, or any other protein of known structure, makes it difficult to accurately predict its structure and mode of operation.

Here we report the crystal structure of the N-terminal domain of the yeast (*Saccharomyces cerevisiae*) mitochondrial magnesium transporter Mrs2 at 1.3 Å resolution and its functional characterization. The structure can provide a partial framework for addressing questions related to regulatory metal sites, conformational changes in regulation and transport events, residues involved in the formation of hydrophobic gates, as well as for evaluating the important common features present in this transporter family.

2. Results and Discussion

Overall structure of Mrs2$_{48\text{-}308}$, and its comparison with prokaryotic magnesium and zinc transporters.

On the basis of our earlier studies (Khan et al., 2010), we designed a stable Mrs2 construct (48–308), denoted Mrs2$_{48\text{-}308}$ (this construct was denoted as Mrs2$_{16\text{-}276}$ in our previous publication where the mitochondrial targeting sequence was not included in numbering) (Khan et al.,2010), which includes the entire N-terminal soluble matrix domain of Mrs2. Analytical size exclusion chromatography studies showed that Mrs2$_{48\text{-}308}$ behaves as a monomer in high ionic strength buffers and as a homo-pentamer in low

ionic strength buffers (Supplementary Figure 1). The circular dichroism (CD) spectrum of Mrs2$_{48-308}$ showed the minima at 208 and 219 nm, characteristic for a protein rich in α-helices (Supplementary Figure 2). Dynamic light scattering (DLS) was used to assess the monodispersity of the protein in solution: a monomodal distribution with a polydispersity of 5% was observed and the gyration radius was estimated to be 4.2 nm in high ionic strength buffers. In low ionic strength buffer conditions the protein solution shows polydispersity of about 25% and the radius of gyration of 14 nm, which is in agreement with analytical size exclusion chromatography. Together, these data suggest that our construct is autonomously folded into the native conformation in solution and that the protein solution is monomeric at high ionic strength and pentameric at low ionic strength.

The monomer of Mrs2$_{48-308}$ was crystallized in the orthorhombic space group P2$_1$2$_1$2$_1$ and its structure solved by experimental phasing exploiting the anomalous signals of sulphur (Khan et al.,2010). Mrs2$_{48-308}$ in general presents a fold similar to that of Tm-CorA (Figure 1B and C). The high-resolution structure of Mrs2$_{48-308}$ enabled us to examine the transporter in more detail.

The overall organization of prokaryotic and eukaryotic magnesium transporters is quite similar. Each subunit can be divided into a N-terminal alpha/beta domain followed by an alpha helical domain. While the first one is a compact alpha-beta-alpha sandwich, the second one contains a trimeric coiled-coil that enters, at the end of the third and last helix, into the membrane with a TM-helix (Figure 2B).

While the coiled-coil domain is nearly identical in Tm-CorA and Mrs2, the first domain is rather different (Figure 2C). The central beta sheet is formed by seven strands in Tm-CorA and by six strands in Mrs2. While the last four strands (named C1-C4 in Figure 1B) are topologically identical in the two proteins – a series of three beta hairpins, the first beta strands are topologically different. The alpha helix, that follows the strand N2, and the strand N3 are missing in Mrs2, making the eukaryotic protein smaller than the prokaryotic one. Although this might be caused by a deletion during molecular evolution,

on the basis of our data we cannot reject other hypotheses. However, it is clear that any structural alignment of these structural moieties would be extremely misleading, since Tm-CorA and Mrs2 adopt different folds.

Although it seems that the first helix of the third strand of Tm-CorA has been deleted during evolution from prokaryotes to eukaryotes, any evolutionary relationship cannot be demonstrated just on the basis of the structural data depicted in (Figure 1C).

The relatively long helices $\alpha 5$ and $\alpha 6$, which extend towards the membrane, are termed the 'willow' helices in case of Tm-CorA "as they hang down like the branches of a weeping willow tree" have high number of glutamic and aspartic residues at the tip region (Lunin et al, 2006). In case of $Mrs2_{48-308}$ the $\alpha 5$ and $\alpha 6$, corresponding to the willow helices of Tm-CorA, have only six acidic residues as compared to ten in Tm-CorA. In Tm-CorA there is also an extended loop between C_5 and C_6, which protrudes like the willow helices, towards the membrane surface. The tip of this loop also has a very high density of aspartic acid and glutamic acid residues in Tm-CorA (Maguire, 2006). On the contrary, in $Mrs2_{48-308}$, the strands C5 and C6 are much shorter and the loop intercalated between them does not protrude towards the willow helices and does not host any acidic residues (Figure 1B and C).

In order to find out the structural neighbourhoods of $Mrs2_{48-308}$, we employed a Dali search (Holm, 1996), using the monomer crystal structure of $Mrs2_{48-308}$. The Dali search found the following homologues with Z-score higher than 9: (i) *Thermotoga maritima* divalent metal ion transporter Tm-CorA (PDB code 2IUB); (ii) *Vibrio parahaemolyticus RIMD* cytoplasmic domain of zinc transporter Vp –ZntB (PDB code 3CK6). The following two hits clearly have a different molecular function, (iii) *Dictyostelium discoideum* STAT protein, (PDB code 1UUS) and (iv) *Escherichia coli* Pore-forming toxins (PDB code 2WCD). All of these structural homologues have low similarity with Mrs2 from *Saccharomyces cerevisiae* at the sequence level and only magnesium metal ion transporter Tm-CorA can be detected using a BLAST (Altschul et al, 1990) search against the sequence data base using the Mrs2 sequence as a query. Despite the low

sequence homology, Tm-CorA and Vp-ZntB have similar structures to that of Mrs2 and carry out similar molecular functions.

Mrs2$_{48\text{-}308}$, Tm-CorA and Vp-ZntB are structurally similar at the level of the subunit. Nevertheless, the protomer and pentamer structures cannot be simply superimposed because the relative orientation of the α/β/α and the helical subdomains are different. Mrs2$_{48\text{-}308}$ and Tm-CorA soluble domain (PDB code 2IUB) can be superimposed with an RMSD value of 2.85 Å (for Cα of 179 residues aligned out of 256 with sequence identity of 16%) (Supplementary Figure 3A). Separately, the sub-domains of Mrs2$_{48\text{-}308}$ and Tm-CorA (α/β/α and helical) align with different RMSDs values. The α/β/α sub-domains of Mrs2$_{48\text{-}308}$ and Tm-CorA can be superimposed over the Cα atoms with an RMSD value of 2.96 Å (for Cα of 69 residues aligned out of 117 with sequence identity of 8%) (Supplementary Figure 3C). Similarly, the corresponding helical sub-domains can be aligned with an RMSD value of 2.62 Å (for Cα of 112 residues aligned out of 131 with a sequence identity of 13%), suggesting the larger difference resides at α/β/α sub-domains (Supplementary Figure 3E).

These differences start right at the N-terminus of Mrs2$_{48\text{-}308}$, the α1 and C1 of Mrs2$_{48\text{-}308}$ do not superpose on any of the structural elements of Tm-CorA. The major structural difference between the two structures is the length and orientation of α4 Mrs2$_{48\text{-}308}$ with respect to the β sheets. Other differences can be found in the loop regions between the C3 and C4. The stalk helix α7 in case of Tm-CorA is bent at the regions between Ser273 and Gly274, while in case of Mrs2$_{48\text{-}308}$ the corresponding helix is much straighter. This might be due to the fact that the Tm-CorA structure is in a closed conformation and in a functional pentameric form which will be more rigid and does not allow too much flexibility compared to Mrs2$_{48\text{-}308}$, which is in a monomeric form and most likely will represent the open conformation of the transporter.

Mrs2$_{48\text{-}308}$ and Vp-ZntB (PDB code 3CK6) can be superimposed with an RMSD value of 2.61 Å (for Cα of 158 residues aligned out of 237 with sequence identity of 14%) (Supplementary Figure 3B). On the other hand the α/β/α sub-domains of Mrs2$_{48\text{-}308}$ and Vp-ZntB can be superimposed with an RMSD value of 2.75 Å (for Cα of 57 residues

aligned out of 116 with sequence identity of 5%) (Supplementary Figure 3D), and the helical subdomains can be aligned with an RMSD value of 2.22 Å (for Cα of 110 residues aligned out of 121 with a sequence identity of 8%). The changes in orientation between the two sub-domains seem to result in a different level of funnel opening in the three different ion transporters.

Superposition of the $Mrs2_{48-308}$ and Vp-ZntB intracellular domains from *Vibrio parahemolyticus* also shows that most of the variations occur at the α/β/α domain, the first two β-strands i.e. C1 and C2 of $Mrs2_{48-308}$ do not superpose on the Vp-ZntB transporter. Similarly, the α4 of $Mrs2_{48-308}$ does not superimpose on any of the structural elements of Vp-ZntB (Supplementary Figure 3B). The small structural element (α7′ helix, not shown in the figure) between the α6 and α7 of $Mrs2_{48-308}$ also does not superpose on the corresponding structural element of Vp-ZntB (Supplementary Figure 3E and F). As the available structure of Vp-ZntB only comprises the soluble domain and does not exhibit the kink in the stalk helix (α7 helix), this helix superposed quite well (Supplementary Figure 3F). This evidence also supports the idea that the funnel domain of Vp-ZntB is reported in an open conformation as there is no bound divalent cation in the structure.

The soluble domains of Tm-CorA (PDB code 2IUB) and Vp-ZntB (PDB code 3CK6) can be superimposed with an RMSD value of 1.89 Å (for Cα of 199 residues aligned out of 237 with a sequence identity of 19%). Separately, the soluble domains α/β/α aligned with RMSD of 1.93 Å (for Cα of 92 residues aligned out of 116 with a sequence identity of 9%), while the helical domain superposed with RMSD value of 1.71 Å (for Cα of 112 residues aligned out of 121 with a sequence identity of 19%).

The structure based sequence alignment (manually corrected) of $Mrs2_{48-308}$ with Tm-CorA explores important residues involved not only in formation of the hydrophobic gate of the transporter but also in propagation of magnesium across the ion conduction pathway in the Mrs2 type of transporters (Figure 1A). Glu295 aligned with Asp277 of Tm-CorA which is highly conserved and is responsible for making an "aspartate ring"

and regulates transport in Tm-CorA. In the TolC (the outer membrane protein of many multidrug efflux pumps) transport system, an "aspartate ring" formed by the carboxylates of three aspartate residues was shown to determine selectivity, as well as to form a binding site for inhibitory cations (Eshaghi et al, 2006; Higgins et al, 2004). The high conservation of Glu295 in eukaryotic Mrs2 transporters together with the localization at the entrance of the pore, suggest that this residue is important for transport or regulation.

Model of Mrs2$_{48-308}$ funnel

In order to generate a model of the functional Mrs2$_{48-308}$ from the monomeric crystal form we superposed the Mrs2$_{48-308}$ structure both on the helical domains of Tm-CorA and of Vp-ZntB. The maximum diameter of the funnel based on Tm-CorA is 106 Å, while the residues at the C-terminus of the stalk (making the wall of the funnel) clash at the tips (Figure 2C and D). This may be because of the structure of Tm-CorA which has been reported in a closed conformation while the monomeric Mrs2$_{48-308}$ is more relaxed and may represent the open conformation of the transporter. In a functional pentameric form each protomer is in contact with two other adjacent molecules. The structural analysis of the generated funnel model based on the Tm-CorA structure indicates that there are five hydrogen bonding interactions and one salt bridge between Glu263 of one protomer and Lys259 of an adjacent protomer. These interacting residues mainly belong to the stalk helix α7 of one protomer and the stalk helix α7 of the adjacent protomer as well as to the residues at the tip of the two willow helix α5, α6.

On the other hand, the funnel model based on Vp-ZntB has a maximum diameter of 102 Å and interestingly there is no clash of the C-termini. This is another evidence that the Vp-ZntB structure is probably in an open conformation. The structural analysis of the funnel model of Mrs2$_{48-308}$ indicates interfaces between the stalk helix α7 of one protomer and the willow helixes α5 and α6 of another adjacent protomer in the form of two hydrogen bonds and two salt bridges between Lys189 and Asn274 of one protomer and Glu173 and Arg273 of an adjacent protomer. On the other hand, eight hydrogen bonds and eight slat bridges can be identified for the funnel domain of Vp-ZntB (PDB code 3CK6) transporter, and sixteen hydrogen bonds and fifteen salt bridges can be found in

Tm-CorA (PDB code 2BBJ). Although the interfaces of the proposed funnel were not optimized. The presence of fewer hydrogen bonds and salt bridges may explain the higher sensitivity of Mrs2 to elevated salt concentrations.

Analysis of electrostatic surface potential of the structure of Mrs2$_{48-308}$, showed that the α7 helices, forming the inner wall of the funnel in the pentamer model, are lined along their length with negative or hydroxyl-bearing residues (Asp264, Glu266, Glu270, Thr274, Asp277, Glu278, Thr281, Thr282, Glu284, Ser285, Thr288, Asp289, Ser292, Glu295, Asp302) (Figure 2A and B). Such an arrangement of charged and polar residues is found in other monovalent cation (KcsA) and divalent cation (CorA, ZntB) channels and may serve as an electrostatic sink to increase the local ion concentration (Roux & MacKinnon, 1999).

TMpred analysis (Online server Prediction of Transmembrane Regions and Orientation *http://www.ch.embnet.org/software/TMPRED_form.html*) on the primary sequence both of Tm-CorA and Mrs2 from *Saccharomyces cerevisiae*, shows that in Tm-CorA the first trans-membrane helix consists of residues Val293 to Met313, while in case of Mrs2 it includes residues from Val315 to Leu336. Based on the TMpred server prediction the two methionine residues Met291 (Tm-CorA) and Met309 (Mrs2) which are involved in hydrophobic gating of the two transporters are located outside of the membrane, either in the cytoplasm or the mitochondrial matrix accordingly, while the second set of hydrophobic gating residues Leu294 in Tm-CorA and Val315 in case of Mrs2 are located in the membrane spanning regions of the helices.

Putative magnesium sensing sites of Mrs2$_{48-308}$

Two divalent cation binding sites, M1 and M2, have been identified by crystallography at the protomer-protomer interface within the funnel domain of Tm-CorA (Eshaghi et al, 2006; Payandeh & Pai, 2006) and have been characterized as a "divalent cation sensor (DCS)". The two sites coordinate the metal ion differently: the first directly by two carboxylates (Asp89 and Asp253) and the second indirectly by coordinating the hydrated ion. According to a model for regulation of Tm-CorA, a torque is generated at the bottom of stalk helix (α7) by releasing bound magnesium from the magnesium binding site and

propagates up toward the hydrophobic gate (Eshaghi et al, 2006; Lunin et al, 2006; Payandeh & Pai, 2006).

Based on structural comparison of Tm-CorA and our model of the Mrs2$_{48-308}$ funnel, we identified amino acid residues that would form the first divalent cation sensing site (DCS) in Mrs2: Asp97 from one subunit and Glu270 from adjacent subunit (Figure 2C and D, Figure 4D) corresponding to DCS1 of Tm-CorA. A sequence alignment of eukaryotic Mrs2 homologues reveals that the Asp97 and Glu270 residues are highly conserved in the whole family of eukaryotic magnesium transporters, and equivalent residues are also found in the prokaryotic CorA family (Figure 1A). In the Mrs2$_{48-308}$ Glu270 is located at the N-terminus of α7, corresponding to the position of Asp253 in Tm-CorA (Figure 4A and C). The Asp97 is located in the α3 corresponding to the Asp89 of Tm-CorA (Figure 4A and B)

In the initial crystallization condition no magnesium was present, but by adding magnesium to the crystallization condition, we obtained crystals with 1.5 mM magnesium chloride and 1.5 mM cobalt chloride. Native crystals soaked in the presence of increasing concentrations of magnesium chloride (1 to 5 mM), and in 5 mM cobalt and nickel chloride were analyzed as well. Structures obtained from magnesium, cobalt and nickel-soaked crystals and magnesium and cobalt co-crystals, are essentially identical to the native crystal structure produced in the absence of any exogenous divalent cation. The addition of magnesium in the crystallization environment did not change the structure of the native protein and corroborate the notion that DCS are composed of ligands coming from adjacent subunits in the pentamer, and that consequently a single subunit cannot bind divalent ions with high affinity.

Protease susceptibility assay, a two-state model

According to the Tm-CorA two state model, the Tm-CorA elbow formed by helices (α5-α6) may function as a "spring" upon metal ion binding to the divalent cation sensor site. Payandeh at all reported that the cations located at the protomer interface may stabilize Tm-CorA, but are not required to maintain its pentameric state (Eshaghi et al, 2005;

Payandeh & Pai, 2006). As portions of the N-terminal region (residues 1-25) are 'invisible' in all available crystal structures of Tm-CorA, this region may become disordered and therefore susceptible to exogenous protease in the open conformation of the transporter (Payandeh & Pai, 2006). In order to validate the two state model for Mrs2, we carried out a protease susceptibility assay in presence and absence of magnesium and cobalt ions.

Prior to experiment the protein was dialyzed against a low ionic strength buffer to induce formation of the functional pentameric form and then incubated with different amounts of magnesium, cobalt EDTA and trypsin. The results showed that in presence of high concentrations of cobalt the protein is less susceptible to trypsin cleavage while in presence of magnesium the protein is comparatively less protected from protease digestion. Interestingly, in presence of EDTA the protein is completely protected from protease digestion. The reaction conditions were tested both at 4 and 37°C for 4 and 15 hours. Interestingly, in contrast to Tm-CorA, Mrs2$_{48-308}$ is less susceptible to protease digestion at 4°C compared to 37°C.

The observed strong protection of the protein in the presence of EDTA may be explained by the fact that during pentamerization of Mrs2$_{48-308}$ in the dialysis process the funnel is in closed conformation which appears to be more susceptible to protease cleavage. This would be exactly opposite to what has been reported for Tm-CorA. Interestingly, addition of EDTA deprived Mrs2 from divalent metal ions and thus led to an open conformation of the Mrs2$_{48-308}$ funnel which is less susceptible to protease cleavage. The observed differential protease susceptibility of the Mrs2$_{48-308}$ funnel domain compared to Tm-CorA suggests a significant conformational change, and thus our results are in line with the proposed different conformations of the pentamer in open and closed state. These differences compared to the Tm-CorA protein susceptibility assay suggest divergent conformational changes or molecular differences in the N-terminal domain of the two types of transporters.

Functional analysis of selected mutants

Gating mutants

It is now well known that Met291 and Leu294 are involved in the formation of hydrophobic gates in Tm-CorA (Lunin et al, 2006; Svidova et al, 2010). As no three-dimensional structure of the full-length Mrs2 transporter is available we modeled the Mrs2 C-terminal moiety on the basis of the structure alignment between $Mrs2_{48-308}$ and the soluble domain of Tm-CorA and extended the sequence in the alignment at the C-terminus (Figure 1A). Our alignment suggests that Met309 and Val315 are putatively involved in the formation of hydrophobic gates. A sequence alignment of eukaryotic members of the Mrs2 family indicates that Met309 is highly conserved in the whole family and we named this amino acid gate 1. Analysis of the pentameric Mrs2 model constructed on the structure of Tm-CorA shows the narrowest constriction of the pore at this residue (Figure 4F), corresponding to Tm-CorA Met291 (Figure 4E).

Amino acid Met309 was therefore mutated to three residues with different properties regarding size and charge i.e. small glycine, negatively charged glutamic acid, and the bulky residue phenylalanine (Table 2). The physiological consequences of these mutations were monitored by means of the following experiments. Strain DBY747 *mrs2Δ* was transformed with high-copy number vector YEp351, or the centromeric plasmid YCp22 harbouring the mutated *MRS2* variants as well as with wild-type *MRS2* and the empty vector as controls. Growth tests showed severely reduced growth of all three mutants on non fermentable carbon sources, indicating that these amino acid substitutions had a considerable effect on magnesium homeostasis in mitochondria. Substitution of methionine by glycine exhibited the strongest effect.

Measurements of magnesium uptake in isolated mitochondria revealed the different effects of these amino acid substitutions. The strongest reduction of magnesium uptake was observed in the Met309Phe variant. This finding can be explained by the size of this bulky residue, leading to narrowing of the pore at this position. The glycine mutant exhibited the highest degree of deregulation in gating of the channel. Exchange of

Met309 to the small Gly residue resulted in a considerably stronger influx compared to the wild-type variant of the protein and significantly elevated final steady state magnesium concentrations (Figure 5B).

A similar effect was observed for Glu at this position. This amino acid substitution yielded higher final steady-state magnesium levels as well. This effect is most probably caused by the charge of this amino acid residue. In the pentameric form, Glu would form a negatively charged ring possibly leading to a stronger transport activity due to increased electrostatic attraction of the magnesium ion.

In the Met309Gly mutant, very strong uptake could be observed after the first magnesium addition, furthermore plateau levels were less pronounced compared to the wild-type control, nevertheless the transporter was still able to close the ion conduction pathway to some extent (Figure 5B). This is in accordance with the assumption that magnesium biding sites in the N-terminal part of Mrs2 act as sensor of the intracellular magnesium concentration. According to this model, alterations in the gating process would lead to higher uptake rates and probably also to elevated magnesium levels in mitochondria; however, as long as the transporter is able to close the pore, magnesium influx is not expected to be completely deregulated.

The second candidate amino acid we investigated was Val315. In the structure based sequence alignment, Val315 aligned with Leu294 of Tm-CorA (Figure 2A). Analysis of the pentameric Mrs2 model constructed on the known structure of Tm-CorA shows the second narrowest constriction of the pore at this residue (Figure 4E and F). In contrast to Met309, sequence alignment of various eukaryotic Mrs2 homologues indicates that Val315 is less conserved than Met309. We termed this amino acid gate 2.

As for Met309, Gly, Glu and Phe were introduced at this position and their effect was examined by growth tests and magnesium uptake measurements in isolated mitochondria. Substitution of Val315 to Glu and Phe had no effect on growth on non-fermentable carbon sources (Figure 6A). In line with this result, also Mg^{2+} uptake was less affected by mutations at this position compared to the first gating mutant at position 309. Mg^{2+}

uptake in the Glu mutant was comparable to wild-type Mrs2. Also the bulky residue Phe was surprisingly well tolerated at this position and obviously did not narrow the ion conduction pathway at this position to an extent leading to a substantial reduction of magnesium uptake (Figure 6B).

Only Gly at this position reduced growth of the cells to a certain degree, which was, however, less pronounced than in the Met309 mutant. Based on the results from mag-fura-2 measurements this effect is again caused by stronger magnesium uptake due to a widening of the channel at this position.

Investigation of the Mrs2 C-terminus

Tm-CorA has a highly conserved positively charged sequence at the C-terminus, mostly composed of lysine residues. This "basic sphincter" is located at the cytoplasmic neck parallel to the hydrophobic gate of the pore and is essential for the function of the transporter (Lunin et al, 2006). The basic sphincter is predicted to draw negative charge away from the middle of the pore at this level, preventing passage of the positively charged Mg^{2+} cation (Lunin et al, 2006).

On the other hand, members of the Mrs2 subfamily have C-termini highly variable in length containing almost no conserved primary sequence motives. The only conserved feature is a surplus of positively charged residues, which may perform the same function as was predicted for the basic sphincter of Tm-CorA transporter (Supplementary Table 1). (Eshaghi et al, 2006; Weghuber et al, 2006). It has also been reported for Mrs2 that the C-terminal moiety contains a segment with characteristics of an amphipathic helix directly after TM2, which serve as internal targeting signals that mediate the N_{in} -C_{in} topology (Baumann et al, 2002).

Yeast Mrs2 has a particularly long C-terminal sequence and a positively charged KRRRK stretch (402-406), which is not conserved. This sequence has been deleted in a previous study with the effect of reduced Mg^{2+} uptake when expressed from a low copy vector. In contrast, over-expression of this mutant restored Mg^{2+} uptake almost to a wild-type levels

(Weghuber et al, 2006). To get more insight into the function of the KRRRK stretch, we reversed charge of this sequence by introducing negatively charged Glu at these positions. This mutant exhibited very good growth on non-fermentable carbon sources either expressed from the centromeric plasmid YCp 22 or when over-expressed (Figure 7A). Mg^{2+} uptake was moderately increased in this mutant. These findings suggest that introduction of a highly negatively charged ring enclosing the ion conduction pathway produces a more active channel without impairing its regulation (Figure 7B).

In order to further explore the role of the C-terminus, we completely removed the extra C-terminus of Mrs2. Interestingly, truncation of the whole C-terminus had a significant negative effect on growth of the cells on non-fermentable carbon sources (Figure 7A); which is in line with the observed strong reduction of Mg^{2+} transport capacity in mag-fura-2 measurements of isolated mitochondria (Figure 7B).

Taken together, the small, non-conserved positively charged stretch (KRRRK, 402-406) at the C-terminus appears to not be critical for the function of Mrs2. On the other hand a complete truncation of the C-terminus (deletion of 94 residues at the C-terminus), negatively affects the transport activity. Not the KRRRK-stretch in particular but the overall surplus of positively charged residues in the C-terminus of Mrs2 might fulfill a similar function than that of the "basic sphincter" in Tm-CorA.

DCS mutants

Employing superposition of the magnesium binding site DCS1 of Tm-CorA and Mrs2$_{48-308}$ of *S. cerevisiae*, we identified a putative DCS site in Mrs2, formed by the amino acid residues Asp97 from one subunit and Glu270 from an adjacent subunit. In order to test the involvement of these amino acids in gating of the channel, we performed site-directed mutagenesis of Asp97 to Ala, Phe and Trp. Surprisingly, these mutants exhibited no growth defect on non-fermentable carbon sources (Figure 8A). Accordingly no significant differences between wild-type Mrs2 and the mutant proteins in Mg^{2+} uptake measurements in isolated mitochondria could be observed (Figure 8B).

Given the high conservation of this residue throughout the Mrs2 subfamily, our results that mutations at this position have no effect is somewhat surprising. However, it cannot

be excluded that also in Mrs2 two or even more Mg^{2+} sensing sites are present, operating jointly in controlling the activity of the channel. Consequently, mutations in only one of these sites might not be sufficient to impair the cation sensing ability of the channel.

3. EXPERIMENTAL PROCEDURES

Preparation of Protein

Details on cloning and purification was reported earlier (Khan et al). The mitochondrial matrix domain of *Saccharomyces cerevisiae* was cloned from genomic DNA into pETM-11 vector (EMBL Hamburg) with a tobacco etch virus (TEV) cleavable N-terminal His_6-tag. The recombinant protein was over expressed in BL-21 star (DE3) at 21 °C, in the presence of 0.025 mg ml^{-1} of kanamycin and induced by 0.5 mM isopropyl β-D-thiogalactopyranoside (IPTG). Cells were sonicated in a suitable buffer. The supernatant after centrifugation was applied onto 5 ml Ni–NTA agarose column (Qiagen). The N-terminal His_6-tag was cleaved using TEV. After the TEV cleavage the purification of protein was take place, the protein was reapplied on a Ni-NTA column, followed by Resource Q column, and HiLoad 26/60 Superdex 200 (GE Healthcare) size exclusion chromatography.

Protein purity and monodispersity controls

The purity of the protein solution used for the crystallization experiments was evaluated by SDS-PAGE analysis and showed a single band of apparent molecular weight of about 30 kDa. Dynamic light scattering (DLS) was used to assess the monodispersity of the protein solution: a monomodal distribution with a polydispersity of 5% was observed and the gyration radius was estimated to be 4.2 nm, suggesting that the protein solution was homogenous and monomeric. Circular dichroism (CD) spectroscopy in the far ultraviolet wavelength range showed that the protein is rich in alpha helical content.

Analytical gel filtration chromatography

Analytical gel filtration chromatography on $Mrs2_{48\text{-}308}$ was performed at 4 °C, using the construct eluted as monomer from Superdex 200 10/300 column (Amersham

Biosciences), after dialyzing the protein against low ionic salt and run onto an analytical gel filtration 200 10/300 column in 15 mM Tris-Hcl (pH 8.0), 15mM NaCl, the protein solution was eluted as a pentamer.

Crystallization

Details on crystallization conditions were reported earlier (Khan et al., 2010). Initial screening crystallization conditions were obtained from sparse matrix screen from MembFac kits and Hampton Research were optimized by hanging drop at 22 °C. Magnesium and cobalt-soaked crystals were obtained by soaking the native crystal with 1-5 mM magnesium chloride and 5 mM cobalt chloride in the crystallization drops. Co-crystals with magnesium or cobalt were grown by vapor diffusion at 22 °C in a solution containing 2.8 mg/ml protein, 22% v/v ethylene glycol 56 mM Na/K phosphate pH 6.3, 1.5 mM magnesium chloride, or cobalt chloride. All the crystals were flash-frozen in a solution containing 30% v/v ethylene glycol 56 mM Na/K phosphate pH 6.3 and mounted on loops at 100 K prior to data collection.

Data collection and processing

All $Mrs2_{48-308}$ X-ray diffraction data sets were collected at 100 K in a cold nitrogen stream using various beamlines at ESRF or Microstar rotating anode at 1.54 Å. The crystals of $Mrs2_{48-308}$ diffracted to 1.83 Å resolution on in-house source and to 1.30 Å at ESRF. Detail of the data collection, statistics and processing are reported earlier (Khan et al). Crystallographic data collected in house was processed (integrated and scaled) with the Proteum2 software suite (Bruker AXS Inc.), while the synchrotron data sets were processed using XDS (Kabsch, 1988). The structure of $Mrs2_{48-308}$ was solved, using a highly redundant data set collected on in-house source by the single-wavelength anomalous dispersion method (SAD) exploiting the Mrs2 native sulphur (S) atoms for phasing using SHELXD (Uson & Sheldrick, 1999). After finding the S atoms, heavy atom refinement and density modification were performed using autoSHARP (Vonrhein et al, 2007). The electron density map obtained from autoSHARP was traced by ARP/wARP (Joosten et al, 2008; Morris et al, 2003), which fitted 243 out of 261 amino acid residues in three different chains with R_{work}/R_{free} = 0.21/0.30. The structure

refinement yielded final R_{work} and R_{free} values of 0.193 and 0.243, respectively. This model contains 258 amino-acid residues and 432 water molecules. Two complete data sets at 1.42 Å and 1.30 Å were collected at ESRF ID14-1, processed individually using XDS. The data sets were than scaled together using SCALA. The structure from S-SAD data was further refine against the merged 1.3 Å data sets using REFMAC5 and phenix. The final model contains 261 amino acid and 392 water and five ethylene glycol molecule with a R_{work} and R_{free} of 0.169 and 0.204 respectively. Details on the refinement statistics are shown in Table 1.

Protease susceptibility Assay

For 50 ml reaction volumes, stock solutions were prepared to obtain the final concentration desired upon dilution: 38.75 ml of protein (2.58 mg/ml), 1µl of trypsin (10 mg/ml; Sigma), and 50µl 3mg/ml of 'substrate'. Reaction solutions were mixed and equilibrated at 4°C for 20 min. Trypsin was then added, and reactions were incubated at 4° or 37°C for the specified times. After adding 50 ml of SDS–PAGE sample buffer, samples were boiled and run immediately on 15% SDS–PAGE gels. To rule out the possibility of trypsin inhibition, controls were performed on a test protein (BSA) over the full range of conditions.

Yeast strains, growth media and genetic procedures:

S. cerevisiae strain DBY747 and the isogenic deletion strain *mrs2Δ* have been described previously (Bui et al, 1999; Wiesenberger et al, 1992). Yeast cells were grown in YPD (1% yeast extract, 2% peptone, 2% glucose) to stationary phase. For growth tests on solid media, yeast cells were grown in YPD over night, washed with dH2O and spotted in ten-fold dilutions on YPD or YPG (1% yeast extract, 2% peptone, 3% glycerol) and incubated at 28°C for 2 (YPD) or 6 days (YPG).

Plasmid constructs:

The plasmid Yep351-*MRS2*-HA (Bui 1999) was used as template in overlap extension PCR. For mutagenesis of Met309, Val315, and the putative sensing site Asp following mutagenic forward and reverse primers were used (changed nucleotides are in bold):

```
MRS2 M309E fw: 5'-CGCAAATAGGAATTCCTTAGAGTTGTTGGAGTTGAAAGTTACC-3'
MRS2 M309E rev: 5'-GGTAACTTTCAACTCCAACAACTCTAAGGAATTCCTATTTGCG-3'
MRS2 M309F fw: 5'-CGCAAATAGGAATTCCTTATTCTTGTTGGAGTTGAAAGTTACC-3'
MRS2 M309F rev: 5'-GGTAACTTTCAACTCCAACAAGAATAAGGAATTCCTATTTGCG-3'
MRS2 M309G fw: 5'-CGCAAATAGGAATTCCTTAGGATTGTTGGAGTTGAAAGTTACC-3'
MRS2 M309Grev: 5'-GGTAACTTTCAACTCCAACAATCCTAAGGAATTCCTATTTGCG-3'
```

```
MRS2 V315E fw: 5'-
CGCAAATAGGAATTCCTTAATGTTGTTGGAGAGGAAAGTTACCATCTACACGTTGGG-3'
MRS2 V315E rev: 5'-
CCCAACGTGTAGATGGTAACTTTCCTCTCCAACAACATTAAGGAATTCCTATTTGCG-3'
MRS2 V315F fw: 5'-
CGCAAATAGGAATTCCTTAATGTTGTTGGATTCGAAAGTTACCATCTACACGTTGGG-3'
MRS2 V315F rev: 5'-
CCCAACGTGTAGATGGTAACTTTCGAATCCAACAACATTAAGGAATTCCTATTTGCG-3'
MRS2 V315G fw: 5'-
CGCAAATAGGAATTCCTTAATGTTGTTGGAGGAGAAAGTTACCATCTACACGTTGGG-3'
MRS2 V315G rev: 5'-
CCCAACGTGTAGATGGTAACTTTCTCCTCCAACAACATTAAGGAATTCCTATTTGCG-3'
```

```
MRS2 D97Afw: 5'-CATTCCCTTTTCCCGAGAGCGCTGAGGAAAATAGATAACTCC-3'
MRS2 D79Arev: 5'- GGAGTTATCTATTTTCCTCAGCGCTCTCGGGAAAAGGGAATG-3'
MRS2 D97Ffw: 5'-CATTCCCTTTTCCCGAGATTTCTGAGGAAAATAGATAACTCC-3'
MRS2 D97Frev:  5'-GGAGTTATCTATTTTCCTCAGAAATCTCGGGAAAAGGGAATG-3'
MRS2 D97Wfw: 5'-CATTCCCTTTTCCCGAGATGGCTGAGGAAAATAGATAACTCC-3'
MRS2 D97Wrev: 5'-GGAGTTATCTATTTTCCTCAGCCATCTCGGGAAAAGGGAATG-3'
```

The above mentioned mutagenic primers were used in combination with the forward primer MRS2Mcsfw: 5'-CGATTAAGTTGGGTAACGCCAGGG-3' and the reverse primer MRS2Mcsrev: 5'-GCACGACAGGTTTCCCGACTGGAAAGC-3'

Verification of positive clones was performed by restriction analysis of the introduced EcoRI (Met309 and Val315) or AvaI (Asp97) sites (underlined). All restriction sites were introduced by silent mutations. No additional mutations were found by sequencing of the complete ORF.

PCR fragments were digested with XbaI and SmaI and cloned in the vector Yep351-MRS2-HA digested with the same enzyme combination.

To create the C-terminal truncation of *MRS2*, the primer MRS2Mcsfw and the reverse primer MRS2 CutCterm rev: GCGCGCGTCGACCGGTCATCTTTGTCAC were used. The XbaI/SalI digested PCR fragment was cloned in vector Yep351.

For the substitution of the positive amino acid stretch by negatively charged amino acid residues in the KRRRK/E mutant the mutagenic primers MRS2 KRRRK/E fw: **5'-**GCGTCTATTGCCCTGACAAATAAACTAGAAGAGGAAGAGGAATGGTGGAA<u>G TCAAC</u>CAAGCAGCGG-3' and MRS2 KRRRK/E rev: 5'-CCGCTGCTTGGTTGACTTCCACCATTCCTCTTCCTCTTCTAGTTTATTTGTCAG GGCAATAGACGC-3' were used with the above mentioned primers in overlap extension PCR. Positive clones were verified by the introduced HincII restriction site (underlined).

Isolation of mitochondria and measurement of [Mg^{2+}]$_m$ by spectrofluorometry

Isolation of mitochondria and the ratiometric determination of intramitochondrial Mg^{2+} concentrations ([Mg2+]$_m$) dependent on various external concentrations ([Mg^{2+}]$_e$) has been performed as reported previously (Kolisek et al, 2003).

References

Altschul SF, Gish W, Miller W, Myers EW, Lipman DJ (1990) Basic local alignment search tool. *J Mol Biol* **215**(3)**:** 403-410

Baumann F, Neupert W, Herrmann JM (2002) Insertion of bitopic membrane proteins into the inner membrane of mitochondria involves an export step from the matrix. *J Biol Chem* **277**(24)**:** 21405-21413

Bui DM, Gregan J, Jarosch E, Ragnini A, Schweyen RJ (1999) The bacterial magnesium transporter CorA can functionally substitute for its putative homologue Mrs2p in the yeast inner mitochondrial membrane. *J Biol Chem* **274**(29)**:** 20438-20443

Chen Y, Wei X, Yan P, Han Y, Sun S, Wu K, Fan D (2009) Human mitochondrial Mrs2 protein promotes multidrug resistance in gastric cancer cells by regulating p27, cyclin D1 expression and cytochrome C release. *Cancer Biol Ther* **8**(7)**:** 607-614

Eshaghi S, Hedren M, Nasser MI, Hammarberg T, Thornell A, Nordlund P (2005) An efficient strategy for high-throughput expression screening of recombinant integral membrane proteins. *Protein Sci* **14**(3)**:** 676-683

Eshaghi S, Niegowski D, Kohl A, Martinez Molina D, Lesley SA, Nordlund P (2006) Crystal structure of a divalent metal ion transporter CorA at 2.9 angstrom resolution. *Science* **313**(5785)**:** 354-357

Froschauer EM, Kolisek M, Dieterich F, Schweigel M, Schweyen RJ (2004) Fluorescence measurements of free [Mg2+] by use of mag-fura 2 in Salmonella enterica. *FEMS Microbiol Lett* **237**(1)**:** 49-55

Gardner RC (2003) Genes for magnesium transport. *Curr Opin Plant Biol* **6**(3)**:** 263-267

Higgins MK, Eswaran J, Edwards P, Schertler GF, Hughes C, Koronakis V (2004) Structure of the ligand-blocked periplasmic entrance of the bacterial multidrug efflux protein TolC. *J Mol Biol* **342**(3)**:** 697-702

Holm L, Sander C (1996) Mapping the protein universe. *Science* **273**(5275)**:** 595-603

Ikari A, Okude C, Sawada H, Yamazaki Y, Sugatani J, Miwa M (2008) TRPM6 expression and cell proliferation are up-regulated by phosphorylation of ERK1/2 in renal epithelial cells. *Biochem Biophys Res Commun* **369**(4)**:** 1129-1133

Joosten K, Cohen SX, Emsley P, Mooij W, Lamzin VS, Perrakis A (2008) A knowledge-driven approach for crystallographic protein model completion. *Acta Crystallogr D Biol Crystallogr* **64**(Pt 4)**:** 416-424

Kabsch W (1988) Automatic-Indexing of Rotation Diffraction Patterns. *Journal of Applied Crystallography* **21:** 67-71

Kehres DG, Lawyer CH, Maguire ME (1998) The CorA magnesium transporter gene family. *Microb Comp Genomics* **3**(3)**:** 151-169

Khan MB, Sjoblom B, Schweyen RJ, Djinovic-Carugo K Crystallization and preliminary X-ray diffraction analysis of the N-terminal domain of Mrs2, a magnesium ion transporter from yeast inner mitochondrial membrane. *Acta Crystallogr Sect F Struct Biol Cryst Commun* **66**(Pt 6)**:** 658-661

Kolisek M, Zsurka G, Samaj J, Weghuber J, Schweyen RJ, Schweigel M (2003) Mrs2p is an essential component of the major electrophoretic Mg2+ influx system in mitochondria. *EMBO J* **22**(6)**:** 1235-1244

Li L, Tutone AF, Drummond RS, Gardner RC, Luan S (2001) A novel family of magnesium transport genes in Arabidopsis. *Plant Cell* **13**(12)**:** 2761-2775

Lunin VV, Dobrovetsky E, Khutoreskaya G, Zhang R, Joachimiak A, Doyle DA, Bochkarev A, Maguire ME, Edwards AM, Koth CM (2006) Crystal structure of the CorA Mg2+ transporter. *Nature* **440**(7085)**:** 833-837

Maguire ME (2006) The structure of CorA: a Mg(2+)-selective channel. *Curr Opin Struct Biol* **16**(4)**:** 432-438

Mobasheri A, Mobasheri R, Francis MJ, Trujillo E, Alvarez de la Rosa D, Martin-Vasallo P (1998) Ion transport in chondrocytes: membrane transporters involved in intracellular ion homeostasis and the regulation of cell volume, free [Ca2+] and pH. *Histol Histopathol* **13**(3)**:** 893-910

Morris RJ, Perrakis A, Lamzin VS (2003) ARP/wARP and automatic interpretation of protein electron density maps. *Methods Enzymol* **374:** 229-244

Payandeh J, Li C, Ramjeesingh M, Poduch E, Bear CE, Pai EF (2008) Probing structure-function relationships and gating mechanisms in the CorA Mg2+ transport system. *J Biol Chem* **283**(17)**:** 11721-11733

Payandeh J, Pai EF (2006) A structural basis for Mg2+ homeostasis and the CorA translocation cycle. *EMBO J* **25**(16)**:** 3762-3773

Roux B, MacKinnon R (1999) The cavity and pore helices in the KcsA K+ channel: electrostatic stabilization of monovalent cations. *Science* **285**(5424)**:** 100-102

Schock I, Gregan J, Steinhauser S, Schweyen R, Brennicke A, Knoop V (2000) A member of a novel Arabidopsis thaliana gene family of candidate Mg2+ ion transporters

complements a yeast mitochondrial group II intron-splicing mutant. *Plant J* **24**(4)**:** 489-501

Svidova S, Sponder G, Schweyen RJ, Djinovic-Carugo K Functional analysis of the conserved hydrophobic gate region of the magnesium transporter CorA. *Biochim Biophys Acta*

Tan K, Sather A, Robertson JL, Moy S, Roux B, Joachimiak A (2009) Structure and electrostatic property of cytoplasmic domain of ZntB transporter. *Protein Sci* **18**(10)**:** 2043-2052

Uson I, Sheldrick GM (1999) Advances in direct methods for protein crystallography. *Curr Opin Struct Biol* **9**(5)**:** 643-648

Vonrhein C, Blanc E, Roversi P, Bricogne G (2007) Automated structure solution with autoSHARP. *Methods Mol Biol* **364:** 215-230

Walker GM, Birchandersen A, Hamburger K, Kramhoft B (1982) Magnesium-Induced Mitochondrial Polymorphism and Changes in Respiratory Metabolism in the Fission Yeast, Schizosaccharomyces Pombe. *Carlsberg Research Communications* **47**(4)**:** 205-214

Weghuber J, Dieterich F, Froschauer EM, Svidova S, Schweyen RJ (2006) Mutational analysis of functional domains in Mrs2p, the mitochondrial Mg2+ channel protein of Saccharomyces cerevisiae. *FEBS J* **273**(6)**:** 1198-1209

Wiesenberger G, Waldherr M, Schweyen RJ (1992) The nuclear gene MRS2 is essential for the excision of group II introns from yeast mitochondrial transcripts in vivo. *J Biol Chem* **267**(10)**:** 6963-6969

Worlock AJ, Smith RL (2002) ZntB is a novel Zn2+ transporter in Salmonella enterica serovar Typhimurium. *J Bacteriol* **184**(16)**:** 4369-4373

Zsurka G, Gregan J, Schweyen RJ (2001) The human mitochondrial Mrs2 protein functionally substitutes for its yeast homologue, a candidate magnesium transporter. *Genomics* **72**(2)**:** 158-168

Table 1 Data collection and refinement statistics

	Data set 1	Data set 2
DATA COLLECTION		
Source	Home source	ID14-1 (ESRF)
Wavelength (Å)	1.54178	0.933
Resolution (Å)	36.89–1.83 (1.90–1.83)[a]	50.0-1.30 (1.35 - 1.31)
Space group	P212121	P212121
Unit cell (Å, º)	a = 54.66, b = 61.70, c = 85.30, α= β= = 90	a = 54.88 = 61.88, c = 85.45 α= β= = 90
Molecules / a.u.	1	1
Unique reflections	48844	69621 (4235)
Completeness (%)	99 (92)	92.1 (79.0)
R_{meas}[b]		0.069 (1.172)
R_{pim}[c]	0.80 (23.0)	
R_{anom}	0.0316	
Multiplicity	80 (13)	12.0 (6.2)
I/sig(I)	40.2 (1.9)	19.9 (1.83)
Software used for integration	*PROTEUM2*	XDS
Software used for scaling	*PROTEUM2*	XSCALE
PHASING		
No. of sites	11	
Phasing power[d]	0.311 (0.069)	
Figure of merit	0.841	
Software used for finding sites	SHELX	
Software used for phasing	SHARP	
Software used for density modification	DM	
REFINEMENT		
R_{cryst}[e]/ R_{free}[f]	0.1932/0.2440	0.169 / 0.204
No. Reflections used for R_{free}	1289	7312
R.m.s.d. bonds (Å)	0.0124	0.004
R.m.s.d. angles (º)	1.3310	0.912
B protein (Å²)		15.062
Software used for refinement	Refmac	Phenix.refine
Refinement method (ML, SA, TLS)	ML	ML

[b]

$$R_{meas} = \frac{\sum_h \sqrt{\frac{n_h}{n_h-1}} \sum_i^{n_h} \left| \hat{I}_h - I_{h,i} \right|}{\sum_h \sum_i^{n_h} I_{h,i}} \text{ with } \hat{I}_h = \frac{1}{n_h} \sum_i^{n_h} I_{h,i}$$

[c]

$$R_{pim} = \sum_{hkl} \sqrt{\frac{1}{N-1}} \sum_i \left| I_i(hkl) - \overline{I(hkl)} \right| / \sum_{hkl} \sum_i I_i(hkl)$$

Where I (hkl) is the mean intensity of multiple I_i (*hkl*) observations of the symmetry-related reflections, N is the redundancy, n_h is the multiplicity, $\hat{I}_h$ is the average intensity and $I_{h,i}$ is the observed intensity.

[d]Anomalous phasing power: $(\Sigma |F_H(\text{imag})|^2 / \Sigma || \Delta F \pm_{PH}(\text{obs})| - |\Delta F \pm_{PH}(\text{calc})||^2)^{1/2}$ where $\Delta F \pm_{PH}$ is the structure factor difference between Bijvoet pairs and $F_H(\text{imag})$ is the imaginary component of the calculated structure factor contribution by the anomalously scattering atoms.

[e]$R_{cryst} = \Sigma |F_o - F_c| / \Sigma F_o$

[f]R_{free} is the cross-validation R_{factor} computed for the test set of reflections (5 %) which are omitted in the refinement process.

Table2:

Table of the mutants designed according to the structure based sequence alignment of Mrs2$_{48-308}$ with Tm-CorA.

Targets	Asp97 Mg^{2+} binding site	Met309 (Gate1)	Val315 (Gate 2)	Lys, Arg,Arg,Arg,Lys (402-406)	Truncation at C- terminus
Mutants	Ala,Phe,Trp	Gly,Glu,Phe	Gly,Glu,Phe	Glu, Glu, Glu,Glu,Glu	truncate after Thr376

Figure 1 Structure-based sequence alignments of Mrs2$_{48-308}$ and its closest structure homologue Tm-CorA
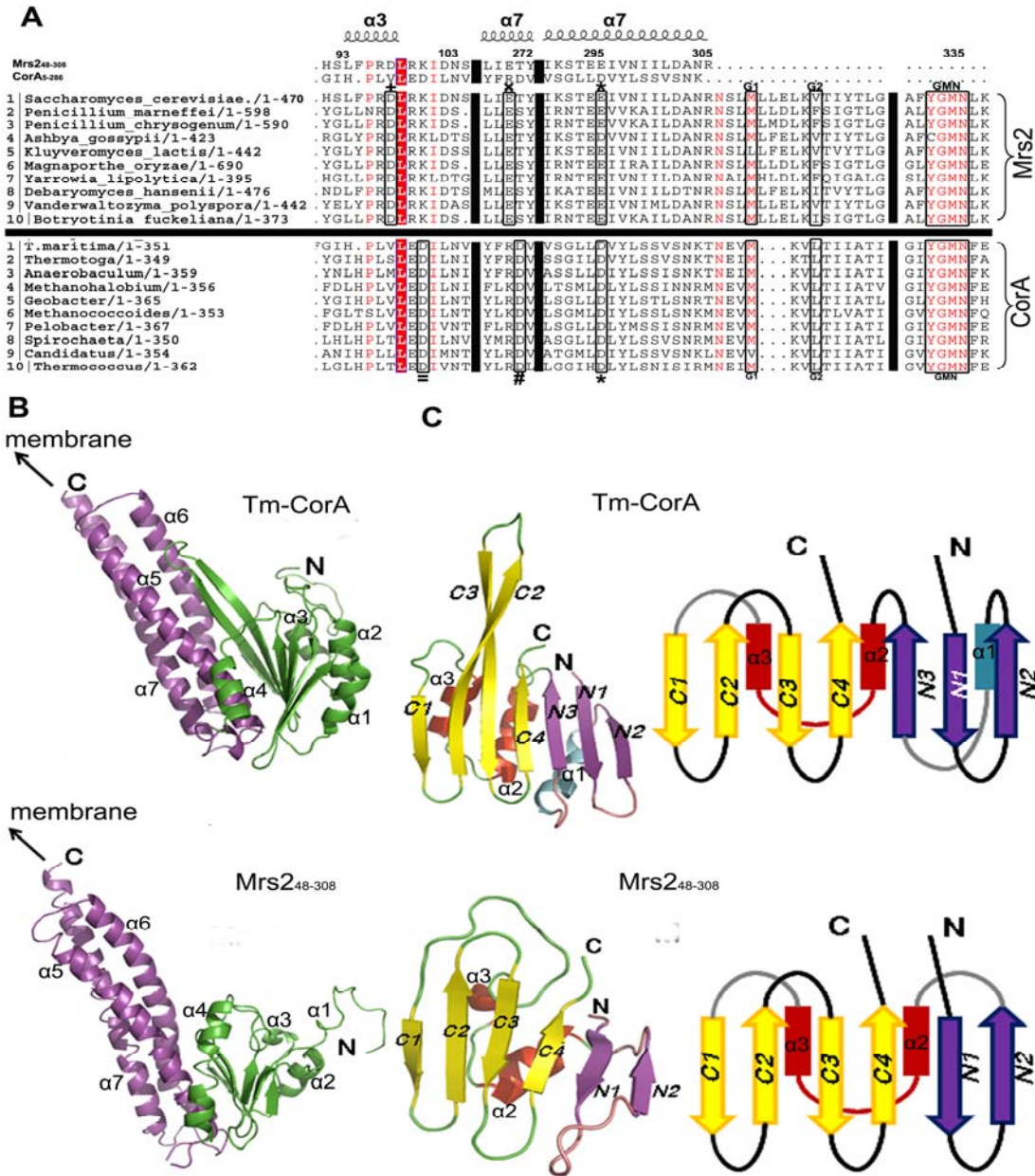
Figure 1 Structure-based sequence alignments of Mrs2$_{48-308}$ and its closest structural homologue Tm-CorA (A) Structure-based sequence alignment of Mrs2$_{48-308}$ and Tm-CorA (PDB code 2IUB), the sequences were then extended to ten species of prokaryotic

magnesium transporter and ten species of eukaryotic magnesium transporters. Identical residues between Mrs2 transporter and Tm-CorA transporter are in red. The gape in the sequence alignment is represented by three solid black lines. The sequences of the two species are separated by a horizontal black solid line. The sequence similarity between the prokaryotic species used in the alignment is about 98 % while between eukaryotic species it is about 82 %. The conserved signature sequence GMN is boxed. Residues of the putative magnesium binding site i.e. Asp97 and Glu270 are boxed in eukaryotes and are denoted by + and × symbols. The prokaryotic magnesium binding site Asp89, Asp253 is boxed and is denoted by = and **#** symbols in the sequence alignment, respectively. The

residue involved in the Asp ring is boxed and is represent by ∗ symbol. The residues involved in the hydrophobic gate formation i.e. Met309, Val315 in case of Mrs2 transporter and Met291, Leu294 in case of Tm-CorA transporter are highlighted (box) and are named G1 and G2 in the sequence alignment (representing gate 1 and gate 2) respectively. The secondary structure derived from Mrs2$_{48-308}$ is shown above its sequence. (B) The structures of the soluble moiety of Tm-CorA and Mrs2 contain a C-terminal trimeric coiled-coil (magenta), which continues into the membrane, and an N-terminal alpha/beta/alpha domain (green). (C) The N-terminal domains of Tm-CaorA and Mrs2$_{48-308}$ are different. While the last four beta strand (C1-C4, yellow) are topologically identical, there are three N-terminal beta strands in Tm-CorA (N1-N3, magenta) and two in Mrs2 (N1 and N2, magenta). The helix, which is intercalated between the second and the third strand of Tm-CorA is missing in Mrs2$_{48-308}$.

Figure 2 Structural features of and proposed funnel model.
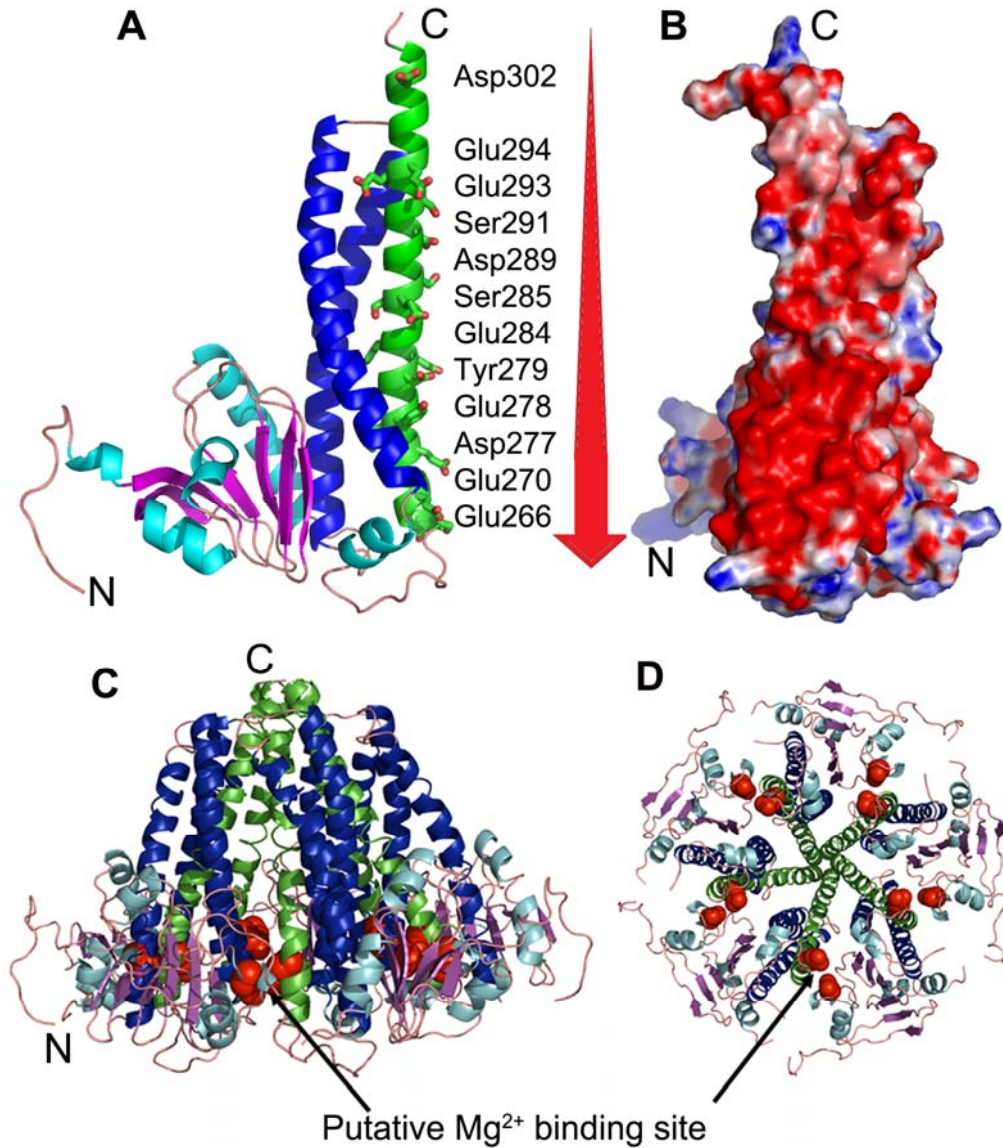
Figure 2 Structural features of Mrs2$_{48\text{-}308}$ and the proposed funnel model. (A) The Mrs2$_{48\text{-}308}$ is represented as ribbon and the side chains of the negatively charged or hydroxyl bearing residues are represented as stick of the helix corresponding to the stalk helix of Tm-CorA which makes the inner side of the pore. (B) Electrostatic surface potential analysis of Mrs2, generated by APBS. Views are from the helix forming the inner wall of the funnel (*red*, negatively charged; *blue*, positively charged; *white*, uncharged). The red arrow shows the gradual increase of negative charge from top to bottom (C) Side view of

the pentamer funnel model of the inner soluble domain of Mrs2 based on Tm-CorA from *Thermotoga maritima*. (D) Bottom view of the pentamer funnel model, highlighting the putative magnesium binding site (red). All structural figures were created with Pymol (http://www.pymol.org/).

Figure 3 Protease susceptibility assay
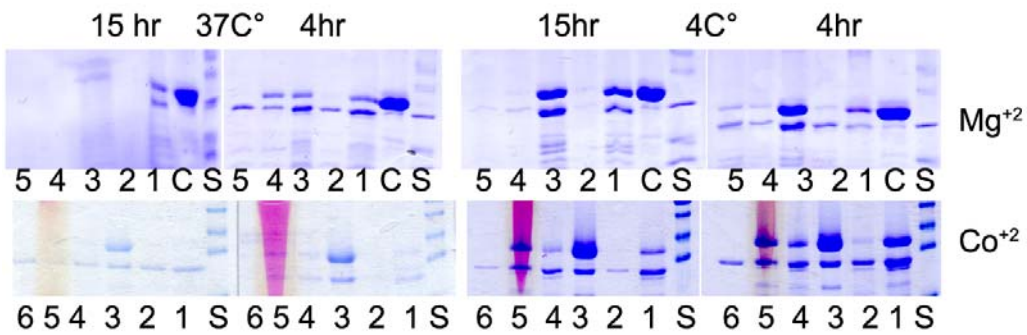
Figure 3 Protease susceptibility assay. Trypsin susceptibility of Mrs2$_{48-308}$ after 4h (right) and 15h (left). Reactions were performed as described in Experimental procedures. Control samples (C) for the different reaction conditions and the molecular weight ladder (S) are shown. The different tested conditions are (1) 20 mM EDTA, (2) 5 mM EDTA, (3) 5 mM EDTA/ 5 mM Mg^{2+}(or 5 mM Co^{2+}), (4) 5 mM Mg^{2+}(or 5 mM Co^{2+}), (5) 20 mM Mg^{2+} (or 20 mM Co^{2+}) and (6) is untreated, native protein.

Figure 4 Evaluation of magnesium binding site in Mrs2$_{48\text{-}308}$ and hydrophobic gate residues in Mrs2 and Tm-CorA
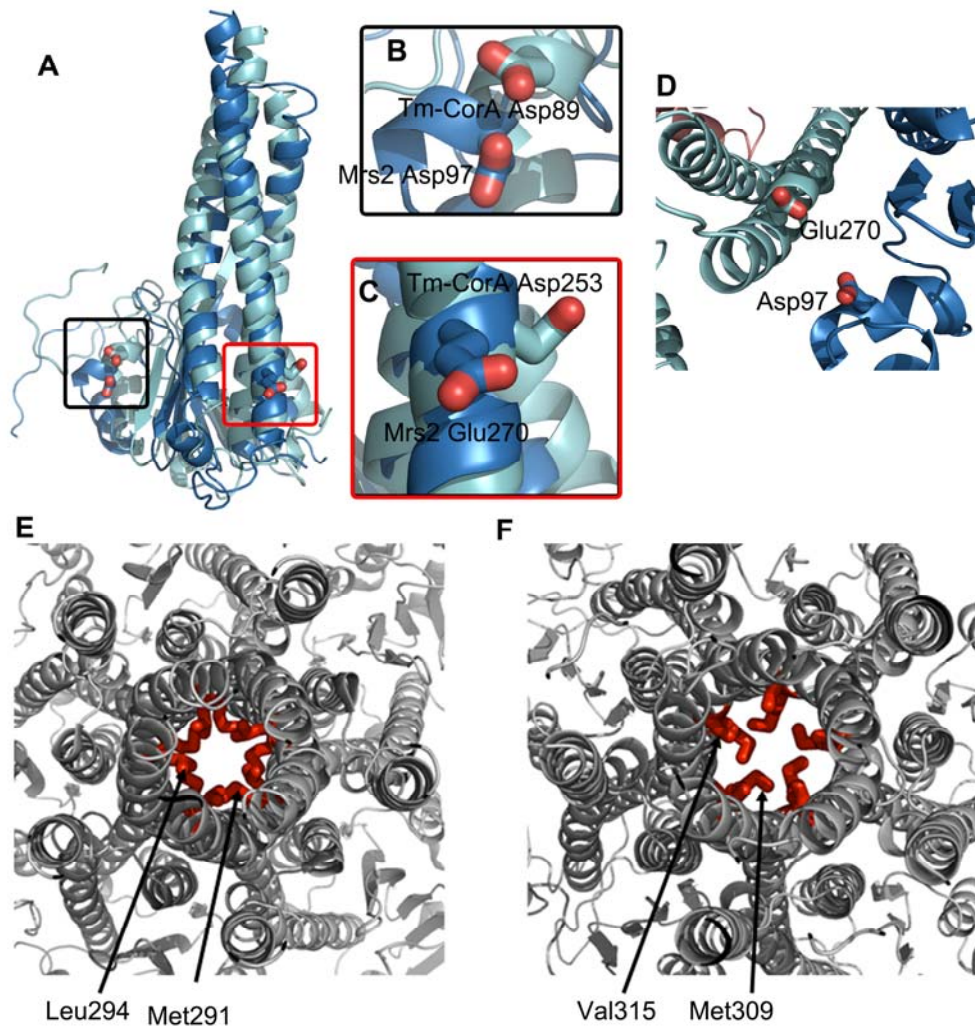
Figure 4 Evaluation of the magnesium binding site in Mrs2$_{48\text{-}308}$ and the hydrophobic gate residues in Mrs2 and Tm-CorA. (A) Superposition of Mrs2$_{48\text{-}308}$ (blue) and Tm-CorA (cyan) soluble domains showing the magnesium binding site of Tm-CorA and the putative magnesium binding site in Mrs2$_{48\text{-}308}$. The coloured boxes relate to panels B and C and show the residues involved in the magnesium sensing. (B) The magnesium binding residue Asp89 of Tm-CorA and the corresponding putative magnesium binding residue Asp97 of Mrs2$_{48\text{-}308}$. (C) The magnesium binding residue Asp253 of Tm-CorA and the corresponding putative magnesium binding residue Glu270 of Mrs2$_{48\text{-}308}$. (D) Putative magnesium binding pocket featuring Asp97 from one monomer (blue) and Glu270 from an adjacent subunit (cyan) in a proposed functional

funnel model. (E) Top view of CorA (PDB code 2IUB) showing the hydrophobic gate residues Met291 and Leu294 (red). (F) Top view of the model of Mrs2 transporter showing the putative hydrophobic gate 1 residue Met309 and gate 2 residue Val315 (red).

Figure 5 Mutations in the hydrophobic gate 1 (Met309) of Mrs2.
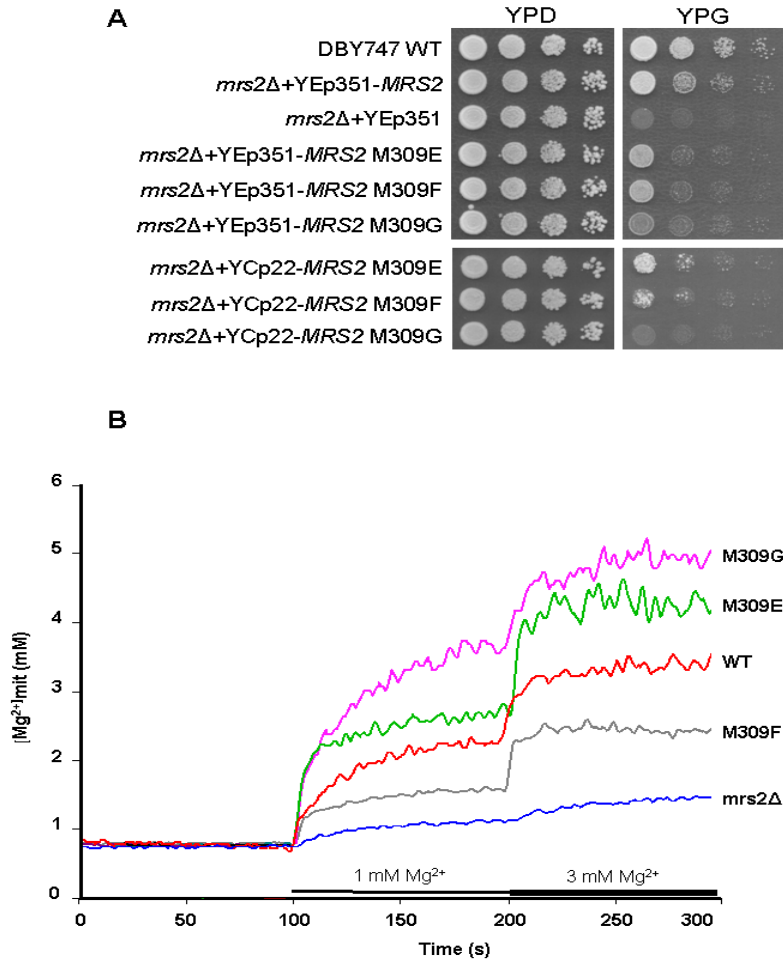
Figure 5 Mutations in the hydrophobic gate 1 (M309) of Mrs2 impairs growth on non fermentable carbon sources and alters the transport activity of the channel. (A) Growth phenotypes of *Saccharomyces cerevisiae* strain DBY747 *mrs2Δ* expressing the corresponding *MRS2* mutant variants from high-copy number vector YEp351 or low copy vector YCp22. Serial dilutions of the different strains were spotted on fermentable (YPD) and non-fermentable (YPG) substrates and grown for three or six days, respectively. (B)

$[Mg^{2+}]_e$-dependent changes in $[Mg^{2+}]_m$ in mitochondria of *mrs2Δ cells*, and cells expressing WT *MRS2* or the mutant variants. Isolated mitochondria were loaded with the Mg^{2+}-sensitive dye mag-fura-2 and changes in the intramitochondrial free Mg^{2+} concentration upon addition of Mg^{2+} to the nominally Mg^{2+}-free buffer, as indicated in the figure, were determined. Representative recordings of four individual measurements are shown.

Figure 6 Characterization of mutants in the hydrophobic gate 2 of Mrs2
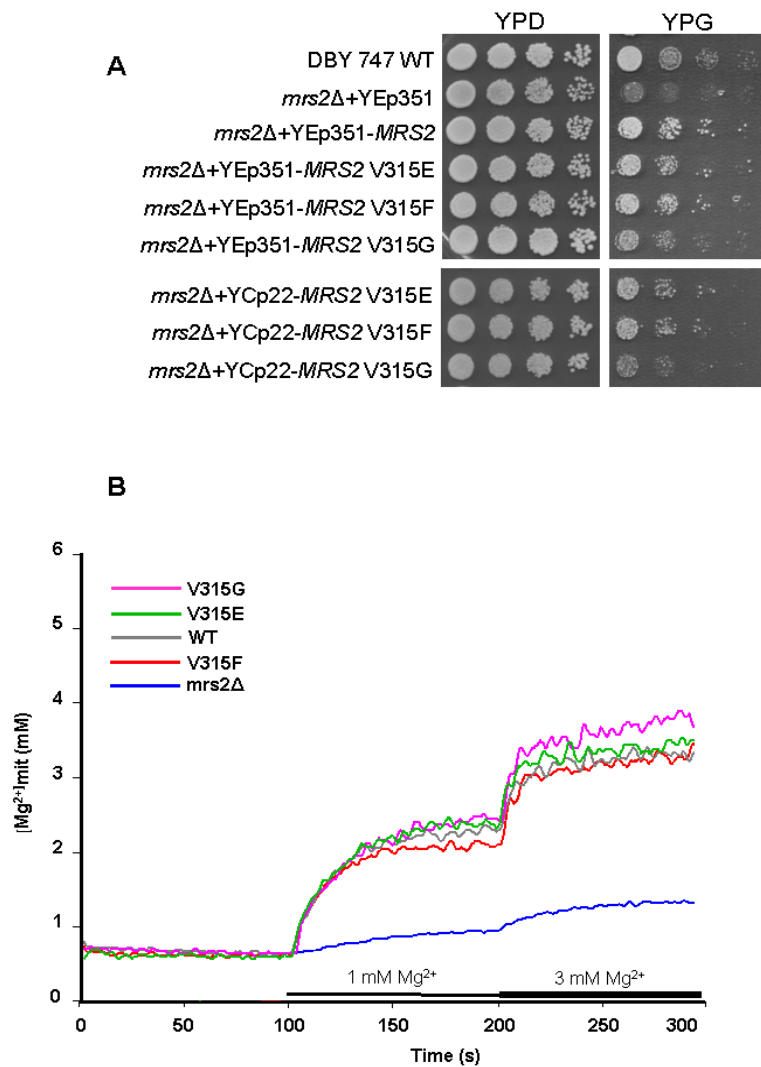
Figure 6 Characterization of mutants in the hydrophobic gate 2 of Mrs2. (A) Serial dilutions of DBY 747 WT and DBY747 *mrs2Δ* cells transformed with the vectors Yep351 and YCp22 expressing *MRS2* or different mutant variants for V315 were spotted on fermentable (YPD) or non-fermentable (YPG) plates and incubated at 28°C for 3 or 6 days, respectively. (B) $[Mg^{2+}]_e$-dependent changes in $[Mg^{2+}]_m$ in mitochondria of DBY747 *mrs2Δ* cells expressing WT *MRS2* or mutant variants of V315. Representative curve traces of three individual measurements are shown.

Figure 7: Characterization of the Mrs2 C-terminus.
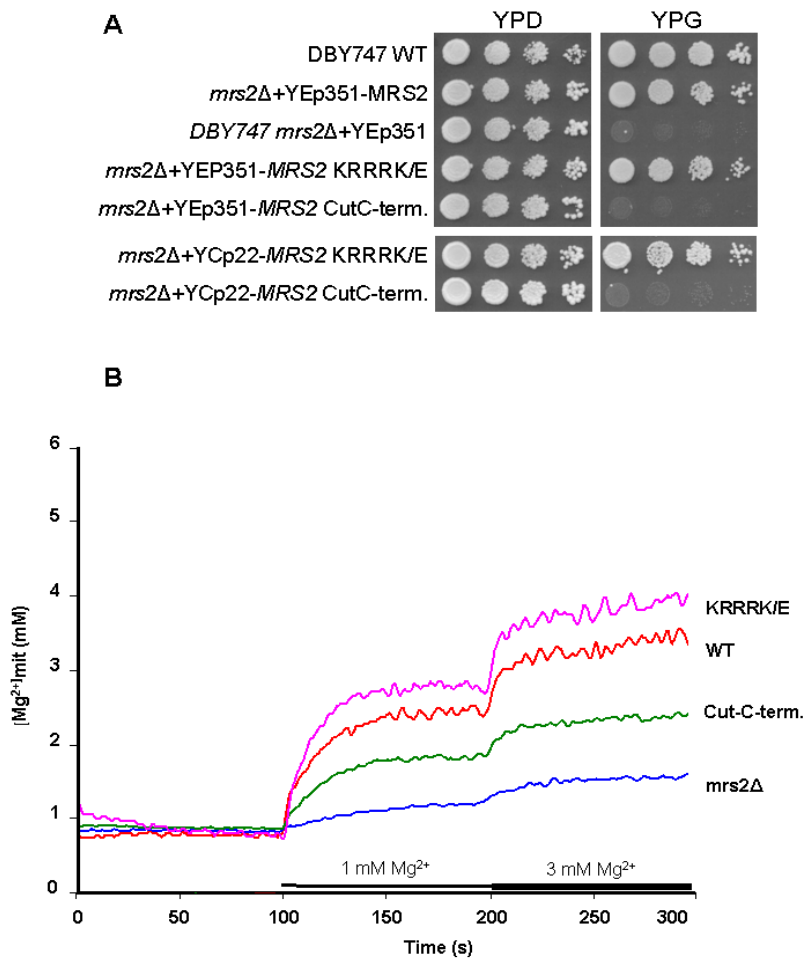
Figure 7 Characterization of the Mrs2 C-terminus. (A) Phenotypes associated with charge reversion of the KRRRK stretch and truncation of the C-terminus after Thr376. Serial dilutions of yeast cultures were spotted on fermentable (YPD) or non-fermentable (YPG) plates and incubated at 28°C for 3 or 6 days, respectively.

(B) $[Mg^{2+}]_e$-dependent changes in $[Mg^{2+}]_m$ in DBY 747 *mrs2Δ* mitochondria expressing the KRRRK/E mutant or the *MRS2* variant with a C-terminal truncation. Representative curve traces of four individual measurements are shown.

Figure 8 Mutation of Asp97 of a putative Mg^{2+} binding site in Mrs2.
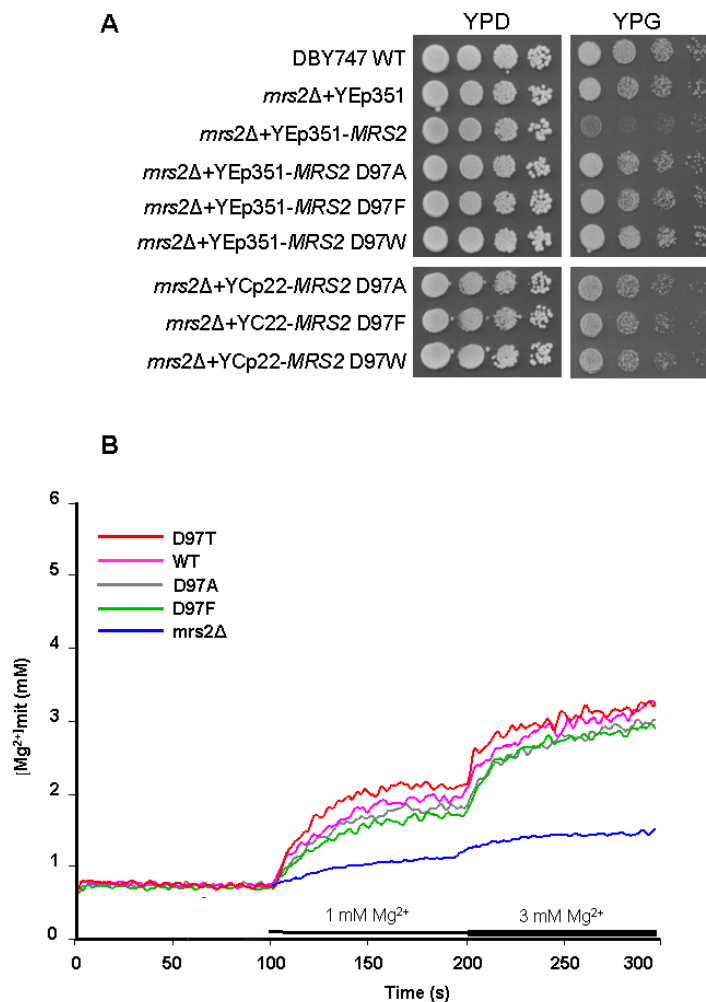
Figure 8 Mutation of Asp97 of a putative Mg^{2+} binding site in Mrs2 does not influence regulation of the transporter. (A) Growth phenotypes of *Saccharomyces cerevisiae* strain DBY747 *mrs2Δ* expressing *MRS2* variants harbouring mutations in the D97 site from high-copy number vector YEp351 or low copy vector YCp22. Serial dilutions of yeast cultures were spotted on fermentable (YPD) or non-fermentable (YPG) plates and incubated at 28°C for 3 or 6 days, respectively. (B) [Mg^{2+}]$_e$-dependent changes in [Mg^{2+}]$_m$ in DBY 747 *mrs2Δ* mitochondria expressing *MRS2* or the mutant variants were determined. Representative curve traces of four individual measurements are shown.

Suppl. Figures:

Supplementary Figure 1 Analytical size exclusion chromatography of Mrs2$_{48-308}$.
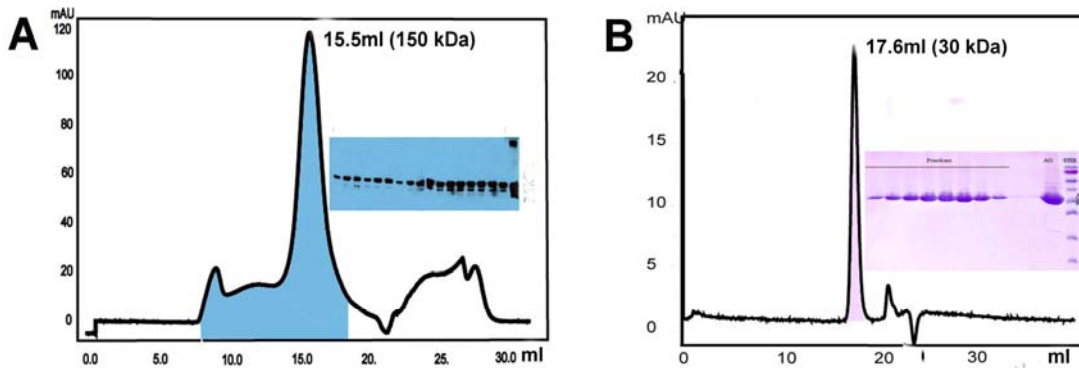
Supplementary Figure 1

Analytical size exclusion chromatography (ASEC) of Mrs2$_{48-308}$. (A) ASEC studies showed that Mrs2$_{48-308}$ behaves as a homo-pentamer in low ionic strength buffers (10 mM Tris-Hcl, 10 mM NaCl) and as a monomer in high ionic strength buffers (50 mM Tris-HCl, 300 mM NaCl) (B). The corresponding peaks are visualized by SDS-PAGE.

Supplementary Figure 2 Circular dichroism spectra of Mrs2₄₈₋₃₀₈.
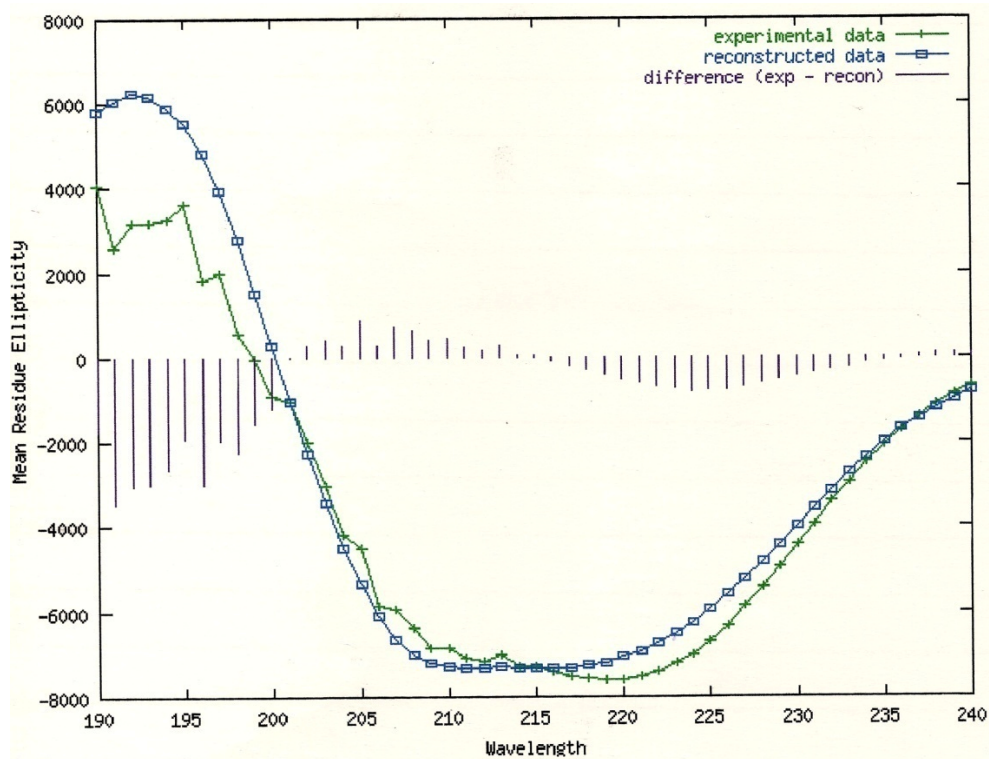
Supplementary Figure 2

Circular dichroism spectra of Mrs2₄₈₋₃₀₈. The mean residual ellipticity of Mrs2₄₈₋₃₀₈ at 1 mg/mL was monitored from 240 to 190 nm. Three scans were performed on individual sample and than averaged. The data were reconstructed and the difference determined by subtracting the reconstructed from the experimental data. It is clear that the circular dichroism (CD) spectrum of Mrs2₄₈₋₃₀₈ showed the minima at 208 and 219 nm, a characteristic for a protein rich in α-helices.

Supplementary Figure 3 Superposition of individual domains of Mrs2$_{48-308}$ on CorA and ZntB.
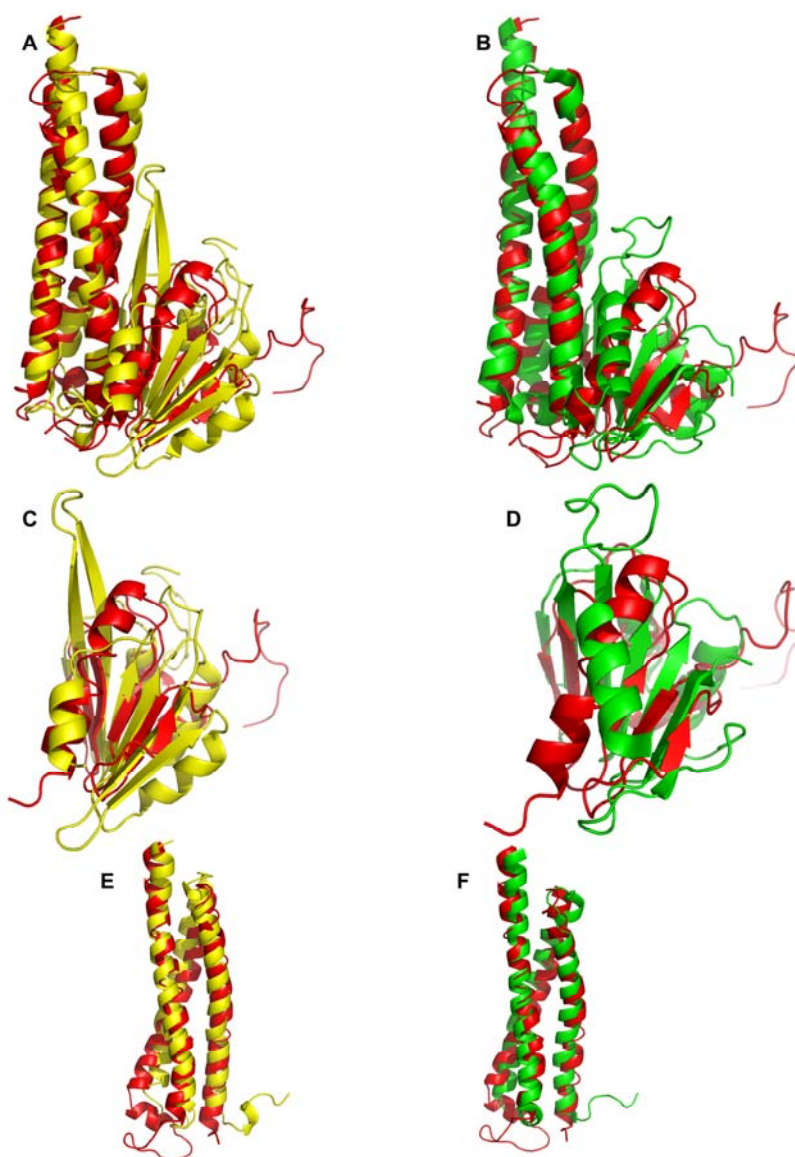
Supplementary Figure 3

Superposition of Mrs2$_{48-308}$ on the soluble domain of Tm-CorA and ZntB. (A) Superposition of the complete soluble domain of Mrs2$_{48-308}$ (red) on soluble domain of Tm-CorA (PDB code 2IUB), with an RMSD of 2.85 Å and mscore 70 % of . (B) Superposition of complete soluble domain of Mrs2$_{48-308}$ (red) on soluble domain of ZntB

(PDB code 3CK6) (green) with an RMSD of 2.61 Å and mscore 67 %. (C) Superposition of α/β/α subdomains of Mrs2$_{48-308}$ (red) and Tm-CorA (yellow) with an RMSD of 2.96 Å and mscore of 59 %. (D) Superposition of α/β/α subdomains of Mrs2$_{48-308}$ (red) and ZntB (green) with an RMSD of 2.75 Å and mscore of 49 %. (E) Superposition of helical subdomains of Mrs2$_{48-308}$ and Tm-CorA with an RMSD of 2.62 Å and mscore of 85 %. (F) Superposition of helical subdomains of Mrs2$_{48-308}$ and ZntB with an RMSD of 2.71 Å and mscore of 91 %. Superpositions were made with a program SHEBA

Supplementary Figure 4 Western Blot analysis of the expression levels of *MRS2* and the different *MRS2* mutant variants.
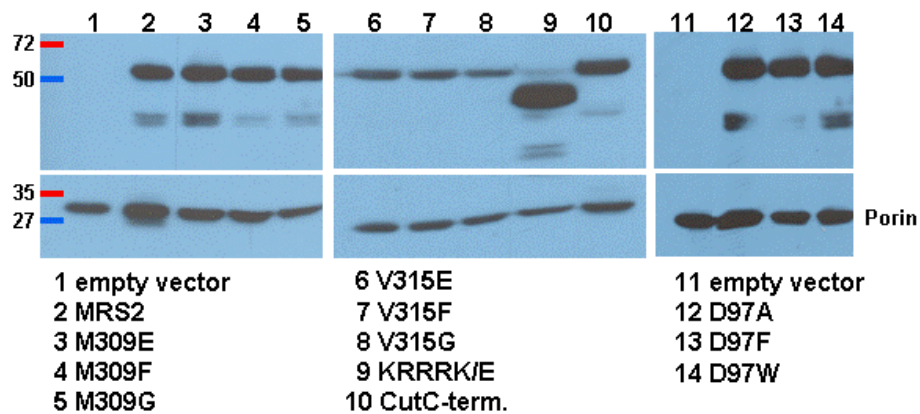
Supplementary Figure 4

Western Blot analysis of the expression levels of *MRS2* and the different *MRS2* mutant variants. Isolated mitochondria of *mrs2Δ* cells transformed with an empty plasmid or high copy number vector Yep351 expressing *MRS2*-HA or the mutant variants were separated by SDS/PAGE and proteins were visualized by immunoblotting with an antiserum against the HA tag. Porin was used as a loading control.

Supplementary Table 1 Number of positively charged residues at the C-terminus of Mrs2 from different species

Name of species	Number of residues at C-terminus	Number of Positively charged residues
Saccharomyces cerevisiae	107	24
Penicillium marneffei	116	21
Penicillium chrysogenum	122	22
Ashbya gossypii	78	16
Kluyveromyces lactis	79	15
Magnaporthe oryzae	198	29
Yarrowia lipolytica	42	14
Debaryomyces hansenii	69	15
Vanderwaltozyma polyspora	83	18
Botryotinia fuckeliana	65	18

3.5. Publication V

Novel components of an active mitochondrial K^+/H^+ exchange

Zotova L., Aleschko M., Sponder G., Baumgartner R., Reipert S., Prinz M., Schweyen R.J., Nowikovsky K.

Novel Components of an Active Mitochondrial K$^+$/H$^+$ Exchange*[s]

Ludmila Zotova[‡1], **Markus Aleschko**[‡1], **Gerhard Sponder**[‡2], **Roland Baumgartner**[‡], **Siegfried Reipert**[§], **Monika Prinz**[‡], **Rudolf J. Schweyen**[†‡], and **Karin Nowikovsky**[‡3]

From the Departments of ‡*Microbiology, Immunobiology, and Genetics* and §*Molecular Cell Biology, Max F. Perutz Laboratories, Vienna University, A-1030 Vienna, Austria*

Defects of the mitochondrial K$^+$/H$^+$ exchanger (KHE) result in increased matrix K$^+$ content, swelling, and autophagic decay of the organelle. We have previously identified the yeast Mdm38 and its human homologue LETM1, the candidate gene for seizures in Wolf-Hirschhorn syndrome, as essential components of the KHE. In a genome-wide screen for multicopy suppressors of the *pet$^-$* (reduced growth on nonfermentable substrate) phenotype of *mdm38Δ* mutants, we now characterized the mitochondrial carriers *PIC2* and *MRS3* as moderate suppressors and *MRS7* and *YDL183c* as strong suppressors. Like Mdm38p, Mrs7p and Ydl183cp are mitochondrial inner membrane proteins and constituents of ~500-kDa protein complexes. Triple mutant strains (*mdm38Δ mrs7Δ ydl183cΔ*) exhibit a remarkably stronger *pet$^-$* phenotype than *mdm38Δ* and a general growth reduction. They totally lack KHE activity, show a dramatic drop of mitochondrial membrane potential, and heavy fragmentation of mitochondria and vacuoles. Nigericin, an ionophore with KHE activity, fully restores growth of the triple mutant, indicating that loss of KHE activity is the underlying cause of its phenotype. Mdm38p or overexpression of Mrs7p, Ydl183cp, or LETM1 in the triple mutant rescues growth and KHE activity. A LETM1 human homologue, HCCR-1/LETMD1, described as an oncogene, partially suppresses the yeast triple mutant phenotype. Based on these results, we propose that Ydl183p and the Mdm38p homologues Mrs7p, LETM1, and HCCR-1 are involved in the formation of an active KHE system.

The high, inside negative membrane potential ($\Delta\psi$) of mitochondria favors uptake of cations through the inner mitochondrial membrane. Potassium is an osmotically active ion and the most abundant cation in the cytosol and in the mitochondrial matrix. The uncontrolled influx of K$^+$ into mitochondria causes an increase of osmotic pressure of the organelles and their swelling. The presence of K$^+$/H$^+$ exchangers in mitochondria which, driven by the inside-directed pH gradient, extrude excess K$^+$ from mitochondria was already postulated in the 1960s by Mitchell (1). Although the KHE[4] has been studied extensively by physiological methods, its molecular identity remained obscure. Recently, our studies identified Mdm38/LETM1 as major players of this extrusion system (2–4).

Phenotypic analyses of *mdm38Δ* are consistent with the loss of KHE activity (4). These included increased matrix K$^+$ content, swelling, and fragmentation of mitochondria, reduced mitochondrial $\Delta\psi$, as well as reduced growth of cells on nonfermentable substrate. Further tests involving submitochondrial inner membrane particles (SMPs) confirmed the near total lack of KHE activity (2). Addition of the synthetic KHE nigericin to *mdm38Δ* cells restored all mitochondrial functions, including growth on nonfermentable substrates, $\Delta\psi$, morphology, and KHE activity (4, 5). This result strongly supported the conclusion that Mdm38 acts as an essential regulator or subunit of the mitochondrial KHE, because it is unlikely that a protein with only one transmembrane domain like Mdm38 forms the KHE itself.

Mdm38p is conserved in all eukaryotic organisms. The human homologue, LETM1, has been implicated in the Wolf-Hirschhorn syndrome (6). The yeast *Saccharomyces cerevisiae* encodes a homologue, *YPR125w*. *YPR125w* had initially been identified as a multicopy suppressor of mutants lacking the mitochondrial Mg^{2+} transporter *MRS2* and was named *MRS7* (7). *YPR125w/MRS7*, also named *YLH47* for yeast LETM1 homologue of 47 kDa (6), encodes a protein located in mitochondria (4, 8). Although disruption of *MRS7* has a weak phenotype, its overexpression restores growth of *mdm38Δ* strains, showing a functional homology to Mdm38p (4). The human genome also encodes a second member of the Mdm38/LETM1 family, named HCCR-1 or LETMD1, which was found to be overexpressed in various human cancer cells (9).

Here, we characterize the role of four yeast multicopy suppressors of *mdm38Δ* as well as of LETM1 and HCCR-1 with

---

[s] The on-line version of this article (available at http://www.jbc.org) contains supplemental Figs. 1–4 and an additional reference.

This paper is dedicated to the memory of Rudolf Schweyen, who tragically passed away during the writing of this manuscript.

† Deceased February 15, 2009.

[1] Both authors contributed equally to this work.

[2] To whom correspondence may be addressed: Dept. of Microbiology, Immunobiology and Genetics, Max F. Perutz Laboratories, Vienna University, Dr. Bohr Gasse 9, A-1030 Wien, Austria. Tel.: 43-1-4277-54619; Fax: 43-1-4277-9546; E-mail: gerhard.sponder@univie.ac.at.

[3] To whom correspondence may be addressed: Dept. of Microbiology, Immunobiology and Genetics, Max F. Perutz Laboratories, Vienna University, Dr. Bohr Gasse 9, A-1030 Wien, Austria. Tel.: 43-1-4277-54619; Fax: 43-1-4277-9546; E-mail: karin.nowikovsky@univie.ac.at.

[4] The abbreviations used are: KHE, K$^+$/H$^+$ exchanger; SMP, submitochondrial particle; FM4-64, *N*-(3-triethylammoniumpropyl)-4-(6-(4-(diethylamino)phenyl)hexatrienyl)pyridinium dibromide; GFP, green fluorescent protein; HA, hemagglutinin; CoIP, coimmunoprecipitation; ORF, open reading frame; Ni-NTA, nickel-nitrilotriacetic acid; GFP, green fluorescent protein; BCECF, 2′,7′-bis(carboxyethyl)-5,6-carboxyfluorescein; BN, Blue Native; YFP, yellow fluorescent protein; PBFI, potassium-binding benzofuran isophthalate.

respect to their potential to restore K$^+$/H$^+$ exchange activity. We find that like Mdm38p, Mrs7p and Ydl183cp are part of a large mitochondrial KHE protein complex. We discuss its putative composition and analyze the additive effects resulting from the triple deletion of *MDM38*, *MRS7,* and *YDL183c.*

EXPERIMENTAL PROCEDURES

Yeast Strains and Growth Media—The *S. cerevisiae* strains W303 (ATCC accession number 2012239) and DBY747 (ATCC accession number 204659) were used as wild type. W303 *mdm38*::HIS3 termed *mdm38*Δ was described previously (4). W303 cells were grown in YPD (yeast extract, bacto peptone, 2% dextrose), YPG (2% glycerol) or YPGal (yeast extract, bacto peptone, 2% galactose) media as indicated. YPG plates were supplemented with 2 μM nigericin when indicated. Synthetic minimal media (S-Gal, synthetic medium containing 2% galactose, or SD, synthetic medium with 2% dextrose, 2% glucose) were supplemented with amino acids and bases when appropriate.

Genomically tagged versions of *MDM38* and *MRS7* were constructed by homologous recombination. The TAP tag and the selection marker *TRP1*-KL were amplified by PCR from the vector pBS1479 (10). The following primers were used to create a C-terminally tagged version of *MDM38* with His$_6$ and the TAP tag consisting of two immunoglobulin binding domains of protein A and the calmodulin-binding peptide: *MDM38*HisTAPfw, 5′-TACCT-CCCATTCCGGCCGATCAAGCTGCGAAGACTTTTGTCA-TTAAGAAAGATCATCACCATCACCATCACTCCATGGA-AAAGAGAAG-3′; *MDM38*HisTAPrev, 5′-CCTGATGTA-CTCACATTTCCATCTGGTGAGGATGGAGGTGGAGA-CGTCGTAGACATGGAACCCTGTTTACGACTCACTA-TAGGG-3′. For tagging *MRS7* with His$_6$ and TAP tag, the following primers were used: *MRS7*HisTAPfw, 5′-AACCG-CATGACACCAAGCCTATCGGAGAAGCCGCTGCCAT-CAAAGAGAAGCATCACCATCACCATCACTCCATGG-AAAAGAGAAG-3′; *MRS7*HisTAPrev, 5′-TAGACACTCT-ATTCTTTGAGTAATTTTGAGGGAGAGCAGCAATG-ATTAACTACGACTCACTATAGGG-3′.

To create chromosomal, C-terminally His$_6$-tagged versions of *MDM38* and *MRS7,* the following forward primers were used: *MDM38*Hisfw, 5′-TTCCGGCCGATCAAGCTGCGAAGACT-TTTGTCATTAAGAAAGATCATCACCATCACCATCACT-GATCCATGGAAAAGAGAAG-3′; *MRS7*Hisfw, 5′-CGCATG-ACACCAAGCCTATCGGAGAAGCCGCTGCCATCAAAGA-GAAGCATCACCATCACCATCACTAATCCATGGAAAAG-AGAAG-3′. *MDM38*HisTAPrev and *MRS7*HisTAPrev served as reverse primers, respectively. To create chromosomal, C-terminally One-STrEP (11)-tagged versions of *MDM38* and *MRS7,* the One-STrEP sequence (based on the plasmid pEXPR-IBA103, IBA BioTAGnology) was synthesized (Eurofins MWG GmbH) and cloned into the BamHI-linearized pBS1479 plasmid. Chromosomal integration was performed using the forward primers: *MDM38*OneSTrEPfw, 5′-CATTCCGGCCGATCAAGCTGCG-AAGACTTTTGTCATTAAGAAAGATGAGAATTTGTATT-TTCAGG-3′, and MRS7OneSTrEPfw 5′-GCATGACACCAA-GCCTATCGGAGAAGCCGCTGCCATCAAAGAGAAGG-

AGAATTTGTATTTTCAGG-3′. *MDM38*HisTAPrev and *MRS7*HisTAPrev served as reverse primers, respectively.

Multicopy Suppressor Screen—The *mdm38*Δ mutant strain was transformed with 1 μg of genomic library (constructed in YEp181, a 2-μm plasmid marked with *LEU*2, gift of Juraj Gregan and Kim Nasmith, IMP, Vienna, Austria). Transformants growing on SD−leu plates were replica-plated on YPG plates and incubated at 37 °C. Three hundred ninety six positive putative candidates were selected and classified into strong or weak suppressors. To confirm that the suppression was plasmid-borne, the plasmids were recovered, amplified in *Escherichia coli*, used for retransformation of W303 *mdm38*Δ, and tested for growth on YPG plates at 37 °C. Confirmed plasmids were then analyzed by restriction digestion patterns to eliminate self-complementation, and the inserts of selected plasmids were sequenced by VBC-Biotech Services GmbH. The suppressor plasmids contained multiple ORFs. Individual ORFs were subcloned and tested for their ability to suppress the growth phenotype. The individual plasmids containing *PIC2*, *MRS3*, *MRS7*, or *YDL183c* were used in all experiments if not otherwise indicated.

Gene Deletions—Deletion of the genes was performed according to the one-step replacement protocol (12). The *MRS7* ORF was disrupted from the start to the stop codon by replacement with the *KANMX4* disruption cassette, which was amplified with the primers 5′-TAGGTTCGAGTAAAGAAA-ATTTCATAAAGAAATCAACAAGACACACGTACGCTG-CAGCTCGAC-3′ and 5′-GCGGAGAGTGTATCGTGCGG-TTTAATGGGCCAGGTGAAAACTGGGATCGATGAATT-CGAGCTCG-3′. To delete *YDL183c* in W303, the whole ORF was replaced with a *URA3* disruption cassette flanked by loxP sites, using the primers 5′-CATCGATAGAATCATTTTATC-ACAATACCAAAACTT-3′ and 5′-CTCAGGAATACCTGT-TATGTATATTTACATGAGATA-3′. Following verification of the correct gene replacement using analytical PCR (12), the selection marker was removed with the CRE recombinase containing vector pSH63 (13). *YDL183c* deletion in DBY747 was performed by replacement with the *LEU2* disruption cassette, using the primers 5′-TCACAATACCAAAACTTCATCCGG-TGTATTTTAGATTAAAGCGTACGCTGCAGGTCGAC-3′ and 5′-ACCTGTTATGTATATTTACATGAGATAGTGGA-CAATCTACATAGGCCACTAGTGGATCTG-3′. Double and triple deletion strains were obtained in W303 by crossing and sporulation of the diploids or in DBY747 by stepwise disruptions.

Plasmid Constructs—To provide *MRS7*, *MDM38*, and *YDL183c* with a C-terminal GFP tag, the entire respective ORFs were cloned into the centromeric vector pUG35 (14). *MRS7* coding sequence was amplified by PCR from YEp351-*MRS7* plasmid (7) with the 5′ primer 5′-ACAA<u>GAATTC</u>ATGCT-GAAATACAGGTC-3′ and the 3′ primer 5′-ACAT<u>GTCGAC</u>-CTTCTCTTTGATGGC-3′ (EcoRI and SalI sites are underlined) and cloned into the EcoRI/SalI sites of the plasmid pUG35 carrying the methionine promoter. To clone *YDL183c* into the pUG35 plasmid, the entire ORF sequence was amplified by PCR from W303 genomic DNA by use of 5′ primer 5′-CG<u>GGATCC</u>ATGATACGTTCAATATTTATACCGC-3′ and 3′ primer 5′-GC<u>GTCGAC</u>AATTTTGTTTTTTCTCTT-

GAGATTTCG-3′ introducing the underlined BamHI and SalI restriction sites. The amplified fragment was cloned into the BamHI- and SalI-linearized pUG35 plasmid. A C-terminally GFP-tagged version of the entire ORF *MDM38* was obtained by cloning *MDM38* in pUG35 by use of the forward primer 5′-TAATATGGATCCATGTTGAATTTCGCATCAAGAGCG-3′ and the reverse primer 5′-AATATCTATCGATCT-TAATGACAAAAGTCTTCGC-3′ (BamHI and ClaI sites *underlined*).

To express *YDL183c* from its own promoter and in fusion with the triple HA epitope at the C-terminal end, the entire ORF and its flanking region, including 217 nucleotides upstream of the ATG, were amplified from W303 genomic DNA with the primers 5′-CTTGAGCTCGGATGGATG-GACTTGACGGC-3′ and 5′-GCGTCGACCAATTTGTTTT-TCTCTTGAGATTTCC-3′ and inserted in the SacI/SalI sites of the YCp33-HA vector. The vectors YCp33-*MDM38*-HA and Yep351-*MDM38*-HA expressing Mdm38p under the control of its native promoter and pVTU103-LETM1-HA expressing the human LETM1 from the *ADH* promoter were described previously (4). To express HCCR-1 in yeast, the entire ORF was amplified from MGC IRAT human (Invitrogen 6009854) with the forward primer 5′-AACGGGATCCCGGATGGCGCTCT-CCAGGGTGTG-3′ and the reverse primer 5′-CATGCTCGA-GTCAGTGGTGGTGGTGGTGGTGGCGCCTTGTCCCA-AGGTAGT-3′ digested with BamHI and XhoI and inserted in the pVTU103 vector.

Isolation and Subfractionation of Mitochondria—Yeast mitochondria used for ion-flux measurements were isolated from cells growing overnight to stationary phase. For all other experiments, cells were grown to $A_{600} = 1$. Mitochondrial isolation and mitoplast preparation were done as described previously (15). Protein extraction with sodium carbonate was performed according to Ref. 16 followed by protein precipitation with trichloroacetic acid and Western blotting analysis. Proteinase K protection experiments were performed as described previously (17). Resuspended mitoplasts were incubated in the presence or absence of proteinase K as indicated for 20 min, and the proteinase K reaction was inactivated with 1 μM phenyl-methylsulfonyl fluoride, and the proteins were trichloroacetic acid-precipitated. 50 μg of protein were loaded in each lane of a 12.5% SDS-PAGE, transferred onto polyvinylidene difluoride membrane, and immunoblotted in Tris-buffered saline/Tween plus 2.5% dry milk with the antibodies against the following: HA (laboratory stock; hexokinase-1 (Biotrend); $F_1\beta$, Tim44, and Yme1 (generous gifts of Gottfried Schatz, Hans van der Spek, and Tom Fox, respectively). The proteins were visualized by use of the SuperSignal™ West Pico system (Pierce).

Blue Native PAGE—Proteins of isolated mitochondria were solubilized as indicated with 1.2% *n*-dodecyl-D-maltoside or Triton X-100, and after a clarifying spin, 200 μg of proteins (25 μl) per lane were separated by BN-PAGE according to Ref. 18 on 5–18% polyacrylamide gradient gels. Following electrophoresis, wet blotting to polyvinylidene difluoride membrane was performed for 1 h at 100 V. Protein complexes were detected by immune decoration. The calibration standards (Amersham Biosciences) used in the BN-PAGE were bovine thyroglobulin (669 kDa), horse spleen apoferritin (440 kDa), bovine

liver catalase (232 kDa), bovine heart lactate dehydrogenase (140 kDa), and bovine serum albumin monomer (67 kDa).

Affinity Chromatography—180 mg of isolated mitochondria were used for standard protein purification. Isolated mitochondria were adjusted to a concentration of 20 mg/ml. For affinity chromatography using Ni-NTA Superflow resin (Qiagen), mitochondria were solubilized with 1.2% Triton X-100 on ice for 30 min in Hi 50 buffer (10 mM Tris-HCl, pH 7.8, 50 mM NaCl, 20 mM imidazole, protease inhibitor mixture (Complete Mini, Roche Applied Science)). After centrifugation at 43,000 × *g* for 30 min (4 °C) to remove nonsolubilized mitochondrial debris, the Triton concentration of the supernatant was reduced to 1% by addition of Hi 50 buffer. Ni-NTA Superflow resin (Qiagen) was washed two times with 10 ml of Hi 50 buffer containing 1% Triton X-100. The clarified supernatant was incubated with the resin for 30 min under gentle shaking and loaded on a Poly-Prep chromatography column (Bio-Rad). The column was washed twice with 15 ml of Hi 50 Wash buffer 1 (0.8% Triton X-100, 20 mM imidazole) and twice with 15 ml of Hi 50 Wash buffer 2 (0.6% Triton X-100, 30 mM imidazole). Finally, bound proteins were eluted with Hi 50 Elution buffer (10 mM Tris-HCl, pH 7.8, 50 mM NaCl, 200 mM imidazole, 0.6% Triton X-100 and, unless otherwise stated, complete protease inhibitor mixture).

For streptavidin affinity chromatography using Strep-Tactin Superflow (Qiagen), mitochondria were solubilized with 1.2% Triton X-100 in Strep 50 buffer (100 mM Tris-HCl, pH 7.8, 50 mM NaCl, protease inhibitor mixture). All other steps were performed as described for the Ni-NTA chromatography except that Strep-Tactin Superflow (Qiagen) was used as affinity resin, and bound proteins were eluted with Strep 50 buffer with a final concentration of 2.5 mM D-desthiobiotin.

All purification steps were performed at 4 °C. Control experiments were performed for each affinity chromatography with untagged or untransformed DBY747 wild-type or *mdm38Δ* strains. Two-dimensional gel electrophoresis was performed as described previously (19). Anti-His antibody was purchased from Qiagen, and anti-Mdm38 was generously provided by P. Rehling.

Coimmunoprecipitation (CoIP)—UltraLink immobilized protein A, covalently bound to HA antiserum with the cross-linker, was kindly provided by A. Pichler. Isolated mitochondria (2 mg of protein) expressing YEp-*MDM38*-HA (70 kDa) and either pUG-*MDM38*-GPF (92 kDa), Y*DL183*-GFP (64 kDa), or *AIF*-GFP (68 kDa) were solubilized for 30 min in RIPA buffer (50 mM Tris, pH 7.4, 150 mM NaCl, 1% Nonidet P-40, 0.5% sodium deoxycholate, 0.1% SDS containing 1.2% *n*-dodecyl-D-maltoside (Sigma)) and protease inhibitor mixture (complete Mini, Roche Applied Science) plus 1 mM phenylmethylsulfonyl fluoride and, after a clarifying spin, incubated under rotation for 1 h with 10 μl of the HA-coupled beads, washed four times in RIPA buffer, and eluted in Laemmli buffer. Proteins were separated on 12.5% SDS-PAGE, transferred, and analyzed by immunoblotting with GFP (Roche Applied Science) and HA (laboratory stock) antibodies.

Measurements of the Mitochondrial Membrane Potential—The membrane potential of isolated mitochondria was recorded in an LS 55 fluorescence spectrometer (PerkinElmer Life Sciences) by monitoring the fluorescence of 5,5′,6,6′-tetra-chloro-1,1,3,3′-tetraethylbenzimidazolylcarbocyanine iodide

(Molecular Probes) according to Ref. 20. Measurements were carried out in breaking buffer (0.6 M sorbitol, 10 mM Tris-HCl, pH 7.4). For calibration, aliquots of the same preparation were hyperpolarized with 1 μM nigericin (Sigma) and depolarized with 1 μM carbonyl cyanide *p*-trifluoromethoxyphenylhydrazone (Sigma) in breaking buffer. The reading after addition of nigericin was set as 100% and that after carbonyl cyanide *p*-trifluoromethoxyphenylhydrazone as 0%. The values were linearized, and the relative membrane potential was calculated using $y = kx + d$.

K^+/H^+ *Exchange Measurements in SMPs*—Preparations of SMPs and loading with the K^+- and H^+-sensitive fluorescent dyes potassium-binding benzofuran isophthalate (PBFI) and BCECF (both Invitrogen) were made as described previously (2). SMPs were treated with 1 μM antimycin A and 1 μM oligomycin prior to measurements. To determine the kinetics of K^+ and H^+ transport across the membrane, 150 mM KCl was added to the SMPs. When indicated, incubation of SMPs with 10 μM nigericin (Sigma) was done at room temperature for 5 min before the measurements. All measurements were repeated at least three times with different preparations of SMPs.

Confocal Microscopy—The plasmids pHS72 (TOM72-YFP) (21) and pYX232-mtGFP (22) were gifts from H. Sesaki and B. Westermann, respectively, and served to label mitochondria. Alternatively, mitochondria were labeled with Mitotracker Red (100 nM). Vacuoles were stained with FM4-64 in a final concentration of 10 μM (Molecular Probes). Microscopy settings were used as described previously (5).

Electron Microscopy—Cells were harvested at logarithmic growth phase ($A_{600} = 1$). Cryofixation, freeze substitution, thin sectioning, and image acquisition were performed as described previously (5).

RESULTS

PIC2, MRS3, MRS7, and a Novel Gene YDL183c Act as Multicopy Suppressors of mdm38Δ—Absence of Mdm38p in yeast cells (*mdm38Δ* mutants) results in reduced growth on nonfermentable substrate (*pet⁻* phenotype) (4). According to our previous data, the antibiotic nigericin, a KHE ionophore, acts as a multivalent suppressor of the *mdm38Δ* deletion phenotype. It restores cell growth on nonfermentable substrate, KHE activity, and $\Delta\psi$ and reverts matrix swelling and fragmentation of mitochondria (5).

To identify proteins substituting similarly for the function of *MDM38*, we have screened a yeast genomic library and selected suppressor genes that, being overexpressed, restored growth of *mdm38Δ* on nonfermentable substrate (Fig. 1). Among the suppressors, we found three previously described genes, *PIC2, MRS3,* and *MRS7,* encoding mitochondrial proteins. *PIC2* and *MRS3* encode mitochondrial carrier proteins involved in P_i transport and Fe^{2+} accumulation, respectively (23, 24). *MRS7* encodes a functional homologue of Mdm38p, located in the inner membrane of mitochondria, with a weak deletion phenotype depending on the strain (7, 8). Additionally, we found one not yet characterized gene, *YDL183c.*

Up-regulation of Pic2, Mrs3, Mrs7, Ydl183c, or Human LETM1 Increases the Mitochondrial Membrane Potential of mdm38Δ—$\Delta\psi$ was found to be moderately reduced in *ydl183cΔ* or *mrs7Δ* and substantially impaired in *mdm38Δ*
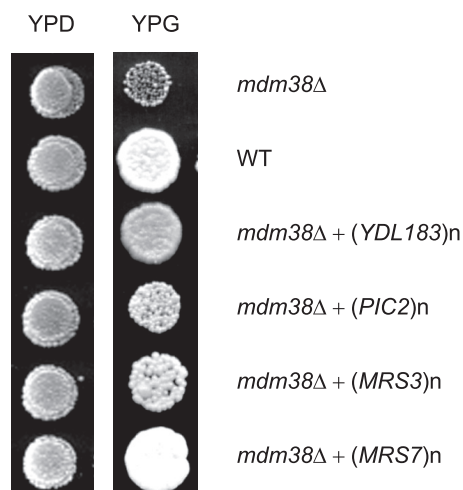
FIGURE 1. **Multicopy suppressors and their growth effects on *mdm38Δ*.** Effects of *YDL183c, PIC2, MRS3,* and *MRS7* on the nonfermentative growth of *mdm38Δ* cells are shown. W303 *mdm38Δ* mutant cells containing an empty vector or a vector overexpressing *YDL183c, PIC2, MRS3,* or *MRS7* and wild-type (*WT*) cells were spotted onto YPD or YPG plates and grown at 28 °C for 3 or 5 days, respectively.

mitochondria. Having determined that overexpression of Pic2p, Mrs3p, Mrs7p, and Ydl183cp rescued the nonfermentative cellular growth of *mdm38Δ*, we asked whether this positive growth effect also correlated with a rise of the mitochondrial $\Delta\psi$ of the *mdm38Δ* mutant. Although $\Delta\psi$ was slightly increased upon overexpression of Pic2p and more significantly upon overexpression of Mrs3p in *mdm38Δ*, overexpression of Mrs7p and Ydl183cp in the mutant restored $\Delta\psi$ close to the wild-type levels (Table 1).

Mitochondrial Morphology Is Restored upon Overexpression of the Suppressor Genes in mdm38Δ—Next, we investigated whether high copy expression of the suppressor genes reversed the fragmentation of *mdm38Δ* mitochondria. For this purpose, *mdm38Δ* cells expressing a GFP targeted to the mitochondrial matrix and a vector with or without the suppressor genes were observed under the confocal microscope. Mitochondria from *mdm38Δ* cells transformed with the empty vector appeared fragmented into large unconnected spheres (Fig. 2a). Compared with wild-type cells, *mdm38Δ* cells displayed wild-type-like elongated tubular mitochondria in only about 3% of the population. Mutant *mdm38Δ* cells overexpressing *PIC2* exhibited a heterogeneous mixture of spherical and tubular mitochondria, indicating a partial reversion of the phenotype (Fig. 2c). Overexpression of *MRS3, YDL183c,* or *MRS7* resulted in a tubular mitochondrial network (Fig. 2, *d–f,* respectively, and Table 2) similar to that displayed by wild-type cells (Fig. 2b). The percentage of elongated tubular mitochondria was shifted to almost 80% upon overexpression of Pic2 and to about 95% when Mrs3, Mrs7, or Ydl183c was overexpressed (Table 2).

YDL183c Is a Strong Suppressor for Mitochondrial KHE Activity in mdm38Δ—Because swelling, depolarization, and fragmentation of *mdm38Δ* mitochondria result from loss of mitochondrial KHE activity and mitochondrial K^+ overload (5), we next asked whether overexpression of the suppressor genes restored the mitochondrial defects by modulating the KHE activity.

TABLE 1

Relative $\Delta\psi$ of *mdm38Δ* (Δ) and *mdm38Δ mrs7Δ ydl183cΔ* ($\Delta\Delta\Delta$) mutants in function of the overexpressed suppressor genes

The relative $\Delta\psi$ of mitochondria are expressed in % relatively to hyperpolarization of the probe with nigericin. ND, no data.

Strains	Vectors						
	Empty	*PIC2*	*MRS3*	*MRS7*	*YDL183*	*MDM38*	*LETM1*
Δ	48	62 ± 3.4	85 ± 2.7	98 ± 3	92 ± 6	95 ± 6	ND
$\Delta\Delta\Delta$	17 ± 2	ND	ND	89 ± 3.3	78.6 ± 3.3	62.3 ± 3.4	82.3 ± 5.2
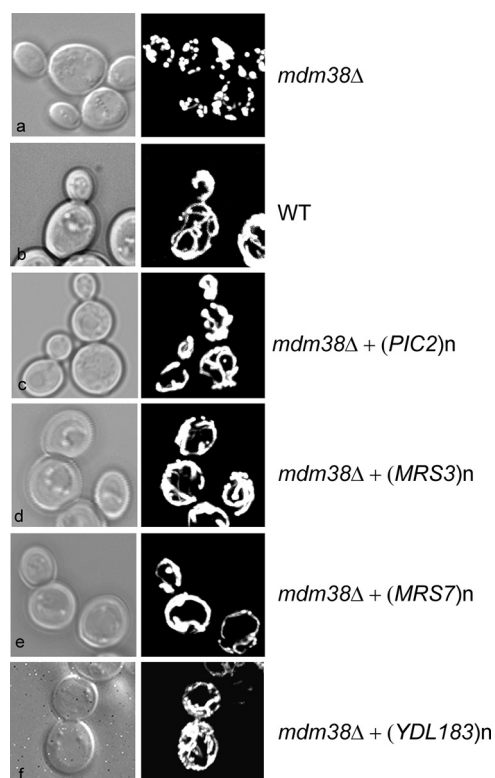
FIGURE 2. **Mitochondrial morphology in function of overexpression of the proteins Pic2, Mrs3, Mrs7, or Ydl183c in W303 *mdm38Δ* mutant cells.** Mitochondrial morphology of cells cotransformed with a mitochondrial matrix targeted GFP (pYX232-mtGFP) and the vector without (*a*) or with the following suppressor genes: *PIC2* (*c*), *MRS3* (*d*), *YDL183c* (*f*), and *MRS7* (*e*) were compared with wild-type (*WT*) cells (*b*). Cells were grown in galactose-containing medium and analyzed by differential interference contrast (Nomarski) and confocal fluorescence microscopy.

TABLE 2

Mitochondrial morphology of W303 *mdm38*D cells in function of the overexpressed suppressor gene

Strains were grown overnight, and mitochondrial morphology was visualized by detection of the expression of the mitochondrial targeted matrix GFP under fluorescence microscopy. Cells were counted with hidden identity.

Strain	Total cells	% cells with fragmented mitochondria
Wild type	602	2.6 ± 1.6
mdm38Δ	680	89.0 ± 5.8
mdm38Δ+(*MRS7*)*n*	1660	7.3 ± 2.6
mdm38Δ+(*PIC2*)*n*	870	20.3 ± 4
mdm38Δ+(*MRS3*)*n*	1126	10.6 ± 6.3
mdm38Δ+(*YDL183c*)*n*	1040	7.7 ± 3.8

We have developed a method to measure the KHE activity across the mitochondrial inner membrane using SMPs with entrapped K^+- and H^+-sensitive fluorescent dyes PBFI and BCECF (2). This approach allows controlling internal and external ion milieus at will and recording of both proton and potassium fluxes. As shown previously and here in Fig. 3, SMPs prepared from wild-type mitochondria exhibited rapid, reciprocal translocation of K^+ and H^+ driven by concentration gradients of either. In contrast, SMPs from *mdm38Δ* failed to exhibit changes in $[H^+]$, and those in $[K^+]$ were drastically reduced. Nigericin restored K^+ and H^+ translocation in mutant SMPs to the wild-type level (Fig. 3*B*) (3).

SMPs were then prepared from *mdm38Δ* mitochondria overexpressing the respective suppressors (Fig. 3*A*). Overexpression of the phosphate carrier Pic2p showed a mild increase in K^+ fluxes and a stronger increase in H^+ fluxes (Fig. 3*A*, *round dotted line*). Interestingly, when K_2HPO_4 was used as K^+ salt instead of KCl, K^+ fluxes were not significantly re-established, whereas H^+ fluxes reached wild-type levels (data not shown), which are consistent with the role of Pic2 as PO_4^-/H^+ transporter (23). Overexpression of Mrs3p poorly restored the K^+ and H^+ fluxes (Fig. 3*A*, *black broken line*). However, overexpression of Ydl183cp restored the K^+ and H^+ exchange activity to a wild-type level, as did overexpression of Mrs7p, the yeast Mdm38p homologue (Fig. 3*A*, *black solid line* and *gray square dotted line*, respectively) or addition of nigericin. These results confirmed that, in contrast to Pic2p or Mrs3p, Ydl183cp, like Mrs7p, can fully substitute for Mdm38p in providing mitochondria with KHE activity.

Ydl183cp Is an Integral Mitochondrial Protein—*YDL183c* encodes a protein of 320 amino acids with a molecular mass of about 37 kDa. The computer programs DAS and TMPRED (available on line) predict one transmembrane domain (196–212 amino acids) and a potential N-terminal mitochondrial targeting sequence. Homologues are found in fungi and in some green plants like *Arabidopsis thaliana* (At1g53760 accession number Q6NQN0). These proteins share one conserved putative transmembrane domain rich in proline residues (Fig. 4*A*). Except for the presence of a proline-rich putative transmembrane domain, there was no obvious sequence similarity between Ydl183cp and proteins of the Mdm38p/LETM1 family.

To determine the cellular localization of Ydl183c, cells expressing the fusion protein Ydl183c-GFP from the *MET* promoter encoded on the centromeric plasmid pUG35 were stained with Mito Tracker Red. Fluorescence confocal microscopy revealed the colocalization of GFP and red fluorescence, indicating the mitochondrial localization of Ydl183-GFP (Fig. 4*B*). To confirm these data, biochemical studies were performed with cells expressing the low copy vector encoding Ydl183cp from its own promoter and C-terminally tagged with the triple hemagglutinin (HA) epitope. Cell fractionation and immunoblotting showed Ydl183c-HA protein to cofractionate with a mitochondrial protein (Porin1, Por1p), whereas the cytosolic protein hexokinase 1 (Hxk1p) was detected in the post-mitochondrial fraction, excluding the possibility of cross-

A

B
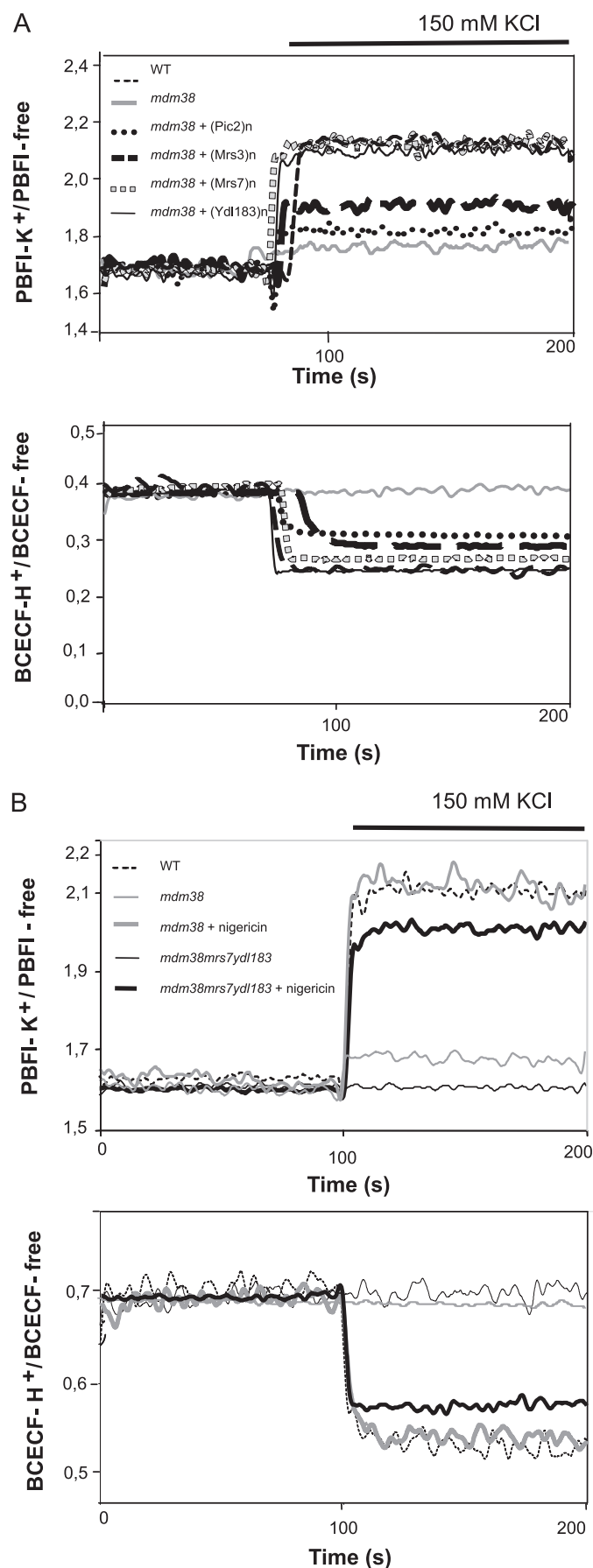
contamination of cytoplasmic and mitochondrial fractions (Fig. 4*C, panel a*). Fractionation of mitochondria into pellet and supernatant upon alkaline sodium carbonate treatment released the membrane-associated β subunit of the F1-ATPase (F1β) almost entirely into the supernatant, whereas the membrane protein Por1p was retained in the pellet fraction containing integral proteins. Ydl183c-HA was found in the membrane pellet (Fig. 4*C, panel b, lane P*). However, in contrast to Por1p, Ydl183c-HA was also partially found in the soluble fraction (Fig. 4*C, panel b, lane SN*). These results indicated that Ydl183cp is inserted into one of the mitochondrial membranes where it can be partly released by alkaline treatment.

For further determination of the topology of Ydl183cp, intact mitochondria were first treated with or without proteinase K. Ydl183cp was not degraded upon addition of proteinase K (data not shown). Mitoplasts were prepared by osmotic swelling and rupture of the mitochondria. Mitoplasts containing the inner membrane were treated with proteinase K (Fig. 4*C, panel c*). To control the intactness of mitoplasts, the topology of known proteins was also tested. Tim44p, a matrix-sided protein of the inner membrane, remained protected from proteinase K, indicating that the mitoplasts were intact. In contrast, Yme1p, an inner mitochondrial membrane protein partially exposed to the outside of mitoplasts, was accessible to proteinase K indicating that the outer membrane was disrupted. The C-terminally tagged Ydl183cp was resistant to 40 μg/ml proteinase K, whereas it became accessible to higher proteinase K concentrations. Proteinase K at 120 μg/ml degraded most of Ydl183-HA without generating proteolytic C-terminal fragments. When mitoplast were lysed with Triton X-100 and then treated with proteinase K, the protein was entirely degraded. Altogether, although alkaline extraction released some of the protein, these results qualify Ydl183p as an integral protein of the inner mitochondrial membrane, with a C_{out} (facing the intermembrane space) topology. Degradation of Ydl183c-HA occurred only in presence of high concentrations of proteinase K as compared with Yme1, either because it is shielded by other proteins or Ydl183cp is intrinsically more resistant to proteinase K.

Synthetic Growth Effect of Triple Disruptions of MDM38, MRS7, and YDL183c—The W303 and DBY *ydl183cΔ* disruptant strain showed reduced growth on nonfermentable carbon sources (YPG) at high temperature (37 °C) (data not shown). Reduced growth on nonfermentable substrate was also reported by Volckaert *et al.* (25) for a FY *ydl183cΔ* mutant at 30 °C and 37 °C. The double disruptants *ydl183cΔ mrs7Δ* exhibited a mild growth reduction on nonfermentable sub-

---

FIGURE 3. **KHE activity of *mdm38Δ* SMPs in the function of the suppressors Pic2, Mrs3, Mrs7, and Ydl183c.** Submitochondrial inner membrane particles were prepared from wild-type and *mdm38Δ* mutant cells with entrapped K^+-sensitive PBFI or H^+-sensitive BCECF. Ratios of K^+-bound or H^+-bound to -unbound dyes were recorded at 25 °C at resting conditions and upon the addition of 150 mM KCl. *A*, shown are the effects on K^+ and H^+ fluxes in SMPs upon overexpression of the suppressor genes in W303 *mdm38Δ*. SMPs were prepared from mitochondria of wild type (*WT*) (*black thin dashed line*) or mutant *mdm38Δ* cells carrying the empty plasmid (*gray solid*) or the suppressor plasmid containing the genes *PIC2* (*black dotted line*), *MRS3* (*black bold dashed line*), *MRS7* (*gray square dotted line*), or *YDL183c* (*black solid line*). *B*, increase of $[K^+]_i$ and $[H^+]_i$ observed in SMPs from DBY wild-type (*black dashed line*), single mutant mdm38 (*gray dashed line*), or triple mutant *mdm38Δ mrs7Δ ydl183cΔ* (*black thin solid line*) in the absence of nigericin or mdm38 (*gray bold solid line*) and mdm38Δ mrs7Δydl183cΔ (*black bold solid line*) in the presence of nigericin.

A

B

Nomarski GFP Mitotracker Overlay

C
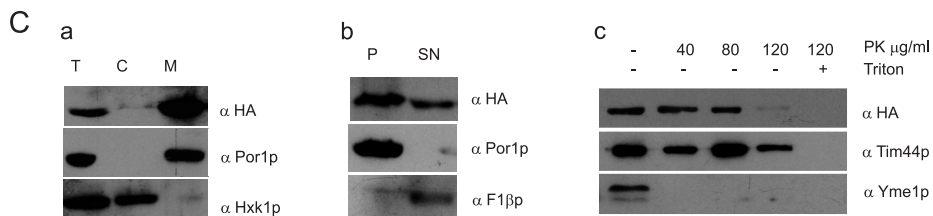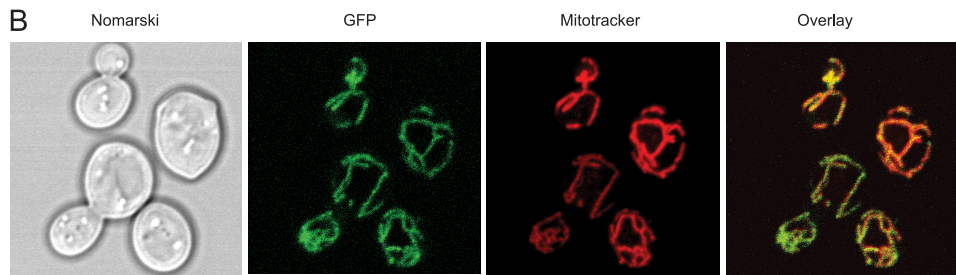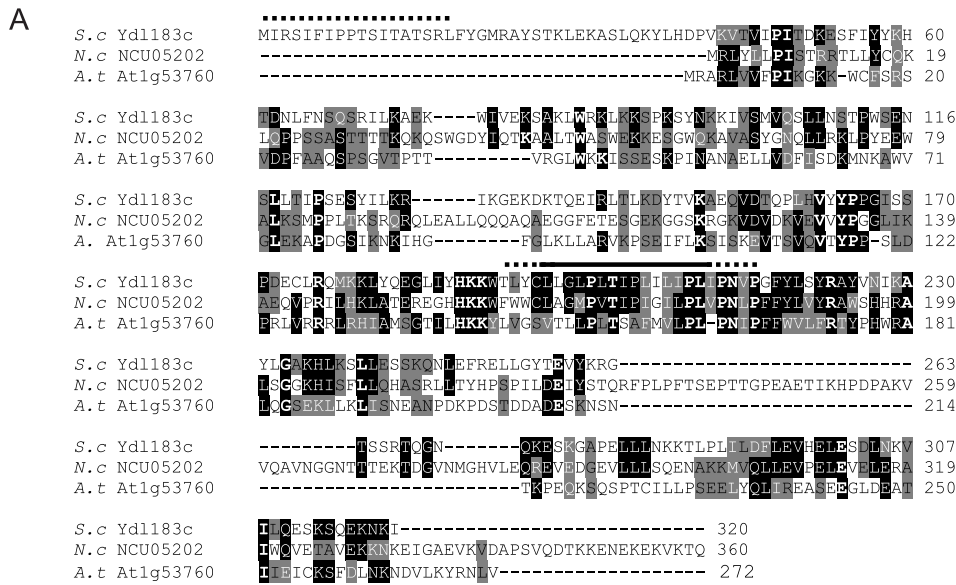
FIGURE 4. **Ydl183cp is a component of the mitochondrial inner membrane.** *A,* Ydl183cp is a member of a novel protein family. Homologous proteins were identified by a BLAST search. A sequence alignment (ClustalW) of Ydl183cp and its homologues in *A. thaliana* (*A.t.*) and *Neurospora crassa* (*N.c.*) is shown here. Identical amino acids are highlighted in *black* and similar amino acids in *gray*. The putative potential N-terminal mitochondrial targeting sequence is marked with a *dotted bar* and the putative transmembrane domain with a *solid bar*. *B,* localization of the Ydl183c-GFP fusion protein analyzed under confocal microscopy. W303 cells expressing C-terminally GFP-tagged *YDL183c* gene were grown to log phase in galactose containing medium at 28 °C. Mitochondria are labeled with MitoTracker red chloromethyl-*X*-rosamine. *C,* subcellular and submitochondrial localization of Ydl183cp. *Panel a,* W303 cells expressing the Ydl183c-HA fusion protein (YCp-*YDL183c*-HA, 42 kDa) were grown to log phase in galactose-containing medium. Protoplasts were homogenized and separated into total cell (*T*), mitochondrial (*M*), and post-mitochondrial (*C*) fractions. Equal amounts of protein of subcellular fractions were subjected to SDS-PAGE, and immunodetection with antisera against the HA tag, Hxk1p and Por1p, was performed. *Panel b,* crude mitochondria (2 mg of protein) were treated with 0.1 M Na$_2$CO$_3$ and fractionated by centrifugation at 100,000 × g into pellet (*P*) and supernatant (*SN*). Both fractions (100 μg of protein/lane) were subjected to SDS-PAGE and immunoblotted with antisera against HA, Por1p, and F$_1$β. *Panel c,* mitoplasts prepared by osmotic shock were separated into supernatant containing the inter-membrane space and pellet. Mitoplasts were aliquoted in equal amounts and incubated with or without proteinase K as indicated. Samples were analyzed by SDS-PAGE and immunoblotted with antisera against the HA tag and against mitochondrial proteins of the inner membrane Tim44p and Yme1p.

thetic phenotypes. Growth on non-fermentable substrates was virtually absent, and the DBY747 triple mutant strain also displayed a significant growth reduction on YPD plates at 28 and 35.5 °C (Fig. 5, *A* and *B*), consistent with a serious disturbance in mitochondrial function(s) essential for cell viability.

Growth of the triple mutant on YPD and YPG was largely restored upon expression of *MDM38* or overexpression of either *MRS7*, *YDL183c*, or human LETM1 (Fig. 5*B*). In comparison, overexpression of *PIC2* in the triple mutant resulted in no growth improvement, and overexpression of *MRS3* rescued the nonfermentable growth of the triple mutant only at 37 °C but not at 16 °C (data not shown).

Addition of nigericin, an electroneutral KHE ionophore, efficiently restored growth of the triple mutant *mdm38Δ mrs7Δ ydl183cΔ* on glycerol at 16 and 28 °C (Fig. 5*C*). This finding is important because it suggests that the growth defects on fermentable and nonfermentable substrates were essentially due to a lack of KHE activity.

Given the strong homology of the yeast proteins Mrs7 and Mdm38, we searched for human homologous proteins of LETM1. A BLAST search of the human protein data base revealed a protein containing a LETM1 domain and named LETMD1 or HCCR-1. The sequence alignment of Mrs7, Mdm38, LETM1, and HCCR-1 shows the conserved domains as highlighted (Fig. 6*A*). The recent work of Kim and co-workers (9, 26) showed that HCCR-1 was overexpressed in various human cancers and might function as a negative regulator of the p53 tumor suppressor. Having shown that overexpression of LETM1 from the *ADH* promoter restored growth of the triple

strate at 16 and 28 °C (data not shown). Double disruptants *mdm38Δ mrs7Δ* in W303 or DBY747 essentially showed the same phenotype as the single mutant *mdm38Δ* at 28 or 35.5 °C, whereas a slight growth improvement was detected on YPG at 16 °C (Fig. 5*A*). Growth of *mdm38Δ ydl183cΔ* double mutants was reduced on YPG at 16 °C (Fig. 5*A*). Importantly, the triple deletion mutant *mdm38Δ mrs7Δ ydl183cΔ* resulted in syn-

mutant, we tested the suppression capacity of HCCR-1 expressed under the same promoter. Overexpression of HCCR-1 restored fermentative growth of the triple mutant to wild-type levels at 28 and 37 °C and nonfermentative growth on YPG at 28 °C (Fig. 6*B*). However, growth was only poorly increased on YPG at 16 °C and not at all at 37 °C (data not shown). As described previously, HCCR-1 was charac-

A

B

C
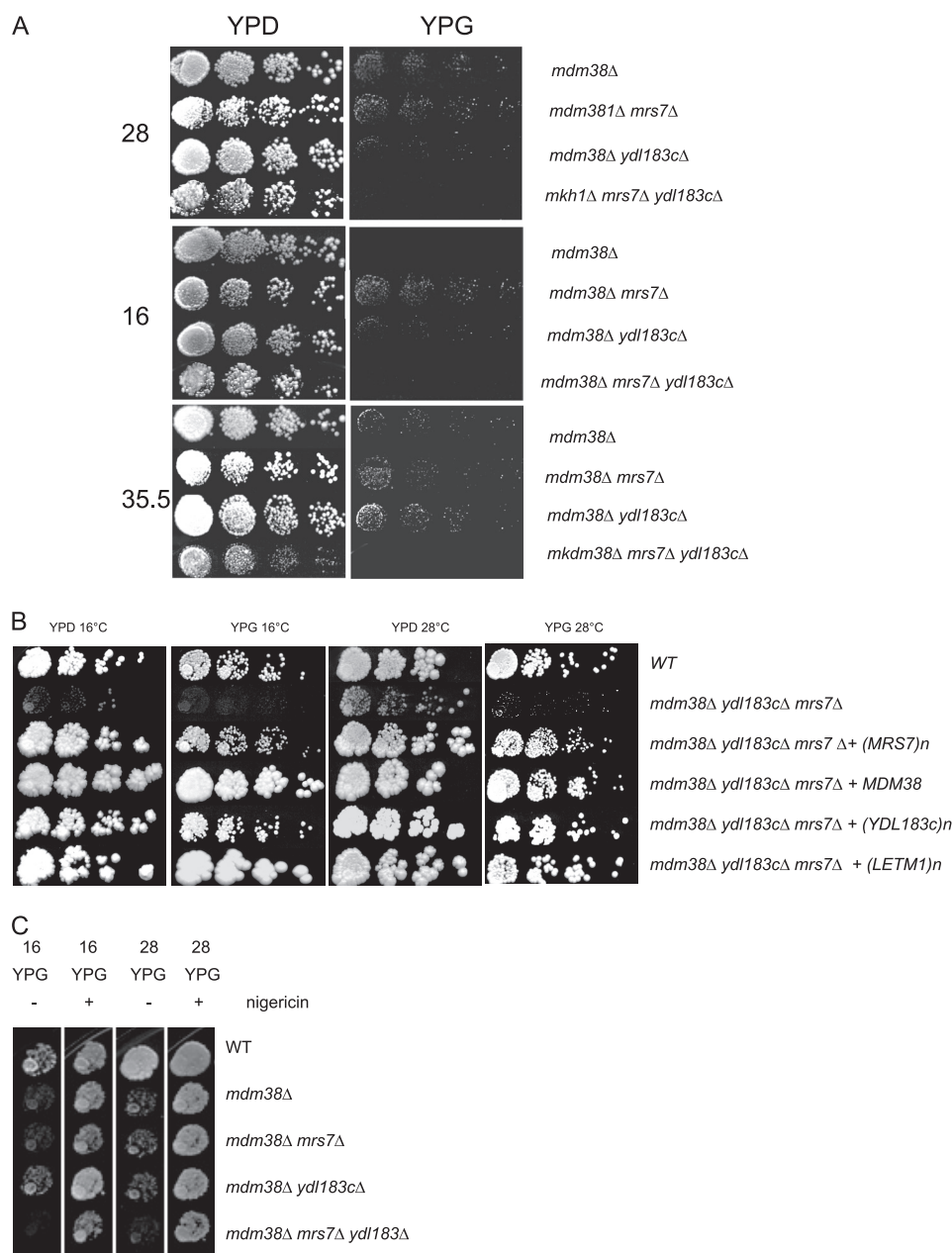
FIGURE 5. **Deletion growth phenotypes.** *A,* serial dilutions of DBY. *mdm38Δ*, *mdm38Δ mrs7Δ*, *mdm38Δ ydl183cΔ*, and *mdm38Δ mrs7Δ ydl183cΔ* mutants were spotted onto YDP and YPG and incubated at the indicated temperatures. Growth on 28, 35.5, and 16 °C was observed after 3, 5, and 8 days, respectively. *B,* DBY wild-type (*WT*) and *mdm38Δ mrs7Δ ydl183cΔ* triple mutant cells expressing an empty control vector (pUG35) or YCp33-*MDM38*-HA, pUG35-*MRS7*-GFP, pUG35-*YDL183c*-GFP, or pVT-U-LETM1-HA. Serial dilutions were spotted onto YPD and YPG plates and incubated for 10 days at 16 °C or 3 or 5 days at 28 and 37 °C on YDP or YPG, respectively. *C,* effect of nigericin on the nonfermentative growth of DBY747 *mdm38Δ* single, *mdm38Δmrs7Δ*, *mdm38Δydl183cΔ* double, and *mdm38Δ mrs7Δ ydl183cΔ* triple mutant cells. Serial dilutions of the wild-type and mutant cells were spotted onto YPD and YPG plates containing (+) or not (−) 2 μM nigericin and incubated 10 days at 16 °C and 5 days at 28 °C.

terized as a mitochondrial protein (26). We verified its subcellular localization when heterologously expressed in yeast. Cell fractionation of wild-type (data not shown) and *mdm38Δ mrs7Δ ydl183Δ* triple mutant cells expressing HCCR-1-His and Western blotting analysis revealed that HCCR-1 was detected as a protein of 35 kDa in the total and mitochondrial fractions (Fig. 6C). Por1p was also recovered in total and mitochondrial fractions and Hxk1p in total and cytoplasmic fractions. Accordingly, in yeast HCCR-1-His

was exclusively found in mitochondria, although in significantly less abundant amounts than Por1p (Fig. 6C).

Severe Loss of the Mitochondrial Membrane Potential in the Absence of Mrs7p, Ydl183cp, and Mdm38p—Most importantly, the mitochondrial Δψ was dramatically reduced in the triple mutant *mdm38Δ mrs7Δ ydl183cΔ* (Table 1). We tested if overexpression of the individual suppressors also restored the mitochondrial Δψ in the triple mutant *mdm38Δ mrs7Δ ydl183cΔ*. We found that expression of Mdm38p and overexpression of Mrs7p or Ydl183cp restored the reduced Δψ of the triple mutant to a reasonable level (Table 1), a result comparable with that observed after overexpression of human LETM1. These findings suggest that cellular growth and increase of mitochondrial Δψ are mechanistically linked.

Dramatic Changes of Organelle Morphology in mdm38Δ mrs7Δ ydl183cΔ Cells—In addition to growth impairment and profound depolarization, the triple deletion mutant *mdm38Δ mrs7Δ ydl183cΔ* differed most strikingly from the mdm38Δ single deletion mutant in its organellar morphology. Confocal microscopic analysis of triple mutant cells expressing the mitochondrial matrix-targeted GFP showed that mitochondria appeared fragmented in spherical units, were less numerous than in the single *mdm38Δ* mutant, and were somewhat clumped together. Furthermore, costaining of cells with the specific vacuole dye FM4-64 consistently showed a multiple lobed morphology of the vacuoles (Fig. 7A). To look into the structure of the organelles at higher resolution, electron microscopy was performed. Remarkably, numerous vesicles were visible in each section, all looking almost alike in size and electron density. The recognition of single or double vesicle-surrounding membranes was the only morphological criterion to discriminate between mitochondrial and vacuolar vesicles. Yet a distinction of the organelles was not always possible (Fig. 7B, *panels a* and *b, right panels*). Surprisingly, a large number of cells showed vesicular mitochondria containing undefined material suggesting either internalized membranes or paracrystalline structures (Fig. 7B, *panel b, right panel*). Most

A

B

SD-ura   YPD   YPG

28   37   28   37   28   °C

WT

Δ Δ Δ

Δ Δ Δ + HCCR-1

C

T   M   C

α HA

α Por1p

α Hxk1p
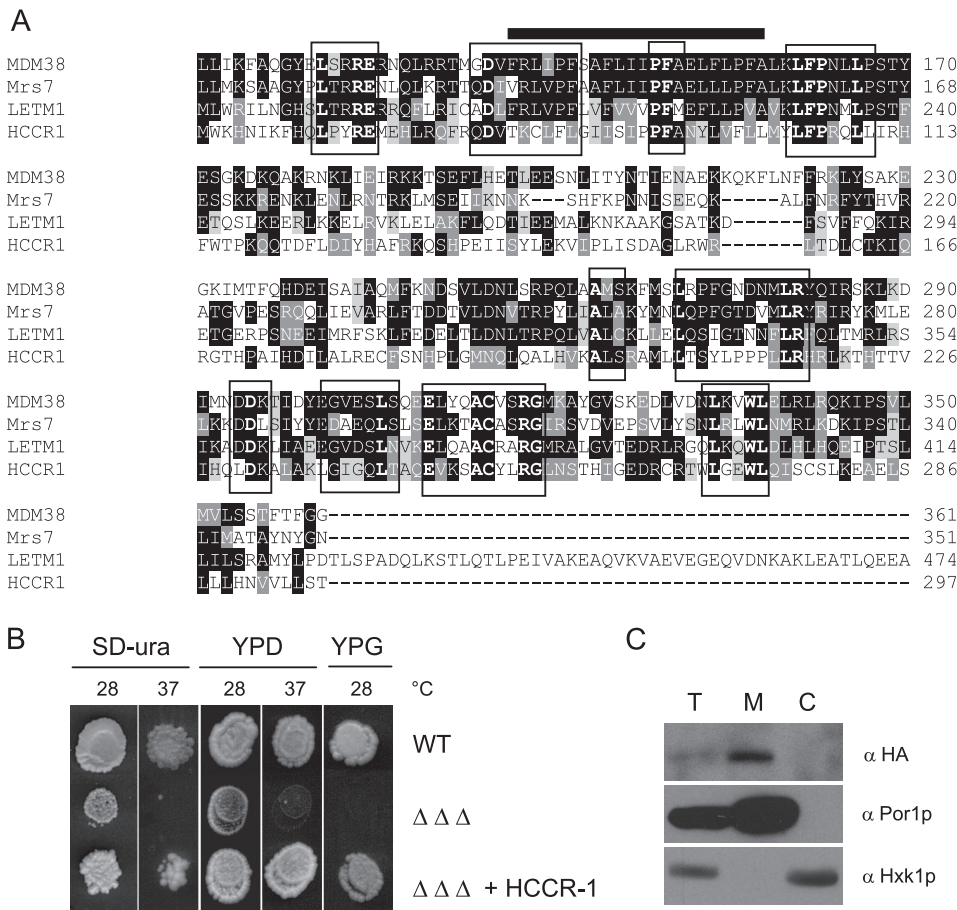
FIGURE 6. **Suppression effect of human HCCR-1.** *A,* sequence alignments of Mdm38, Mrs7, Letm1, and HCCR-1. ClustalW alignments of the amino acid sequences over the homologous regions are shown. Identities are highlighted in *black* and similarities in *gray.* Amino acid residues identical over all four sequences are in *boldface* and *boxed. Bar* is over the transmembrane domain. *B,* growth effect of HCCR-1 expression in yeast triple *mdm38Δ mrs7Δ ydl183Δ* mutants (ΔΔΔ). Wild-type (*WT*) and triple mutant cells expressing pVTU103 with or without HCCR-1 were spotted onto SD−ura, YPD, and YPG plates and grown at the indicated temperatures for 6, 3, and 6 days, respectively. *C,* subcellular localization of HCCR-1 in yeast. Yeast triple *mdm38Δ mrs7Δ ydl183Δ* mutants (ΔΔΔ) expressing HCCR-1 were fractionated into total (*T*), mitochondrial (*M*), and post-mitochondrial (*C*) fractions, and Western blotting was performed.

in the *mdm38Δ* single mutant SMPs were fully eliminated in the triple mutant (Fig. 3*B*). However, KHE was fully active in *ydl183cΔ* and moderately reduced in *mrs7Δ* (data not shown). Consistent with data reported above on cell growth and Δψ, disruption of all three genes had additive effects on the KHE activity. However, preincubation of the *mdm38Δ mrs7Δ ydl183cΔ* SMPs with nigericin led to the activation of the K$^+$ and H$^+$ transport across the SMPs membrane, although not to full wild-type levels (Fig. 3*B*).

K$^+$ and H$^+$ flux measurements carried out in triple mutant SMPs revealed efficient restoration of activities by Mdm38p expressed from a single copy vector, whereas its homologue Mrs7p required expression from a multicopy vector (Fig. 8, *B, black solid line,* and *A, black square dotted line*, respectively). Overexpression of Ydl183cp also restored some of the K$^+$/H$^+$ fluxes in the triple mutant but not fully (Fig. 8*A, black broken line*). Finally, overexpression of the human homologue of Mdm38p, LETM1 in the triple mutant strains, restored most of the KHE activity (Fig. 8*B, gray solid line*).

Ydl183cp, Mrs7p, and Mdm38p Form High Molecular Weight Complexes—The genetic data presented here support the notion that Mdm38, Mrs7, and Ydl183c proteins are functionally equivalent in contributing to the formation of an active KHE. All three proteins are single-pass transmembrane proteins and thus are unlikely to form an exchanger without self-association or without association with other yet unidentified proteins (homo- or hetero-oligomerization, respectively). To address the question of whether the proteins were part of high molecular weight complexes, we first performed chemical cross-linking. We used crude mitochondria expressing Mdm38p or Ydl183cp in cross-linking experiments using disuccinimidyl suberate at increasing concentrations. Based on the electrophoretic mobility of the cross-linked products, our data confirmed that Mdm38p and Ydl183cp were part of large protein complexes (supplemental material). To improve the molecular weight size resolution of the complexes, we performed BN-gel electrophoresis followed by immunodetection. Mitochondria were isolated from DBY wild-type strains expressing chromosomally tagged Mdm38-His or Mrs7-His or extra-chromosomal Ydl183-GFP from the pUG vector. Isolated mitochondria were solubilized with mild detergents and separated on nondenaturing gels prior to Western blotting and immunodetection. Probing with

importantly, wild-type-like morphology of the cells was restored upon addition of nigericin (Fig. 7*B, panel c*) with reversion of mitochondria from swollen, fragmented, and electron-transparent to condensed, elongated, and electron-dense organelles. This key finding links the morphological phenotype of the triple mutant to a defect of K$^+$ homeostasis, which can be compensated by nigericin.

For better discrimination of the origin of the visualized organelles, we used a mitochondrial YFP targeted to the outer membrane (pHS72) and the vacuolar stain FM4-64. Confocal microscopy showed stained wild-type mitochondria and vacuoles as clearly distinct organelles (Fig. 7*C, panels a–d*). In contrast, triple mutant cells exhibited widely overlapping fluorescence of FM4-64 (vacuoles) and YFP directed to the outer mitochondrial membrane (Fig. 7*C, panels e–h*), indicative of the colocalization of both organelle markers that occurs in mitophagy (27).

Mitochondrial KHE Is Totally Absent in the Triple Deletion Strain mdm38Δ mrs7Δ ydl183cΔ—Remarkably, SMPs from the triple mutant *mdm38Δ mrs7Δ ydl183cΔ* failed to exhibit H$^+$ fluxes, and most importantly, residual K$^+$ fluxes observed

the anti-His antibody revealed that Mdm38-His (~67 kDa) migrated at ~500, <232, and <140 kDa (Fig. 9*A, left panel*). Of note, Mdm38-His was detected in protein complexes of the same molecular weights irrespective of the presence of Mrs7p or Ydl183cp (data not shown). Furthermore, Mrs7-His (53 kDa) appeared in three bands around ~500 kDa and an additional band of >232 kDa (Fig. 9*B, lane 1*). BN-PAGE analysis of solubilized mitochondria expressing Ydl183-GFP yielded a product of an apparent molecular mass of about 67 kDa, which corresponds to its molecular weight as GFP-tagged monomer and to additional bands of <232 kDa, representing YDL183GFP-containing complexes. However, in the background of a mutant *mdm38Δ* strain, Ydl183-GFP partly shifted to a major band of ~500 kDa (Fig. 9*C*).

Next, we affinity-purified the chromosomally His-tagged Mdm38p and Mrs7p. The proteins were bound to the resin and eluted from the column prior to analysis on BN-PAGE. Surprisingly, despite changing the experimental conditions such as the incubation times with the Ni-NTA beads or using different detergents or NaCl concentrations, the eluted Mdm38-His exclusively appeared as a single band of a molecular mass slightly smaller than 232 kDa (Fig. 9*A, middle panel*). This was an unexpected result. To find out if the protein complex of ~500 kDa containing the His-tagged Mdm38p as detected on BN prior affinity purification had become inaccessible to the column possibly because it was hidden by additional proteins of the larger complex, we decided to affinity-purify Mdm38 fused to the One-STrEP tag. This tag containing a *linker* region makes the tagged component of a protein complex more accessible to the column. In fact, using the chromosomal One-STtrEP-tagged version of *MDM38*, the purified Mdm38p was recovered within high molecular complexes ranging between ~500 and < 600 kDa in addition to the complex of <232 kDa (Fig. 9*A, right panel*).

Affinity chromatography of solubilized mitochondria chromosomally expressing Mrs7-His followed by BN-PAGE recovered Mrs7-His within three complexes of <140, >232, and between 440 and 669 kDa as seen in Fig. 9*B, left panel, lane 2*. Similar results were obtained using Mrs7OneStrep instead of Mrs7His (Fig. 9, *right panel*). In the next step, we solubilized mitochondria from chromosomally Mrs7-His-tagged cells coexpressing either YCp-Mdm38-HA or YCp-Ydl183-HA. Mitochondrial expression of Mdm38-HA and Ydl183c-HA was confirmed by Western blotting (data not shown). Affinity purification followed by BN-PAGE and Western blotting analyses, including immunodetection with anti-His and HA antibodies, was performed. Although the anti-His antibody recognized Mrs7-His, neither Mdm38-HA nor Ydl183-HA was detectable when the eluted fractions were probed with the anti-HA anti-

body, excluding a direct interaction of Mrs7-His and Mdm38-HA or Mrs7-His and Ydl183-HA (Fig. 10, *A* and *C*, respectively). Second dimension SDS-PAGE confirmed that Mdm38-HA was not part of the Mrs7-His complex (Fig. 10*B, right panel*). Taken together, our experiments did not suggest any direct interaction between Mdm38-HA and Mrs7-His.

These results are in contrast to data reported previously by Frazier *et al.* (8), indicating a direct interaction of a protein A-tagged Mdm38 with numerous other mitochondrial proteins, including Mrs7p. In fact, when we used a strain expressing the Mrs7 protein C-terminally tagged with a His fused to protein A (Mrs7-His-TAP), we found that Mdm38 coeluted with Mrs7-His-TAP in the ~232-kDa complex (Fig. 11, *B* and *C*). However, a direct interaction between Mrs7-His-TAP and Ydl183c was not detectable (Fig. 10*C*). We asked whether the tags affected the suppression of the mutant phenotype. Mrs7-His or Mrs7-His-TAP was introduced into the *mdm38Δ* mutant, and nonfermentative growth was tested. We found that *mdm38Δ* cells expressing Mrs7-His-TAP did not grow as well as Mrs7-His or wild-type cells (Fig. 11*D*). Thus, these data altogether suggest that Mrs7p and Mdm38p are not interacting directly.

We used CoIP to ask whether Mdm38 homo- or heterooligomerizes with Ydl183cp. Mdm38 self-oligomerization was confirmed by CoIP experiments performed on *mdm38Δ* cells coexpressing Mdm38-HA (72 kDa) and Mdm38-GFP (92 kDa). Although Mdm38-HA was successfully bound to HA-coated protein A beads, only Mdm38-GFP was pulled down, and Ydl183c-GFP did not copurify in the protein A-bound fractions like Aif-GFP serving as negative control (Fig. 12).

DISCUSSION

We previously characterized Mdm38p as a mitochondrial protein essential for KHE activity (2, 4). Because this protein has only one transmembrane domain, it appears unlikely to be solely responsible for the KHE process. To explore the possible existence of additional proteins involved in KHE, we carried out a genome-wide suppressor screen.

We identified the mitochondrial carriers Pic2p and Mrs3p as weak suppressors. Their overexpression rescued the growth defect of *mdm38Δ*. We showed that mitochondrial morphology of *mdm38Δ* was restored to wild-type upon overexpression of *PIC2* and *MRS3*. However, in *mdm38Δ* SMPs, KHE was not seen after overexpression of Pic2p and was only marginally restored by Mrs3p. Because overexpression of Pic2p, a P_i carrier, had no effect on mitochondrial K^+ fluxes in *mdm38Δ* mitochondria and resulted in a marginal increase of the mitochondrial $\Delta\psi$, we hypothesize that a contribution to $\Delta\psi$ above a threshold is sufficient to heal the growth and morphology phe-

FIGURE 7. **Mitochondrial and vacuolar morphology in absence of Mdm38p, Mrs7p, and Ydl183cp.** Cells were grown to logarithmic phase in galactose (*A* and *B*)- or galactose- and raffinose (*C*)-containing medium. Shown are representative fluorescent and electron microscopy images. *A,* confocal microscopy analysis of W303 wild-type cells (*a*), isogenic *mdm38Δ* (*b*) and isogenic *mdm38Δ mrs7Δ ydl183cΔ* triple mutant cells (*c*) expressing the mitochondrial matrix targeted GFP. Vacuoles were stained with FM4-64. *B,* electron micrographs of *mdm38Δ mrs7Δ ydl183cΔ* cells. *Panels a* and *b* show the organellar ultrastructure of the triple mutant grown as described above. Whole cells are shown in *right panels*. The cells display mitochondria with aberrant morphologies (details showing mitochondria are in the *left panels*). *Panel c* shows the organellar ultrastructure of cells from the same culture to which nigericin (2 nM) has been added for the last growth generation. *Right panel,* whole cells; *left panel,* mitochondrion after nigericin treatment. *Bar,* 200 nm (*left panels*) and 1 μm (*right panels*). *C,* confocal microscopy analysis of wild-type cells (*panels a–d*) and *mdm38Δ mrs7Δ ydl183cΔ* cells (*panels e–h*) expressing the mitochondrial targeted YFP (*panels a* and *e*) to the outer membrane (pHS72). Vacuoles are indicated by FM4-64 (*panels b* and *f*). Merged fluorescence is shown in *panels c* and *g*. The yellow fluorescence detected indicates the colocalization of mitochondria and vacuoles. Differential interference contrast microscopy of wild-type (*panel d*) and *mdm38Δ mrs7Δ ydl183cΔ* (*panel h*) cells is shown.

A

B
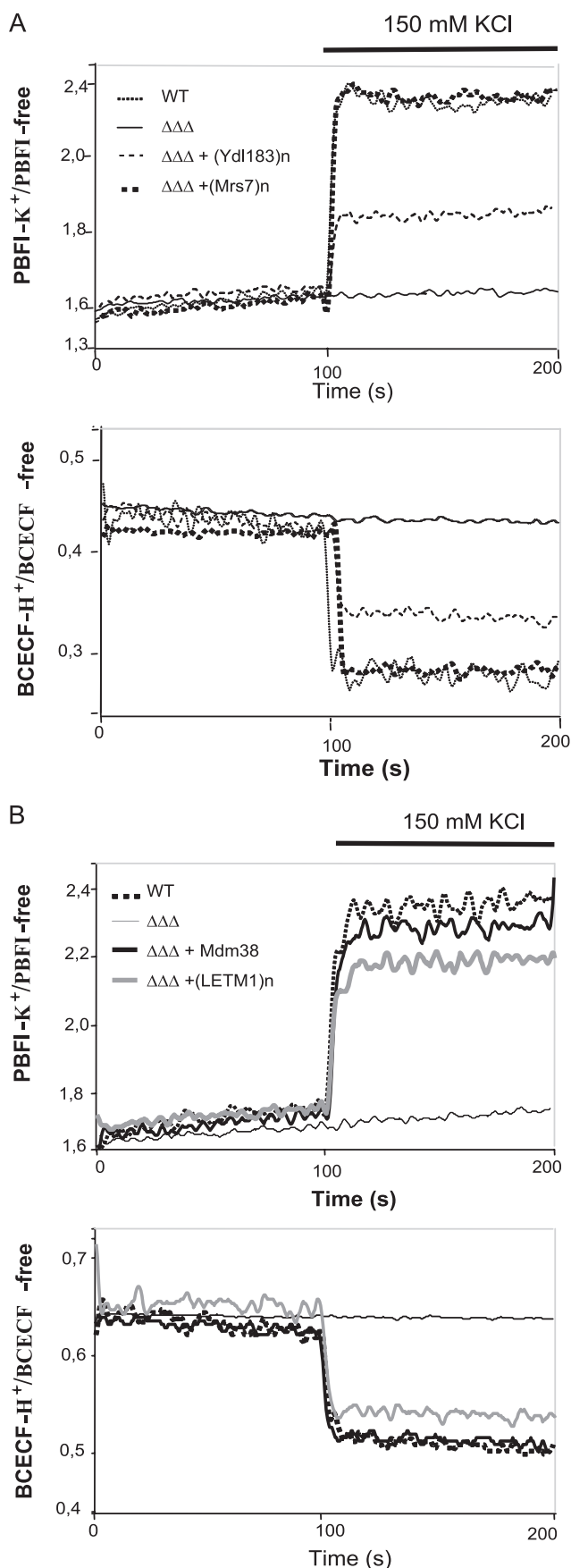
notype. Alternatively, Pic2p might act indirectly by modulating proton fluxes or mitochondrial pH. Overexpression of Mrs3p, a Fe^{2+} carrier, increased the mitochondrial $\Delta\psi$ and moderately the KHE. Deletion of *MRS3* had no effect on KHE, and *mrs3Δ mdm38Δ* mutants remained without synthetic phenotype,[5] excluding a role of Mrs3p as the KHE. These findings suggest an indirect role of Mrs3p on the KHE activity. In fact, several ions have been stated to play a direct or indirect role in mitochondrial K^+ homeostasis (28–31).

The suppressor screen also identified two additional genes, *MRS7* and the novel gene *YDL183c* encoding an unknown protein, which were found to restore both growth and KHE activity of *mdm38Δ* mutant cells. Although Mdm38p and Mrs7p are phylogenetically related, Ydl183cp is likely not related to them. Each of these proteins contains a single transmembrane domain and appears to be part of a high molecular weight protein complex. They are functionally redundant in establishing a functional KHE in mitochondria.

In contrast to Mdm38p, absence of either Mrs7p or Ydl183cp alone or in combination did not seriously affect the growth of yeast cells. Yet the triple mutant *mdm38Δ mrs7Δ ydl183cΔ* had a dramatically stronger negative growth phenotype than the single *mdm38Δ* mutant or double mutants. This mutant completely failed to grow on respiratory substrates and exhibited a strain- and temperature-dependent reduced growth on fermentable substrates. This synthetic phenotype of the triple mutant indicates the following: (i) all three proteins are functionally expressed in yeast; (ii) loss of all three proteins dramatically impairs mitochondrial volume homeostasis through a disturbance that can be rescued by nigericin; and (iii) impaired volume homeostasis causes mitochondrial dysfunction affecting cell vitality as indicated by the reduction in growth on fermentable substrates.

Overexpression of Mrs7p or Ydl183cp fully compensated the growth defects of the *mdm38Δ* single and the *mdm38Δ mrs7Δ ydl183cΔ* triple disruptant. Accordingly, either protein could fully substitute for Mdm38p when expressed at high abundance. Addition of the exogenous KHE nigericin equally compensated for the growth defect of *mdm38Δ* single as well as for the even stronger growth defects of the triple mutant. This finding supports the conclusion that the triple mutant growth phenotype is essentially due to a lack of KHE activity.

This important point was proved by a direct test for KHE activity on inner membrane SMPs, a system that entirely avoids any interference of osmotically swollen mutant mitochondria.

---

[5] G. Wiesenberger and K. Nowikovsky, unpublished data.

FIGURE 8. **KHE activity of *mdm38Δ mrs7Δ ydl183c Δ* SMPs.** $[K^+]$-driven changes of $[K^+]_i$ and $[H^+]_i$ in submitochondrial inner-membrane particles prepared from wild-type and *mdm38Δ mrs7Δ ydl183cΔ* mutant cells with entrapped K^+-sensitive PBFI or H^+-sensitive BCECF were recorded as described in Fig. 3. *A,* effect of overexpression of Mrs7p (*black square dotted line*) or Ydl183cp (*black thin dashed line*) on $[K^+]$-driven changes of $[K^+]_i$ and $[H^+]_i$ in DBY triple mutant *mdm38Δ mrs7Δ ydl183cΔ* SMPs (*black solid line*) in comparison with wild-type SMPs (*black dotted line*). *B,* effect of Mdm38p (expressed from YCp33, *bold black solid line*) or LETM1 (expressed from pVTU- (*bold gray solid line*) on $[K^+]$-driven changes of $[K^+]_i$ and $[H^+]_i$ in DBY *mdm38Δ mrs7Δ ydl183cΔ* SMPs (*black thin solid line*) in comparison with wild-type SMPs (*bold square dotted line*).
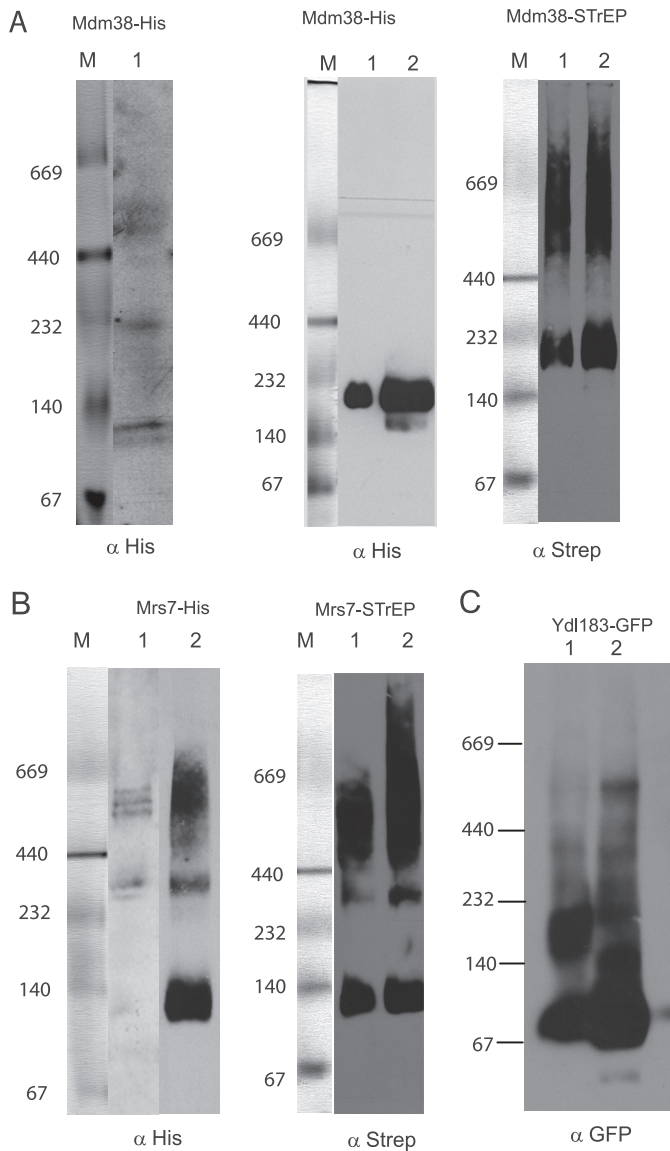
FIGURE 9. **Mdm38p, Mrs7p, and Ydl183cp are part of a high molecular weight complex.** *A,* DBY chromosomally Mdm38-His-tagged mitochondria were solubilized with 1.2% Triton X-100. *Left panel,* one part of the preparation was immediately separated on BN-PAGE. The anti-His antibody recognized three protein complexes of ~500, <232, and < 40 kDa. *Middle panel,* other part of the same preparation was used for a further step involving nickel-affinity chromatography. Mdm38-His was recovered as part of a complex of <232 kDa. *Right panel* shows Mdm38-STrEP after STrEP-affinity chromatography elution separated on BN-PAGE. The anti-STrEP antibody recognized the complexes of <232 and >440 kDa. *M,* marker. *B,* DBY mitochondria expressing the chromosomally His-tagged Mrs7 were solubilized as in *A* and analyzed by BN-PAGE (*left panel, lane 1*), and parallel fractions were used for further isolation of a Mrs7-His complex by affinity chromatography (*left panel, lane 2*). Solubilized mitochondrial proteins and elution fractions from the affinity purification were separated on the same BN gel, transferred to a common membrane for Western blotting, and probed with an antiserum against His. DBY mitochondria expressing the chromosomal Mrs7-STrEP were solubilized, affinity-purified, and recovered in complexes of <140, >232, and >440 kDa. *C,* mitochondria expressing pUG-*YDL183c*-GFP in different backgrounds as follows: wild-type (*lane 1*) or *mdm38Δ* (*lane 2*) were solubilized with 1.2% *n*-dodecyl β-D-maltoside. Equal amounts of proteins were separated on BN-PAGE and immunoblotted with an antibody against GFP.

A comparison between single and triple mutants clearly revealed that the single *mdm38Δ* mutant retained a minor KHE activity, whereas the triple mutant totally lacked this activity. Thus, single and triple mutants most likely differ only in the degree to which they have lost KHE activity. These data correlate well with the reduction in growth of the single and triple mutants. However, mild reduction in KHE activity detected in single mutants *mrs7Δ* and *ydl183cΔ* indicates that expression of Mrs7p and/or Ydl183p is necessary for full KHE activity in wild-type cells. Yet the physiological effects of *mrs7Δ* or *ydl183cΔ* mutations are too weak to result in reduced growth of mutant cells. In assays performed on the single *mdm38Δ* mutant, overexpression of Ydl183cp or Mrs7 could equally restore transmitochondrial K^+/H^+ fluxes, like Mdm38p or LETM1. However, in the triple mutant *mdm38Δ mrs7Δ ydl183c*, Ydl183cp restored the mitochondrial KHE to a lesser extent than Mdm38p Mrs7p, or LETM1, most likely resulting from a less abundant expression of Ydl183c as compared with Mdm38 or Mrs7 (shown in supplemental Fig. S4). Taken together, these results indicate that Mdm38p, Mrs7p, and Ydl183cp are functionally redundant, but only Mdm38p is essential.

Mitochondrial depolarization in the mutants and its rescue by expression of either Mdm38p or Mrs7p or Ydl183cp correlated with loss and recovery of KHE activity, respectively, and with cell growth that was mildly affected on YPG when Δψ fell below 60% of wild-type values and increasingly more with lower values. The lowest Δψ values observed in the triple mutant also affected growth on fermentable substrate, indicating that essential functions of mitochondria, possibly protein import, were affected. The loss of Δψ in mitochondria of the disruptants may be a direct consequence of the absence of H^+ fluxes into the mitochondria in exchange for the efflux of K^+ rather than an additional effect resulting from the K^+ accumulation and swelling of mitochondria.

Total loss of KHE activity of the triple mutant was accompanied by more dramatic changes in organelle morphology than in the single *mdm38Δ* mutant. Both mitochondria and vacuoles appeared to be heavily fragmented and were shown to frequently colocalize, suggesting intense mitophagy. Notably, hyperosmotic stress has been reported to result in significant changes of the vacuole morphology of wild-type cells. In fact, the one to three large vacuoles usually present in wild-type cells underwent fragmentation to numerous smaller multilobe vacuoles (32). Interestingly, treatment of triple mutant cells with the K^+/H^+ ionophore nigericin efficiently reversed swelling and restored a near normal mitochondrial network. As this involves the mitochondrial fusion (33, 34), we assume that proteins regulating the fusion activity are not affected by the absence of Mdm38, Mrs7, and Ydl183c. Vacuolar fragmentation was efficiently reverted together with re-establishing mitochondrial KHE activity by nigericin (data not shown). This raises the question of how the loss of KHE and swelling of mitochondria cause fragmentation of the vacuole. In sum, this study provides strong evidence for a role of all three proteins in contributing to an active mitochondrial KHE.

A genome-wide screen in *Drosophila* S2 cells recently identified LETM1 as strongly affecting mitochondrial Ca^{2+} and H^+ homoeostasis. Absence of LETM1 resulted in reduced mitochondrial Ca^{2+} uptake *in situ*, a finding that led the authors to conclude that Letm1 is the mitochondrial Ca^{2+}/H^+ antiporter (35). This conclusion is puzzling, because down-regulation of the mitochondrial Ca^{2+}/H^+ exchanger would rather have been expected to result in decreased Ca^{2+} efflux and therefore in increased mito-
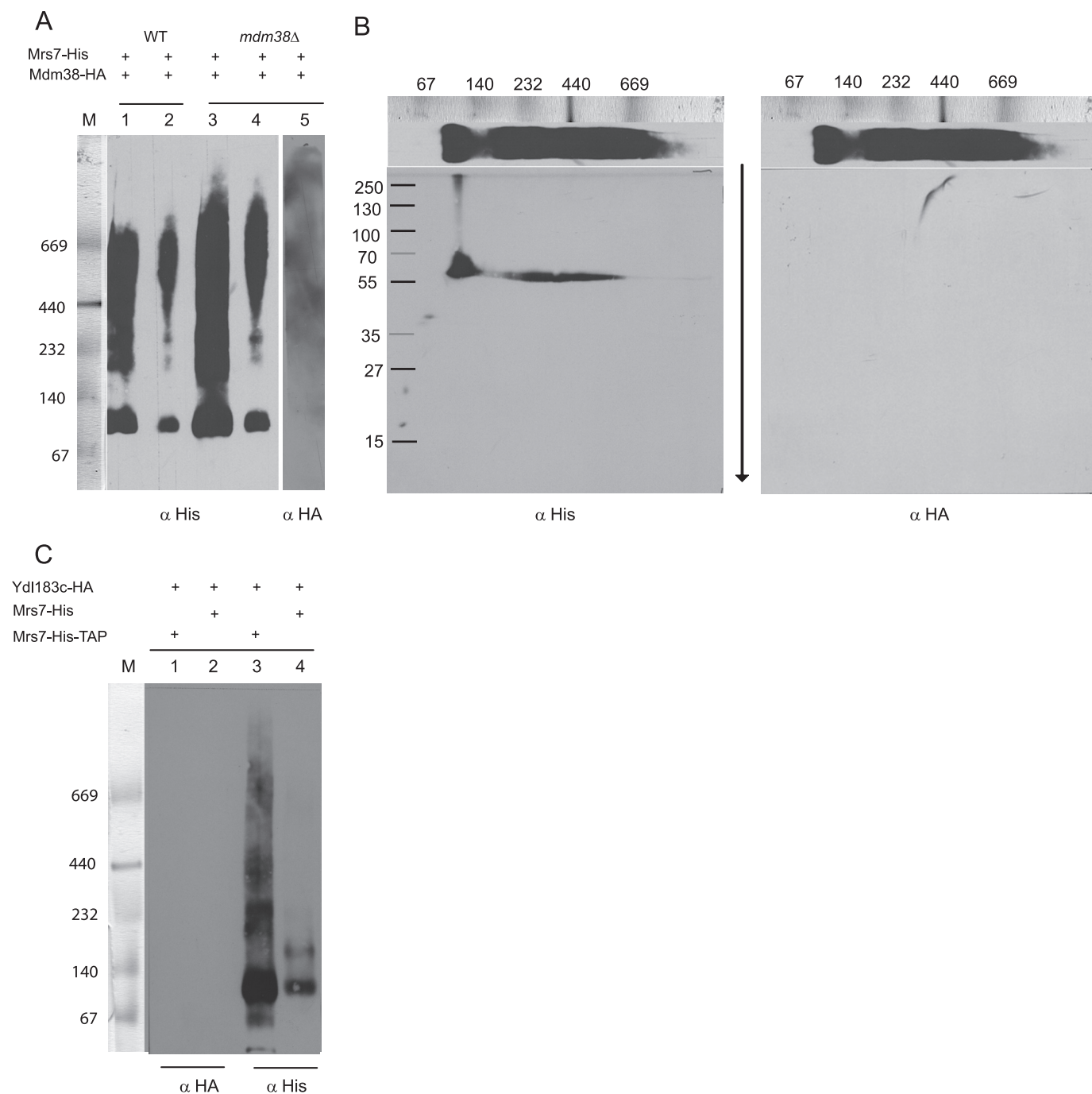
FIGURE 10. **Interaction of Mrs7-His with Mdm38-HA and YDL183c-HA.** *A,* affinity chromatography and preparative BN-PAGE of solubilized mitochondria coexpressing chromosomally His-tagged Mrs7 and extra-chromosomal YCp-Mdm38-HA in different backgrounds as follows: wild-type (*WT*) (*lanes 1* and *2*) and *mdm38Δ* (*lanes 3–5*). 120 μl (*lanes 1, 3,* and *5*) and 60 μl (*lanes 2* and *4*) of the eluted fractions were applied to the same gel. *Lanes 1–4* were probed with an antibody against His. *Lane 5* served for the additional immunodetection with an antibody against HA. *M,* marker. *B,* second dimension SDS-PAGE of *lane 3.* *Left panel,* the antibody against His recognizes a product of ~55 kDa corresponding to Mrs7-His. The signal is in perfect agreement with the signals of the first dimension (BN-PAGE). *Right panel,* immunodetection with anti-HA antibody of the same blot after mild stripping. *C,* affinity chromatography and BN-PAGE of solubilized mitochondria coexpressing chromosomally His-tagged Mrs7 (*lanes 1* and *3*) or His-TAP-tagged Mrs7 (*lanes 2* and *4*) and extra-chromosomal Ydl183-HA (*lanes 1–4*). *Lanes 1* and *2* and *lanes 3* and *4* were probed with antibodies against HA and His, respectively.

chondrial Ca²⁺ accumulation, because mitochondrial cation/H⁺ antiporters protect cells from mitochondrial cation overload by mediating cation *efflux* from energized mitochondria (1). Jiang *et al.* (35) also found that reconstitution of LETM1 in liposomes catalyzed Ruthenium red-sensitive Ca²⁺/H⁺ exchange, which raises further questions since decades of work on mitochondria indicate

that Ca²⁺/H⁺ exchange is insensitive to Ruthenium red (36). Previous evidence that LETM1 is essential for mitochondrial K⁺/H⁺ exchange is compelling (4, 5, 37), and the present study demonstrated that LETM1 fully restores mitochondrial KHE activity of the yeast triple mutant *mdm38Δ mrs7Δ ydl183c* like the exogenous *bona fide* KHE nigericin. We believe that further studies will

A

Mrs7-His   +   +   +   +
Mrs7-His-TAP   +   +   +   +

D
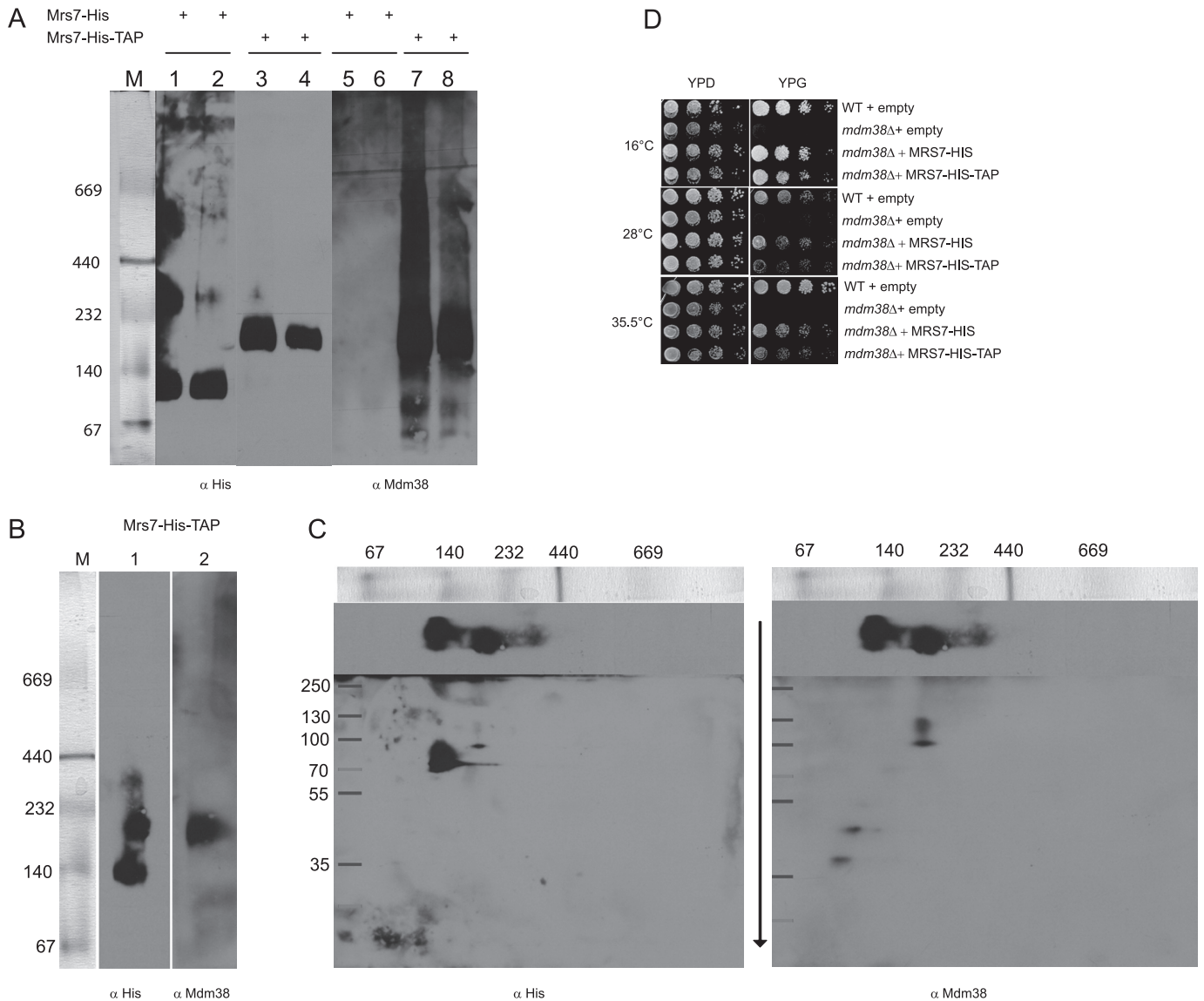
FIGURE 11. **Interaction of Mdm38p with Mrs7-His and Mrs7-His-TAP.** *A,* affinity chromatography and BN-PAGE of solubilized DBY mitochondria expressing either chromosomally His-tagged or His-TAP-tagged Mrs7. Eluted fractions 1–2 containing Mrs7-His were applied on *lanes 1* and *2* and *5* and *6* and eluted fractions 1–2 containing Mrs7-His-TAP on *lanes 3* and *4* and *7* and *8.* BN-PAGE was performed and followed by immunostaining with an antibody against His (*lanes 1–4*) and Mdm38p (*lanes 5–8*). *M,* marker. *B,* preparative affinity chromatography and BN-PAGE of DBY mitochondria expressing chromosomally Mrs7-His-TAP prior to second dimension SDS-PAGE. The membrane was first incubated with an anti-His primary antibody (*lane 1*). Thereafter, the blot was mildly stripped and reincubated with an antibody against Mdm38p (*lane 2*). *C,* second dimension SDS-PAGE. *Left panel,* the blot was probed with the anti His antibody. *Right panel,* same blot probed with the anti Mdm38p antibody after mild stripping of the membrane. *D,* suppression effect of Mrs7-His and Mrs7-His-TAP in *mdm38Δ.* DBY wild type (*WT*) with YEp112 empty and *mdm38Δ* with YEp112 empty, MRS7-His, or MRS7-His-TAP were grown overnight. Serial dilutions were spotted onto YPD and YPG plates and incubated at the indicated temperatures.
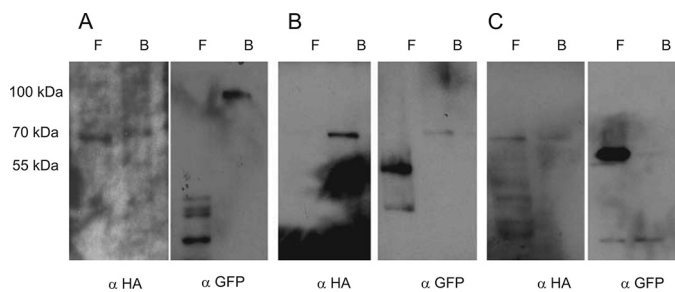
FIGURE 12. **CoIP of isolated *mdm38Δ* mitochondria coexpressing YEp-*MDM38*-HA (72 kDa) and pUG-*MDM38*-GFP (92 kDa) (*A*), YDL183-GFP (65 kDa) (*B*), or AIF-GFP (68 kDa) (*C*).** *F,* flow-through fraction; *B,* HA-coated protein A-bound fraction.

be needed to clarify whether the highly conserved LETM1 proteins exert different cation-specific functions in different eukaryotic organisms or rather disturbances of mitochondrial K$^+$ homeostasis can secondarily affect mitochondrial cation transport. Relevant to this discussion, we have shown that yeast mitochondria depleted of Mdm38p display a considerably reduced influx of Mg^{2+} and Ca^{2+} resulting from decreased mitochondrial $\Delta\psi$ (4).

Human LETM1 has previously been shown to be part of a complex of about 550 kDa by CoIP of GFP- and HA-tagged isomers (38). Rehling and co-workers (8) reported an interaction of Mdm38-protein A with various proteins, including numerous mitochondrial ribosomal proteins and Mrs7p. In our hands, hetero-oligomerization of Mrs7p with Mdm38p was not

detected unless Mrs7p was fused to a tag, including protein A and calmodulin-binding protein.

We have shown that the Mdm38p, Mrs7p, and Ydl183cp form oligomers. Data provided here confirmed that Mdm38p self-dimerizes in mitochondria. However, it may hetero-oligomerize also with a yet unknown protein as suggested by BN and affinity chromatography data. Mdm38p appeared as part of high molecular complexes of ∼140, 232, and 500 kDa. Ydl183cp appeared as part of protein complexes with variable molecular sizes depending on the presence or absence of Mdm38p. Remarkably, in the absence of Mdm38p, Ydl183-GFP appeared as part of a complex of ∼500 kDa. In any case, a direct interaction between Ydl183cp and Mdm38p was not found according to the CoIP experiments performed in this work. Furthermore, Mrs7 was shown to be part of several protein complexes, including a complex of ∼500 kDa, independently of the presence or absence of Mdm38p. Thus, data presented here exclude a direct interaction between Mrs7p and Mdm38p or Ydl183cp. Altogether, the three proteins may act as cofactors interacting with a so far unidentified KHE, which in their absence would be completely inactive. This would be reminiscent of what has been observed for plasma membrane cation exchangers, where the exchanger is regulated by essential cofactors (39, 40). We propose that either Mdm38p or Mrs7p or Ydl183cp bind to a yet unknown protein or protein complex to activate the KHE activity. Although the composition of the 500-kDa complex and the molecular mechanisms through which Mdm38p, Mrs7p, and Ydl183cp modulate KHE activity remain to be elucidated, this study has identified intriguing new players that are amenable to further genetic analysis.

Finally, we included here for the first time a human gene, *HCCR-1*, which has been shown to play a role in cancer development (34). Furthermore, HCCR-1 shows sequence homologies to LETM1. We suggest a related role of HCCR1 to LETM1. Discrepancies in the quality as suppressor might result from its weak expression in yeast. Further studies will be required to test the direct role of HCCR-1 in the KHE.

REFERENCES

1. Mitchell, P. (1966) *Biol. Rev. Camb. Philos. Soc.* **41,** 445–502
2. Froschauer, E., Nowikovsky, K., and Schweyen, R. J. (2005) *Biochim. Biophys. Acta* **1711,** 41–48
3. McQuibban, A. G., Joza, N., Megighian, A., Scorzeto, M., Zanini, D., Reipert, S., Richter, C., Schweyen, R. J., and Nowikovsky, K. (2010) *Hum. Mol. Genet.* **19,** 987–1000
4. Nowikovsky, K., Froschauer, E. M., Zsurka, G., Samaj, J., Reipert, S., Kolisek, M., Wiesenberger, G., and Schweyen, R. J. (2004) *J. Biol. Chem.* **279,** 30307–30315
5. Nowikovsky, K., Reipert, S., Devenish, R. J., and Schweyen, R. J. (2007) *Cell Death Differ.* **14,** 1647–1656
6. Zollino, M., Lecce, R., Fischetto, R., Murdolo, M., Faravelli, F., Selicorni, A., Buttè, C., Memo, L., Capovilla, G., and Neri, G. (2003) *Am. J. Hum. Genet.* **72,** 590–597
7. Waldherr, M., Ragnini, A., Jank, B., Teply, R., Wiesenberger, G., and Schweyen, R. J. (1993) *Curr. Genet.* **24,** 301–306
8. Frazier, A. E., Taylor, R. D., Mick, D. U., Warscheid, B., Stoepel, N., Meyer, H. E., Ryan, M. T., Guiard, B., and Rehling, P. (2006) *J. Cell Biol.* **172,** 553–564
9. Cho, G. W., Shin, S. M., Namkoong, H., Kim, H. K., Ha, S. A., Hur, S. Y., Kim, T. E., Chai, Y. G., and Kim, J. W. (2006) *Gene* **384,** 18–26
10. Rigaut, G., Shevchenko, A., Rutz, B., Wilm, M., Mann, M., and Séraphin, B. (1999) *Nat. Biotechnol.* **17,** 1030–1032
11. Junttila, M. R., Saarinen, S., Schmidt, T., Kast, J., and Westermarck, J. (2005) *Proteomics* **5,** 1199–1203
12. Wach, A., Brachat, A., Pöhlmann, R., and Philippsen, P. (1994) *Yeast* **10,** 1793–1808
13. Thorpe, H. M., and Smith, M. C. (1998) *Proc. Natl. Acad. Sci. U.S.A.* **95,** 5505–5510
14. Cormack, B. P., Bertram, G., Egerton, M., Gow, N. A., Falkow, S., and Brown, A. J. (1997) *Microbiology* **143,** 303–311
15. Zinser, E., and Daum, G. (1995) *Yeast* **11,** 493–536
16. Fujiki, Y., Hubbard, A. L., Fowler, S., and Lazarow, P. B. (1982) *J. Cell Biol.* **93,** 97–102
17. Daum, G., Gasser, S. M., and Schatz, G. (1982) *J. Biol. Chem.* **257,** 13075–13080
18. Schägger, H., and von Jagow, G. (1991) *Anal. Biochem.* **199,** 223–231
19. Schamel, W. W. (2008) *Curr. Protoc. Cell Biol.* **6,** Unit 6.10.1–6.10.21
20. Nowikovsky, K., Devenish, R. J., Froschauer, E., and Schweyen, R. J. (2009) *Methods Enzymol.* **457,** 305–317
21. Sesaki, H., Southard, S. M., Yaffe, M. P., and Jensen, R. E. (2003) *Mol. Biol. Cell* **14,** 2342–2356
22. Westermann, B., and Neupert, W. (2000) *Yeast* **16,** 1421–1427
23. Hamel, P., Saint-Georges, Y., de Pinto, B., Lachacinski, N., Altamura, N., and Dujardin, G. (2004) *Mol. Microbiol.* **51,** 307–317
24. Mühlenhoff, U., Stadler, J. A., Richhardt, N., Seubert, A., Eickhorst, T., Schweyen, R. J., Lill, R., and Wiesenberger, G. (2003) *J. Biol. Chem.* **278,** 40612–40620
25. Volckaert, G., Voet, M., Van der Schueren, J., Robben, J., Vanstreels, E., and Vander Stappen, J. (2003) *Yeast* **20,** 79–88
26. Ha, S. A., Shin, S. M., Lee, Y. J., Kim, S., Kim, H. K., Namkoong, H., Lee, H., Lee, Y. S., Cho, Y. S., Park, Y. G., Jeon, H. M., Oh, C., and Kim, J. W. (2008) *Int. J. Cancer* **122,** 501–508
27. Kissová, I., Salin, B., Schaeffer, J., Bhatia, S., Manon, S., and Camougrand, N. (2007) *Autophagy* **3,** 329–336
28. Cortés, P., Castrejón, V., Sampedro, J. G., and Uribe, S. (2000) *Biochim. Biophys. Acta* **1456,** 67–76
29. Lee, W. K., Spielmann, M., Bork, U., and Thévenod, F. (2005) *Am. J. Physiol. Cell Physiol.* **289,** C656–C664
30. Rasheed, B. K., Diwan, J. J., and Sanadi, D. R. (1984) *Eur. J. Biochem.* **144,** 643–647
31. Wojtczak, L., Nikitina, E. R., Czyz, A., and Skulskii, I. A. (1996) *Biochem. Biophys. Res. Commun.* **223,** 468–473
32. Bonangelino, C. J., Nau, J. J., Duex, J. E., Brinkman, M., Wurmser, A. E., Gary, J. D., Emr, S. D., and Weisman, L. S. (2002) *J. Cell Biol.* **156,** 1015–1028
33. Okamoto, K., and Shaw, J. M. (2005) *Annu. Rev. Genet* **39,** 503–536
34. Zhang, Y., and Chan, D. C. (2007) *FEBS Lett.* **581,** 2168–2173
35. Jiang, D., Zhao, L., and Clapham, D. E. (2009) *Science* **326,** 144–147
36. Bernardi, P. (1999) *Physiol. Rev.* **79,** 1127–1155
37. Dimmer, K. S., Navoni, F., Casarin, A., Trevisson, E., Endele, S., Winterpacht, A., Salviati, L., and Scorrano, L. (2008) *Hum. Mol. Genet.* **17,** 201–214
38. Hasegawa, A., and van der Bliek, A. M. (2007) *Hum. Mol. Genet.* **16,** 2061–2071
39. Pang, T., Su, X., Wakabayashi, S., and Shigekawa, M. (2001) *J. Biol. Chem.* **276,** 17367–17372
40. Weinman, E. J., Cunningham, R., Wade, J. B., and Shenolikar, S. (2005) *J. Physiol.* **567,** 27–32

3.6. Identification of interaction partners of Mrs7p

3.6.1. Strategies to identify interaction partners of Mrs7p

Deletion of *MRS7* leads only to a weak growth defect on non-fermentable carbon sources. Furthermore, Mrs7p has only one membrane-spanning helix. This makes it rather unlikely that this protein forms the active K^+/H^+ exchanger alone by homo-oligomerization.

Based on our assumption that Mrs7p is a regulatory factor associated with the mitochondrial K^+/H^+ exchanger, we aimed at identifying other proteins constituting the high molecular weight protein complex of ~ 550 kDa.
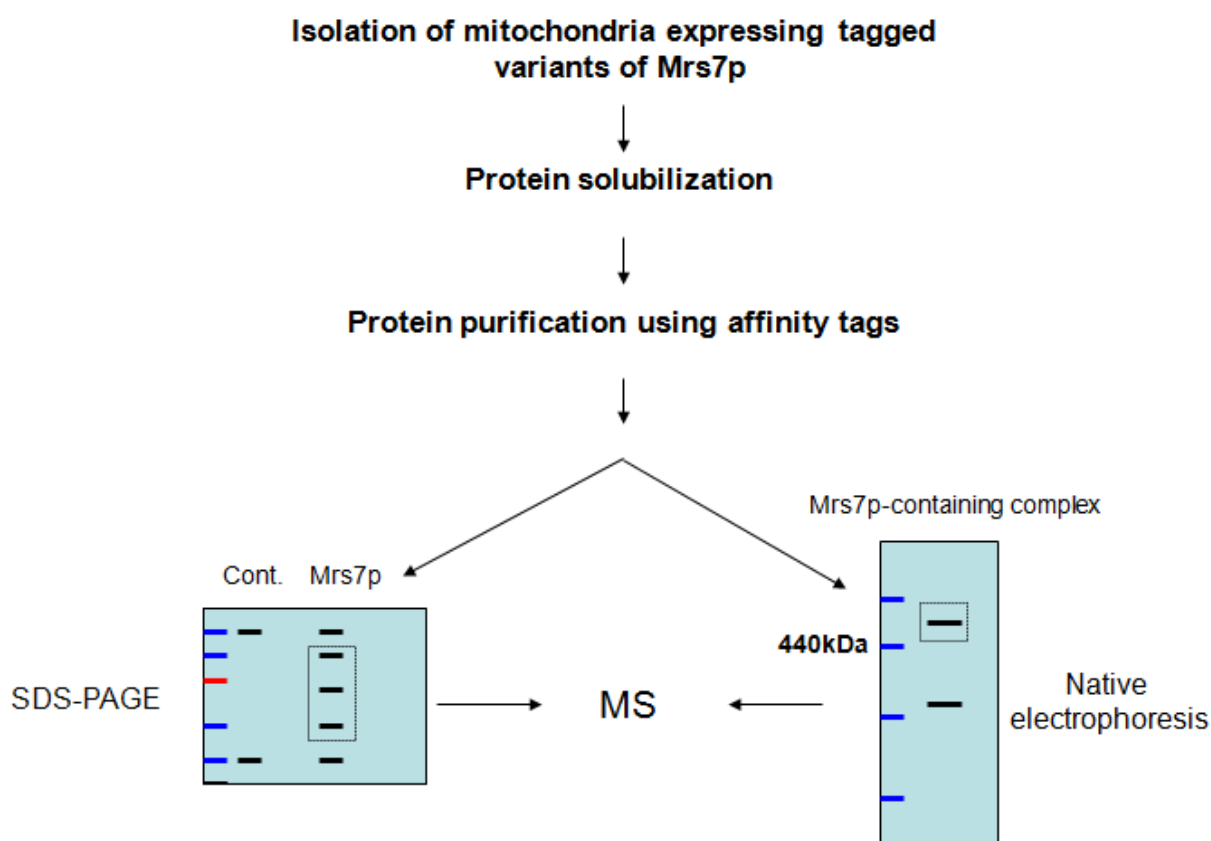
Figure 8: Schematic representation of the two strategies used to identify complex partners of Mrs7p. After the preparation of crude mitochondrial extracts from yeast cells expressing tagged variants of Mrs7p, mitochondrial membrane proteins are solubilized using detergents. Affinity chromatographic methods are used to isolate Mrs7p together with its interaction partners. Bound proteins are eluted from the column under mild conditions and purified proteins are subsequently separated on denaturing SDS-PAA gels or the whole protein complex is analyzed by Blue Native gel electrophoresis. Protein bands not present in the control experiment are cut out and proteins are identified by mass spectrometry.

We employed a combination of one to two affinity chromatography steps with mass spectrometry, which is a powerful tool to isolate protein complexes and identify their molecular composition (Figure 8). To identify putative interacting proteins, different tagged variants of Mrs7p were used as bait in affinity chromatography (Figure 9).

The tags were selected based on their properties to allow for mild binding and elution conditions, offering the possibility to isolate the high molecular weight complex in its intact form. The whole complex is subsequently subjected to Blue native electrophoresis or eluted proteins are separated on denaturing SDS-PAA gels. Candidate protein bands representing potential interaction partners of Mrs7p are analyzed by mass spectrometry (Figure 8).
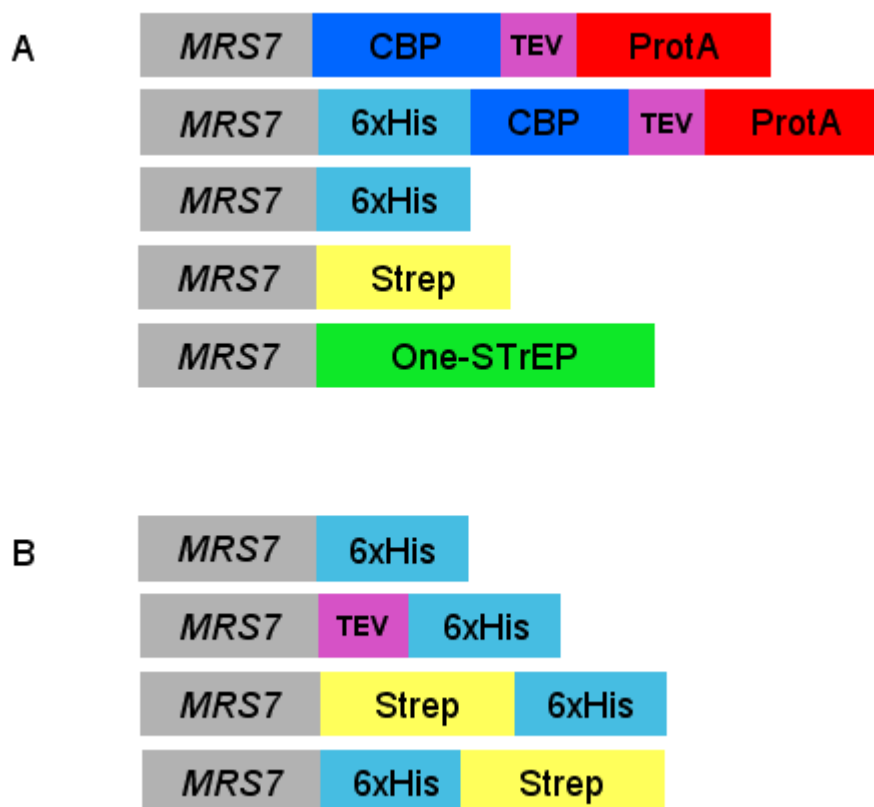

Figure 9: Overview of the different tags used for Mrs7p affinity purifications. The classical TAP-tag, consisting of two IgG–binding domains of Protein A (ProtA) and the Calmodulin binding peptide (CBP), separated by a TEV protease recognition site, as well as the 6xHis-TAP and the One-STrEP-tag (two Strep-tag II moieties separated by a linker sequence (GGGSGGGSGGSA) were chromosomally integrated by homologous recombination (**A**).
The different 6xHis- and Strep-tag II (WSHPQFEK) constructs presented in (**B**) are vector-based and expressed from the centromeric plasmid YCp22 or multi-copy vector YEp351

Since *MRS7* has an N-terminal mitochondrial targeting sequence, which is proteolytically cleaved off during the protein import into mitochondria, C-terminal tags were used. Most experiments were performed with yeast strains bearing different chromosomally tagged *MRS7* variants to keep protein expression at physiological levels (Figure 9A). Strong overexpression of single components of a potential multi-protein complex could have had negative effects on the composition of the high molecular weight complex and lead to aberrant protein interactions or elevated Mrs7p self-oligomerization. Nevertheless, given the higher flexibility and easy cloning procedure also low and high copy number vectors expressing tagged variants of *MRS7* were constructed (Figure 9B).

To achieve a high purity of the isolated complexes, the classical TAP-tag, consisting of the Calmodulin binding peptide (CBP) and two IgG binding domains of Protein A was used. This method was applied successfully for the purification of protein complexes in yeast (Puig, et al., 2001). Besides this, we introduced an additional 6xHis-tag between the gene and the TAP-tag (Figure 8) to allow for an extra purification step and a convenient detection in Western Blots. Furthermore, constructs with 6xHis-tag, Strep-tag, and different combinations of the two tags were designed (Figure 9). Both tags are widely used for the purification of proteins. They provide high yields, mild purification and elution conditions and due to their small size, the danger of having negative effects on protein function is minimized (Lichty, et al., 2005). We also constructed a variant of *MRS7* tagged with the One-STrEP-tag which was specifically designed for the purification of protein complexes (Figure 9B) (Junttila, et al., 2005).

Fusing tags to the protein of interest may interfere with protein stability, folding or negatively affect protein-protein interactions. To exclude this possibility, particularly for the relatively large TAP-tag (22 kDa), serial dilutions of strain DBY747 WT and strains harboring different tagged variants of *MRS7* were spotted on fermentable (YPD) and different non-fermentable media (YPG and YPEG).

Strain DBY747 *mrs7Δ* exhibited a weak growth defect on non-fermentable carbon sources, the deletion of its homolog *MKH1* resulted in a stronger defect. The strongest growth reduction was observed in the triple deletion strain DBY747 *mkh1Δmrs7Δydl183Δ* which exhibited a growth defect also on full-medium (YPD) plates. Strains expressing different chromosomally tagged variants of *MRS7* exhibited growth comparable to the wild-type strain (Figure 10A).

It has previously been shown that overexpression of *MRS7* rescues the growth defect of the *mkh1Δ* and the triple deletion strain (*mkh1Δmrs7Δydl183Δ*) (Zotova, et al., 2010). This effect was also observed with 6xHis/Strep-tagged variants of *MRS7* expressed from the multi-copy vector Yep351 indicating that the tags did not affect protein function (Figure 10B).
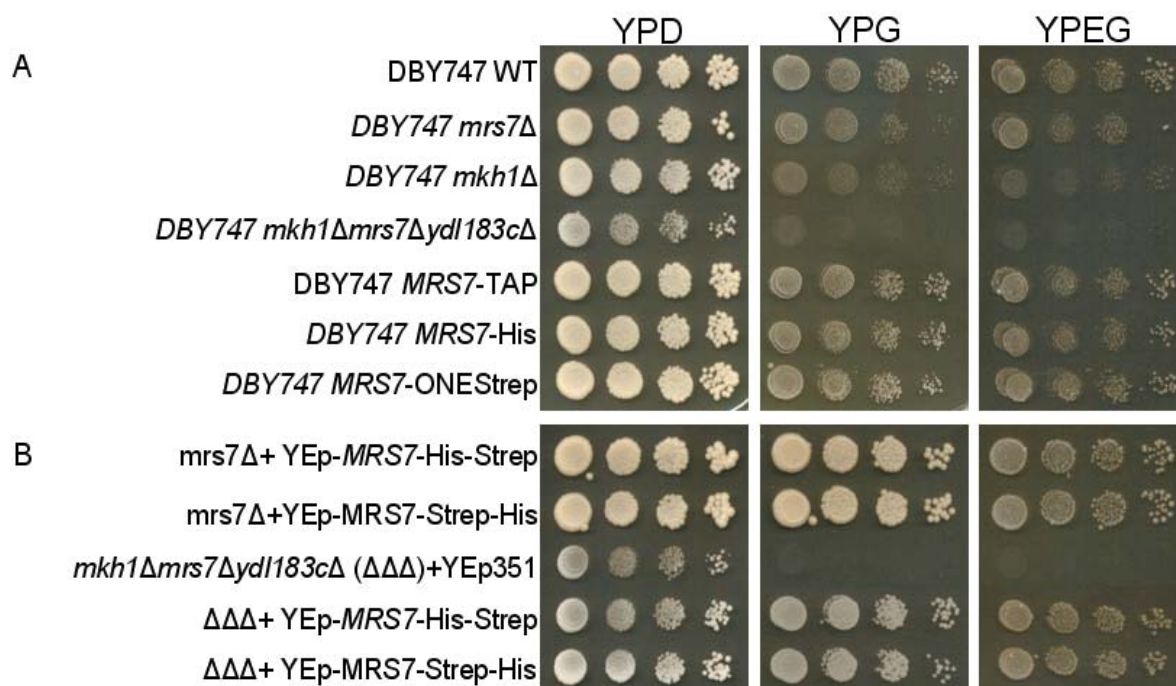

Figure 10: Growth phenotype-overview of the strains DBY747 WT, the deletion strains *mrs7Δ* and *mkh1Δ* as well as the triple deletion strain *mkh1Δmrs7Δydl183cΔ* (ΔΔΔ). Overnight cultures of different strains were adjusted to an OD_{600} of 1 and ten-fold serial dilutions were spotted on YPD, YPG and YPEG plates and incubated at 28°C for 3 (YPD) or 6 days (YPG, YPEG), respectively. (**A**) shows the growth phenotype of DBY747 WT, the triple deletion strain and DBY747 WT bearing chromosomally tagged variant of *MRS7*. In (**B**) the growth phenotypes of DBY747 *mrs7Δ* and the triple deletion strain *(ΔΔΔ)* transformed with different vector-based constructs are shown.

3.6.2. Implementation of efficient conditions for solubilization and complex purification

An important prerequisite for the identification of complex partners of Mrs7p is an efficient solubilization of the membrane proteins. Since other proteins of this high molecular weight complex are unknown, all experiments for finding suitable solubilization conditions were based on the solubilization efficiency of Mrs7p. In general only low concentrations of the detergents (0.8-1.2%) and low salt concentrations were used to keep the risk of loosing

possible binding partners minimal. Different buffers and detergents were tested for their efficiency in solubilizing Mrs7p. All buffers used had a pH of 7.8, which is similar to the pH value in the mitochondrial matrix. The NaCl concentration was varied in the range of 20 to 300 mM, various detergents, in particular Triton X-100, laurylmaltoside, digitonin as well as NP-40 were tested. Best results were obtained with the detergent digitonin (not shown), however, due to its high costs this chemical could not be used in large scale experiments. Figure 11 shows a small selection of some of the tested solubilization conditions in low ionic strength buffers. Triton X-100 at a final concentration of 1.2% in Hi10/50 buffer (10 mM Tris-HCl pH 7.8, 50 mM NaCl and 20 mM imidazol) yielded a solubilization efficiency of ~ 90% and was therefore used for all further experiments.
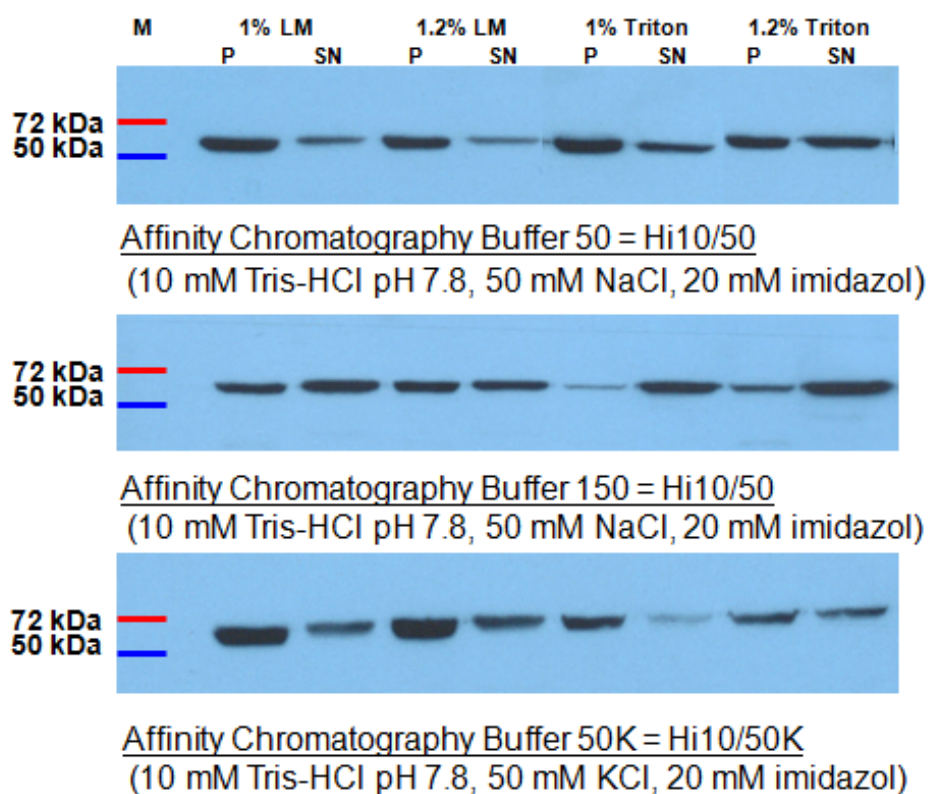

Figure 11: Solubilization efficiency of Mrs7p in different buffers and with different detergents. Mitochondria from DBY747 cells chromosomally expressing Mrs7p-HisTAP were resuspended in the buffers stated above to a final concentration of 20 mg/ml and incubated on ice for 30 min. After a clarifying spin (30 min at 42 000 rpm, 4°C), equal amounts of the supernatant (solubilized protein) and the pellet (insoluble fraction) were loaded on a 10% SDS-PAA gel and Western Blot was performed with an anti-6xHis antibody.

After establishing efficient conditions for Mrs7p solubilization, the presence of the intact high molecular weight complex was verified by Blue native PAGE. Isolated mitochondria were solubilized in the buffer described above with or without 100 mM NaCl. After removal of unsolubilized debris by centrifugation, the supernatant was either loaded directly on a 5-18% polyacrylamide gradient gel, or imidazol was added to the protein sample in order to mimic the high imidazol concentrations during the elution from a Ni-NTA affinity column.
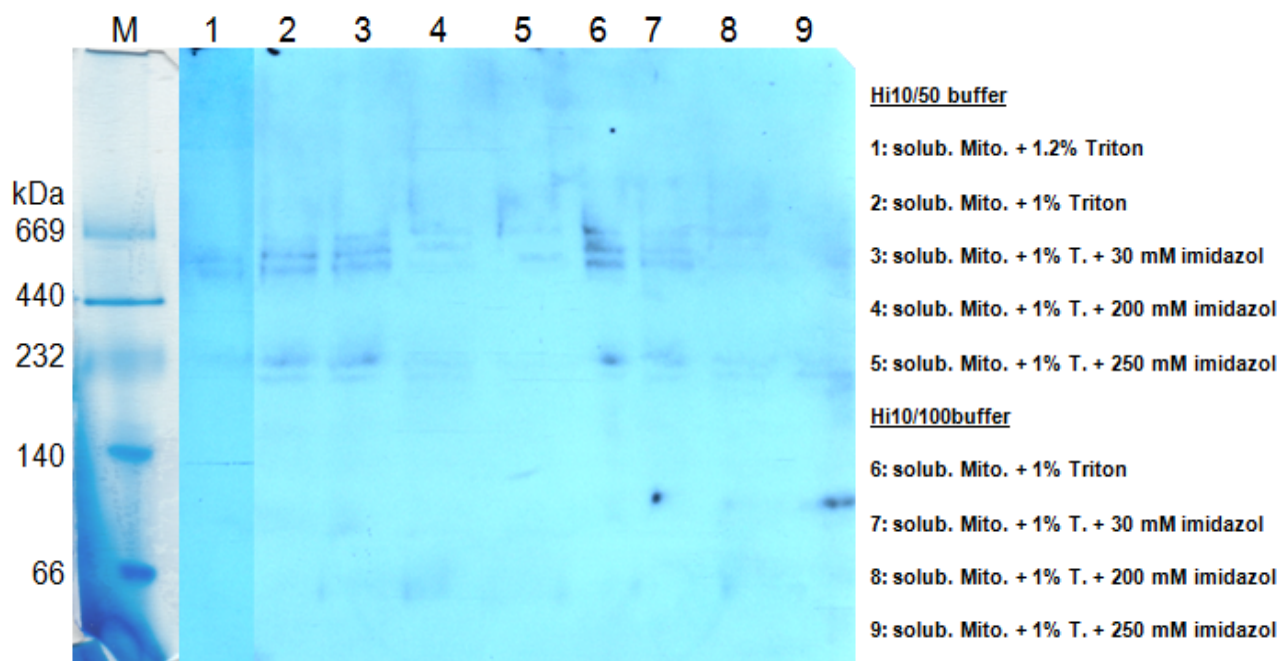

Figure 12: Initial stability test of the Mrs7p-containing high molecular weight complex. Mitochondria from DBY747 cells chromosomally expressing Mrs7p-HisTAP were solubilized in buffers containing 10 mM Tris-HCl pH 7.8, 50 or 100 mM NaCl, with or without 30 mM imidazol and the detergent Triton X-100. After a clarifying spin to remove unsolubilized debris higher imidazol concentrations, to simulate the conditions during elution of the proteins from a Ni-NTA chromatography column, were added to the supernatant. The samples were run on a 5-18% BN-PAA gradient gel and Western Blot was performed with an antibody directed against the 6xHis-tag. M, high molecular weight protein standard.

Mrs7p was detected in a high molecular weight complex between 440 and 669 kDa and in a smaller complex of approximately 230 kDa in most tested conditions (Figure 12). The lower signal intensity for samples with high imidazol concentration (Figure 12 lanes 4, 5, 8 and 9) is most probably caused by dilution of the protein sample by subsequent addition of imidazol. Under higher ionic strength and a high imidazol concentration (Figure 12 lane 9) a potential

Mrs7p dimer of approx. 120 kDa was detected. This experiment indicated that the tested solubilization conditions, particularly in Hi10/50 buffer were mild enough not to affect stability of the protein complexes.

Table 1 gives an overview of all tested purification methods, their applicability for the purification of Mrs7p as well as yield and purity of the affinity chromatographic methods.

Table 1: Comparison of yield and purity of the tested single-step and tandem affinity purification methods.

Yield and purity of the different purification strategies were tested in small scale affinity purifications with 180 mg isolated crude mitochondrial extracts. The yield was estimated based on the signal strength in Western Blots and purity was assessed by Coomassie-staining of the gels. A successful tandem affinity purification with the tag combination Protein A and Calmodulin failed, since none of the tested conditions allowed cleavage at the TEV recognition site. Consequently the Mrs7p-containing complex could not be eluted from the first column under non-denaturing conditions. The two-step purification strategy using Ni-NTA affinity chromatography as first step and Strep-affinity chromatography as second step resulted in high enrichment of the Mrs7p containing complex combined with the highest purity in any of the tested strategies.

Method	Applicability	Yield	Purity
Protein A	✔	low	medium
Calmodulin	✔	medium	medium
Protein A + Calmodulin	✘	---	---
Calmodulin + Protein A	✔	very low	medium
6xHis	✔	**high**	**low**
Strep	✔	**high**	**medium**
6xHis + Protein A	✔	very low	medium
6xHis + Calmodulin	✔	low	medium
One-STrEP	✔	medium	medium
6xHis + Strep	✔	**very high**	**high**

All purifications *via* Protein A or CBP were tested with 180 or 360 mg total mitochondrial protein with different volumes of the specific resin and various washing and elution conditions. For affinity chromatography *via* Protein A, solubilized mitochondrial proteins

were incubated with IgG sepharose beads and incubated for 60 min at 4°C under gentle shaking. The bead suspension was loaded on a column and unbound proteins were eluted by gravity flow. The interaction between the Protein A-tag and IgG is very strong. Proteins cannot be eluted under mild native conditions, but the tag has to be cleaved off by TEV protease. Various conditions were tested for the TEV cleavage reaction. Higher concentrations of the enzyme, reduction of the Triton X-100 concentration to 0.1% and elevated temperatures to increase the cleavage efficiency had no effect. Mrs7p could not be detected in the elution fraction after TEV cleavage. Only after treatment of the sepahrose beads with 0.1 M glycine pH 3.0, Mrs7p could be eluted form the column (Figure 13). Since Mrs7p was not detected in the flow through and wash fraction, insufficient binding of the protein can be excluded. A possible explanation is that the TEV recognition site is not accessible in the Mrs7p protein complex.
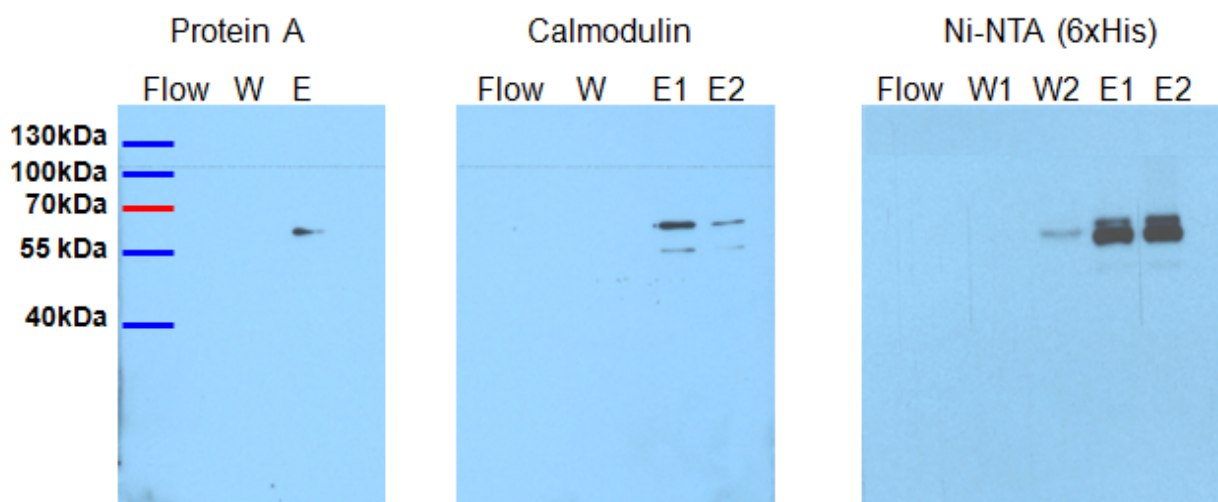

Figure 13: Typical example for the higher yield of Ni-NTA chromatography in comparison to affinity chromatography *via* the Protein A- or Calmodulin-tag. Mitochondria were isolated from strains expressing Mrs7p-HisTAP and solubilized in Hi10/50 Buffer (1.2% Triton X-100) After a clarifying spin to remove unsolubilized mitochondrial debris, Mrs7p and associated proteins were purified on gravity flow columns. Equal amounts of the flow through (Fl), wash fractions (W) as well as elution fractions (E) were run on 10% SDS-PAA gels. Western Blot was performed with an antibody against the 6xHis-tag.

The finding that Mrs7p was not eluted from the column under native conditions qualified the classical tandem affinity purification as not suitable for Mrs7p.

Affinity chromatography *via* the CBP-tag was also tested. The Calmodulin binding protein binds in the presence of calcium to the Calmodulin affinity resin. Solubilized mitochondria were incubated in the presence of 2 mM $CaCl_2$ with the resin for 60 min at 4°C under gentle shacking. After two washing steps, bound proteins were eluted with Hi10/50 buffer supplemented with 4 mM EGTA to complex calcium ions. This method worked well for Mrs7p, however, compared to Ni-NTA affinity chromatography the yield was very low (Figure 13).

Though, as stated previously the classical TAP method was not efficient, this purification method can also be performed in the reverse order. However, in this case, the proteins bound to IgG sepharose had to be eluted under very harsh conditions (0.1 M glycine, pH 3) destroying protein-protein interactions, thus excluding further experiments with an intact complex. Nevertheless it would allow the analysis of the eluted proteins by SDS-PAGE and Coomassie staining. The TAP purification in reverse order worked but protein yields were extremely low and Mrs7p could hardly be detected by Western Blot (data not shown). The low yield combined with the impossibility to verify intactness of the high molecular weight complex after affinity chromatography made this method not applicable.

3.6.3. Single-step affinity chromatography via the 6xHis- and Strep-tag

Attempts to combine the high yield of Ni-NTA affinity chromatography in the first step and purification *via* Protein A or *via* CBP as second step similarly resulted in low yields, which could not be enhanced.

We therefore focused on Ni-NTA and Strep affinity chromatography. Both methods were optimized and yielded satisfactory amounts of Mrs7p. Since isolation of mitochondria from yeast cells is quite laborious, small amounts of mitochondria were used for optimization experiments. In these small scale experiments, Mrs7p was of relatively low abundance. As Mrs7p could not be detected by Coomassie staining, immunoblots served to evaluate the protein yield.

For Ni-NTA affinity chromatography 90 mg of crude mitochondrial extracts were solubilized and after centrifugation the supernatant was incubated with Ni-NTA superflow resin (Qiagen) for 10 min. The strong affinity of the 6xHis-tag to the resin allows short incubation times. Bound proteins were eluted by washing the column with Hi10/50 buffer supplemented with 200 mM imidazol. The yield of Ni-NTA chromatography was slightly higher compared to Strep purifications (Figure 14).
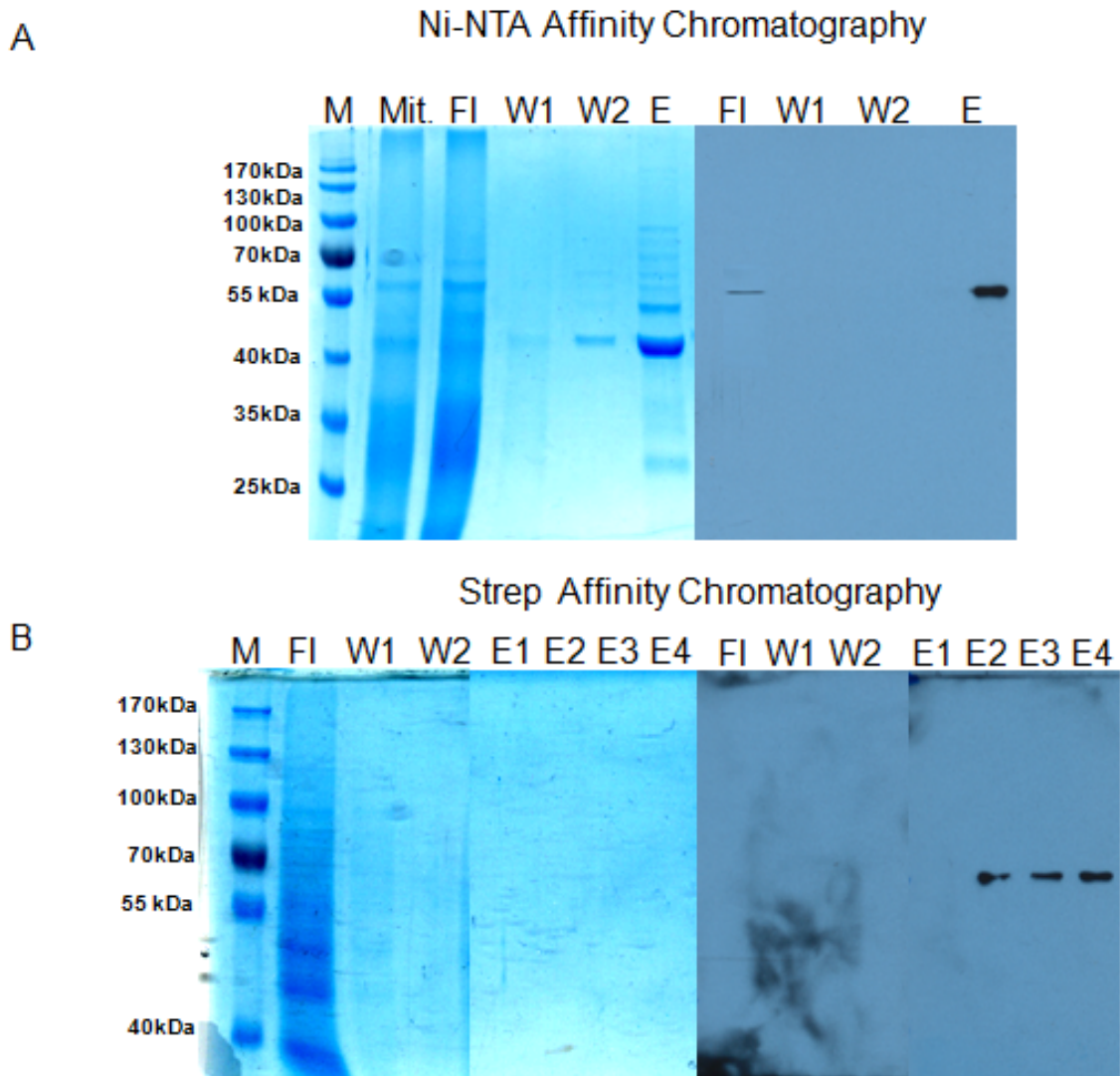
Figure 14: Purity of Ni-NTA and Strep affinity chromatography. Mitochondria were isolated form strains expressing *MRS7* chromosomally tagged either with the 6xHis-tag (**A**) or the Strep-tag (**B**) and solubilized in Hi10/50 Buffer (1.2% Triton X-100). After removing unsolubilized mitochondrial debris, Mrs7p and associated proteins were purified on gravity flow columns. Equal amounts of the flow through (Fl), wash fractions (W1 and W2) as well as elution fractions (E) were run on 10% SDS-PAA gels. Gels were stained with Coomassie brilliant blue or Western Blot was performed with an antibody against the 6xHis-tag or the Strep-tag, respectively.

However a disadvantage of using the 6xHis-tag in eukaryotic organisms is the considerable higher number of proteins with successive histidines in their amino acid sequence, which therefore have strong affinity to the Ni-NTA resin, eventually leading to a relatively low purity (Figure 14A). Strep affinity purifications were carried out as described for Ni-NTA affinity chromatography, but with Strep-sepharose (IBA). The resin was incubated with

solibilized proteins for 20 min and after a washing step proteins were eluted in the presence of 2.5 mM D-desthiobiotin. In contrast to the Ni-NTA affinity chromatography the purity was considerably higher, albeit the yield was slightly lower (Figure 14B).
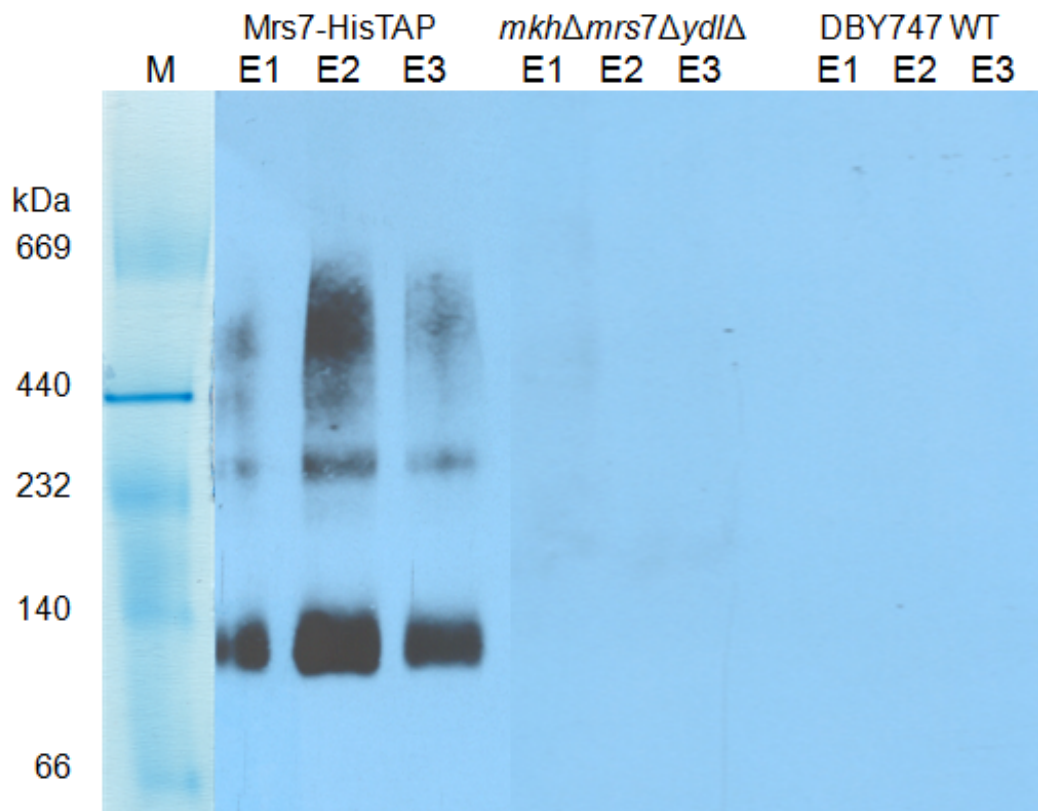

Figure 15: Ni-NTA affinity purification of Mrs7p-containing high molecular weight complexes and control of signal specificity. Isolated mitochondria of DBY747 WT cells, the triple deletion strain *mkhΔmrs7ΔydlΔ* and cells expressing a chromosomally 6xHis-tagged version of *MRS7* were solubilized and purified *via* Ni-NTA affinity chromatography. Elution fractions were loaded on a 6-18% Blue Native gradient gel and Western Blot was performed with an anti-6xHis antibody.

Elution fractions obtained after Ni-NTA affinity chromatography were analyzed by Blue native electrophoresis to verify the presence of the Mrs7p containing high molecular weight complexes. The first three elution fractions were run on a 5-18% PAA gradient gel and Western Blot was performed with an antibody directed against the 6xHis-tag.

Mrs7p was detected as part of high molecular weight complexes of ~ 550 and 240 kDa, furthermore a faint signal with an apparent molecular weight of 440 kDa was observed. Surprisingly, the anti-6xHis antibody recognized an additional, highly abundant complex of 100-120 kDa which might be a Mrs7p dimer (Figure 15).

This dimeric form of Mrs7p was not observed in previous experiments when mitochondria were solubilized in low ionic strength buffer and loaded directly on a Blue native gel (Figure 12). Consequently, this signal likely resulted from the partial dissociation of the complex during the purification procedure. In our preliminary stability test we only examined if the used buffers were in principle compatible with the Mrs7p containing high molecular weight complex. Obviously affinity purification exposes the protein complex to much stronger forces eventually leading to the dissociation of some of the involved proteins.

3.6.4. Chemical cross-linking of Mrs7p

To avoid the loss of possible interaction partners of Mrs7p, we took chemical cross-linking into consideration to "stabilize" the complex. Several cross-linking agents were tested e.g. the amine-reactive bis(maleimido)hexane (BMH1), dithiobis(succinimidyl propionate) (DSP), bis(sulfosuccinimidyl)suberate (BS3), o-phenylenedimaleimide (oPDM), disuccinimidyl suberate (DSS) and formaldehyde. Cross-linking experiments were initially performed with intact mitochondria. Due to the relatively low expression level of Mrs7p, 3 to 5 mg total mitochondrial protein had to be used. No significant cross-linking activity could be observed under various tested conditions where we explored a number of cross-linker concentrations, buffer conditions and incubation times. However, with DSS and formaldehyde surprising results were obtained: addition of the cross-linker led, as expected, to a weaker signal for monomeric Mrs7p, but no cross-linking products of higher molecular weight could be detected (Figure 16A). Interestingly this effect was only observed in small reaction volumes (100-200 μl), while in larger volumes no change in signal strength for the Mrs7p monomer could be observed, although the ratio between protein and cross-linking agent ratio was kept constant.

A possible explanation for this surprising finding that addition of the cross-linker decreases the signal strength for the monomer without resulting in a detectable cross-linked product, could be that the 6xHis-tag is no longer accessible when Mrs7p is part of a protein complex. Due to the limitations of cross-linking in whole mitochondria we could not verify this hypothesis. Instead of using mitochondrial extracts we therefore performed chemical cross-linking with the elution fractions obtained after Ni-NTA affinity purification (Figure 16B).
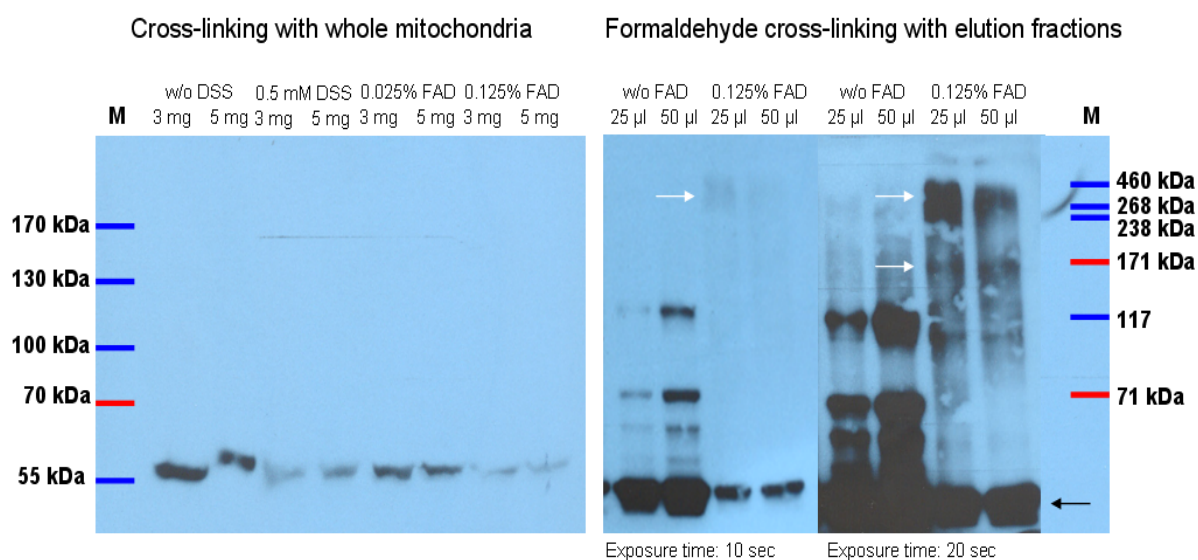
Figure 16: Chemical cross-linking of Mrs7p. (**A**) Cross-linking was performed with isolated mitochondria from strain DBY747 expressing Mrs7p-6xHis from a multicopy plasmid. Isolated mitochondria (3 mg/ml or 5 mg/ml) were incubated in Hi10/50 buffer without or with increasing concentrations of the cross-linking agents disuccinimidyl suberate (DSS) and formaldehyde (FAD) for 30 min on ice. Proteins were separated by SDS-PAGE and immunoblotted against the 6xHis epitope. (**B**) Isolated mitochondria from strain DBY747 expressing Mrs7p-6xHis from a multicopy plasmid were solubilized and Mrs7p-containing high molecular weight complexes were purified *via* Ni-NTA affinity chromatography. Chemical cross-linking with 0.125% formaldehyde was performed in two different reaction volumes (25 µl and 50 µl). Proteins were separated on a 5-16% SDS-PAA mini gradient gel. Western Blot was performed with an antibody against the 6xHis-tag. The monomeric form of Mrs7p (black arrow) and higher molecular weight complexes containing Mrs7p (white arrows) were detected.

Addition of formaldehyde to the eluted proteins similarly led to a decrease in signal strength for the monomer with no formation of higher Mrs7p containing cross-linking products as detected by Western Blotting. However, due to the higher abundance of Mrs7p after affinity purification, a longer exposure time revealed high molecular weight cross-linking products (Figure 16B, white arrows). These findings confirmed that accessibility of the 6xHis-tag is reduced when Mrs7p interacts with other proteins, probably caused by steric hindrance or an altered fold of the protein.

This supports the possibility that also the percentage of Mrs7p found in the dimeric form after Ni-NTA affinity chromatography and Blue native electrophoresis is not as high as judged by signal intensities in Western Blots (Figure 15) and that a reasonable amount of the high molecular weight complex is still intact after the purification.

3.6.5. The Mrs7p-containing complex is intact after affinity chromatography and size exclusion chromatography (SEC)

To better estimate the remaining amount of intact high molecular weight complex after affinity purification, Ni-NTA affinity chromatography was combined with size exclusion chromatography (SEC). SEC is a relatively mild method where proteins and protein complexes are separated based on their hydrodynamic radius. Affinity chromatography with 6xHis-tagged Mrs7p was performed as described previously; the elution fractions were pooled and diluted with Hi10/50 buffer to reduce the Triton X-100 concentration to 0.1% to be compatible with SEC. The protein sample was run on a 26/60 Superdex 200 column (Amersham).
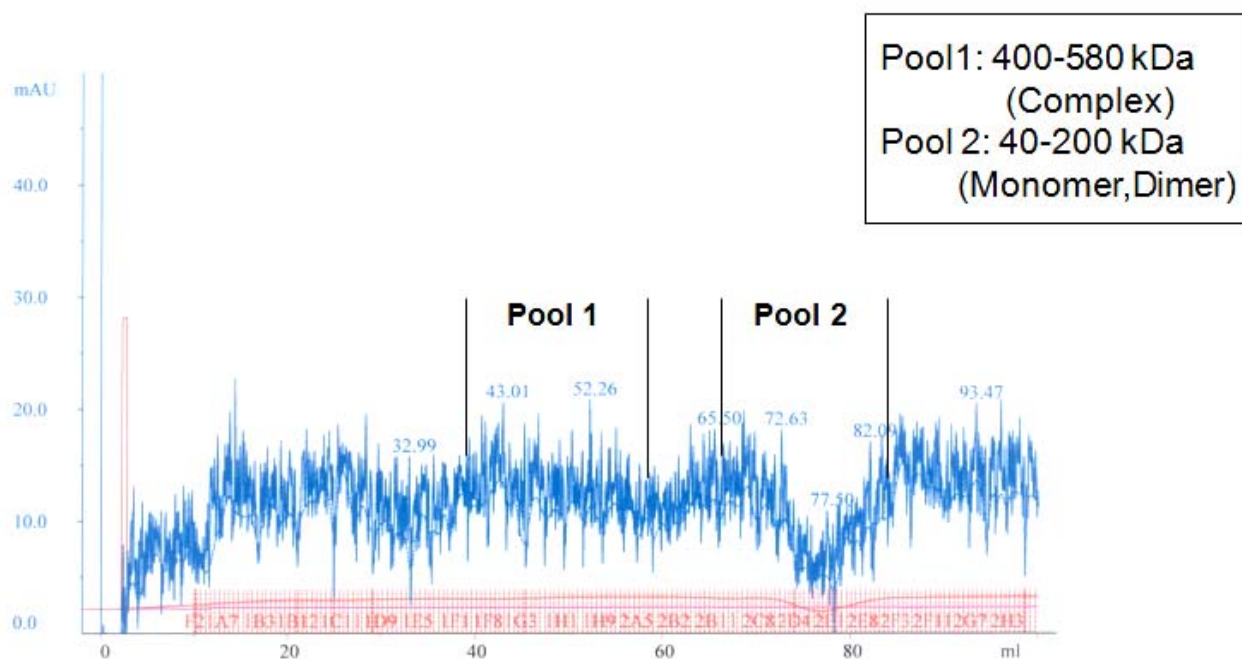

Figure 17: Size determination of the Mrs7p containing high molecular weight complex after Ni-NTA affinity chromatography. Isolate mitochondria of DBY747 cells expressing a chromosomally 6xHis-tagged version of Mrs7p were solubilized with 1.2% Triton X-100, after centrifugation the Triton X-100 concentration of the supernatant was reduced to 1% and during the washing and elution steps to 0.8%. Elution fractions were further diluted to a final concentration of 0.1% by addition of Hi10/50 buffer. The sample was run on a 26/60 Superdex 200 column. Fractions containing proteins and protein complexes with a size of 580-400 kDa (Pool1) and 40-200 kDa (Pool2) were pooled and the volume of the pools was reduced using a Vivaspin concentrator. Abscissa indicates the elution volume in millilitres, ordinate gives the absorbance. mAu, milliampere units.

Based on the chromatogram (Figure 17) individual elution fractions representing proteins with a size of 400-580 kDa, containing Mrs7p as part of a high molecular weight complex, as well as fractions in which the momomeric and dimeric form of Mrs7p should be enriched were pooled. Due to the eight-fold dilution of the protein sample prior to SEC to reduce the Triton X-100 concentration and the further dilution during SEC, the volume of the two pools had to be reduced. Equal amounts of the two pools were concentrated using a Vivaspin concentrator.


Exposure time: 20 sec   Exposure time: 40 sec
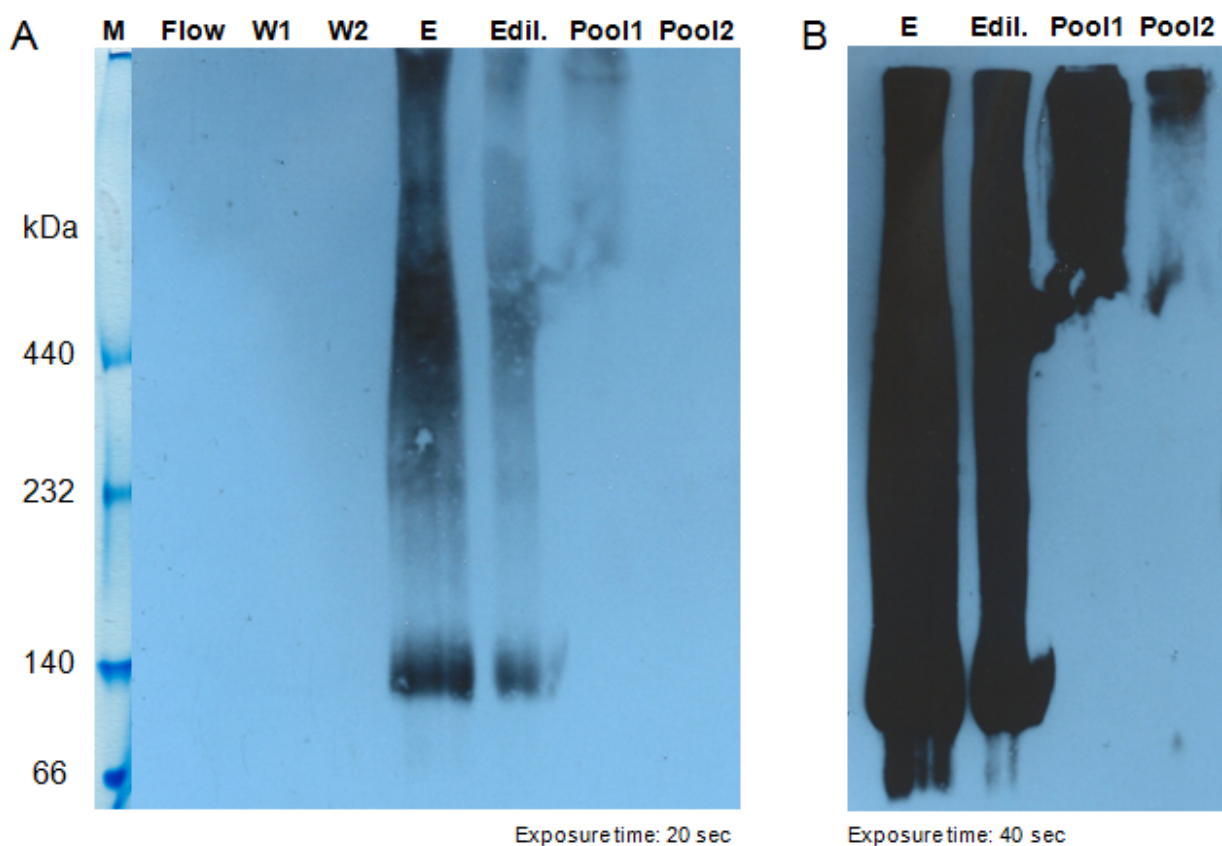
Figure 18: Blue native electrophoresis of different fractions obtained from Ni-NTA affinity purification and of pool 1 and pool 2 after SEC. (**A**) After Ni-NTA chromatography, flow through, wash fractions, the elution fraction and the elution fraction diluted to a final Triton X-100 concentration of 0.1% (Edil.) as well as the pools 1 and 2 obtained from SEC after concentration using a Vivaspin concentrator were run on a 5-18% blue native gradient gel, Western Blot was performed with an antibody against the 6xHis-tag. The higher salt concentration of the concentrated pools was not compatible with Blue native electrophoresis. However, the predominant amount of Mrs7p was detected in pool 1 (high molecular weight fraction containing proteins/complexes of 400-500 kDa). (**B**) shows the same Blot after prolonged exposure time.

Equal amounts of the eluate after affinity chromatography, the diluted sample as well as the concentrated pools after SEC were subsequently applied to a 5-18% native gradient gel and Western Blot was performed with an antibody directed against the 6xHis-tag (Figure 18). Signals obtained for the elution fraction after affinity chromatography and the diluted sample were comparable to previous purifications, while samples taken from pool 1 and pool 2 did not separate well in Blue native electrophoresis (Figure 18A and B, pool 1 and pool 2). This was most likely caused by the higher salt concentration after the volume reduction. Although a stronger signal for 6xHis-tagged Mrs7p is apparent in the first pool containing high molecular weight proteins and protein complexes (Figure 18B, pool 1), samples were also run on a denaturing 10% SDS-PAA gel and Western Blot was performed. The Western Blot after SDS-PAGE clearly demonstrated that most of Mrs7p is found in the high molecular weight pool (Figure 19, pool 1) indicating that the predominant part of the protein complex is still intact after affinity chromatography and SEC. The stronger signal intensity for the Mrs7p dimer is likely caused by a higher accessibility of the 6xHis-tag in the dimeric conformation compared to the full-size protein complex.
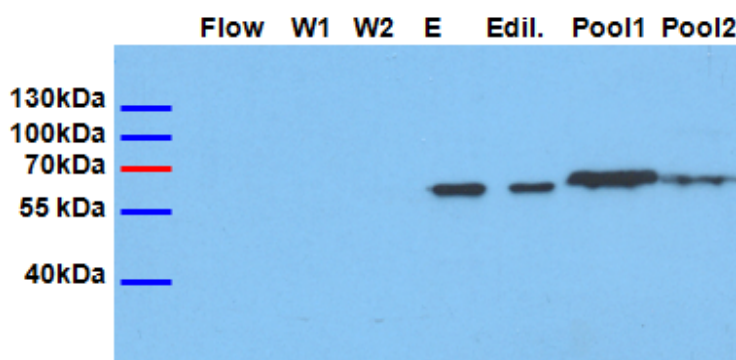
Figure 19: Analysis of the various fractions obtained from Ni-NTA affinity purification and after SEC and concentration by SDS-PAGE. Flow through (Flow), wash fractions 1 and 2 (W1 and 2), the eluted proteins (E) and the elution fraction diluted to a final Triton X-100 concentration of 0.1% (Edil.) of the Ni-NTA affinity chromatography as well as the concentrated pools 1 and 2 from size exclusion chromatography were analyzed on a 10% SDS-PAA gel and Western Blot was performed with an antibody against the 6xHis-tag. The major part of Mrs7p was detected in pool 1 indicating that a high percentage of the Mrs7p containing high molecular weight complex is intact after affinity chromatography and size exclusion chromatography.

3.6.6. Optimization of single step affinity chromatography via the Strep-tag

Ni-NTA affinity chromatography has proven to be efficient for isolation of Mrs7p together with interacting proteins, although the purity was not as high as expected.

In search for a second affinity chromatography method we tried to optimize purifications *via* the Strep-tag. Two different bead materials were tested for their effectiveness in gravity flow columns compared to our standard Ni-NTA superflow resin. To test the different resins, equal amounts of isolated mitochondria from strain DBY747 + YCp22-*MRS7*-Strep-6xHis were solubilized and purifications were performed on gravity flow columns packed with the respective bead materials (Figure 20).
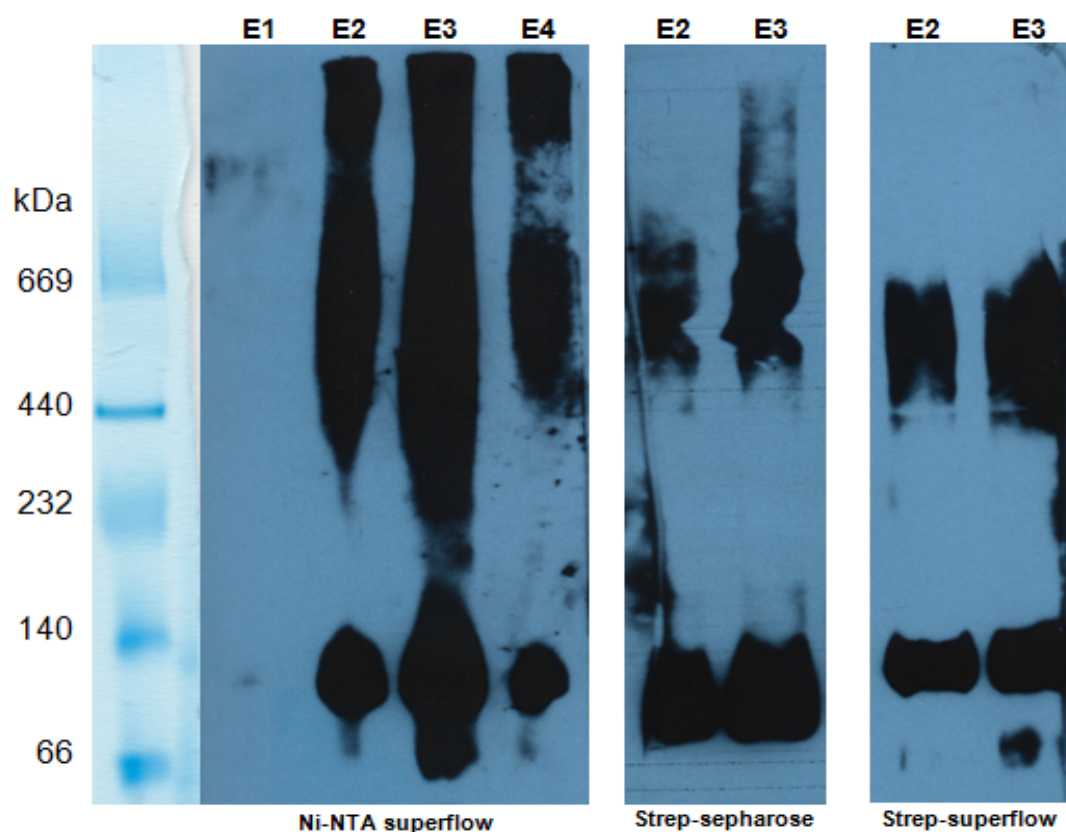

Figure 20: Efficiency of complex purification with Ni-NTA superflow compared to different Strep-tactin resins: Mitochondria isolated from strain DBY747 expressing 6xHis-Strep-tagged Mrs7p from the vector Yep351 were solubilized using 1.2% Triton X-100 in Hi10/50 buffer. After solubilization, the supernatant, containing tagged Mrs7p was subjected to affinity chromatography on different resins. After purification, elution fractions (E1-E4) were separated by Blue native electrophoresis on a native 5-18 % polyacrylamide gradient gel, transferred to a PVDF membrane and immunoblotted against the Strep epitope.

143

As shown in Figure 20, no significant difference between Strep-sepharose and Strep-superflow resin could be observed. Again purification efficiency was judged by immunodetection of Western blots with an antibody directed against the Strep-tag. Compared to Ni-NTA affinity purification, signals obtained after purifications *via* the Strep-tag were weaker, nevertheless relatively high amounts of the high molecular weight complex could be purified and the lower yield of this method is counterbalanced by its remarkable higher purity.

Recently an improved version of the classical Strep-tag II, the One-STrEP-tag, has been developed consisting of two Strep II moieties, separated by a linker sequence. This tag should give higher yields particularly in the isolation of low abundant protein complexes. Because of the two Strep II moieties a higher binding affinity and a higher accessibility due to its almost threefold longer amino acid sequence was expected.

Mitochondria were isolated from strain DBY747 bearing chromosomally tagged *MRS7* either fused to the Strep-tag II or the One-STrEP-tag. In order to avoid misinterpretation of Western Blots, large scale purifications with 360 mg total mitochondrial protein were performed. Equal amounts of the elution fractions were run either on a Blue native gel with subsequent immunodetection of the Strep-tag II or applied to a large 10% SDS-PAA gel and stained with Coomassie brilliant blue. Signals obtained for Mrs7p tagged with the One-STrEP-tag were extremely strong in the Western Blot (Figure 21A). Surprisingly, in the Coomassie stained gel the ratio was reversed, Strep-tag II was significantly more efficient than One-STrEP (Figure 21B). This effect is most likely caused by the fact, that the One-STrEP-tag consists of two Strep II parts and therefore has the two-fold amount of binding sites for the Strep antibody, eventually leading to a much stronger signal. Accordingly, the One-STrEP-tag did not represent a suitable method for the identification of complex partners of Mrs7p.
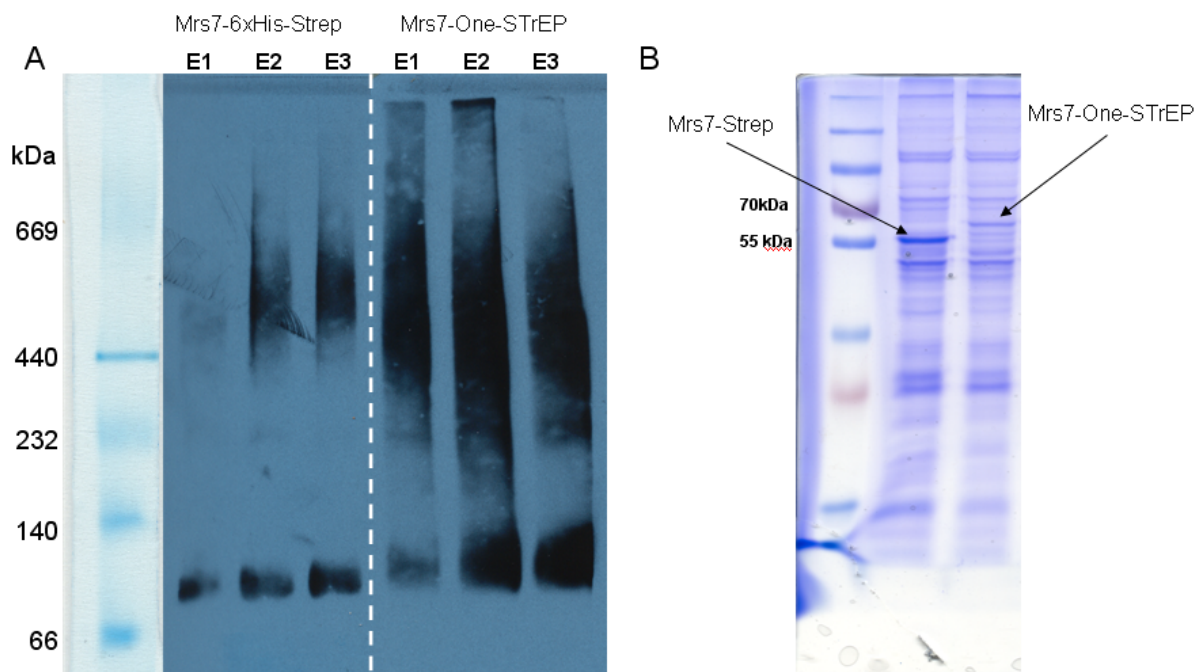
Figure 21: The One-STrEP-tag is less efficient in purification of Mrs7p containing high molecular weight complexes compared to the classical Strep-tag. Mitochondria isolated from strain DBY747 expressing genomically tagged Mrs7p-Strep or Mrs7p-One-STrEP were solubilized using 1.2% TX-100 in Hi10/50 buffer. After solubilization, the supernatant, containing tagged Mrs7p was subjected to affinity chromatography on Strep-sepharose resin. (**A**) After purification, equal amounts of the elution fractions (E1-E4) were separated by Blue native electrophoresis on a native 5-18 % polyacrylamide gradient gel, transferred to a PVDF membrane and immunoblotted against the Strep epitope. (**B**) Equal amounts of the elution fraction E2 of Mrs7p-Strep and Mrs7p-ONE-Strep were separated on a large 10% SDS-PAA gel and Coomassie-stained.

In general identification of proteins by mass spectrometry is successful if the protein band can be visualized by Coomassie staining of the gel. In the next step we tested the needed amount of purified mitochondria to obtain a signal for the high molecular weight complex in Blue native gradient gels. To obtain a Coomassie stainable band for the potential Mrs7p containing complex, 360 mg isolated crude mitochondria extracts, equivalent to twelve liters of yeast culture were needed to obtain a signal putatively originating from the complex (Figure 22, black arrows). No clear sharp band could be observed, probably due to the relatively low sensitivity of Coomassie staining of Blue native gels. Mass spectrometry analysis was performed with the two obtained bands. However, more than 200 proteins were identified in the gel piece cut out from the gel after Ni-NTA affinity chromatography and around 60 after Strep affinity purification.

Mrs7p was identified with relatively high scores but the large number of proteins made the identification of potential interaction partners impossible.
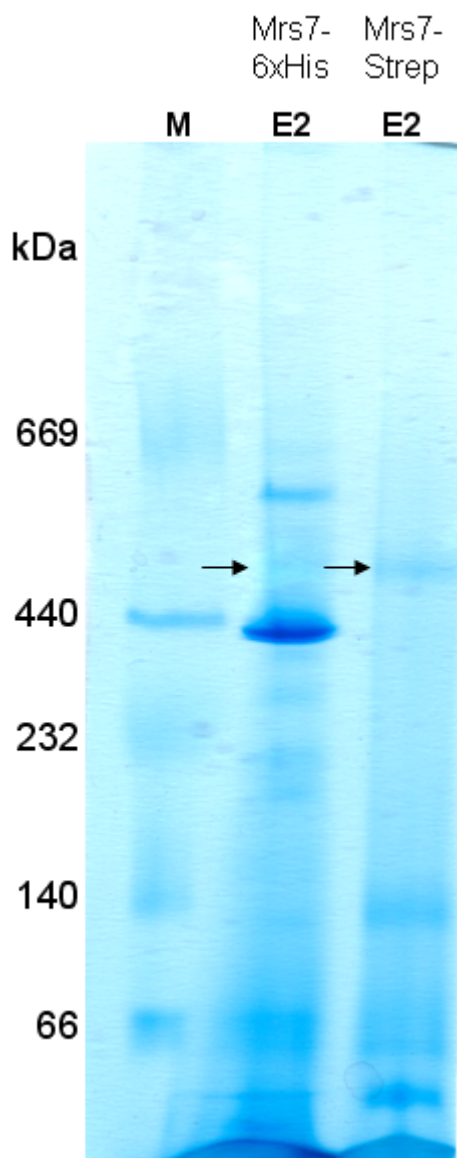

Figure 22: Result of large scale purifications using Mrs7p-6xHis and Mrs7p-Strep. Mitochondria isolated form strain DBY747 expressing either a 6xHis- or a Strep-tagged variant of the protein were solubilized using 1.2% Triton X-100 and subjected to affinity chromatography on gravity flow columns. The second elution fraction (E2) was separated on a 5-18% native polyacrylamide gel and proteins were detected by Coomassie staining. The potential Mrs7p containing high molecular weight complex is marked (*black arrows*)

3.6.7. Tandem affinity purification via 6xHis and Strep-tag – large scale purifications to identify interaction partners by mass spectrometry

We therefore decided to combine the two methods to achieve a further enrichment of the high molecular weight complexes and to improve the purity of the preparations. Since we demonstrated that the Mrs7p containing high molecular weight complex can be purified in its intact form by these two methods, the analysis of the eluted proteins by SDS-PAGE appeared to be the more reliable technique compared to Blue native electrophoresis. First, Coomassie

staining of SDS-PAA gels is more sensitive than staining of Blue native gels. Second, protein bands are usually sharper, which facilitates cutting out of the desired band for mass spectrometry analysis. Furthermore, the implementation of a control is easier. Affinity purifications are performed in parallel with mitochondria isolated from strains bearing tandemly tagged *MRS7* and a WT strain.
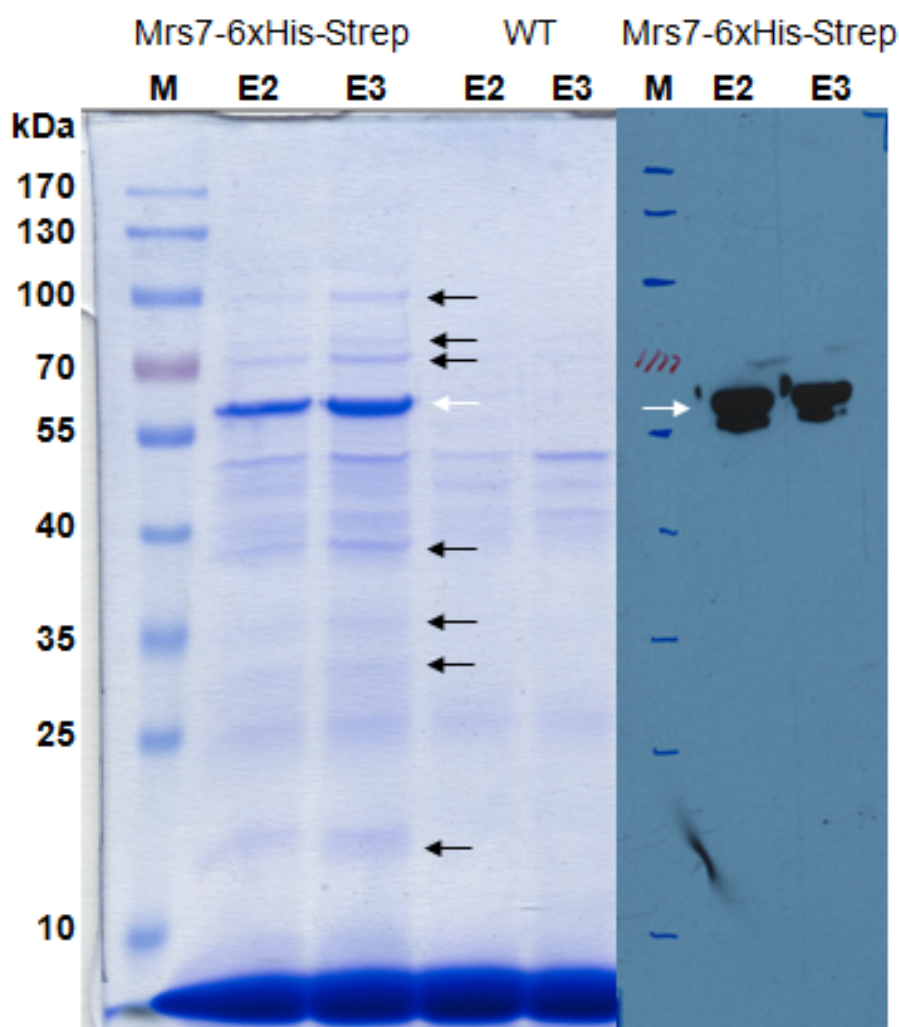

Figure 23: Representative result of the large scale purifications. After the tandem purification *via* Ni-NTA and Strep affinity chromatography of isolated mitochondria expressing Mrs7p-6xHis-Strep or mitochondria from strain DBY747 WT. The elution fractions containing the highest amount of the Mrs7p protein complex and the corresponding WT elution fractions were separated on a 10% SDS-PAA gel and stained with Coomassie brilliant blue. Interesting bands solely appearing in the Mrs7p-6xHis-Strep lane (*black arrows*) were cut out and analyzed by mass spectrometry. A Western Blot control was performed in parallel to confirm that the strongest signal originates from the full-length tagged Mrs7p (*white arrows*) and that lower molecular weight bands present only in the Mrs7p lanes are not derived from shorter, degraded versions of the protein.

Figure 23 shows an example of a large scale purification of Mrs7p. For these experiments 900 mg isolated mitochondria, equivalent to 20 liters of yeast culture were processed. Ni-NTA and Strep affinity purifications were performed in tandem. Eluted proteins were separated on large 10% SDS-PAA gels and stained with Coomassie brilliant blue. Strong

signals were obtained for the bait Mrs7p (Figure 23, white arrows). Bands exclusively appearing in the Mrs7p lanes were cut out and analyzed by mass spectrometry (Figure 23, black arrows).

Table 2 gives a list of all proteins identified as potential interaction partners of Mrs7p.

Systematic name	Standard name	Description
YPR125W	**YLH47 (MRS7)**	Mitochondrial inner membrane protein exposed to the mitochondrial matrix, associates with mitochondrial ribosomes, NOT required for respiratory growth; homolog of human Letm1, a protein implicated in Wolf-Hirschhorn syndrome
YGR149W	-	Uncharacterized, predicted to be an integral membrane protein
YMR102C	-	Protein of unknown function; transcription is activated by paralogous transcription factors Yrm1p and Yrr1p along with genes involved in multidrug resistance
YPL224C	MMT2	Putative metal transporter involved in mitochondrial iron accumulation; closely related to Mmt1p
YJR077C	MIR1	Mitochondrial phosphate carrier, imports inorganic phosphate into mitochondria; functionally redundant with Pic2p but more abundant than Pic2p under normal conditions; phosphorylated
YBR085W	AAC3	Mitochondrial inner membrane ADP/ATP translocator, exchanges cytosolic ADP for mitochondrially synthesized ATP; expressed under anaerobic conditions; similar to Pet9p and Aac1p; has roles in maintenance of viability and in respiration
YCL044C	MGR1	Subunit of the mitochondrial (mt) i-AAA protease supercomplex, which degrades misfolded mitochondrial proteins; forms a subcomplex with Mgr3p that binds to substrates to facilitate proteolysis; required for growth of cells lacking mtDNA
YCL009C	ILV6	Regulatory subunit of acetolactate synthase, which catalyzes the first step of branched-chain amino acid biosynthesis; enhances activity of the Ilv2p catalytic subunit, localizes to mitochondria
YNR008W	LRO1	Acyltransferase that catalyzes diacylglycerol esterification; one of several acyltransferases that contribute to triglyceride synthesis; putative homolog of human lecithin cholesterol acyltransferase
YEL030W	ECM10	Heat shock protein of the Hsp70 family, localized in mitochondrial nucleoids, plays a role in protein translocation, interacts with Mge1p in an ATP-dependent manner; overexpression induces extensive mitochondrial DNA aggregations
YLR056W	ERG3	C-5 sterol desaturase, catalyzes the introduction of a C-5(6) double bond into episterol, a precursor in ergosterol biosynthesis; mutants are viable, but cannot grow on non-fermentable carbon sources
YFR031C	RPL2A	Protein component of the large (60S) ribosomal subunit, identical to Rpl2Bp and has similarity to E. coli L2 and rat L8 ribosomal proteins
YBR191W	RPL21A	Protein component of the large (60S) ribosomal subunit, nearly identical to Rpl21Bp and has similarity to rat L21 ribosomal protein
YIL133C	RPL16A	N-terminally acetylated protein component of the large (60S) ribosomal subunit, binds to 5.8 S rRNA; has similarity to Rpl16Bp, E. coli L13 and rat L13a ribosomal proteins; transcriptionally regulated by Rap1p
YLR344W	RPL26A	Protein component of the large (60S) ribosomal subunit, nearly identical to Rpl26Bp and has similarity to E. coli L24 and rat L26 ribosomal proteins; binds to 5.8S rRNA
YOR063W	RPL3	Protein component of the large (60S) ribosomal subunit, has similarity to E. coli L3 and rat L3 ribosomal proteins
YNL178W	RPS3	Protein component of the small (40S) ribosomal subunit, has apurinic/apyrimidinic (AP) endonuclease activity; essential for viability; has similarity to E. coli S3 and rat S3 ribosomal proteins
YGR112W	SHY1	Mitochondrial inner membrane protein required for assembly of cytochrome c oxidase (complex IV); associates with complex IV assembly intermediates and complex III/complex IV supercomplexes; similar to human SURF1 involved in Leigh Syndrome

Two hitherto uncharacterized proteins were found. Ygr149wp was predicted to be an integral membrane protein (Kim, et al., 2003) and exhibits seven or eight transmembrane domains (predicted with the program TMHMM, http://www.cbs.dtu.dk/services/TMHMM/). The second protein Ymr102cp is implicated to play a role in multidrug resistance (Anderson, et al., 2003). It has no predicted transmembrane domains and no data about its subcellular localization is available. Several other mitochondrial transport proteins were identified by mass spectrometry, e.g. the putative metal transporter Mmt2p, the phosphate carrier Mir1p and the ADP/ATP translocator Aac3p. Also a relatively high number of proteins constituting cytosolic ribosomes were found.

4. Discussion

4.1. Functional studies on CorA/Mrs2p family proteins

4.1.1. Lpe10p is important for maintenance of the mitochondrial membrane potential and modulates the activity of the Mrs2p channel

Mrs2p forms the major Mg^{2+} uptake system in the inner mitochondrial membrane, with a remarkably high conductance of 155pS (Schindl, et al., 2007; Sponder, et al., 2010). This conductance is obtained in patch clamping experiments with giant lipid vesicles of *mrs2Δlpe10Δ*, overexpressing Mrs2p and therefore does not necessarily represents the natural situation in mitochondria. In comparison, the mammalian TRPM7 channel mediates Mg^{2+} uptake across the plasma membrane with a conductance of 40 pS (Monteilh-Zoller, et al., 2003; Nadler, et al., 2001).

Lpe10p exhibits 32% sequence identity with Mrs2p and it is also localized in the inner mitochondrial membrane. The growth defect caused by deletion of *LPE10* is similar to the one observed upon deletion of *MRS2*. In both deletion strains, splicing of mitochondrial group II introns is impaired and cells exhibit a pronounced growth reduction on non-fermentable carbon sources (Gregan, et al., 2001a). Deletion of *LPE10* furthermore results in weaker Mg^{2+} influx in mag-fura-2 measurements in isolated mitochondria (Sponder, et al., 2010).

These results characterize Mrs2p and Lpe10p as homologous proteins fulfilling similar functions. However, the two proteins cannot substitute for each other. Only high-copy expression of *MRS2* in the double deletion strain *mrs2Δlpe10Δ* restored growth of cells on non-fermentative media to some extent.

In our study we could demonstrate that the deletion of *LPE10* resulted in a 70% reduction of the mitochondrial membrane potential (ΔΨ) compared to wild-type levels, whereas *mrs2Δ* mitochondria do not show a loss of ΔΨ. Preincubation of isolated of *lpe10Δ* mitochondria with nigericin artificially restored the membrane potential to wild-type levels and restored Mg^{2+} influx in mag-fura-2 measurements. Furthermore, in patch clamping experiments Lpe10p alone did not yield a conductance for Mg^{2+} (Sponder, et al., 2010; Schindl, et al., 2007). This suggests an essential function of *LPE10* in maintenance of the mitochondrial membrane potential. The

reduced Mg^{2+} influx observed in mag-fura-2 measurements upon deletion of *LPE10* is therefore caused by the reduction of the membrane potential, the driving force for Mg^{2+} influx.

Still, Lpe10p is obviously also directly involved in the Mrs2p mediated Mg^{2+} transport into mitochondria since it was shown that Mrs2p and Lpe10p are able to form hetero-oligomers. Interestingly, coexpression of Lpe10p and Mrs2p reduced the Mrs2p channel conductance by ~ 70%. Besides of its impact on the membrane potential, Lpe10p appears to be also a structural as well as a modulating factor of the Mrs2p channel (Sponder, et al., 2010).

To get more insight into the bifunctional role of Lpe10p, we tried to identify which parts of the protein are responsible for Mg^{2+} transport or maintenance of the membrane potential, respectively.

Even conservative mutations in the universally conserved F/Y-G-M-N motif of the CorA/Mrs2p family are not tolerated and lead to a complete loss of Mg^{2+} transport activity (Szegedy and Maguire, 1999; Kolisek, et al., 2003). Replacing the F/Y-G-M-N motif of Lpe10p with A-S-S-V reduced growth of the cells on non fermentable carbon sources and almost completely abolished Mg^{2+} influx in mag-fura-2 measurements but had only a minor impact on the membrane potential (Sponder, et al., 2010). Given the high conservation of this motif the observed reduction in Mg^{2+} transport is not surprising. In the heteromeric Mrs2p/Lpe10p channel complex an intact G-M-N motif is required for Mg^{2+} transport activity. In contrast, this motif appears to be dispensable for maintenance of the membrane potential.

The creation of chimeric Mrs2p/Lpe10p proteins gave further indications which parts of Lpe10p are important for its role in maintaining the membrane potential. The fusion of the N-terminal domain of Lpe10p with the C-terminal part of Mrs2p, exhibited better growth complementation than the Mrs2p-Lpe10p fusion. Furthermore Lpe10p-Mrs2p restored $\Delta\Psi$ to 80% of the wild-type level, whereas Mrs2p-Lpe10p only slightly increased the membrane potential above the level of the double deletion strain *mrs2Δlpe10Δ*. Based on these findings, the N-terminal part of Lpe10p to the extent of α7 appears to be associated with Lpe10p's role in maintenance of the membrane potential.

The mechanism by which Lpe10p influences $\Delta\Psi$ is unknown. A possible explanation is that the high transport capacity of a homopentameric Mrs2p channel reduces the inside negative membrane potential by accumulating positively charged Mg^{2+} in the mitochondrial matrix. Hetero-oligomerization of Mrs2p and Lpe10p reduces the conductance of the channel. Consequently, the effect of Lpe10p on the membrane potential would be a secondary effect of the reduced activity of a Mrs2p/Lpe10p heteromeric channel. This hypothesis is not supported by our data. If Mg^{2+} transport via Mrs2p were in a scale influencing the membrane potential,

overexpression of Mrs2p should lead to a reduction of $\Delta\Psi$, which was not observed in our experiments. Overexpression of Mrs2p in mitochondria of *mrs2Δlpe10Δ* cells does not further decrease $\Delta\Psi$, in contrary; $\Delta\Psi$ is slightly increased compared to mitochondria of *mrs2Δlpe10Δ* cells (Sponder, et al., 2010).

There is no data available about a direct interaction of Lpe10p with other proteins except of Mrs2p. Nevertheless, it seems plausible that Lpe10p acts as a regulatory factor on other protein/proteins thereby influencing the mitochondrial membrane potential.

4.1.2. Gating mechanisms in CorA and Mrs2p

Two areas in the pentameric channel appear to be of central importance in the gating process. First, the five asparagines of the G-M-N motif seal the ion conduction pathway at the membrane-periplasm interface in the closed conformation (Lunin, et al., 2006; Eshaghi, et al., 2006; Payandeh and Pai, 2006).

The second control point is the MM stretch (residues Met291 to Met301. This region, and in particular bulky, hydrophobic leucine at position 294 and methionine at position 291 create a steric and electrostatic bottleneck for Mg^{2+} flux (Lunin, et al., 2006; Eshaghi, et al., 2006; Payandeh and Pai, 2006; Chakrabarti, et al., 2010; Payandeh, et al., 2008). Our mutational analysis of Leu294 of *T. maritima CorA* verified the importance of this amino acid in the gaiting process. Interestingly, in CorA the hydrophobic gate formed by Leu294 appears to be of such outstanding importance that mutations at this position led to a complete deregulation of ion transport. Substitution of Leu by Asp at this position resulted in slow, constant influx of Mg^{2+} in mag-fura-2 measurements. Small glycine residue at position 294 led to an even stronger, uncontrolled Mg^{2+} influx which eventually was lethal for the cells (Svidova, et al., 2010). Although several constrictions are present along the ion conduction pathway, which are supposed to play a role in gating of the channel, this hydrophobic gate seems to be essential for the complete closing of the CorA channel.

In contrast to that, the gating process of Mrs2p seems to be controlled at more than one site. Recently the crystal structure of the funnel domain including TM 1 of Mrs2p has been solved (Khan, et al., 2010). By superposition of the monomeric Mrs2p structure on the funnel domain of TmCorA and VpZntB, we could generate a model for the pentameric form of Mr2p. Based on this model of the N-terminal domain and TM 1, we identified Met309 and Val315 of Mrs2p as

being functionally equivalent to Met291 and Leu294 in CorA. Met309 is highly conserved throughout the Mrs2p family and according to our pentameric Mrs2p model, forms the narrowest constriction of the ion conduction pathway. Val315 forms the second narrowest constriction in the pore of Mrs2p. However, this position appears to be less conserved (Khan MB et al., manuscript in preparation).

Three different amino acids were introduced at these two positions (Met309 and Val315) in Mrs2p: negatively charged glutamic acid, bulky phenylalanine and small glycine. All substitutions of Met309 exhibited a strong growth reduction on non-fermentable carbon sources compared to cells expressing wild-type *MRS2*. Phe at position 309 narrowed the pore diameter and thereby reduced Mg^{2+} influx in mag-fura-2 measurements. The formation of a negatively charged ring by Glu increased Mg^{2+} uptake, possibly due to stronger electrostatic attraction of the ion. The strongest effect was observed in the Gly mutant, which exhibited very strong Mg^{2+} flux and incipient signs of deregulation of the closing process (Khan MB et al., manuscript in preparation). Nevertheless, closing of the ion conduction pathway was not completely deregulated as observed for mutations at position 294 in CorA. (Svidova, et al., 2010)

In line with the observed lower sequence conservation of Val315 in the Mrs2p family, all three amino acid substitutions at this position were relatively well tolerated. Again, introduction of small glycine had the strongest effect in growth tests on non fermentable carbon sources but led only to a moderate increase of Mg^{2+} uptake in mag-fura-2 measurements (Khan MB et al., manuscript in preparation).

Taken together, these findings suggest a higher degree of regulation of the Mrs2p channel in comparison to CorA. Mutations at only one of several positions putatively involved in gating do not abolish the ability of the channel to close the ion conduction pathway. The strong inside negative membrane potential of mitochondria represents a strong driving force for the positively charged Mg^{2+} ion. The homomeric Mrs2p channel exhibits a high conductance of 155 pS in patch clamping experiments (Sponder, et al., 2010). A stringent control of the transport activity at more than one site of the ion conduction pathway may therefore be essential to assure an adequate Mg^{2+} level in the mitochondrial matrix and thereby normal mitochondrial function.

4.1.3. The role of the G-M-N motif for Mg^{2+} transport and ion selectivity

The sequence G-M-N at the end of the first transmembrane helix is the only universally conserved motif in the large CorA/Mrs2p/Alr1p family (Knoop, et al., 2005). Mutational studies on *S. typhimurium* CorA showed that even conservative single point mutations are not tolerated (Szegedy and Maguire, 1999). However, sequences divergent from G-M-N (e.g. G-V-N and G-I-N) occur in nature but have been proposed to be involved in transport of ions different from Mg^{2+} (Knoop, et al., 2005). Based on the CorA crystal structure, different roles of this sequence for the function of the channel were proposed. In the closed conformation the Asn ring of G-M-N occludes the ion conduction pathway in *T. maritima* CorA (Lunin, et al., 2006). Furthermore, the G-M-N motif is supposed to be responsible for positioning of the short, periplasmatic loop (Lunin, et al., 2006; Moomaw and Maguire, 2010). This loop presumably is the initial site of interaction between the hydrated ion and the channel and is suggested to assist in the dehydration process as well as to be involved in cation selectivity (Lunin, et al., 2006; Moomaw and Maguire, 2010). The main-chain carbonyl groups of G-M-N are oriented towards the center of the pore entrance which allows an interaction with the hydrated ion and consequently these amino acids may play an important role in the dehydration process (Moomaw and Maguire, 2010).

The importance of this motif for the function of the channel was also confirmed for Mrs2p, mutation of G-M-N to A-M-N completely abolished Mg^{2+} transport activity (Kolisek, et al., 2003).

In our study we chose a different approach to get more insight into the role of this motif. We took advantage of the fact, that heterologous expression of *MRS2* complements the Mg^{2+}-dependent growth defect of *S. typhimurium* strain MM281, deficient for all major bacterial Mg^{2+} transport systems (CorA, MgtA and MgtB). We performed random mutagenesis of all three amino acids, which, in principle, allows all possible amino acid combinations at these positions and screened for mutants still able to transport Mg^{2+} (Svidova S. et al. manuscript in preparation). The advantage of investigating G-M-N mutants in a bacterial system is that besides of an altered transport activity also alterations in ion selectivity of the channel can be assessed directly.

Surprisingly, we found plenty of mutants still able to transport Mg^{2+} with sequences completely different to G-M-N. However, mutant variants of *MRS2* required higher expression levels to complement the growth defect of MM281 cells, indicating reduced Mg^{2+} transport compared to wild-type Mrs2p (Svidova S. et al. manuscript in preparation).

These findings show that the G-M-N motif can be replaced by several amino acid combinations, although is highly conserved. Moreover, the high divergence of functional sequences from the original G-M-N sequence is astonishing. A positively charged amino acid in the first position and a hydrophobic amino acid in the third position were frequently observed. The second position appeared to be relatively variable (Svidova S. et al. manuscript in preparation).

All tested mutants exhibited altered ion selectivity leading to a growth defect on plates supplemented with Mn^{2+} or Zn^{2+}. This effect may be caused by a blockage of the pore or transport of these ions leading to toxic effects (Svidova S. et al. manuscript in preparation). Patch clamping experiments are necessary to clarify, if these ions are transported by mutant Mrs2p variants.

The G-M-N motif therefore appears to act in concert with the periplasmatic loop in selecting and dehydrating the Mg^{2+} ion. The G-M-N motif is located at the end of the first transmembrane helix TM 1, directly at the membrane-periplasm/intermembrane space interface. This location at the mouth of the channel is an ideal site to control selectivity and dehydration of the incoming Mg^{2+} ion. Not the individual amino acids of this motif seem to be important but the structural properties generated collectively by these residues. This can be in part accomplished by amino acid combinations completely different from the original sequence, albeit with reduced selectivity. Thus, G-M-N appears to be the best combination nature found to ensure a high selectivity of the Mrs2p channel and concomitant high transport capacity.

4.1.4. The role of the Mrs2p C-terminus in Mg^{2+} transport

The Lpe10p-Mrs2p chimeric protein consists of the N-terminal part of Lpe10p and the C-terminal moiety of Mrs2p starting with the long α7 helix forming the funnel domain. The higher transport capacity of this fusion protein, compared to the Mrs2p-Lpe10p chimeric protein may be in part based on the fact that this fusion protein contains the pore of Mrs2p (Sponder, et al., 2010). However, also the exceptionally long C-terminus of Mrs2p seems to play an important role for the transport activity.

For CorA a role of the C-terminus in regulation of Mg^{2+} transport has been proposed. The helix forming TM 2 of CorA ends with the highly positively charged motif KKKKWL. Compared to Mrs2p, the C-terminus is extremely short, placing the motif directly at the membrane-cytosol interface. This high accumulation of positive charge in the form of 20 lysine residues in the pentamer has been termed basic sphincter. The basic sphincter, in combination with the

hydrophobic constrictions formed by Leu294 and Met291 appear to be the major barrier for Mg^{2+} transport in CorA (Lunin, et al., 2006; Eshaghi, et al., 2006; Payandeh and Pai, 2006). In contrast, TM 2 of Mrs2p end with two lysine residues, putatively resulting in a ring of only ten positively charged residues located directly at the membrane-matrix interface.

The C-terminus of Mrs2p also contains an arginine-rich motif (ARM) (Weghuber, et al., 2006). The end of TM 2 and the arginine-rich motif are separated by ~ 40 amino acids. A tertiary structure for the ~ 106 amino acid long C-terminus is not available. This makes predictions about the molecular function of this part of the protein difficult. Despite of its distance from TM 2, the arginine-rich motif of Mrs2p may be located near the membrane and would represent a potential candidate for a basic sphincter in Mrs2p. However, our data do not argue for a major role of this motif in regulation of the transport activity. Deletion of this motif (aa 400-414) resulted in weaker Mg^{2+} influx upon low copy expression. In contrast, high-copy expression of this mutant exhibited no growth defect on non-fermentable carbon sources and exhibited Mg^{2+} influx comparable to WT (Weghuber, et al., 2006).

However, deletion of a whole motif could result in major structural changes and a different orientation of the residual C-terminus in regard to the funnel domain. This renders the evaluation of the importance of this motif for Mg^{2+} transport difficult. In a subsequent study we reversed the charge of the KRRRK sequence of this motif (aa 402-406) by introducing negatively charged glutamic acid residues at these positions. This mutant exhibited normal growth on non-fermentable carbon sources and slightly elevated Mg^{2+} uptake rates in mag-fura-2 measurements. The observed higher transport capacity is likely due to the formation of a highly negatively charged ring surrounding the ion conduction pathway and consequently in a stronger electrostatic attraction of the Mg^{2+} ion. At the same time this mutation obviously had no dramatic effect on regulation of the channel (Khan MB et al., manuscript in preparation).

In contrast, deletion of almost the complete C-terminus (after Thr376) resulted in a growth defect on non-fermentable carbon sources, comparable to *mrs2Δ* cells. This is in accordance with the significantly reduced transport activity of this mutant observed in mag-fura-2 measurements (Khan MB et al., manuscript in preparation).

Besides of the arginine-rich motif, the whole C-terminus of Mrs2p exhibits a surplus of positively charged amino acid residues. (24 positively versus 5 negatively charged residues). The extensive deletion did not lead to an increased instability of the protein, in contrary, protein levels were slightly elevated. These findings suggest that, maybe not in particular the arginine-rich motif, but the overall positively charged C-terminus of Mrs2p plays an important role for transport activity/regulation of the channel. This is also in line with Mg^{2+} uptake measurements with the

two chimeric Mrs2p/Lpe10p proteins. The fusion protein Mrs2p-Lpe10p lacking the Mrs2p specific C-terminus exhibited weaker Mg^{2+} influx in mag-fura-2 measurements (Sponder, et al., 2010). Furthermore, the C-terminus may be also directly involved in structural changes regulating opening/closing of the pore, apart from providing a surplus of positive charge surrounding the ion conduction pathway. Consequently, deletion of the whole sequence may result in a reduced opening capability.

4.1.5. Divalent cation sensing sites in CorA and Mrs2p

Opening and closing of the CorA channel is likely to be controlled by a Mg^{2+} sensor located in the intracellular portion of the protein. As the intracellular Mg^{2+} concentration decreases, Mg^{2+} is released from the sensing site/sites leading to conformational changes and opening of the ion conduction pathway (Lunin, et al., 2006; Eshaghi, et al., 2006; Payandeh and Pai, 2006). Based on the crystal structure of *T. maritima* CorA, putative Mg^{2+} binding sites in the intracellular, funnel domain of the protein have been identified. A site termed M 1 is formed by residues Asp89 in helix α3 and Asp253 of the stalk helix and directly coordinates Mg^{2+}. M 1 is considered to be the primary regulatory sensing site (Lunin, et al., 2006; Eshaghi, et al., 2006; Payandeh and Pai, 2006; Maguire, 2006b). A second site (M 2) formed by residues Glu88, Asp175 and Asp179 seems to coordinate the ion indirectly via water molecules (Payandeh and Pai, 2006; Niegowski and Eshaghi, 2007). Results on the M 1 site obtained from a protease protection assay (Payandeh and Pai, 2006) and mutational analysis (Payandeh, et al., 2008) argue for an involvement of this sensing site in CorA function.

According to our structure based sequence analysis of CorA and Mrs2p, we identified Asp97 as being equivalent to Asp89 in *T. maritima* CorA. Asp89 from one monomer possibly coordinates the ion with Glu270 from the long α7 helix of another monomer (Khan, MB et al., manuscript in preparation). Furthermore, both amino acids are well conserved throughout the Mrs2p subfamily, which also argues for an involvement of these amino acids in the formation of a divalent cation sensing site. Thus, we exchanged negatively charged Asp97 to small alanine and to the bulky, hydrophobic amino acids tryptophan and phenylalanine.

Surprisingly, none of the mutations had an effect on growth of the cells on non-fermentable carbon sources or led to changes in Mg^{2+} uptake in isolated mitochondria compared to wild-type Mrs2p – an unexpected finding given the high conservation of these amino acids (Khan, MB et

al., manuscript in preparation). A possible explanation is that Mrs2p has like CorA two or even more Mg^{2+} binding sites and mutations in only one of these sites is not sufficient to impair the sensing ability of the Mrs2p channel. Alternatively, the chosen amino acids did not alter the conformation of this domain in the desired manner. Mutational analysis of this divalent cation sensing site in CorA also yielded unexpected results. Mutation of Asp89 by phenylalanine had no effect and substitution of Asp253 to phenylalanine had only a minor effect on the regulation of Mg^{2+} transport (Payandeh, et al., 2008). Further experiments will be necessary to clarify which amino acids are involved in sensing of the mitochondrial matrix Mg^{2+} concentration thereby controlling opening and closing of the channel.

4.2. Mitochondrial K^+/H^+ exchange in *S. cerevisiae*

4.2.1. The long search for the mitochondrial K^+/H^+ exchanger

Half a century ago, Peter Mitchell postulated the existence of cation/proton exchangers in the inner mitochondrial membrane (Mitchell, 1961). The high, inside negative membrane potential of mitochondria is essential for energy conversion by the ATP-synthase but at the same time, it turns mitochondria into infinite sinks for positively charged ions in particular for the most abundant ion, potassium (Garlid and Paucek, 2003). The existence of coupled K^+ and H^+ gradients across the inner mitochondrial membrane has been studied extensively in isolated mitochondria (for review see Bernardi, 1999 and Garlid and Paucek, 2003). Furthermore, reconstitution experiments with purified protein fractions in liposomes were shown to mediate K^+/H^+ exchange (Martin, et al., 1984). However the molecular identity of the protein/proteins constituting the antiporter remained unclear.

Recently, Mdm38p and Mrs7p of *S. cerevisiae* and their human homolog Letm1 have been identified as factors involved in mitochondrial K^+/H^+ homeostasis (Froschauer, et al., 2005; Nowikovsky, et al., 2007; McQuibban, et al., 2011). Deletion of *MDM38* causes a complete loss of K^+/H^+ exchange activity accompanied by a strongly reduced membrane potential, increased K^+-content and fragmentation of the mitochondrial network (Froschauer, et al., 2005; Nowikovsky, et al., 2007). Knock-down of LETM1 in human cells and in *Drosophila* exhibited

similar effects (Dimmer, et al., 2008; McQuibban, et al., 2011). Furthermore, deletion of *LETM1* seems to be the cause for seizures in Wolf-Hischhorn syndrome (Zollino, et al., 2003).

Mdm38p, Mrs7p and Letm1 have been implicated in different biological processes. For Mdm38p and Mrs7p a function in the translation and export of mitochondrially encoded proteins has previously been proposed (Frazier, et al., 2006). Recently, *LETM1* has been characterized as mitochondrial Ca^{2+}/H^+ exchanger (Jiang, et al., 2009). Typical exchangers contain six to twelve transmembrane domains (Wakabayashi, et al., 2000). In contrast, Mdm38p, Mrs7p and Letm1 have only one predicted transmembrane domain (Zotova, et al., 2010; Frazier, et al., 2006). This makes it rather unlikely that these proteins form an active exchanger by homo-oligomerization, although this cannot be fully excluded.

4.2.2. Identification of interaction partners of Mrs7p

Deletion of *MRS7* itself leads only to a weak growth reduction on non-fermentable carbon sources. Nevertheless, it is a strong suppressor of the *mdm38Δ* deletion phenotype when overexpressed (Nowikovsky, et al., 2004; Zotova, et al., 2010). For members of the Na^+/H^+ exchanger family it has previously been shown that these exchangers require essential cofactors for their activity (Pang, et al., 2001). We found that Mrs7p is able to dimerize and that the protein is part of a high molecular weight complex of ~ 500 kDa (Zotova, et al., 2010). Taken together, these facts led us to the hypothesis that Mrs7p may be a regulatory factor of the mitochondrial K^+/H^+ exchanger. Identification of the molecular composition of this complex therefore represents a promising approach to identify other regulatory proteins involved in K^+/H^+ exchange or the exchanger itself.

We employed different affinity chromatography approaches to purify the Mrs7p containing high molecular weight complex. Various tags were tested for their applicability to isolate the intact high molecular weight complex of ~ 500 kDa. The relatively low expression level of Mrs7p made it difficult to obtain sufficient protein amounts for reliable analysis by mass spectrometry. Best results were obtained with a two-step purification protocol via the 6xHis- and the Strep-tag. An analysis of the complete complex by mass spectrometry after Blue native electrophoresis could not be achieved. Elution fractions of the affinity purifications were therefore analyzed on denaturing SDS-PAA gels.

Mass spectrometry analysis of proteins co-purified with Mrs7p-6xHis-Strep yielded the candidate protein Ygr149wp. In a recent study applying theoretical topology prediction combined with C-terminal reporter fusions, Ygr149wp was characterized as a membrane protein with eight transmembrane domains with a N_{in}-C_{in} topology. However, results from the reporter assay suggest a localization of the C-terminus in the cytosol which would exclude localization in the inner mitochondrial membrane (Kim, et al., 2003).

No experimental data on the subcellular localization of Ymr102cp, the second uncharacterized protein identified by mass spectrometry, are available. Prediction of a mitochondrial targeting sequence (using Mitoprot II, http://ihg.gsf.de/ihg/mitoprot.html) for Ymr102cp, yielded only a very low probability of export to mitochondria of 3.66%. Consequently, Ygr149wp and Ymr102cp do not appear to be ideal candidates for constituting the K^+/H^+ exchanger or to act as regulatory factor thereof.

Interestingly, several proteins constituting cytosolic ribosomes but no mitochondrial ribosomal protein was identified by mass spectrometry. This is at variance with results obtained by Frazier et al. who reported a strong interaction of Mdm38p and Mrs7p with mitochondrial ribosomes (Frazier, et al., 2006). The high number of cytosolic ribosomal proteins identified in our approach may represent contaminations. Crude mitochondrial extracts were used for solubilization and affinity purifications. Under the mild purification conditions used to prevent dissociation of the complex, a co-purification of Mrs7p with high abundant proteins seems to be plausible.

The signal strength of protein bands containing possible interaction partners of Mrs7p were significantly weaker compared to the band for the bait Mrs7p (Figure 22). This allows two possible explanations. First, the high molecular weight complex is mainly composed of Mrs7p. Second, a significant fraction of the interaction partners is lost during the purification process. As discussed in the results section, an estimation of the relative amounts of the Mrs7p dimer and high molecular weight complexes in Western Blots is difficult. Although the presence of the Mrs7p containing high molecular weight complexes after affinity chromatography was demonstrated, Mrs7p was also found in a dimeric form. A Mrs7p dimer could not be observed when mitochondrial were only solubilized and directly applied on a Blue native gel (Figure 11). This suggests that, although very mild conditions were used in affinity chromatography, the complex dissociates during this process to a certain degree, which impairs the identification of interacting proteins.

It is known, that certain membrane proteins do not stain well with Coomassie (Ladner, et al., 2004). It can therefore not be ruled out, that the K^+/H^+ exchanger was co-purified with Mrs7p but

was not visualized under our conditions. Furthermore, the identification of hydrophobic membrane proteins by standard MALDI-TOF (matrix-assisted laser desorption/ionization-time of flight) and PMF (peptide mass fingerprinting) is often difficult (Zischka, et al., 2004). Consequently, it cannot be excluded that one of the analyzed bands contained the protein encoding the K^+/H^+ exchanger but identification by mass spectrometry failed due to the low amounts of peptides generated and the resulting insufficient signal intensity.

Further experiments with different protein staining methods and improved mass spectrometric analyses are necessary to rule out that some of the co-purified proteins were not visualized or not detected.

5. References

Anderson, J. B., Sirjusingh, C., Parsons, A. B., Boone, C., Wickens, C., Cowen, L. E. and Kohn, L. M. (2003). Mode of selection and experimental evolution of antifungal drug resistance in Saccharomyces cerevisiae. *Genetics* **163,** 1287-98.

Azzi, A., Casey, R. P. and Nalecz, M. J. (1984). The effect of N,N'-dicyclohexylcarbodiimide on enzymes of bioenergetic relevance. *Biochim Biophys Acta* **768,** 209-26.

Azzone, G. F., Massair, S. and Pozzan, T. (1976). Mechanism of active shrinkage in mitochondria. II. Coupling between strong electrolyte fluxes. *Biochim Biophys Acta* **423,** 27-41.

Azzone, G. F. and Massari, S. (1971). Thermodynamic and kinetic aspects of the interconversion of chemical and osmotic energies in mitochondria. *Eur J Biochem* **19,** 97-107.

Bauerschmitt, H., Mick, D. U., Deckers, M., Vollmer, C., Funes, S., Kehrein, K., Ott, M., Rehling, P. and Herrmann, J. M. (2010). Ribosome-binding proteins Mdm38 and Mba1 display overlapping functions for regulation of mitochondrial translation. *Mol Biol Cell* **21,** 1937-44.

Baumann, F., Neupert, W. and Herrmann, J. M. (2002). Insertion of bitopic membrane proteins into the inner membrane of mitochondria involves an export step from the matrix. *J Biol Chem* **277,** 21405-13.

Beavis, A. D. and Garlid, K. D. (1990). Evidence for the allosteric regulation of the mitochondrial K+/H+ antiporter by matrix protons. *J Biol Chem* **265,** 2538-45.

Beeler, T., Bruce, K. and Dunn, T. (1997). Regulation of cellular Mg2+ by Saccharomyces cerevisiae. *Biochim Biophys Acta* **1323,** 310-8.

Bernardi, P. (1999). Mitochondrial transport of cations: channels, exchangers, and permeability transition. *Physiol Rev* **79,** 1127-55.

Bernardi, P., Angrilli, A., Ambrosin, V. and Azzone, G. F. (1989). Activation of latent K+ uniport in mitochondria treated with the ionophore A23187. *J Biol Chem* **264,** 18902-6.

Bernardi, P. and Azzone, G. F. (1983). Electroneutral H+-K+ exchange in liver mitochondria. Regulation by membrane potential. *Biochim Biophys Acta* **724,** 212-23.

Blondin, G. A., Vail, W. J. and Green, D. E. (1969). The mechanism of mitochondrial swelling. II. Pseudoenergized swelling in the presence of alkali metal salts. *Arch Biochem Biophys* **129,** 158-72.

Brett, C. L., Tukaye, D. N., Mukherjee, S. and Rao, R. (2005). The yeast endosomal Na+K+/H+ exchanger Nhx1 regulates cellular pH to control vesicle trafficking. *Mol Biol Cell* **16,** 1396-405.

Brierley, G. P., Baysal, K. and Jung, D. W. (1994). Cation transport systems in mitochondria: Na+ and K+ uniports and exchangers. *J Bioenerg Biomembr* **26,** 519-26.

Brierley, G. P. and Jung, D. W. (1988). K+/H+ antiport in mitochondria. *J Bioenerg Biomembr* **20,** 193-209.

Brierley, G. P., Jurkowitz, M. S., Farooqui, T. and Jung, D. W. (1984). K+/H+ antiport in heart mitochondria. *J Biol Chem* **259,** 14672-8.

Brunet, S., Scheuer, T., Klevit, R. and Catterall, W. A. (2005). Modulation of CaV1.2 channels by Mg2+ acting at an EF-hand motif in the COOH-terminal domain. *J Gen Physiol* **126,** 311-23.

Bui, D. M., Gregan, J., Jarosch, E., Ragnini, A. and Schweyen, R. J. (1999). The bacterial magnesium transporter CorA can functionally substitute for its putative homologue Mrs2p in the yeast inner mitochondrial membrane. *J Biol Chem* **274,** 20438-43.

Chakrabarti, N., Neale, C., Payandeh, J., Pai, E. F. and Pomes, R. (2010) An iris-like mechanism of pore dilation in the CorA magnesium transport system. *Biophys J* **98,** 784-92.

Chappell, J. B. (1968). Systems used for the transport of substrates into mitochondria. *Br Med Bull* **24,** 150-7.

Cockrell, R. S. (1973). Energy-linked ion translocation in submitochondrial particles. 3. Transport of monovalent cations by submitochondrial particles. *J Biol Chem* **248,** 6828-33.

de Valk, H. W. (1999). Magnesium in diabetes mellitus. *Neth J Med* **54,** 139-46.

Dimmer, K. S., Fritz, S., Fuchs, F., Messerschmitt, M., Weinbach, N., Neupert, W. and Westermann, B. (2002). Genetic basis of mitochondrial function and morphology in Saccharomyces cerevisiae. *Mol Biol Cell* **13,** 847-53.

Dimmer, K. S., Navoni, F., Casarin, A., Trevisson, E., Endele, S., Winterpacht, A., Salviati, L. and Scorrano, L. (2008). LETM1, deleted in Wolf-Hirschhorn syndrome is required for normal mitochondrial morphology and cellular viability. *Hum Mol Genet* **17,** 201-14.

DiResta, D. J., Kutschke, K. P., Hottois, M. D. and Garlid, K. D. (1986). K^+-H^+ exchange and volume homeostasis in brown adipose tissue mitochondria. *Am J Physiol* **251,** R787-93.

Dordick, R. S., Brierley, G. P. and Garlid, K. D. (1980). On the mechanism of A23187-induced potassium efflux in rat liver mitochondria. *J Biol Chem* **255,** 10299-305.

Douglas, M. G. and Cockrell, R. S. (1974). Mitochondrial cation-hydrogen ion exchange. Sodium selective transport by mitochondria and submitochondrial particles. *J Biol Chem* **249,** 5464-71.

Duszynski, J. and Wojtczak, L. (1977). Effect of Mg^{2+} depletion of mitochondria on their permeability to K^+: the mechanism by which ionophore A23187 increases K^+ permeability. *Biochem Biophys Res Commun* **74,** 417-24.

Endele, S., Fuhry, M., Pak, S. J., Zabel, B. U. and Winterpacht, A. (1999). LETM1, a novel gene encoding a putative EF-hand Ca(2+)-binding protein, flanks the Wolf-Hirschhorn syndrome (WHS) critical region and is deleted in most WHS patients. *Genomics* **60,** 218-25.

Eshaghi, S., Niegowski, D., Kohl, A., Martinez Molina, D., Lesley, S. A. and Nordlund, P. (2006). Crystal structure of a divalent metal ion transporter CorA at 2.9 angstrom resolution. *Science* **313,** 354-7.

Frazier, A. E., Taylor, R. D., Mick, D. U., Warscheid, B., Stoepel, N., Meyer, H. E., Ryan, M. T., Guiard, B. and Rehling, P. (2006). Mdm38 interacts with ribosomes and is a component of the mitochondrial protein export machinery. *J Cell Biol* **172,** 553-64.

Froschauer, E., Nowikovsky, K. and Schweyen, R. J. (2005). Electroneutral K^+/H^+ exchange in mitochondrial membrane vesicles involves Yol027/Letm1 proteins. *Biochim Biophys Acta* **1711,** 41-8.

Garcia Vescovi, E., Soncini, F. C. and Groisman, E. A. (1996). Mg^{2+} as an extracellular signal: environmental regulation of Salmonella virulence. *Cell* **84,** 165-74.

Garfinkel, D. and Garfinkel, L. (1988). Magnesium and regulation of carbohydrate metabolism at the molecular level. *Magnesium* **7,** 249-61.

Garlid, K. D. (1978). Unmasking the mitochondrial K/H exchanger: swelling-induced K^+-loss. *Biochem Biophys Res Commun* **83,** 1450-5.

Garlid, K. D. (1979). Unmasking the mitochondrial K/H exchanger: tetraethylammonium-induced K^+-loss. *Biochem Biophys Res Commun* **87,** 842-7.

Garlid, K. D. (1980). On the mechanism of regulation of the mitochondrial K^+/H^+ exchanger. *J Biol Chem* **255,** 11273-9.

Garlid, K. D., DiResta, D. J., Beavis, A. D. and Martin, W. H. (1986). On the mechanism by which dicyclohexylcarbodiimide and quinine inhibit K+ transport in rat liver mitochondria. *J Biol Chem* **261,** 1529-35.

Garlid, K. D. and Paucek, P. (2003). Mitochondrial potassium transport: the K(+) cycle. *Biochim Biophys Acta* **1606,** 23-41.

Garlid, K. D., Shariat-Madar, Z., Nath, S. and Jezek, P. (1991). Reconstitution and partial purification of the Na(+)-selective Na+/H+ antiporter of beef heart mitochondria. *J Biol Chem* **266,** 6518-23.

Goytain, A. and Quamme, G. A. (2005a). Functional characterization of human SLC41A1, a Mg2+ transporter with similarity to prokaryotic MgtE Mg2+ transporters. *Physiol Genomics* **21,** 337-42.

Goytain, A. and Quamme, G. A. (2005b). Functional characterization of the mouse [corrected] solute carrier, SLC41A2. *Biochem Biophys Res Commun* **330,** 701-5.

Graschopf, A., Stadler, J. A., Hoellerer, M. K., Eder, S., Sieghardt, M., Kohlwein, S. D. and Schweyen, R. J. (2001). The yeast plasma membrane protein Alr1 controls Mg2+ homeostasis and is subject to Mg2+-dependent control of its synthesis and degradation. *J Biol Chem* **276,** 16216-22.

Gregan, J., Bui, D. M., Pillich, R., Fink, M., Zsurka, G. and Schweyen, R. J. (2001a). The mitochondrial inner membrane protein Lpe10p, a homologue of Mrs2p, is essential for magnesium homeostasis and group II intron splicing in yeast. *Mol Gen Genet* **264,** 773-81.

Gregan, J., Kolisek, M. and Schweyen, R. J. (2001b). Mitochondrial Mg(2+) homeostasis is critical for group II intron splicing in vivo. *Genes Dev* **15,** 2229-37.

Groisman, E. A. (2001). The pleiotropic two-component regulatory system PhoP-PhoQ. *J Bacteriol* **183,** 1835-42.

Hattori, M., Iwase, N., Furuya, N., Tanaka, Y., Tsukazaki, T., Ishitani, R., Maguire, M. E., Ito, K., Maturana, A. and Nureki, O. (2009). Mg(2+)-dependent gating of bacterial MgtE channel underlies Mg(2+) homeostasis. *Embo J* **28,** 3602-12.

Hattori, M., Tanaka, Y., Fukai, S., Ishitani, R. and Nureki, O. (2007). Crystal structure of the MgtE Mg2+ transporter. *Nature* **448,** 1072-5.

Hmiel, S. P., Snavely, M. D., Florer, J. B., Maguire, M. E. and Miller, C. G. (1989). Magnesium transport in Salmonella typhimurium: genetic characterization and cloning of three magnesium transport loci. *J Bacteriol* **171,** 4742-51.

Hmiel, S. P., Snavely, M. D., Miller, C. G. and Maguire, M. E. (1986). Magnesium transport in Salmonella typhimurium: characterization of magnesium influx and cloning of a transport gene. *J Bacteriol* **168,** 1444-50.

Hu, J., Sharma, M., Qin, H., Gao, F. P. and Cross, T. A. (2009). Ligand binding in the conserved interhelical loop of CorA, a magnesium transporter from Mycobacterium tuberculosis. *J Biol Chem* **284,** 15619-28.

Humphries, S., Kushner, H. and Falkner, B. (1999). Low dietary magnesium is associated with insulin resistance in a sample of young, nondiabetic Black Americans. *Am J Hypertens* **12,** 747-56.

Jiang, D., Zhao, L. and Clapham, D. E. (2009). Genome-wide RNAi screen identifies Letm1 as a mitochondrial Ca2+/H+ antiporter. *Science* **326,** 144-7.

Johnson, V. P., Mulder, R. D. and Hosen, R. (1976). The Wolf-Hirschhorn (4p-) syndrome. *Clin Genet* **10,** 104-12.

Jung, D. W. and Brierley, G. P. (1999). Matrix free Mg(2+) and the regulation of mitochondrial volume. *Am J Physiol* **277,** C1194-201.

Jung, D. W., Farooqui, T., Utz, E. and Brierley, G. P. (1984). Effects of quinine on K+ transport in heart mitochondria. *J Bioenerg Biomembr* **16,** 379-90.

Jung, D. W., Panzeter, E., Baysal, K. and Brierley, G. P. (1997). On the relationship between matrix free Mg2+ concentration and total Mg2+ in heart mitochondria. *Biochim Biophys Acta* **1320,** 310-20.

Junttila, M. R., Saarinen, S., Schmidt, T., Kast, J. and Westermarck, J. (2005). Single-step Strep-tag purification for the isolation and identification of protein complexes from mammalian cells. *Proteomics* **5,** 1199-203.

Kakar, S. S., Mahdi, F., Li, X. Q. and Garlid, K. D. (1989). Reconstitution of the mitochondrial non-selective Na+/H+ (K+/H+) antiporter into proteoliposomes. *J Biol Chem* **264,** 5846-51.

Kao, W. H., Folsom, A. R., Nieto, F. J., Mo, J. P., Watson, R. L. and Brancati, F. L. (1999). Serum and dietary magnesium and the risk for type 2 diabetes mellitus: the Atherosclerosis Risk in Communities Study. *Arch Intern Med* **159,** 2151-9.

Kapus, A., Lukacs, G. L., Cragoe, E. J., Jr., Ligeti, E. and Fonyo, A. (1988). Characterization of the mitochondrial Na+-H+ exchange. The effect of amiloride analogues. *Biochim Biophys Acta* **944,** 383-90.

Kehres, D. G., Lawyer, C. H. and Maguire, M. E. (1998). The CorA magnesium transporter gene family. *Microb Comp Genomics* **3,** 151-69.

Khan, M. B., Sjoblom, B., Schweyen, R. J. and Djinovic-Carugo, K. (2010). Crystallization and preliminary X-ray diffraction analysis of the N-terminal domain of Mrs2, a magnesium ion transporter from yeast inner mitochondrial membrane. *Acta Crystallogr Sect F Struct Biol Cryst Commun* **66,** 658-61.

Kim, H., Melen, K. and von Heijne, G. (2003). Topology models for 37 Saccharomyces cerevisiae membrane proteins based on C-terminal reporter fusions and predictions. *J Biol Chem* **278,** 10208-13.

Knoop, V., Groth-Malonek, M., Gebert, M., Eifler, K. and Weyand, K. (2005). Transport of magnesium and other divalent cations: evolution of the 2-TM-GxN proteins in the MIT superfamily. *Mol Genet Genomics* **274,** 205-16.

Kolisek, M., Launay, P., Beck, A., Sponder, G., Serafini, N., Brenkus, M., Froschauer, E. M., Martens, H., Fleig, A. and Schweigel, M. (2008). SLC41A1 is a novel mammalian Mg2+ carrier. *J Biol Chem* **283,** 16235-47.

Kolisek, M., Zsurka, G., Samaj, J., Weghuber, J., Schweyen, R. J. and Schweigel, M. (2003). Mrs2p is an essential component of the major electrophoretic Mg2+ influx system in mitochondria. *Embo J* **22,** 1235-44.

Koll, H., Schmidt, C., Wiesenberger, G. and Schmelzer, C. (1987). Three nuclear genes suppress a yeast mitochondrial splice defect when present in high copy number. *Curr Genet* **12,** 503-9.

Kucharski, L. M., Lubbe, W. J. and Maguire, M. E. (2000). Cation hexaammines are selective and potent inhibitors of the CorA magnesium transport system. *J Biol Chem* **275,** 16767-73.

Ladner, C. L., Yang, J., Turner, R. J. and Edwards, R. A. (2004). Visible fluorescent detection of proteins in polyacrylamide gels without staining. *Anal Biochem* **326,** 13-20.

Li, X. Q., Hegazy, M. G., Mahdi, F., Jezek, P., Lane, R. D. and Garlid, K. D. (1990). Purification of a reconstitutively active K+/H+ antiporter from rat liver mitochondria. *J Biol Chem* **265,** 15316-22.

Lichty, J. J., Malecki, J. L., Agnew, H. D., Michelson-Horowitz, D. J. and Tan, S. (2005). Comparison of affinity tags for protein purification. *Protein Expr Purif* **41,** 98-105.

Lunin, V. V., Dobrovetsky, E., Khutoreskaya, G., Zhang, R., Joachimiak, A., Doyle, D. A., Bochkarev, A., Maguire, M. E., Edwards, A. M. and Koth, C. M. (2006). Crystal structure of the CorA Mg2+ transporter. *Nature* **440,** 833-7.

MacDiarmid, C. W. and Gardner, R. C. (1998). Overexpression of the Saccharomyces cerevisiae magnesium transport system confers resistance to aluminum ion. *J Biol Chem* **273,** 1727-32.

Maguire, M. E. (2006a). Magnesium transporters: properties, regulation and structure. *Front Biosci* **11,** 3149-63.

Maguire, M. E. (2006b). The structure of CorA: a Mg(2+)-selective channel. *Curr Opin Struct Biol* **16,** 432-8.

Maguire, M. E. and Cowan, J. A. (2002). Magnesium chemistry and biochemistry. *Biometals* **15,** 203-10.

Martin, W. H., Beavis, A. D. and Garlid, K. D. (1984). Identification of an 82,000-dalton protein responsible for K+/H+ antiport in rat liver mitochondria. *J Biol Chem* **259,** 2062-5.

Martin, W. H., DiResta, D. J. and Garlid, K. D. (1986). Kinetics of inhibition and binding of dicyclohexylcarbodiimide to the 82,000-dalton mitochondrial K+/H+ antiporter. *J Biol Chem* **261,** 12300-5.

McCarthy, T. J., Plog, M. A., Floy, S. A., Jansen, J. A., Soukup, J. K. and Soukup, G. A. (2005). Ligand requirements for glmS ribozyme self-cleavage. *Chem Biol* **12,** 1221-6.

McQuibban, A. G., Joza, N., Megighian, A., Scorzeto, M., Zanini, D., Reipert, S., Richter, C., Schweyen, R. J. and Nowikovsky, K. (2010). A Drosophila mutant of LETM1, a candidate gene for seizures in Wolf-Hirschhorn syndrome. *Hum Mol Genet* **19,** 987-1000.

Menze, M. A., Hutchinson, K., Laborde, S. M. and Hand, S. C. (2005). Mitochondrial permeability transition in the crustacean Artemia franciscana: absence of a calcium-regulated pore in the face of profound calcium storage. *Am J Physiol Regul Integr Comp Physiol* **289,** R68-76.

Mitchell, P. (1961). Coupling of phosphorylation to electron and hydrogen transfer by a chemi-osmotic type of mechanism. *Nature* **191,** 144-8.

Mitchell, P. (1966). Chemiosmotic coupling in oxidative and photosynthetic phosphorylation. *Biol Rev Camb Philos Soc* **41,** 445-502.

Mitchell, P. and Moyle, J. (1969). Translocation of some anions cations and acids in rat liver mitochondria. *Eur J Biochem* **9,** 149-55.

Monteilh-Zoller, M. K., Hermosura, M. C., Nadler, M. J., Scharenberg, A. M., Penner, R. and Fleig, A. (2003). TRPM7 provides an ion channel mechanism for cellular entry of trace metal ions. *J Gen Physiol* **121,** 49-60.

Moomaw, A. S. and Maguire, M. E. (2010). Cation selectivity by the CorA Mg2+ channel requires a fully hydrated cation. *Biochemistry* **49,** 5998-6008.

Murphy, E. (2000). Mysteries of magnesium homeostasis. *Circ Res* **86,** 245-8.

Nadler, M. J., Hermosura, M. C., Inabe, K., Perraud, A. L., Zhu, Q., Stokes, A. J., Kurosaki, T., Kinet, J. P., Penner, R., Scharenberg, A. M. and Fleig, A. (2001). LTRPC7 is a Mg.ATP-regulated divalent cation channel required for cell viability. *Nature* **411,** 590-5.

Nakashima, R. A., Dordick, R. S. and Garlid, K. D. (1982). On the relative roles of Ca2+ and Mg2+ in regulating the endogenous K+/H+ exchanger of rat liver mitochondria. *J Biol Chem* **257,** 12540-5.

Nakashima, R. A. and Garlid, K. D. (1982). Quinine inhibition of Na+ and K+ transport provides evidence for two cation/H+ exchangers in rat liver mitochondria. *J Biol Chem* **257,** 9252-4.

Nass, R. and Rao, R. (1999). The yeast endosomal Na+/H+ exchanger, Nhx1, confers osmotolerance following acute hypertonic shock. *Microbiology* **145 (Pt 11),** 3221-8.

Niegowski, D. and Eshaghi, S. (2007). The CorA family: structure and function revisited. *Cell Mol Life Sci* **64,** 2564-74.

Nowikovsky, K., Froschauer, E. M., Zsurka, G., Samaj, J., Reipert, S., Kolisek, M., Wiesenberger, G. and Schweyen, R. J. (2004). The LETM1/YOL027 gene family encodes a factor of the mitochondrial K+ homeostasis with a potential role in the Wolf-Hirschhorn syndrome. *J Biol Chem* **279,** 30307-15.

Nowikovsky, K., Reipert, S., Devenish, R. J. and Schweyen, R. J. (2007). Mdm38 protein depletion causes loss of mitochondrial K+/H+ exchange activity, osmotic swelling and mitophagy. *Cell Death Differ* **14,** 1647-56.

Numata, M., Petrecca, K., Lake, N. and Orlowski, J. (1998). Identification of a mitochondrial Na+/H+ exchanger. *J Biol Chem* **273,** 6951-9.

Pang, T., Su, X., Wakabayashi, S. and Shigekawa, M. (2001). Calcineurin homologous protein as an essential cofactor for Na+/H+ exchangers. *J Biol Chem* **276,** 17367-72.

Payandeh, J., Li, C., Ramjeesingh, M., Poduch, E., Bear, C. E. and Pai, E. F. (2008). Probing structure-function relationships and gating mechanisms in the CorA Mg2+ transport system. *J Biol Chem* **283,** 11721-33.

Payandeh, J. and Pai, E. F. (2006). A structural basis for Mg2+ homeostasis and the CorA translocation cycle. *Embo J* **25,** 3762-73.

Pfeiffer, D. R. and Lardy, H. A. (1976). Ionophore A23187: the effect of H+ concentration on complex formation with divalent and monovalent cations and the demonstration of K+ transport in mitochondria mediated by A23187. *Biochemistry* **15,** 935-43.

Priault, M., Salin, B., Schaeffer, J., Vallette, F. M., di Rago, J. P. and Martinou, J. C. (2005). Impairing the bioenergetic status and the biogenesis of mitochondria triggers mitophagy in yeast. *Cell Death Differ* **12,** 1613-21.

Puig, O., Caspary, F., Rigaut, G., Rutz, B., Bouveret, E., Bragado-Nilsson, E., Wilm, M. and Seraphin, B. (2001). The tandem affinity purification (TAP) method: a general procedure of protein complex purification. *Methods* **24,** 218-29.

Qiu, Q. S. and Fratti, R. A. (2010) The Na+/H+ exchanger Nhx1p regulates the initiation of Saccharomyces cerevisiae vacuole fusion. *J Cell Sci* **123,** 3266-75.

Robinson, H. and Wang, A. H. (1996). Neomycin, spermine and hexaamminecobalt (III) share common structural motifs in converting B- to A-DNA. *Nucleic Acids Res* **24,** 676-82.

Romani, A. (2007). Regulation of magnesium homeostasis and transport in mammalian cells. *Arch Biochem Biophys* **458,** 90-102.

Romani, A. and Scarpa, A. (1992). Regulation of cell magnesium. *Arch Biochem Biophys* **298,** 1-12.

Rosen, B. P. and Futai, M. (1980). Sodium/proton antiporter of rat liver mitochondria. *FEBS Lett* **117,** 39-43.

Schindl, R., Weghuber, J., Romanin, C. and Schweyen, R. J. (2007). Mrs2p forms a high conductance Mg2+ selective channel in mitochondria. *Biophys J* **93,** 3872-83.

Schmidt, U., Maue, I., Lehmann, K., Belcher, S. M., Stahl, U. and Perlman, P. S. (1998). Mutant alleles of the MRS2 gene of yeast nuclear DNA suppress mutations in the catalytic core of a mitochondrial group II intron. *J Mol Biol* **282,** 525-41.

Shi, G. Y., Jung, D. W., Garlid, K. D. and Brierley, G. P. (1980). Induction of respiration-dependent net efflux of K+ from heart mitochondria by depletion of endogenous divalent cations. *J Biol Chem* **255,** 10306-11.

Smith, R. L., Banks, J. L., Snavely, M. D. and Maguire, M. E. (1993). Sequence and topology of the CorA magnesium transport systems of Salmonella typhimurium and Escherichia coli. Identification of a new class of transport protein. *J Biol Chem* **268,** 14071-80.

Smith, R. L., Kaczmarek, M. T., Kucharski, L. M. and Maguire, M. E. (1998). Magnesium transport in Salmonella typhimurium: regulation of mgtA and mgtCB during invasion of epithelial and macrophage cells. *Microbiology* **144 (Pt 7),** 1835-43.

Smith, R. L. and Maguire, M. E. (1998). Microbial magnesium transport: unusual transporters searching for identity. *Mol Microbiol* **28,** 217-26.

Smith, R. L., Thompson, L. J. and Maguire, M. E. (1995). Cloning and characterization of MgtE, a putative new class of Mg2+ transporter from Bacillus firmus OF4. *J Bacteriol* **177,** 1233-8.

Snavely, M. D., Florer, J. B., Miller, C. G. and Maguire, M. E. (1989). Magnesium transport in Salmonella typhimurium: 28Mg2+ transport by the CorA, MgtA, and MgtB systems. *J Bacteriol* **171,** 4761-6.

Sponder, G., Svidova, S., Schindl, R., Wieser, S., Schweyen, R. J., Romanin, C., Froschauer, E. M. and Weghuber, J. (2010). Lpe10p modulates the activity of the Mrs2p-based yeast mitochondrial Mg2+ channel. *Febs J* **277,** 3514-25.

Svidova, S., Sponder, G., Schweyen, R. J. and Djinovic-Carugo, K. (2010). Functional analysis of the conserved hydrophobic gate region of the magnesium transporter CorA. *Biochim Biophys Acta*.

Szegedy, M. A. and Maguire, M. E. (1999). The CorA Mg(2+) transport protein of Salmonella typhimurium. Mutagenesis of conserved residues in the second membrane domain. *J Biol Chem* **274,** 36973-9.

Tao, T., Snavely, M. D., Farr, S. G. and Maguire, M. E. (1995). Magnesium transport in Salmonella typhimurium: mgtA encodes a P-type ATPase and is regulated by Mg2+ in a manner similar to that of the mgtB P-type ATPase. *J Bacteriol* **177,** 2654-62.

Townsend, D. E., Esenwine, A. J., George, J., 3rd, Bross, D., Maguire, M. E. and Smith, R. L. (1995). Cloning of the mgtE Mg2+ transporter from Providencia stuartii and the distribution of mgtE in gram-negative and gram-positive bacteria. *J Bacteriol* **177,** 5350-4.

Wabakken, T., Rian, E., Kveine, M. and Aasheim, H. C. (2003). The human solute carrier SLC41A1 belongs to a novel eukaryotic subfamily with homology to prokaryotic MgtE Mg2+ transporters. *Biochem Biophys Res Commun* **306,** 718-24.

Wachek, M., Aichinger, M. C., Stadler, J. A., Schweyen, R. J. and Graschopf, A. (2006). Oligomerization of the Mg2+-transport proteins Alr1p and Alr2p in yeast plasma membrane. *Febs J* **273,** 4236-49.

Wakabayashi, S., Pang, T., Su, X. and Shigekawa, M. (2000). A novel topology model of the human Na(+)/H(+) exchanger isoform 1. *J Biol Chem* **275,** 7942-9.

Waldherr, M., Ragnini, A., Jank, B., Teply, R., Wiesenberger, G. and Schweyen, R. J. (1993). A multitude of suppressors of group II intron-splicing defects in yeast. *Curr Genet* **24,** 301-6.

Weghuber, J., Dieterich, F., Froschauer, E. M., Svidova, S. and Schweyen, R. J. (2006). Mutational analysis of functional domains in Mrs2p, the mitochondrial Mg2+ channel protein of Saccharomyces cerevisiae. *Febs J* **273,** 1198-209.

Welihinda, A. A., Trumbly, R. J., Garlid, K. D. and Beavis, A. D. (1993). On the regulation of Na+/H+ and K+/H+ antiport in yeast mitochondria: evidence for the absence of an Na(+)-selective Na+/H+ antiporter. *Biochim Biophys Acta* **1144,** 367-73.

Wiesenberger, G., Steinleitner, K., Malli, R., Graier, W. F., Vormann, J., Schweyen, R. J. and Stadler, J. A. (2007). Mg2+ deprivation elicits rapid Ca2+ uptake and activates Ca2+/calcineurin signaling in Saccharomyces cerevisiae. *Eukaryot Cell* **6,** 592-9.

Wiesenberger, G., Waldherr, M. and Schweyen, R. J. (1992). The nuclear gene MRS2 is essential for the excision of group II introns from yeast mitochondrial transcripts in vivo. *J Biol Chem* **267,** 6963-9.

Wilson, M. G., Towner, J. W., Coffin, G. S., Ebbin, A. J., Siris, E. and Brager, P. (1981). Genetic and clinical studies in 13 patients with the Wolf-Hirschhorn syndrome [del(4p)]. *Hum Genet* **59,** 297-307.

Zeth, K. and Thein, M. (2010). Porins in prokaryotes and eukaryotes: common themes and variations. *Biochem J* **431,** 13-22.

Zischka, H., Gloeckner, C. J., Klein, C., Willmann, S., Swiatek-de Lange, M. and Ueffing, M. (2004). Improved mass spectrometric identification of gel-separated hydrophobic membrane proteins after sodium dodecyl sulfate removal by ion-pair extraction. *Proteomics* **4,** 3776-82.

Zollino, M., Di Stefano, C., Zampino, G., Mastroiacovo, P., Wright, T. J., Sorge, G., Selicorni, A., Tenconi, R., Zappala, A., Battaglia, A., Di Rocco, M., Palka, G., Pallotta, R., Altherr, M. R. and Neri, G. (2000). Genotype-phenotype correlations and clinical diagnostic criteria in Wolf-Hirschhorn syndrome. *Am J Med Genet* **94,** 254-61.

Zollino, M., Lecce, R., Fischetto, R., Murdolo, M., Faravelli, F., Selicorni, A., Butte, C., Memo, L., Capovilla, G. and Neri, G. (2003). Mapping the Wolf-Hirschhorn syndrome phenotype outside the currently accepted WHS critical region and defining a new critical region, WHSCR-2. *Am J Hum Genet* **72,** 590-7.

Zotova, L., Aleschko, M., Sponder, G., Baumgartner, R., Reipert, S., Prinz, M., Schweyen, R. J. and Nowikovsky, K. (2010) Novel components of an active mitochondrial K(+)/H(+) exchange. *J Biol Chem* **285,** 14399-414.

Acknowledgements

First of all I would like to thank a very special person and outstanding scientist, Professor Rudolf Schweyen, for his support during my studies, my diploma work and also this thesis would not have been possible without him. I was impressed by his attitude towards science and his humanity; it was a pleasure to work in his lab.

I am also deeply grateful to Professor Kristina Djinovic-Carugo for her great support after Rudolf's tragic death and for taking over the supervision of my thesis.

I am very thankful to my long time colleague and very good friend Markus Aleschko for the fruitful work on our common projects, the great fun we had together and for teaching me the carinthian dialect. I really enjoyed the time we spent together.

I am indebted to Elisabeth "Lisi" Froschauer-Neuhauser for sharing her great knowledge about mag-fura-2 measurements and mitochondria with me, for pleasant teamwork, critical reading of manuscripts and my thesis and our chats in her office in the morning. I would like to thank our "lab-mom" Mirjana for her helpfulness, excellent technical assistance and especially for supplying us with delicious food and sparkling wine (of course only occasionally). I would also like to thank Dr. Karin Nowikovsky for our successful work on mitochondrial K^+/H^+ exchange and critical reading of my thesis, Julian Weghuber, Muhammad Bashir Khan and Sona Svidova for our teamwork on *MRS2*, CorA and *LPE10*. I thank Dr. Anton Graschopf for helping me with his experience and having an answer on almost every question and of course for hilarious after-work meetings with some drinks.

I value the support of Professor Christoph Romanin (University of Linz) and thank him for being a member of my PhD committee. I am also grateful to DDr Martin Kolisek for successful collaborations, for his encouragement and the pleasant stay in Berlin.

Furthermore, I would like to thank the whole MRS group for the pleasant working atmosphere and for being the best colleagues one could have, especially Michael Aichinger, Monika Prinz, Katharina Steinleitner, Melanie Hassler and Tamás Henics.

I am specially indebt to my parents for their support throughout my life and for giving me the chance to follow my interests and of course my darling Lene for her love and selfless support.

Curriculum vitae

Name:	Gerhard Sponder
Date of birth:	13.07.1981
Place of birth:	Vienna
Nationality:	Austria
Marital status:	single
Private address:	Am Ölberg 111
	3400 Klosterneuburg, Austria

Education

1987 - 1991	Volksschule Klosterneuburg
1991 - 1999	Bundesgymnasium Klosterneuburg
2000 – 2006	Studies at the University of Vienna in Microbiology and Genetics
April 2006 - June 2007	Diploma work in the lab of Prof. Dr. Rudolf J. Schweyen
	Diploma thesis: Characterization of eukaryotic Mg^{2+} transport systems in Salmonella typhimurium
June 2007 - October 2007	Research associate at Max F. Perutz Laboratories GmbH
October 2007 - May 2011	Start of PhD thesis in the lab of Prof. Dr. Rudolf J. Schweyen
	Thesis: Functional and molecular characterization of proteins involved in Mg^{2+} and K^+ homeostasis

Publications:

- **Pun1p is a metal ion - inducible, calcineurin/Crz1p - regulated plasma membrane protein required for cell wall integrity**
  Hosiner D., Sponder G., Graschopf A., Reipert S., Schweyen R.J., Schüller C., and Aleschko M.
  Biochim Biophys Acta. 2011 Jan 9. [Epub ahead of print]

- **Functional analysis of the conserved hydrophobic gate region of the magnesium transporter CorA**
  Svidová S., Sponder G., Schweyen RJ., Djinović-Carugo K.
  Biochim Biophys Acta. 2010 Nov 11. [Epub ahead of print]

- **Lpe10p modulates the activity of the Mrs2p-based yeast mitochondrial Mg^{2+} channel**
  Sponder G., Svidova S., Schindl R., Wieser S., Schweyen RJ., Romanin C., Froschauer EM., Weghuber J.
  FEBS J. 2010 Sep;277(17):3514-25. Epub 2010 Jul 23.

- **Splice-variant 1 of the ancient domain protein 2 (ACDP2) complements the magnesium-deficient growth phenotype of Salmonella enterica sv. typhimurium strain MM281**
  Sponder G., Svidova S., Schweigel M., Vormann J., Kolisek M.
  Magnes Res. 2010 Jun;23(2):105-14. Epub 2010 Jun 2.

- **Novel components of an active mitochondrial K^+/H^+ exchange**
  Zotova L.[1], Aleschko M.[1], Sponder G.[2], Baumgartner R., Reipert S., Prinz M., Schweyen R.J., and Nowikovsky K.[2]
  Journal of Biological Chemistry, 2010, May; 285(19):14399-414.
  [1]equal contributing authors, [2]co-corresponding authors

- **SLC41A1 is a novel mammalian Mg^{2+} carrier**
  Kolisek M.1, Launay P.1, Beck A.1, Sponder G., Serafini N., Brenkus M., Froschauer EM., Martens H., Fleig A., Schweigel M.
  J. Biol. Chem., Vol. 283, Issue 23, 16235-16247, June 6, 2008
  [1] equal contribution

Conference:

- **35th FEBS Congress 2010 - Molecules of life**
  June 26th - July 1st, Göteborg (Gothenburg), Sweden
  Talk and poster presentation: 'Lpe10p modulates the activity of the Mrs2p-based yeast mitochondrial Mg2+ channel'